Stem Cells International

Stem Cell-Based Therapy in Transplantation and Immune-Mediated Diseases

Lead Guest Editor: Vladislav Volarevic
Guest Editors: Majlinda Lako, Slaven Erceg, and Miodrag Stojkovic

Stem Cell-Based Therapy in Transplantation and Immune-Mediated Diseases

Stem Cells International

Stem Cell-Based Therapy in Transplantation and Immune-Mediated Diseases

Lead Guest Editor: Vladislav Volarevic
Guest Editors: Majlinda Lako, Slaven Erceg,
and Miodrag Stojkovic

Editorial Board

Contents

Hindawi
Stem Cells International
Volume 2017, Article ID 7379136, 3 pages
https://doi.org/10.1155/2017/7379136

Editorial

Stem Cell-Based Therapy in Transplantation and Immune-Mediated Diseases

Vladislav Volarevic,[1] Majlinda Lako,[2] Slaven Erceg,[3] and Miodrag Stojkovic[4,5]

[1]*Faculty of Medical Sciences, Department of Microbiology and Immunology, Center for Molecular Medicine and Stem Cell Research, University of Kragujevac, Kragujevac, Serbia*
[2]*Institute of Genetic Medicine, Newcastle University, Newcastle, UK*
[3]*Principe Felipe Research Center, Valencia, Spain*
[4]*Faculty of Medical Sciences, Department of Genetics, University of Kragujevac, Kragujevac, Serbia*
[5]*Spebo Medical, Leskovac, Serbia*

Correspondence should be addressed to Vladislav Volarevic; drvolarevic@yahoo.com

Received 14 August 2017; Accepted 14 August 2017; Published 6 September 2017

Despite the enormous scientific progress in the field of regenerative medicine, there are no cells that provide a cure for everything and everyone. Stem cells have raised tremendous expectations among the medical doctors, researchers, patients, and the general public due to their capacity to differentiate into a broad range of cell types. Stem cell researchers are engaged in different endeavors, including treating genetic disorders and generating new stem cell-derived human tissues and biomaterials for use in pharmacy, genomics, and regenerative medicine. Results obtained from completed and on-going clinical studies during the last decades demonstrate rapid progress and the increased importance of stem cells in both basic research and the long-term future of modern medicine indicating the huge therapeutic potential of stem cells in the treatment of degenerative, autoimmune, and genetic disorders.

Mesenchymal stem cells (MSCs) are considered as new therapeutic agents in the treatment of immune-mediated diseases, particularly due to their immunomodulatory characteristics. In cell-to-cell contact and through the production of soluble mediators, MSCs can regulate the proliferation, activation, and effector function of T lymphocytes, professional antigen presenting cells, NK cells, NKT cells, and neutrophils.

MSCs suppress inflammatory (M1) macrophages and promote their conversion in alternative (M2) phenotype in prostaglandin E2 (PGE2), tumor necrosis factor alpha- (TNF-α-) stimulated gene/protein 6 (TSG-6), interleukin- (IL-) 6, and indoleamine 2,3-dioxygenase- (IDO-) dependent manner. In line with these findings, in their article published in this special issue, S. Ravanidis and coworkers described molecular mechanisms involved in interplay between macrophages and multipotent adult progenitor cells (MAPC), a stem cell population sharing common mesodermal origin with MSCs. S. Ravanidis et al. showed that MAPC, in a cyclooxygenase 2- (COX-2-) dependent manner, suppressed the secretion of TNF-α in M1 inflammatory macrophages while, at the same time, inflammatory macrophages triggered the immunomodulatory properties of MAPC, including an increased expression of immunomodulatory mediators (inducible nitric oxide synthase (iNOS) and COX-2), chemokines, and chemokine receptors. Moreover, S. Ravanidis and colleagues showed that the MAPC secretome suppressed the antigen-specific proliferation of autoreactive T cells and attenuated their capacity to activate inflammatory macrophages. Data published in this article revealed mechanisms involved in the interactions between MAPC and inflammatory macrophages, which could be important for the design of new MAPC-based therapeutic strategies for the treatment of inflammatory disorders in which myeloid cells play a crucial role.

MSCs are adult stem cells that can be isolated from various numbers of postnatal tissues. Bone marrow (BM) has been the main source for the isolation of multipotent MSCs. BM-MSCs have many properties that enable their therapeutic use: easy acquisition, quick proliferation *in vitro*, low surface expression of major histocompatibility complex (MHC) antigens and minor immunological rejection, long-term coexistence in the host, maintenance of differentiation potential after repeated passages, and ease of transplantation. Since the derivation of BM-MSCs involves harvesting of BM that is a highly invasive procedure, alternative sources have been strongly pursued. In this special issue, immunomodulatory characteristics of BM-MSC, synovial-membrane-derived MSCs (SM-MSCs), human placenta-derived MSCs (hP-MSCs), and adipose tissue-derived MSCs (AT-MSCs) were described and their therapeutic potential was investigated in well-established animal models of acute renal injury, arthritis, and liver fibrosis.

Since AT-MSCs can be easily isolated from liposuctions, AT represents an important source of MSCs. Accordingly, Y. Wu and coworkers investigated cytokine secretion profile of AT-MSCs in order to further emphasize their potential in cellular immunotherapy. As it was described by Y. Wu et al., AT-MSC cultures were heterogeneous in phenotype indicating that all AT-MSCs did not contribute to the immune-suppression in the same manner. Although all AT-MSCs were capable to produce IL-6, only 10–20% of AT-MSCs expressed IL-6 receptor (CD130) on their surface. Similarly, IFN-γ was produced by only 1.4% of AT-MSCs, but 18–31% of AT-MSCs expressed receptor of IFN-γ (CD119) indicating that AT-MSCs did not produce inflammatory cytokines but had the capacity to respond on them. Results obtained by Y. Wu and colleagues demonstrate that AT-MSCs are heterogeneous in their cytokine secretion and receptor expression profiles which are an important information for their future therapeutic use.

AT-MSCs were also in the focus of the research conducted by I. Muñoz-Criado et al. who investigated regenerative potential of AT-MSCs in the animal model of severe osteoarthritis (OA). They showed that transplantation of suprapatellar-derived AT-MSCs significantly diminished the OA-associated knee inflammation and cartilage degenerative grade by increasing the production of glycosaminoglycan and by inducing endogenous chondrogenesis. Results obtained by I. Muñoz-Criado and colleagues strongly suggest transplantation of autologous suprapatellar-derived AT-MSCs as a new therapeutic approach for patients with multiple degenerative OA.

Advanced liver fibrosis results in cirrhosis, liver failure, and portal hypertension and often requires liver transplantation. However, liver transplantation has several limitations, including lack of donors, complications of surgical interventions, side effects of immuno-suppressive drugs, and high medical costs. Accordingly, the alternative approaches such as stem cell transplantation have been suggested as an effective alternate therapy to liver transplantation. In line with these findings, J. Yu and coworkers showed that transplantation of hP-MSCs efficiently repaired carbon tetrachloride- (CCl_4-) induced liver fibrosis in rats, as evaluated by enhanced liver function tests, improved histopathology, reduced Sirius red-stained collagen area, and downregulated expression of fibrotic markers: transforming growth factor beta (TGF-β) and alpha smooth muscle actin (α-SMA). Moreover, by using green fluorescent protein, J. Yu et al. demonstrated that transplanted hP-MSCs successfully engrafted in the injured livers where it were able to restore liver function, suggesting their therapeutic potential in the treatment of liver fibrosis.

In many cisplatin-treated patients, kidney injury is irreversible, requiring substitution, reduction, or discontinuation of cisplatin treatment. Since currently there is no compatible and convenient chemotherapeutic agent with similar potent, anticancer efficacy as cisplatin, clinical use of cisplatin cannot be abandoned. Accordingly, an urgent demand exists for researchers to develop new adjuvant therapy for attenuation of cisplatin-induced nephrotoxicity and inflammation. B. S. Markovic and coworkers demonstrated that BM-MSCs can attenuate cisplatin-induced acute renal failure by suppressing migration and activation of immune cells in inducible nitric oxide synthase- (iNOS-) dependent manner. They noticed significantly decreased levels of inflammatory cytokines TNF-α and IL-17 and increased levels of anti-inflammatory cytokines IL-10, IL-6, nitric oxide (NO), and kynurenine in sera of cisplatin-treated mice that received BM-MSCs or MSC-conditioned medium (MSC-CM) indicating that MSCs exert their beneficial effects in paracrine manner. Moreover, BM-MSC or MSC-CM treatment significantly attenuated influx of immune cells: macrophages, dendritic cells, neutrophils, and T lymphocytes in damaged kidneys and attenuated their capacity to produce TNF-α and IL-17. Importantly, inhibition of iNOS completely diminished renoprotective and immuno-suppressive effects of MSC-CM. Results obtained by B. S. Markovic and colleagues provide the evidence that BM-MSCs, in paracrine, iNOS-dependent manner, attenuate inflammation in cisplatin-induced nephrotoxicity. These findings could be helpful in developing new BM-MSC-based therapeutic approaches for attenuation of cisplatin-induced nephrotoxicity.

Rheumatoid arthritis is an autoimmune, systemic inflammatory disease characterized by persistent inflammation, extensive synovial hyperplasia, and cartilage and bone destruction that is developed as a consequence of enhanced Th1 and Th17 immune response and suppressed activity of T regulatory and B regulatory cells. MSCs have the potential to suppress both Th1- and Th17-driven inflammation and to promote expansion of regulatory cells in peripheral lymph organs. Accordingly, in this special issue, M. Yan and coworkers demonstrated that intra-articular injection of SM-MSCs ameliorated clinical and histological severity of collagen-induced arthritis by decreasing production of Th1 and Th17 inflammatory cytokines (TNF-α, IFN-γ, and IL-17A) and by increasing production of anti-inflammatory and immuno-suppressive IL-10. Moreover, cellular makeup of the spleens revealed decreased number of Th1 and Th17 cells and increased presence of Th2 lymphocytes, PD-1+ CXCR5+FoxP3+ follicular T regulatory cells, and CD19+ CD5+CD1d+IL-10+ regulatory B cells in mice that received SM-MSCs. Data obtained by M. Yan and colleagues

demonstrated therapeutic potential of SM-MSCs for the suppression of immune response and inflammation during the progression and development of rheumatoid arthritis.

Although immuno-suppressive characteristics of MSCs are beneficial in the treatment of inflammatory and autoimmune diseases, they can represent a serious problem if patient that received MSCs has primary or metastatic tumor. By using mice model of metastatic lung cancer, M. Gazdic and coworkers showed that intravenous application of BM-MSCs significantly suppressed systemic antitumor immune response, reduced total number of lung-infiltrated dendritic cells, macrophages, and CD4+ T lymphocytes, and attenuated antitumor cytotoxicity of cytotoxic T lymphocytes and NK cells resulting with the expansion of metastatic lesions in the lungs. This phenomenon was abrogated by inhibitors of iNOS and IDO, suggesting importance of iNOS and IDO for MSC-mediated suppression of antitumor immune response. Data obtained by M. Gazdic and colleagues raise serious concerns regarding safety of MSC-based therapy in patients who have genetic susceptibility for malignant diseases.

In summing up, articles in this special issue present novel findings regarding molecular and cellular mechanisms involved in MSC-based suppression of immune response in inflammatory and malignant diseases underlining the importance of preclinical studies in the development of efficient and low-cost regenerative medicine.

Vladislav Volarevic
Majlinda Lako
Slaven Erceg
Miodrag Stojkovic

Hindawi
Stem Cells International
Volume 2017, Article ID 1315378, 15 pages
https://doi.org/10.1155/2017/1315378

Research Article

Mesenchymal Stem Cells Attenuate Cisplatin-Induced Nephrotoxicity in iNOS-Dependent Manner

Bojana Simovic Markovic,[1] Marina Gazdic,[2] Aleksandar Arsenijevic,[1] Nemanja Jovicic,[3] Jovana Jeremic,[4] Valentin Djonov,[5] Nebojsa Arsenijevic,[1] Miodrag L. Lukic,[1] and Vladislav Volarevic[1]

[1]*Center for Molecular Medicine and Stem Cell Research, Faculty of Medical Sciences, University of Kragujevac, 34000 Kragujevac, Serbia*
[2]*Department of Genetics, Faculty of Medical Sciences, University of Kragujevac, 34000 Kragujevac, Serbia*
[3]*Department of Histology and Embryology, Faculty of Medical Sciences, University of Kragujevac, 34000 Kragujevac, Serbia*
[4]*Department of Pharmacy, Faculty of Medical Sciences, University of Kragujevac, 34000 Kragujevac, Serbia*
[5]*Institute of Anatomy, University of Bern, 3000 Bern 9, Switzerland*

Correspondence should be addressed to Vladislav Volarevic; drvolarevic@yahoo.com

Received 9 March 2017; Revised 28 June 2017; Accepted 4 July 2017; Published 30 July 2017

Academic Editor: Silvia Brunelli

Mesenchymal stem cells (MSCs) are, due to their immunomodulatory characteristics, utilized in therapy of immune-mediated diseases. We used murine model of cisplatin nephrotoxicity to explore the effects of MSCs on immune cells involved in the pathogenesis of this disease. Intraperitoneal application of MSCs significantly attenuated cisplatin nephrotoxicity, decreased inflammatory cytokines TNF-α and IL-17, and increased anti-inflammatory IL-10, IL-6, nitric oxide (NO), and kynurenine in sera of cisplatin-treated mice. MSC treatment significantly attenuated influx of leukocytes, macrophages, dendritic cells (DCs), neutrophils, CD4+ T helper (Th), and CD8+ cytotoxic T lymphocytes (CTLs) in damaged kidneys and attenuated the capacity of renal-infiltrated DCs, CD4+ Th, and CD8+ CTLs to produce TNF-α and IL-17. Similar effects were observed after intraperitoneal injection of MSC-conditioned medium (MSC-CM) indicating that MSCs exert their beneficial effects in paracrine manner. Inhibition of inducible nitric oxide synthase (iNOS) in MSC-CM resulted with increased number of TNF-α-producing DCs and IL-17-producing CTLs, decreased number of IL-10-producing tolerogenic DCs and regulatory CD4+FoxP3 + T cells, and completely diminished renoprotective effects of MSC-CM. In conclusion, MSCs, in iNOS-dependent manner, attenuated inflammation in cisplatin nephrotoxicity by reducing the influx and capacity of immune cells, particularly DCs and T lymphocytes, to produce inflammatory cytokines.

1. Introduction

Acute renal injury, characterized by tubular cell damage and kidney dysfunction, may be developed as a consequence of drug-induced toxicity [1]. As one of the most effective chemotherapeutics, cisplatin has been used for the therapy of a broad range of solid tumors including lung, ovarian, bladder, gastric, and testicular cancers [2]. However, clinical application of cisplatin is limited because of nephrotoxicity that, as a serious side effect, occurs in nearly 30% of cisplatin-treated patients [3]. Cisplatin, which could be metabolized to a potent nephrotoxin-reactive thiol, selectively accumulates in proximal tubular cells to five times higher degree of the serum concentration and damages proximal tubular epithelial cells, contributing to nephrotoxicity [3]. Acute cisplatin-induced nephrotoxicity is associated with a robust inflammatory response followed by infiltration of immune cells that promotes further progression of renal tissue damage leading to the development of renal failure [4, 5].

In many cisplatin-treated patients, kidney injury, manifested by increased serum creatinine and blood urea nitrogen (BUN) levels and decreased renal blood flow, hypomagnesemia, hypocalcemia, and proteinuria [3], is irreversible, requiring substitution, reduction, or discontinuation of cisplatin treatment. Since currently there is no compatible and convenient chemotherapeutic agent with similar potent, anticancer efficacy as cisplatin, the clinical use of cisplatin cannot be abandoned. Accordingly, an urgent demand exists for researchers to develop new adjuvant therapy for attenuation of cisplatin-induced nephrotoxicity and inflammation.

Mesenchymal stem cells (MSCs) are adult, self-renewable, multipotent cells which are, due to their differentiation and immunomodulatory characteristics, used in preclinical and clinical studies of degenerative and immune-mediated diseases [6–8].

Recently, MSC-based therapeutic approach for attenuation of cisplatin-induced nephrotoxicity has been extensively investigated, and several possible mechanisms were proposed. As demonstrated by Ashour et al. [9], renoprotective effects of intraperitoneally injected MSCs were based on MSC-mediated reduction of oxidative stress. Significantly decreased renal tissue malondialdehyde, increased reduced glutathione level, and superoxide dismutase activity were noticed in cisplatin-treated rats that received MSCs [9].

Additionally, Kim et al. [10] and Yao et al. [11] demonstrated that MSCs markedly improved cisplatin-induced renal failure by suppressing apoptosis in paracrine and p53-dependent manner. Alleviated kidney injury was accompanied by decreased expression of cyclooxygenase COX-2 and tumor necrosis factor alpha (TNF-α), a key mediator in the inflammatory response triggered by cisplatin, indicating that MSC attenuated cisplatin-induced nephrotoxicity by modulating kidney inflammation. In line with these findings, Park et al. [12] recently showed that early but not late treatment with MSCs attenuates cisplatin-induced nephrotoxicity and modulates inflammation in the injured kidneys.

Although data presented in these studies [9–12] clearly demonstrated that MSCs were able to protect the kidney from the cisplatin-induced toxicity, the effects of MSC on immune cell-mediated mechanisms involved in induction and progression of cisplatin-caused kidney inflammation are still unknown. The aim of our study was to investigate the cellular mechanisms underlying the protective effects of MSCs on kidney function in order to suggest new pathways that can be used for the modulation of MSC-dependent protection of cisplatin-induced nephrotoxicity.

Herewith, we show that single intraperitoneal injection of MSCs and MSC-conditioned medium (MSC-CM) diminished influx of immune cells (dendritic cells (DCs), macrophages, neutrophils, effector CD4+ T helper, and cytotoxic CD8+ CTL lymphocytes) into the cisplatin-injured kidneys and attenuated their capacity to produce nephrotoxic and inflammatory cytokines (TNF-α and interleukin- (IL-) 17) in inducible nitric oxide synthase- (iNOS-) dependent manner.

2. Materials and Methods

2.1. Cells. Mouse bone marrow-derived MSCs were purchased from Gibco (catalog number S1502-100). The cells were cultured in complete Dulbecco's Modified Eagle Medium (DMEM) containing 10% heat-inactivated fetal bovine serum (FBS), 100 IU/mL penicillin G, and 100 μg/mL streptomycin (Sigma-Aldrich, Munich, Germany), at 37°C in a 5% CO_2 incubator. MSCs in passage 4 were used throughout the experiments.

2.2. Generation of MSC-Conditioned Medium (MSC-CM). MSCs were seeded at a density of 10,000 cells/cm^2. In order to collect the MSC-CM, MSCs were first cultured in serum-containing complete medium and incubated at 37°C in a humid atmosphere with 5% CO_2. At 80% confluence, the cells were washed twice with 1x phosphate-buffered saline (PBS, Invitrogen), and the medium was then changed to serum-free medium. After 48 h, the medium was collected, centrifuged at 13000 ×g at 4°C for 10 min, and stored at −80°C until used [13].

2.3. Pharmacological Inhibition of iNOS and Indoleamine 2,3-Dioxygenase (IDO). To block iNOS activity, mMSCs or hMSCs were cultured for 48 h in the presence of 1 mM of an iNOS inhibitor, L-N^G-monomethyl arginine citrate (L-NMMA, Sigma-Aldrich, St. Louis, MO) [14].

MSCs were cultured for 48 h in culture medium containing 1 mM 1-methyltryptophan, (1-MT, Sigma-Aldrich, St. Louis, MO), an inhibitor of IDO enzymatic activity [15].

2.4. In Vitro Activation of MSCs. For in vitro activation, MSCs were cultured 48 h in the presence of 10 ng/mL recombinant mouse TNF-α (Ebioscience, San Diego, USA). IDO activity in supernatants of TNF-α-activated MSCs was determined by spectrophotometric measuring of kynurenine (described under Section 2.11) while expression of iNOS and IDO was determined by real-time RT-PCR, as described under Section 2.12.

2.5. Animals. 6–8-week-old male BALB/c mice were randomly divided in control and experimental groups ($n = 10$ mice/group). All animals received human care, and all experiments were approved by and conducted in accordance with the Guidelines of the Animal Ethics Committee of the Faculty of Medical Sciences of the University of Kragujevac, Serbia. Mice were housed in a temperature-controlled environment with a 12 hour light-dark cycle and were administered with standard laboratory chow and water ad libitum.

2.6. Induction of Cisplatin Nephrotoxicity and Application of MSCs and MSC-CM. Cisplatin nephrotoxicity was induced by intraperitoneal injection of cisplatin (16 mg/kg body weight) [16]. One hour after the injection of cisplatin, MSC-treated mice intraperitoneally received 5×10^5 MSCs and resuspended in 200 μL of saline, while MSC-CM-treated mice intraperitoneally received 200 μL of MSC-CM. Mice were randomized to receive cisplatin only, cisplatin and MSCs, cisplatin and MSC-CM, MSCs, MSC-CM, or saline only (control mice). After mouse euthanasia (72 h after

cisplatin treatment), both the kidneys were excised and blood samples were drawn from the inferior vena cava, as previously described [16].

2.7. Determination of BUN and Creatinine Levels. Serum levels of BUN and creatinine were determined to assess the renal function. After blood collection, serum levels of these toxicity markers were measured immediately using assay kits and blood chemistry analyzer, as described [17].

2.8. Histopathological Analysis. The isolated kidneys were fixed in 10% formalin and embedded in paraffin, and consecutive 5 μm tissue sections were mounted on slides. Sections were stained with Hematoxylin and Eosin (H&E) and examined under low-power (100x) light microscopy- (Zeiss Axioskop 40, Jena, Germany) equipped digital camera. Histological sections were scored using a semiquantitative scale designed to assess acute kidney injury-associated tubular injury (tubular epithelial cell loss, necrosis, tubular epithelial simplification, intratubular debris, and casts) by a pathologist unaware of the experimental groups (using >5 random fields/section, 4-5 mice/group). Tubule injury scores (ranging between 0 and 4) were based on the percentage of tubules affected as follows: $0 \leq 10\%$, $1 = 10$–25%, $2 = 26$–50%, $3 = 51$–75%, and $4 \geq 75\%$, as previously described [18].

Periodic acid-Schiff (PAS) staining was performed on paraffin-embedded kidney tissue sections using PAS Kit (Sigma-Aldrich, St. Louis, MO) according to the manufacturer's protocol.

2.9. Isolation of Renal-Infiltrated Immune Cells. The kidneys were washed with sterile phosphate-buffered saline (PBS) and placed in Petri dishes with DMEM supplemented with 10% FBS. The kidneys were cut into small pieces (1-2 mm in dimension) using a regular metal shaping blade and placed into the collagenase solution for 30–45 min in the incubator at 37°C. The cells were filtered through a 70 μm nylon cell strainer into a clean 50 mL conical tube. Then, cells were pelleted by centrifuging 10 min at 400 ×g, at 4°C. Pellet was resuspended in 4 mL of 40% Percoll solution and gently overlaid onto 4 mL of 80% Percoll solution. Slight whitish translucent layers of cells were collected from the interface of the two Percoll phases after centrifugation at 1500 ×g for 30 minutes, at room temperature. These cells were then collected and pelleted by centrifuging 10 min at 400 ×g, at 4°C. Pellet was resuspended in 1 mL of DMEM, and the total number of cells was determined by using trypan blue exclusion on a hemocytometer [19].

2.10. Flow Cytometry Analysis and Intracellular Staining of Renal-Infiltrated Immune Cells. Renal-infiltrated immune cells were screened for various cell surface and intracellular markers with flow cytometry. Briefly, 1×10^6 cells were incubated with anti-mouse CD45, F4/80, CD4, CD8, CD11c, CD11b, Ly6G, and monoclonal antibodies conjugated with fluorescein isothiocyanate (FITC), phycoerythrin (PE), peridinin chlorophyll protein (PerCP), or allophycocyanin (APC) (all from BD Biosciences, San Jose, CA, USA) following the manufacturer's instructions. Immune cells derived from the kidneys were concomitantly stained for the intracellular content of TNF-α, IL-10, IL-17, and forkhead box P3 (FoxP3) by using the fixation/permeabilization kit and anti-mouse monoclonal antibodies conjugated with fluorescein isothiocyanate (FITC), phycoerythrin (PE), peridinin chlorophyll protein (PerCP), and allophycocyanin (APC) (BD Bioscience). For intracellular cytokine staining, cells were stimulated with 50 ng/mL PMA and 500 ng/mL ionomycin for 5 h, and GolgiStop (BD Biosciences) was added. Cells were fixed in Cytofix/Cytoperm, permeated with 0.1% saponin, and stained with fluorescent Abs. Flow cytometric analysis was conducted on a BD Biosciences FACSCalibur and analyzed by using the Flowing Software analysis program.

2.11. Measurement of Cytokines and Growth Factors. Levels of TNF-α, IL-17, IL-10, and IL-6 in the mouse serum were measured using ELISA kits specific for the mouse cytokines (R&D Systems, Minneapolis, MN, USA) according to the manufacturer's instructions.

Serum concentrations of nitric oxide (NO) were measured by Griess reagent while IDO activity in serum and supernatants of TNF-α-stimulated MSCs was determined by spectrophotometric measuring of kynurenine since IDO catalyzes the metabolism of tryptophan in the kynurenine [20].

2.12. Expression of Genes in Cisplatin-Injured Kidneys and in TNF-α-Activated MSCs. Total RNA was extracted from frozen mouse kidneys (for determination of IL-6 and TNF-α) or from cultured MSCs (for determination of NO and IDO) using TRIzol (Invitrogen, Carlsbad, CA) according to the manufacturer's instructions. Total RNA (2 μg) was reverse transcribed to cDNA using High-Capacity cDNA Reverse Transcription Kit (Applied Biosystems, Foster City, California, USA). qRT-PCR was performed using Power SYBR MasterMix (Applied Biosystems) and miRNA-specific primers for IL-6, TNF-α, NO, IDO, and β-actin as a housekeeping gene. qPCR reactions were initiated with a 10-minute incubation time at 95°C followed by 40 cycles of 95°C for 15 seconds and 60°C for 60 seconds in a Mastercycler ep realplex (Eppendorf, Hamburg, Germany). Relative expression of genes was calculated according to the formula $2^{-(C_t - C_{tactin})}$, where C_t is the cycle threshold of the gene of interest and C_{tactin} is the cycle threshold value of the housekeeping gene (β-actin) [21].

2.13. Statistical Analysis. The results were analyzed using Student's *t*-test. All data in this study were expressed as the mean ± standard error of the mean (SEM). Values of $p < 0.05$ were considered as statistically significant.

3. Results

3.1. Intraperitoneal Application of MSCs Significantly Attenuates Cisplatin-Induced Acute Kidney Injury. Cisplatin caused significant renal dysfunction as determined by biochemical analysis and histological examination.

As shown in Figure 1(a), cisplatin administration resulted with 4-fold increase in BUN and creatinine when compared to control mice, indicating the induction of severe nephrotoxicity. Single, intraperitoneal injection of MSCs did

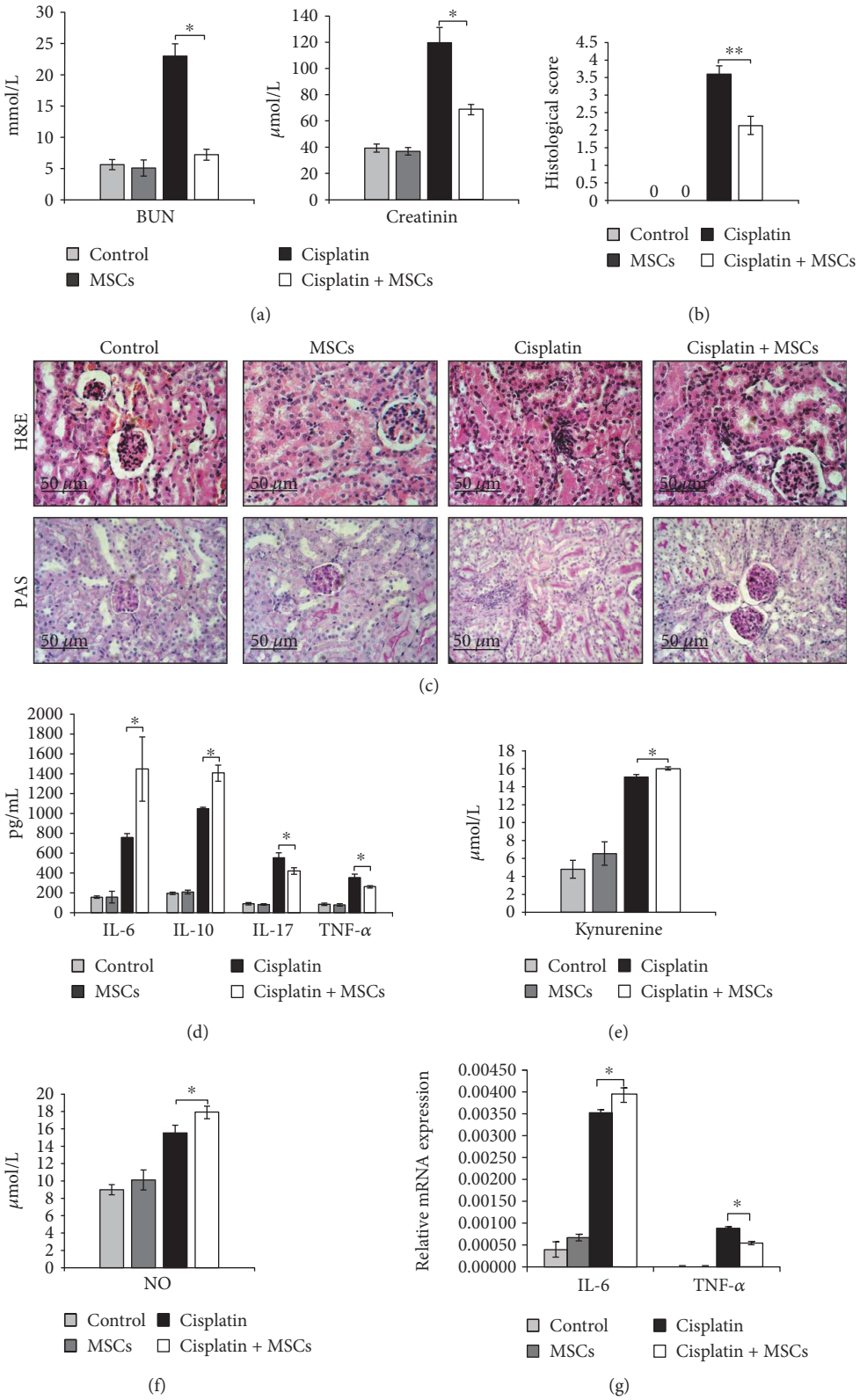

Figure 1: MSCs attenuate cisplatin-induced acute kidney injury. (a) Blood urea nitrogen (BUN) and plasma creatinine levels are evaluated. (b) Histological scores (ranging between 0 and 4) were determinated and calculated on the percentage of tubules affected ($0 \leq 10\%$, $1 = 10$–25%, $2 = 26$–50%, $3 = 51$–75%, and $4 \geq 75\%$). (c) Representative H&E- and PAS-stained mouse kidney. H&E staining images of kidney tissue samples are shown at the same magnifications (×200). Concentration of (d) cytokines, (e) kynurenine, and (f) NO in mice sera. (g) IL-6 and TNF-α gene expression in mouse kidneys. Values are mean ± SEM; $n = 10$ mice/group. $^{*}p < 0.05$, $^{**}p < 0.001$.

not alter serum levels of BUN and creatinine in cisplatin-untreated mice. However, MSCs significantly downregulated serum levels of both BUN ($p < 0.05$) and creatinine ($p < 0.05$) in cisplatin-treated animals suggesting beneficent effects of MSCs in the treatment of cisplatin-induced nephrotoxicity.

As shown in Figure 1(c), the kidneys obtained from control and MSC-only treated animals had normal histology. Partial tubular cell necrosis with citoplasmatic vacuolar transformation of the tubular epithelium due to hydropic degeneration and mild interstitial edema with discrete focal monocyte infiltration was noticed in cisplatin-treated mice. On the contrary, cisplatin + MSC-treated mice showed significant reduction in renal injury followed by reduced infiltration of inflammatory cells (Figure 1(c)). The histological scores also showed increased tubular injury score after cisplatin treatment, which was significantly reversed by MSCs (Figure 1(b)).

In accordance with the biochemical and histological analysis, MSCs did not affect serum levels of cytokines in cisplatin-untreated mice indicating that the differences in their concentration, between cisplatin + MSC-treated and cisplatin-treated mice (Figure 1(d)), are a consequence of MSC-mediated suppression of immune cells that produce these mediators. The concentrations of nephrotoxic and inflammatory cytokines TNF-α ($p < 0.05$) and IL-17 ($p < 0.05$) were significantly lower while concentrations of anti-inflammatory IL-10 ($p < 0.01$) and IL-6 ($p < 0.05$) were significantly higher in sera of cisplatin-treated mice that received MSCs (Figure 1(d)). In line with these findings, the expression of TNF-α was significantly lower ($p < 0.05$) while expression of IL-6 was significantly higher ($p < 0.05$) in the kidneys of cisplatin + MSC-treated mice when compared to animals that received only cisplatin (Figure 1(g)). Immunosuppressive kynurenine ($p < 0.05$, Figure 1(e)) and NO ($p < 0.05$, Figure 1(f)) were also elevated in the serum of cisplatin + MSC-treated mice suggesting that the production of IDO and NO by MSCs may be important for their beneficent effects.

3.2. Influx of Immune Cells and Their Capacity to Produce Nephrotoxic and Inflammatory Cytokines Have Been Significantly Attenuated by MSCs. To assess the role of MSCs for inflammatory cell accumulation in the kidneys after cisplatin injection, different populations of renal-infiltrated immune cells were analyzed by flow cytometry. MSCs did not alter the total number of renal-infiltrated immune cells in cisplatin-untreated animals. Nevertheless, in cisplatin-treated mice, influx of immune cells and their capacity to produce nephrotoxic and inflammatory cytokines have been significantly attenuated by MSCs. As shown in Figure 2(a), 72 hours after cisplatin injection, accumulation of CD45+ leukocytes was much less pronounced ($p < 0.05$) in the kidneys from cisplatin + MSC-treated mice compared to cisplatin-only-treated animals.

Cellular make-up of the kidneys (Figure 2(b)) showed that MSC treatment significantly attenuated influx of CD45+CD11b+ myeloid cells ($p < 0.05$), CD45+F4/80+ macrophages ($p < 0.05$), CD45+CD11c+DCs ($p < 0.01$), CD45+CD11b+Ly6G+ neutrophils ($p < 0.05$), CD45+CD4+ helper T cells ($p < 0.01$), and CD45+CD8+ cytotoxic T cells (CTLs) ($p < 0.01$).

Moreover, MSCs attenuate the capacity of DCs, CD4+T helper, and CD8+ CTLs to produce inflammatory cytokines in cisplatin-injured kidneys. Intracellular staining revealed significantly decreased number of TNF-α-producing DCs (Figure 2(c), $p < 0.05$), IFN-γ- and IL-17-producing CD4+ T cells (Figure 2(d), $p < 0.01$), and IFN-γ- and IL-17-producing CD8+ CTLs (Figure 2(e), $p < 0.01$) in the kidneys of cisplatin-injured mice that received MSCs when compared to the cisplatin-only-treated animals.

3.3. MSCs Attenuate Cisplatin-Induced Nephrotoxicity in Paracrine Manner. To investigate whether soluble factors were responsible for the MSC-mediated attenuation of cisplatin-induced nephrotoxicity, cisplatin-treated mice intraperitoneally received MSC-CM.

Biochemical analysis showed that MSC-CM did not alter serum levels of BUN and creatinine in cisplatin-untreated mice but managed to markedly decrease both BUN and creatinine in cisplatin-treated animals (Figure 3(a)).

Histological analysis revealed reduced necrosis, vacuolization, and desquamation of epithelial cells in the renal tubules of cisplatin + MSC-CM-treated mice when compared to the animals that received only cisplatin (Figure 3(c)). Histological score confirmed significant reduction of acute renal injury in cisplatin-treated mice that received MSC-CM (Figure 3(b)).

As shown in Figures 3(d), 3(e), and 3(f), MSC-CM treatment significantly downregulated serum levels of nephrotoxic and inflammatory TNF-α ($p < 0.05$) and IL-17 ($p < 0.05$) and increased serum levels of immunosuppressive IL-10 ($p < 0.05$), IL-6 ($p < 0.05$), kynurenine ($p < 0.05$), and NO ($p < 0.05$) in cisplatin-treated mice. Accordingly, MSC-CM significantly downregulated expression of TNF-α ($p < 0.05$) and increased expression of IL-6 ($p < 0.05$) in the kidneys of cisplatin-treated animals (Figure 3(g)).

3.4. MSC-CM Decreases Inflammatory Cell Accumulation in the Kidneys of Cisplatin-Treated Mice. Application of MSC-CM did not affect influx of renal-infiltrated immune cells in cisplatin-untreated animals (Figures 3(h) and 4(a), 4(b), and 4(c)). Nevertheless, similar as it was observed after injection of MSCs, MSC-CM managed to significantly reduce the presence of CD45+ leukocytes ($p < 0.05$), CD45+CD11b+ myeloid cells ($p < 0.01$), CD45+F4/80+ macrophages ($p < 0.01$), CD45+CD11c+ DCs ($p < 0.01$), CD45+CD11b+Ly6G+ neutrophils ($p < 0.01$), CD45+CD4+ helper T cells ($p < 0.01$), and CD45+CD8+ CTLs ($p < 0.01$) in the kidneys of cisplatin-injured mice (Figure 3(g)).

As determined by intracellular staining, in comparison to cisplatin-only-treated mice, MSC-CM treatment significantly increased the total number of immunosuppressive IL-10-producing DCs ($p < 0.01$, Figure 4(a), left panel) and regulatory T cells ($p < 0.01$, Figure 4(a), right panel) and attenuated the total number of inflammatory TNF-α-producing DCs ($p < 0.05$, Figure 4(b)), IFN-γ- and IL-17-producing CD8+ cytotoxic T cells ($p < 0.01$, Figure 4(c)).

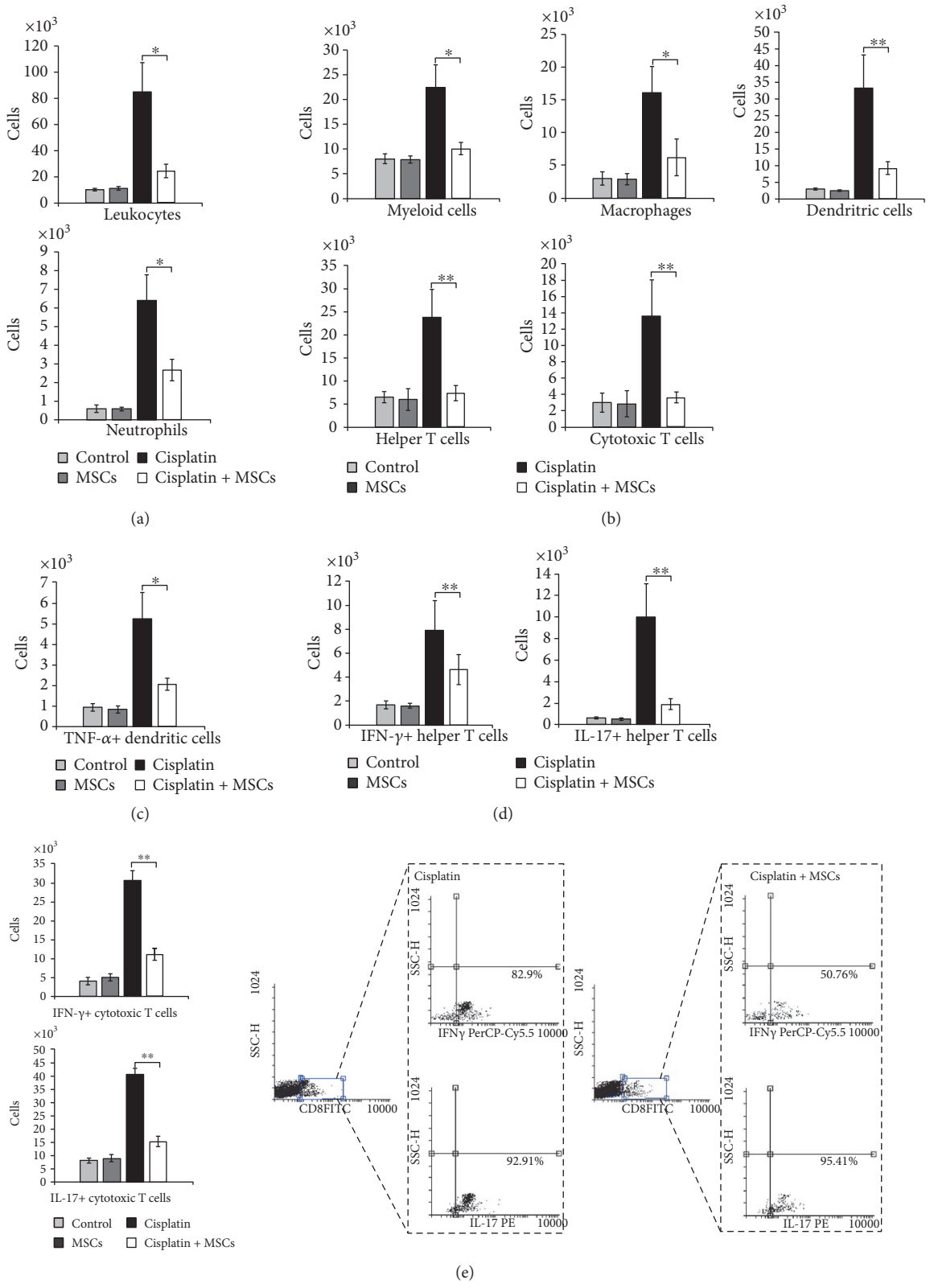

Figure 2: MSCs significantly attenuate influx of immune cells and their capacity to produce nephrotoxic and inflammatory cytokines. Total number of (a) CD45+ leukocytes, (b) CD45+CD11b+ myeloid cells, CD45+F4/80+ macrophages, CD45+CD11c+ dendritic cells, CD45+CD11b+Ly6G+ neutrophils, CD45+CD4+ T helper cells, CD45+CD8+ cytotoxic T cells, (c) TNF-α+CD11c+ dendritic cells, (d) IFN-γ+CD4+ T helper cells, and IL-17+CD4+ T helper cells in cisplatin- and cisplatin + MSC-treated mice. (e) Total number and representative flow cytometry dot plots of IFN-γ- and IL-17-producing cytotoxic CD8+ T cells. Data presented as mean ± SEM; $n = 10$ mice/group. $^{*}p < 0.05$, $^{**}p < 0.01$.

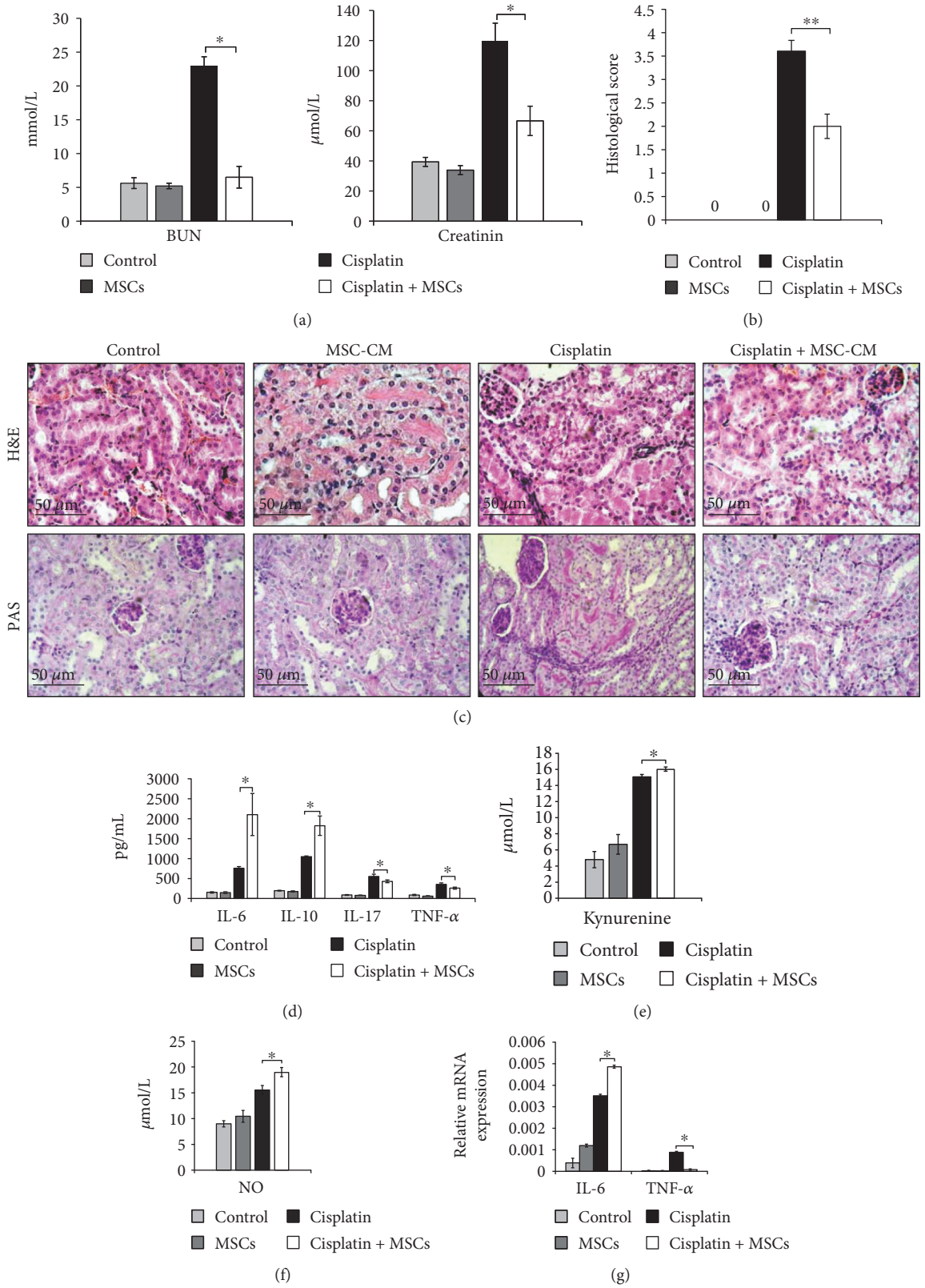

Figure 3: Continued.

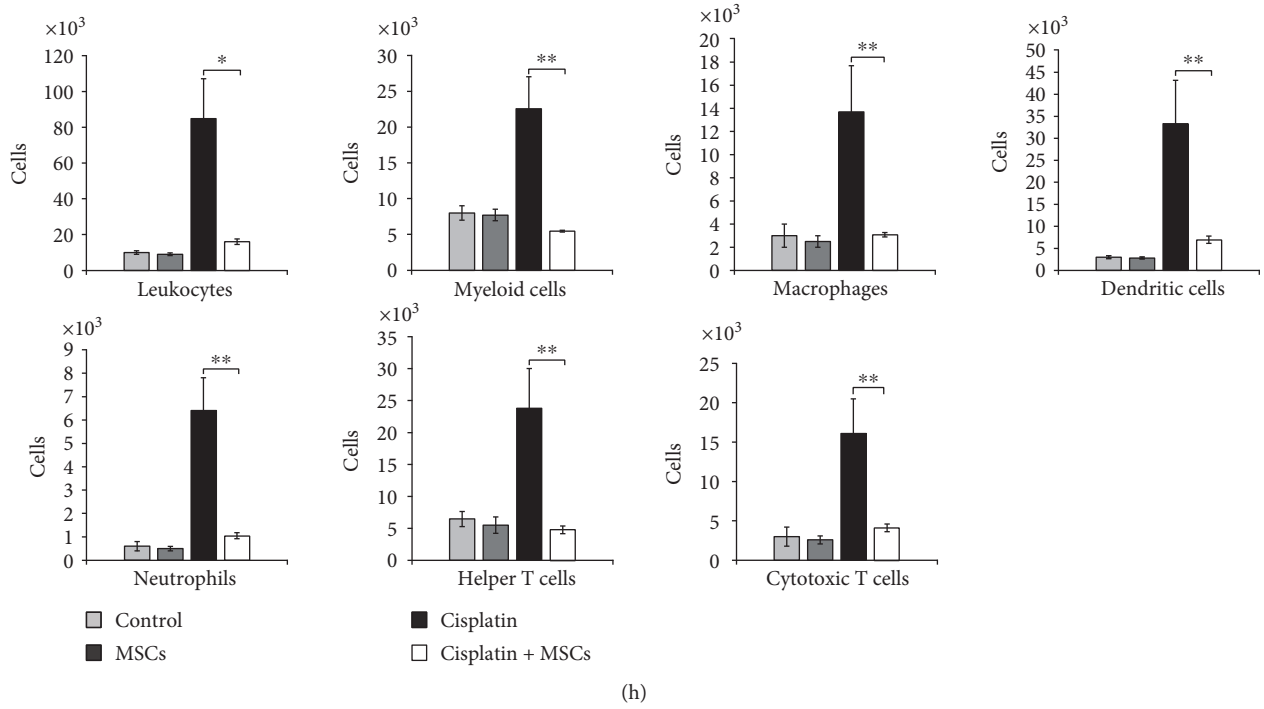

Figure 3: MSCs reduce cisplatin-induced nephrotoxicity via soluble factors. (a) Mice were euthanized 72 h after cisplatin administration, and blood urea nitrogen (BUN) and plasma creatinine levels are measured. (b) Histological examination was performed with H&E staining. (c) H&E and PAS staining images of representative kidney tissues are shown at the same magnifications (200x). Concentration of (d) cytokines, (e) kynurenine, and (f) NO in mouse serum. (g) Expression of IL-6 and TNF-α genes in mouse kidneys. (h) Total number of renal-infiltrated CD45+ leukocytes, CD45+CD11b+ myeloid cells, CD45+F4/80+ macrophages, CD45+CD11c+ dendritic cells, CD45 +CD11b+Ly6G+ neutrophils, CD45+CD4+ T helper cells, and CD45+CD8+ cytotoxic T cells. Data presented as mean ± SEM; $n = 10$ mice/group. $^{*}p < 0.05$, $^{**}p < 0.01$.

3.5. The Capacity of MSC-CM to Protect from Cisplatin-Induced Acute Kidney Injury Is Completely Abrogated by iNOS Inhibitor. Various mediators are proposed to be responsible for the immunosuppressive effects of MSCs, including NO, IDO, TGF-β, HGF, PGE_2, and IL-10 [22–24]. IDO plays a key role in immunomodulation mediated by human MSCs while murine MSCs mainly use iNOS-dependent suppression of immune response [25]. Accordingly, we investigated the effects of iNOS or IDO inhibition on MSC-CM-dependent attenuation of cisplatin-induced nephrotoxicity.

As it is shown in Figure 5, blockade of iNOS by L-NMMA almost completely diminished the renoprotective effects of MSC-CM as determined by increased serum levels of BUN and creatinine ($p < 0.05$, Figure 5(a)) and histological analysis (Figures 5(b) and 5(c)).

Almost normal morphology with well-preserved brush border membranes and no loss of tubular epithelial cells was noticed in cisplatin +MSC-CM-treated animals. On the contrary, cisplatin + MSC-CM + L-NMMA-treated kidneys exhibited severe histological changes which included tubular necrosis and dilation (Figure 5(c)). These findings were confirmed by histological scores (Figure 5(b)).

Similar as it was noticed by biochemical and histological analysis, blockade of iNOS resulted with elevated serum levels of TNF-α ($p < 0.05$, Figure 5(d)) and decreased serum concentration of immunosuppressive IL-10 ($p < 0.01$, Figure 5(d)) in the kidneys of cisplatin + MSC-CM + L-NMMA-treated mice. Significantly higher number of inflammatory TNF-α-producing DCs ($p < 0.05$, Figure 5(e), left panel), followed with increased number of IL-17-producing CTLs ($p < 0.05$, Figure 5(e), right panel), was noticed in the kidneys of cisplatin + MSC-CM + L-NMMA-treated mice when compared to cisplatin + MSC-CM-treated animals (Figure 4(f)). Interestingly, iNOS inhibition also attenuates the capacity of MSC-CM to affect influx of regulatory cells in the injured kidneys. There was significantly lower number of tolerogenic IL-10-producing DCs ($p < 0.05$, Figure 5(f), left panel) and IL-10-producing regulatory T cells ($p < 0.05$, Figure 5(f), right panel) in the kidneys of cisplatin + MSC-CM + L-NMMA-treated mice when compared to cisplatin + MSC-CM-treated animals.

Biochemical and histological analyses indicate that, in contrast to L-NMMA, IDO inhibitor (1-MT) did not manage to completely abrogate renoprotective effects of MSC-CM (Figures 5(a), 5(b), and 5(c)). Significant difference was not observed for serum levels of creatinine and BUN (Figure 5(a)) and histological scores (Figure 5(b)) between cisplatin + MSC-CM- and cisplatin + MSC-CM + 1-MT-treated animals.

In accordance with results obtained by biochemical and histological analyses, cellular make-up of cisplatin-injured kidneys revealed that 1-MT only affected MSC-CM-mediated suppression of TNF-α production in DCs

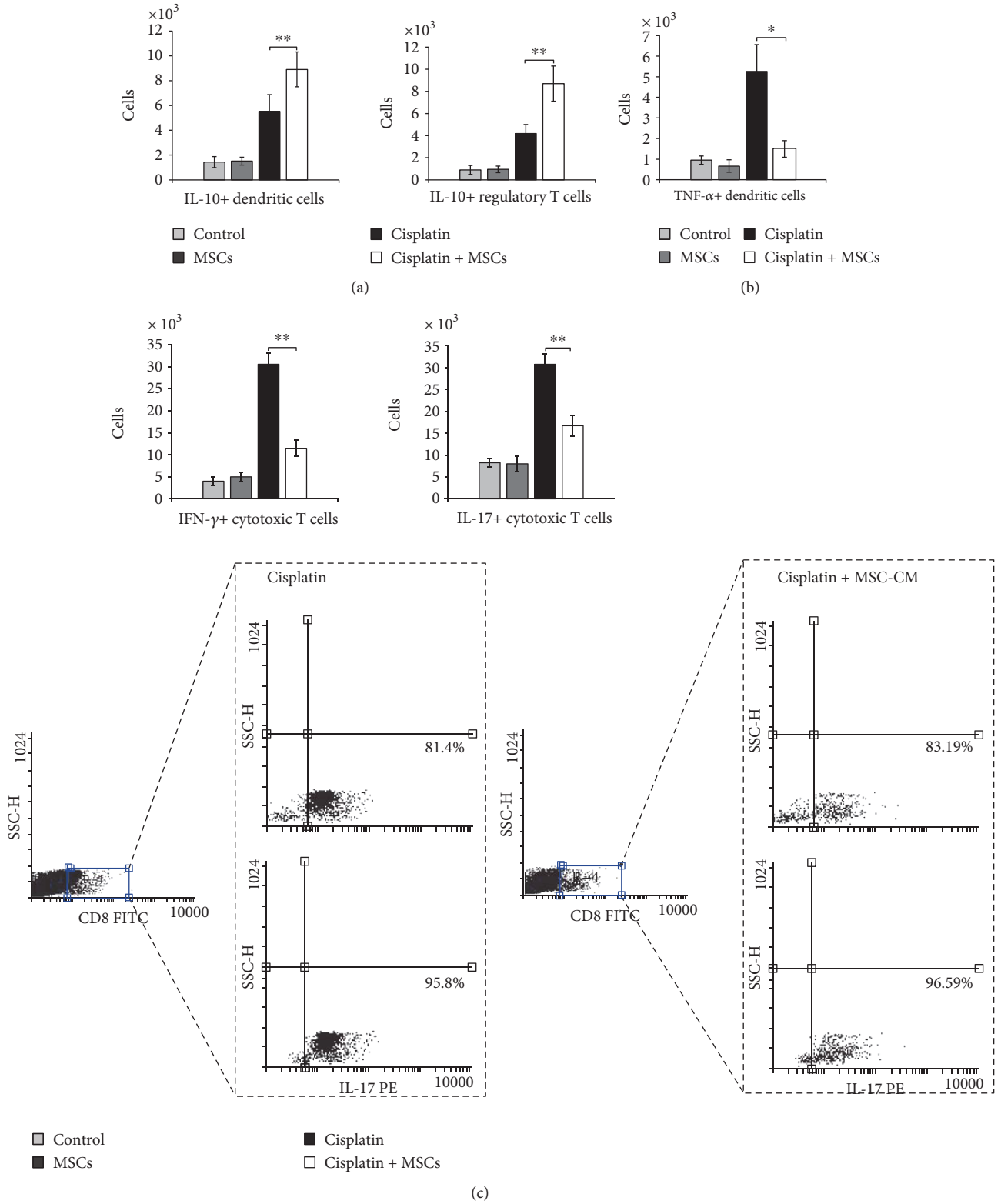

Figure 4: MSC-CM reduces influx of inflammatory DCs and CTLs in cisplatin-induced acute kidney injury and alters their cytokine profile. Total number of (a) IL-10-producing CD45+CD11c+ DCs, CD4+CD25+FoxP3+ T regulatory cells, (b) TNF-α+CD45+CD11c+ DCs, (c) IFN-γ- and IL-17-producing CD8+ CTL cells that infiltrated kidneys of the control and experimental animals. Representative flow cytometry dot plots are shown. Values are mean ± SEM; $n = 10$ mice/group. $^{*}p < 0.05$, $^{**}p < 0.001$.

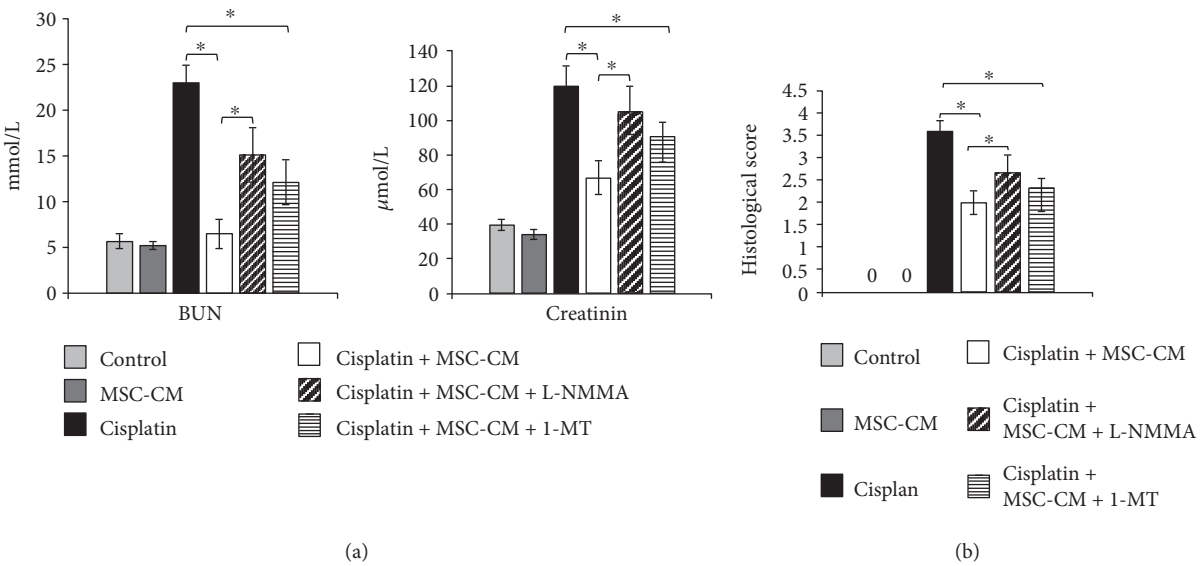

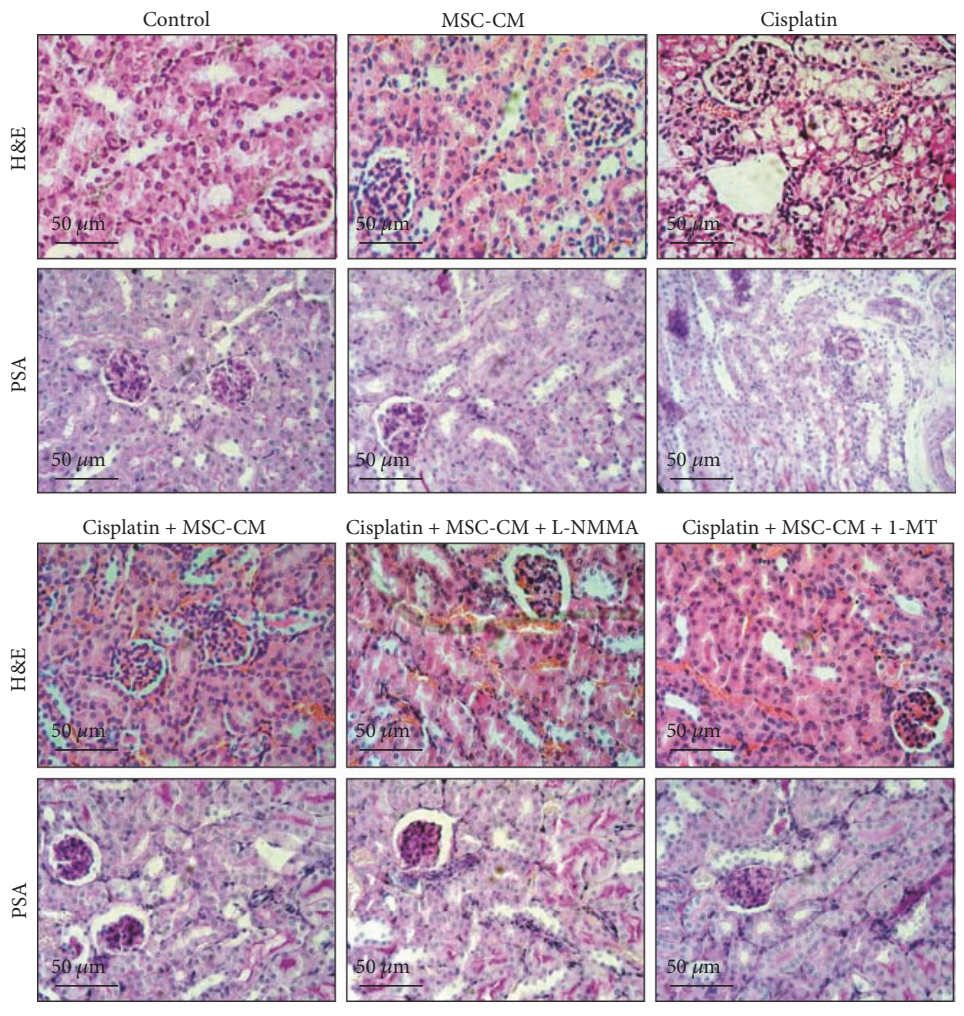

Figure 5: Continued.

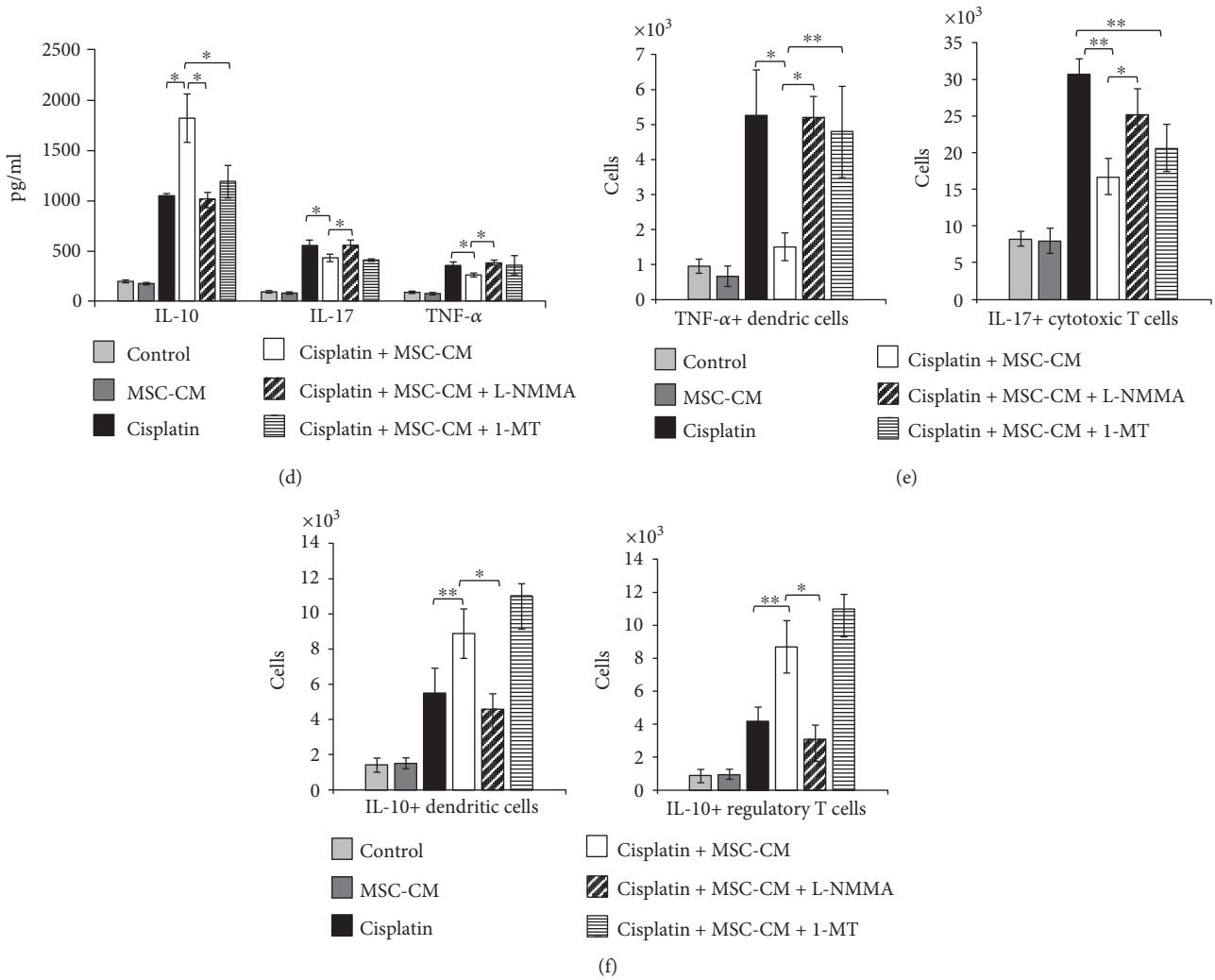

Figure 5: MSCs attenuate cisplatin-induced acute kidney injury in iNOS-dependent manner. (a) Serum levels of BUN and creatinine. (b) Histological scores. (c) Representative H&E and PAS-stained mouse kidney (magnifications ×200). (d) Serum levels of cytokines. Total numbers of (e) TNF-α-producing CD45+CD11c+ dendritic cells and IL-17-producing CD8+ cytotoxic T cells, (f) IL-10-producing CD45+CD11c+ DCs and CD4+CD25+FoxP3+ T regulatory cells. Values are mean ± SEM; $n = 10$ mice/group. $^{*}p < 0.05$, $^{**}p < 0.001$.

(Figure 5(e)) and did not significantly alter MSC-CM-dependent modulation of CTLs and regulatory cells (Figure 5(f)).

3.6. iNOS Is Important for Activation of IDO in TNF-α-Stimulated MSCs. Nonstimulated MSCs express both iNOS and IDO but their expression significantly increased after activation of MSCs by TNF-α (Figure 6(a)). In order to evaluate the interplay between MSC-derived NO and IDO, concentration of kynurenine was measured in supernatants of TNF-α-activated MSCs that were cultured with or without iNOS inhibitor, L-NMMA. As shown in Figure 6(b), L-NMMA significantly attenuated the concentration of kynurenine in TNF-α-primed MSCs indicating the importance of iNOS for IDO activity in TNF-α-stimulated MSCs.

4. Discussion

Here, we provide the evidence that intraperitoneal application of MSCs and MSC-CM attenuates cisplatin-induced nephrotoxicity by suppressing infiltration and activation of immune cells in iNOS-dependent manner.

Cisplatin-induced renal injury is followed by increased release of inflammatory TNF-α. As a response to these inflammatory cytokines, endothelial cells in injured kidneys increase expression of selectins and chemokines which are involved in leukocyte trafficking, resulting with massive influx of inflammatory cells in injured kidneys [26]. MSCs interact with endothelial cells and, by producing IL-6, down-regulate expression of adhesion molecules on endothelial cells, reducing recruitment of leukocytes into the damaged kidneys [27]. Accordingly, decreased expression of TNF-α in the kidneys, attenuated serum levels of TNF-α, and increased expression of IL-6 in renal tissue accompanied with elevated serum concentration of IL-6, noticed in cisplatin + MSC-treated mice (Figures 1(d) and 1(g)), were accompanied with reduced infiltration of leukocytes in injured kidneys of these animals (Figure 2(a)).

Among renal-infiltrated immune cells, MSC treatment significantly attenuates influx of neutrophils, DCs,

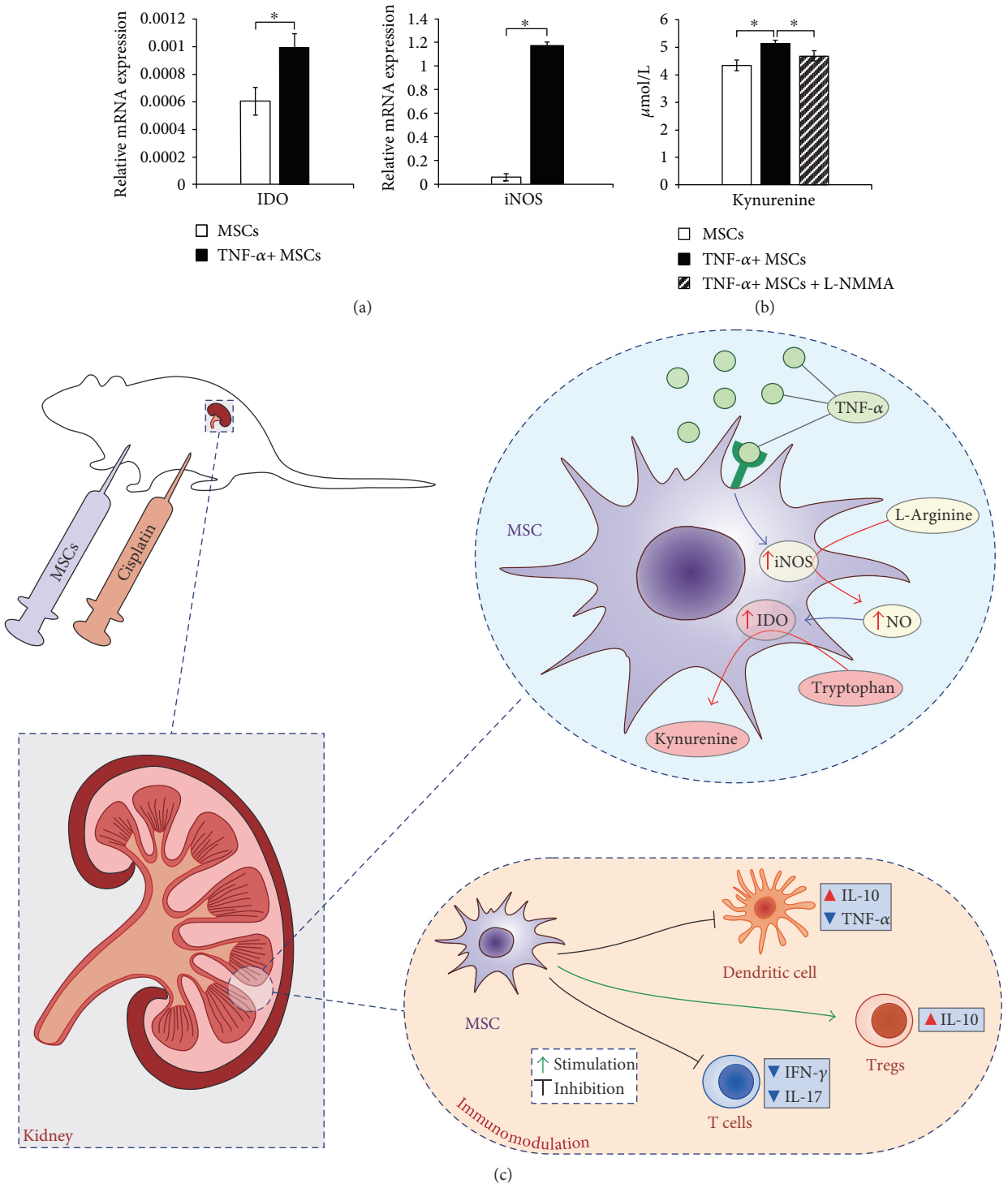

Figure 6: MSC-derived NO is important for activation of IDO in TNF-α-stimulated MSCs. (a) Expression of IDO and iNOS in nonstimulated and TNF-α-stimulated MSCs. (b) Concentration of kynurenine in supernatants of nonstimulated MSCs, TNF-α-stimulated MSCs, and TNF-α-stimulated MSCs cultured in the presence of L-NMMA. $^{*}p < 0.05$. (c) Proposed mechanism of MSC-based immunomodulation of cisplatin-induced nephrotoxicity: After cisplatin-induced kidney injury, MSCs migrate in the kidneys as a response to the inflammatory cytokines and chemokines. Under inflammatory conditions, TNF-α provokes MSCs to express iNOS and to produce NO which, in turn, increases IDO activity and augment MSC-based immunomodulation resulting with attenuated number of inflammatory TNF-α-producing DCs and IFN-γ- and IL-17-producing T cells and increased number of immunosuppressive IL-10-producing DCs and regulatory T cells in injured kidneys.

macrophages, and CD4+ helper and CD8+ CTLs (Figure 2(b)) in the kidneys of cisplatin-injured mice.

Neutrophils are reported to infiltrate and exacerbate cisplatin-induced acute kidney injury 24 to 48 h after cisplatin administration. Although the extent of neutrophil infiltration coincided with the severity of acute kidney injury and renal dysfunction, their depletion had no impact on the extent of cisplatin-induced nephrotoxicity [27]. As recently demonstrated by Tadagavadi et al. [27], cisplatin-mediated acute kidney injury is not mediated by neutrophils, while DCs play the most important role in stimulation or suppression of inflammation in cisplatin-induced renal failure. Renal DCs are immune sentinels with the ability to induce immunity or tolerance in acute kidney injury. IL-10, mainly produced by renal DCs, attenuates cisplatin nephrotoxicity and protects from cisplatin-mediated acute kidney injury [28]. Additionally, depletion of IL-10-producing and tolerogenic renal-infiltrated DCs results with aggravation of cisplatin-induced nephrotoxicity [28, 29].

It is well known that MSCs may suppress maturation of DCs in IL-10-dependent manner, promoting generation of their tolerogenic, immunosuppressive phenotype [30]. In inflammatory microenvironment, DCs exposed to TNF-alpha (produced by inflammatory cells) and IL-10 (produced by MSCs) failed to upregulate maturation markers [31]. These immature DCs are strongly hampered in their ability to produce TNF-α and to promote inflammation [32].

In line with these observations, downregulated serum levels of TNF-α and increased serum concentration of IL-10, noticed in cisplatin + MSC-treated mice (Figure 1(d)), were accompanied with significantly lower number of renal-infiltrated TNF-α-producing DCs (Figure 2(c)).

MSCs are also able to suppress migration of DCs to the draining lymph nodes and inflamed tissues significantly affecting their ability for antigen presentation to CD4+ T helper (Th) cells and cross-presentation to CD8+ T cells [33, 34] resulting with attenuated generation and activation of IFN-γ-producing Th1 and IL-17-producing Th17 cells and CTLs [35]. Accordingly, we noticed reduced renal infiltration of IFN-γ- and IL-17-producing Th1 and Th17 cells (Figure 2(d)) and CTLs (Figure 2(e)), accompanied with decreased serum levels of IL-17 (Figure 1(d)) in cisplatin + MSC-treated mice when compared to cisplatin-only-treated animals. An important proinflammatory role of IL-17 in the nephrotoxicity induced by cisplatin was demonstrated by observing protection from cisplatin-induced functional and histological renal injury in IL-17 and RORγt-deficient mice and in mice treated with anti-IL-17 antibodies [36].

Homing of MSCs to the sites of renal injury and their integration and differentiation into tubular cells were rare or absent in animal models of acute kidney injury [37]. Accordingly, it is generally considered that MSCs exert their beneficial effects in paracrine manner, through the production of growth factors and cytokines that suppress oxidative stress, apoptosis, and inflammation in damaged kidneys [22, 23, 25, 38, 39]. In line with these findings, we showed here that MSC-CM also attenuates cisplatin-induced nephrotoxicity (Figure 3) in a similar manner as it was observed after injection of MSCs (Figure 1).

IDO and NO are important for MSC-mediated suppression of immune response in acute inflammation [25, 40]. IDO promotes the degradation of tryptophan into kynurenine and toxic metabolites (quinolinic acid and 3-hydroxyanthranillic acid) which suppress proliferation or induce apoptosis of T cells. NO inhibits phosphorylation of signal transducer and activator of transcription-5 (Stat5) in T cells, leading to cell-cycle arrest [22, 23, 25]. Under inflammatory conditions, mouse MSCs increase expression of iNOS [38]. Activation of MSCs by TNF-α resulted with the increased expression of both iNOS and IDO (Figure 6(a)) whose interplay is important for MSC-mediated immunosuppression [40]. Since, in the presence of inflammatory cytokines, NO increased IDO activity [39], we assume that cisplatin-induced inflammation increased production of TNF-α in DCs (Figure 2(c)) resulting with increased generation and activation of IFN-γ-producing CD4+ Th1 cells and CD8+ CTLs (Figures 2(d) and 2(e)) that provoked MSCs to express iNOS and produce NO. MSC-derived NO increased IDO activity and MSC-mediated immunosuppression and led to the attenuation of cisplatin-induced cytotoxicity and inflammation (Figure 6(c)). In line with these observations are increased serum levels of immunosuppressive NO, kynurenine (product of IDO activity), and IL-10 (Figures 3(d), 3(e), and 3(f)) accompanied with reduced infiltration of immune cells in the kidneys of cisplatin-treated mice that received MSC-CM (Figure 3(h)) and attenuated concentration of kynurenine in supernatants of TNF-α-stimulated MSCs that were cultured in the presence of iNOS inhibitor, L-NMMA (Figure 6(b)). Blockade of iNOS by L-NMMA resulted with increased infiltration and activation of inflammatory DCs, effector T helper cells, and CTLs, decreased influx of tolerogenic DCs and regulatory T cells, and almost completely diminished renoprotective effects of MSC-CM (Figure 5).

In conclusion, our study provides the evidence that MSCs, in paracrine, iNOS-dependent manner, attenuate inflammation in cisplatin-induced nephrotoxicity by reducing influx and the capacity of immune cells, particularly DCs and T lymphocytes, to produce inflammatory cytokines. These findings could be helpful in developing new, MSC-based therapeutic approaches for attenuation of cisplatin-induced nephrotoxicity.

Conflicts of Interest

The authors declare that there is no conflict of interests regarding the publication of this paper.

Acknowledgments

This study was supported by "Start Up for Science" grant funded by the Phillip Morris and Center for Leadership Development, Swiss National Science Foundation Project (SCOPES IZ73Z0_152454/1), Serbian Ministry of Science (ON175069 and ON175103), and Faculty of Medical Sciences, University of Kragujevac (MP01/14 and MP01/12).

References

[1] F. Ghane Shahrbaf and F. Assadi, "Drug-induced renal disorders," *Journal of Renal Injury Prevention*, vol. 4, no. 3, pp. 57–60, 2015.

[2] G. Y. Ho, N. Woodward, and J. I. Coward, "Cisplatin versus carboplatin: comparative review of therapeutic management in solid malignancies," *Critical Reviews in Oncology/Hematology*, vol. 102, pp. 37–46, 2016.

[3] S. Manohar and N. Leung, "Cisplatin nephrotoxicity: a review of the literature," *Journal of Nephrology*, pp. 1–11, 2017.

[4] P. Ma, S. Zhang, X. Su, G. Qiu, and Z. Wu, "Protective effects of icariin on cisplatin-induced acute renal injury in mice," *American Journal of Translational Research*, vol. 7, no. 10, pp. 2105–2114, 2015.

[5] N. Pabla and Z. Dong, "Cisplatin nephrotoxicity: mechanisms and renoprotective strategies," *Kidney International*, vol. 73, no. 9, pp. 994–1007, 2008.

[6] V. Pistoia and L. Raffaghello, "Mesenchymal stromal cells and autoimmunity," *International Immunology*, vol. 29, no. 2, pp. 49–58, 2017.

[7] L. T. Wang, C. H. Ting, M. L. Yen et al., "Human mesenchymal stem cells (MSCs) for treatment towards immune- and inflammation-mediated diseases: review of current clinical trials," *Journal of Biomedical Science*, vol. 23, no. 1, p. 76, 2016.

[8] K. N. Yarygin, A. Y. Lupatov, and G. T. Sukhikh, "Modulation of immune responses by mesenchymal stromal cells," *Bulletin of Experimental Biology and Medicine*, vol. 161, no. 4, pp. 561–565, 2016.

[9] R. H. Ashour, M. A. Saad, M. A. Sobh et al., "Comparative study of allogenic and xenogeneic mesenchymal stem cells on cisplatin-induced acute kidney injury in Sprague-Dawley rats," *Stem Cell Research & Therapy*, vol. 7, no. 1, p. 126, 2016.

[10] J. H. Kim, D. J. Park, J. C. Yun et al., "Human adipose tissue-derived mesenchymal stem cells protect kidneys from cisplatin nephrotoxicity in rats," *American Journal of Physiology*, vol. 302, no. 9, pp. F1141–F1450, 2012.

[11] W. Yao, Q. Hu, Y. Ma et al., "Human adipose-derived mesenchymal stem cells repair cisplatin-induced acute kidney injury through antiapoptotic pathways," *Experimental and Therapeutic Medicine*, vol. 10, no. 2, pp. 468–476, 2015.

[12] J. H. Park, H. R. Jang, D. H. Kim et al., "Early, but not late treatment with human umbilical cord blood-derived mesenchymal stem cells attenuates cisplatin nephrotoxicity through immunomodulation," *American Journal of Physiology - Renal Physiology*, 2017.

[13] I. Linero and O. Chaparro, "Paracrine effect of mesenchymal stem cells derived from human adipose tissue in bone regeneration," *PLoS One*, vol. 9, no. 9, article e107001, 2014.

[14] G. Ren, L. Zhang, X. Zhao et al., "Mesenchymal stem cell-mediated immunosuppression occurs via concerted action of chemokines and nitric oxide," *Cell Stem Cell*, vol. 2, no. 2, pp. 141–150, 2008.

[15] S. H. Yang, M. J. Park, I. H. Yoon et al., "Soluble mediators from mesenchymal stem cells suppress T cell proliferation by inducing IL-10," *Experimental & Molecular Medicine*, vol. 41, no. 5, pp. 315–324, 2009.

[16] S. Lee and D. Ahn, "Expression of endothelin-1 and its receptors in cisplatin-induced acute renal failure in mice," *The Korean Journal of Physiology and Pharmacology*, vol. 12, no. 4, pp. 149–153, 2008.

[17] M. Yang, R. Wang, J. Sun et al., "The liver X receptor agonist TO901317 protects mice against cisplatin-induced kidney injury," *Experimental Biology and Medicine*, vol. 240, no. 12, pp. 1717–1727, 2015.

[18] M. H. Solanki, P. K. Chatterjee, X. Xue et al., "Magnesium protects against cisplatin-induced acute kidney injury without compromising cisplatin-mediated killing of an ovarian tumor xenograft in mice," *American Journal of Physiology. Renal Physiology*, vol. 309, no. 1, pp. F35–F47, 2015.

[19] M. N. Martina, S. Bandapalle, H. Rabb, and A. R. Hamad, "Isolation of double negative $\alpha\beta$ T cells from the kidney," *Journal of Visualized Experiments*, vol. 87, 2014.

[20] W. Ling, J. Zhang, Z. Yuan et al., "Mesenchymal stem cells use IDO to regulate immunity in tumor microenvironment," *Cancer Research*, vol. 74, no. 5, pp. 1576–1587, 2014.

[21] T. Saksida, I. Nikolic, M. Vujicic et al., "Galectin-3 deficiency protects pancreatic islet cells from cytokine-triggered apoptosis in vitro," *Journal of Cellular Physiology*, vol. 7, no. 228, pp. 1568–1576, 2013.

[22] K. Sato, K. Azaki, I. Oh et al., "Nitric oxide plays a critical role in suppression of T-cell proliferation by mesenchymal stem cells," *Blood*, vol. 109, no. 1, pp. 228–234, 2007.

[23] R. Meisel, A. Zibert, M. Laryea, U. Göbel, W. Däubener, and D. Dilloo, "Human bone marrow stromal cells inhibit allogeneic T-cell responses by indoleamine 2,3-dioxygenase-mediated tryptophan degradation," *Blood*, vol. 103, no. 12, pp. 4619–4621, 2004.

[24] A. Nasef, A. Chapel, C. Mazurier et al., "Identification of IL-10 and TGF-beta transcripts involved in the inhibition of T-lymphocyte proliferation during cell contact with human mesenchymal stem cells," *Gene Expression*, vol. 13, no. 4-5, pp. 217–226, 2007.

[25] G. Ren, J. Su, L. Zhang et al., "Species variation in the mechanisms of mesenchymal stem cell-mediated immunosuppression," *Stem Cells*, vol. 27, no. 8, pp. 1954–1962, 2009.

[26] N. T. Luu, H. M. McGettrick, C. D. Buckley et al., "Crosstalk between mesenchymal stem cells and endothelial cells leads to downregulation of cytokine-induced leukocyte recruitment," *Stem Cells*, vol. 31, no. 12, pp. 2690–2702, 2013.

[27] R. K. Tadagavadi, G. Gao, W. W. Wang, M. R. Gonzalez, and W. B. Reeves, "Dendritic cell protection from cisplatin nephrotoxicity is independent of neutrophils," *Toxins (Basel)*, vol. 7, no. 8, pp. 3245–3256, 2015.

[28] R. K. Tadagavadi and W. B. Reeves, "Endogenous IL-10 attenuates cisplatin nephrotoxicity: role of dendritic cells," *The Journal of Immunology*, vol. 185, no. 8, pp. 4904–4011, 2010.

[29] R. K. Tadagavadi and W. B. Reeves, "Renal dendritic cells ameliorate nephrotoxic acute kidney injury," *Journal of the American Society of Nephrology*, vol. 21, no. 1, pp. 53–63, 2010.

[30] W. H. Liu, J. J. Liu, J. Wu et al., "Novel mechanism of inhibition of dendritic cells maturation by mesenchymal stem cells via interleukin-10 and the JAK1/STAT3 signaling pathway," *PloS One*, vol. 8, no. 1, article e55487, 2013.

[31] X. Jiang, Y. Zhang, B. Liu et al., "Human mesenchymal stem cells inhibit differentiation and function of monocyte-derived dendritic cells," *Blood*, vol. 105, no. 10, pp. 4120–4126, 2005.

[32] A. Nauta, A. Kruisselbrink, E. Lurvink, R. Willemze, and W. Fibbe, "Mesenchymal stem cells inhibit generation and function of both CD34+-derived and monocyte-derived dendritic cells," *Journal of Immunology*, vol. 177, no. 4, pp. 2080–2087, 2006.

[33] S. Chiesa, S. Morbelli, S. Morando et al., "Mesenchymal stem cells impair in vivo T-cell priming by dendritic cells," *Proceedings of the National Academy of Sciences*, vol. 108, no. 42, pp. 17384–17389, 2011.

[34] K. English, F. P. Barry, and B. P. Mahon, "Murine mesenchymal stem cells suppress dendritic cell migration, maturation and antigen presentation," *Immunology Letters*, vol. 115, no. 1, pp. 50–58, 2008.

[35] M. Gazdic, V. Volarevic, N. Arsenijevic, and M. Stojkovic, "Mesenchymal stem cells: a friend or foe in immune-mediated diseases," *Stem Cell Reviews and Reports*, vol. 11, no. 2, pp. 280–287, 2015.

[36] A. J. Chan, M. A. Alikhan, D. Odobasic et al., "Innate IL-17A-producing leukocytes promote acute kidney injury via inflammasome and toll-like receptor activation," *The American Journal of Pathology*, vol. 184, no. 5, pp. 1411–1418, 2014.

[37] F. Tögel, A. Cohen, P. Zhang, Y. Yang, Z. Hu, and C. Westenfelder, "Autologous and allogeneic marrow stromal cells are safe and effective for the treatment of acute kidney injury," *Stem Cells and Development*, vol. 18, no. 3, pp. 475–485, 2009.

[38] W. Li, G. Ren, Y. Huang et al., "Mesenchymal stem cells: a double-edged sword in regulating immune responses," *Cell Death & Differentiation*, vol. 19, no. 9, pp. 1505–1513, 2012.

[39] A. S. López, E. Alegre, A. Díaz, C. Mugueta, and A. González, "Bimodal effect of nitric oxide in the enzymatic activity of indoleamine 2,3-dioxygenase in human monocytic cells," *Immunology Letters*, vol. 106, no. 2, pp. 163–171, 2006.

[40] M. Gazdic, B. Simovic Markovic, L. Vucicevic et al., "Mesenchymal stem cells protect from acute liver injury by attenuating hepatotoxicity of liver NKT cells in iNOS and IDO dependent manner," *Journal of Tissue Engineering and Regenerative Medicine*, 2017.

Hindawi
Stem Cells International
Volume 2017, Article ID 6294717, 11 pages
https://doi.org/10.1155/2017/6294717

Research Article

Mesenchymal Stem Cells Promote Metastasis of Lung Cancer Cells by Downregulating Systemic Antitumor Immune Response

Marina Gazdic,[1] Bojana Simovic Markovic,[2] Nemanja Jovicic,[3] Maja Misirkic-Marjanovic,[4] Valentin Djonov,[5] Vladimir Jakovljevic,[6] Nebojsa Arsenijevic,[2] Miodrag L. Lukic,[2] and Vladislav Volarevic[2]

[1]*Department of Genetics, Faculty of Medical Sciences, University of Kragujevac, 34000 Kragujevac, Serbia*
[2]*Department of Microbiology and Immunology, Center for Molecular Medicine and Stem Cell Research, Faculty of Medical Sciences, University of Kragujevac, 69 Svetozar Markovic Street, 34000 Kragujevac, Serbia*
[3]*Department of Histology and Embryology, Faculty of Medical Sciences, University of Kragujevac, 34000 Kragujevac, Serbia*
[4]*Institute of Microbiology and Immunology, School of Medicine, University of Belgrade, 11000 Belgrade, Serbia*
[5]*Institute of Anatomy, University of Bern, 3000 Bern 9, Switzerland*
[6]*Department of Physiology, Faculty of Medical Sciences, University of Kragujevac, 34000 Kragujevac, Serbia*

Correspondence should be addressed to Vladislav Volarevic; drvolarevic@yahoo.com

Received 9 March 2017; Revised 4 June 2017; Accepted 5 June 2017; Published 16 July 2017

Academic Editor: Franca Fagioli

Since majority of systemically administered mesenchymal stem cells (MSCs) become entrapped within the lungs, we used metastatic model of lung cancer, induced by intravenous injection of Lewis lung cancer 1 (LLC1) cells, to investigate the molecular mechanisms involved in MSC-mediated modulation of metastasis. MSCs significantly augmented lung cancer metastasis, attenuate concentrations of proinflammatory cytokines (TNF-α, IL-17), and increase levels of immunosuppressive IL-10, nitric oxide, and kynurenine in sera of LLC1-treated mice. MSCs profoundly reduced infiltration of macrophages, TNF-α-producing dendritic cells (DCs), TNF-α-, and IL-17-producing CD4+ T cells but increased IL-10-producing CD4+ T lymphocytes in the lungs of tumor-bearing animals. The total number of lung-infiltrated, cytotoxic FasL, perforin-expressing, TNF-α-, and IL-17-producing CD8+ T lymphocytes, and NKG2D-expressing natural killer (NK) cells was significantly reduced in LLC1 + MSC-treated mice. Cytotoxicity of NK cells was suppressed by MSC-conditioned medium. This phenomenon was abrogated by the inhibitors of inducible nitric oxide synthase (iNOS) and indoleamine 2,3-dioxygenase (IDO), suggesting the importance of iNOS and IDO for MSC-mediated suppression of antitumor cytotoxicity of NK cells. This study provides the evidence that MSCs promote lung cancer metastasis by suppressing antitumor immune response raising concerns regarding safety of MSC-based therapy in patients who have genetic susceptibility for malignant diseases.

1. Introduction

Mesenchymal stem cells (MSCs) are self-renewable adult stem cells with fibroblast-like morphology that can be found in almost all postnatal tissues [1]. MSCs are currently used in broad number of clinical trials due to their multilineage differentiation potential and immunomodulatory characteristics. MSCs differentiate into the cells of mesodermal origin in vitro and in vivo, but recently published data suggest that under specific culture conditions, plasticity of MSCs should be extended to nonmesenchymal lineages of neuroectodermal (neurons, astrocytes, and oligodendrocytes) or endodermal (hepatocytes) origin [2].

MSCs may promote angiogenesis by transdifferentiation into endothelial cells and through the production of several proangiogenic factors (hepatocyte growth factor (HGF), vascular endothelial growth factor (VEGF), transforming growth factor beta (TGF-β), and interleukin- (IL-) 6) [3].

MSCs suppress immune response by attenuating migration and maturation of dendritic cells (DCs), promoting

alternative activation of macrophages, and reducing proliferation, activation, and effector function of B and T lymphocytes, natural killer (NK), and natural killer T (NKT) cells [1].

Although proangiogenic and immunosuppressive characteristics of MSCs are beneficial in the treatment of degenerative and autoimmune diseases, they can represent a serious problem if patient that received MSCs have primary or metastatic tumor. Accordingly, safeness of MSC-based therapy is still a matter of debate. The primary concern was the potential malignant transformation of the administered MSCs. A recent meta-analysis partly reassured the scientific community by showing that malignancies which were noticed in MSC-treated patients occurred only in patients with previous or current malignancies, with no formation of de novo tumors [4]. However, potential of MSCs to promote neovascularization and suppress antitumor immunity is still existing as major concerns regarding the safety of MSC-based therapy and should be further explored in preclinical and clinical studies.

MSCs have at least three functions that can promote tumor metastasis: homing to the site where tissues are damaged, including metastatic lesions, production of immunomodulatory factors, and secretion of proangiogenic cytokines and growth factors that promote neovascularization enabling metastasis of tumor cells [1, 4].

Lung-infiltrated cells as well as their products which contribute to tumor escape mechanisms and host immunosuppression are emerging as important mediators in promoting lung cancer growth and metastasis [5, 6].

Since vast majority of intravenously injected MSCs initially become entrapped within the lungs where MSCs interact with tumor-infiltrated immune cells [1], we used metastatic model of murine lung cancer to investigate molecular and cellular mechanisms involved in MSC-mediated modulation of antitumor immune response and progression of lung cancer metastasis.

Herewith, we showed that intravenous application of MSCs in tumor-bearing mice significantly suppressed systemic antitumor immune response, reduced total number of lung-infiltrated DCs, macrophages, CD4+ T lymphocytes, CTLs, and NK cells, and attenuated antitumor cytotoxicity of CTLs and NK cells resulting with the expansion of metastatic lesions in the lungs.

2. Materials and Methods

2.1. Cells. MSCs isolated from bone marrow of C57BL/6 mice were purchased from Gibco (Catalog number S1502-100). The cells were cultured in complete Dulbecco's Modified Eagle Medium (DMEM) containing 10% heat-inactivated fetal bovine serum (FBS), 100 IU/mL penicillin G, and 100 μg/mL streptomycin (Sigma-Aldrich, Munich, Germany), at 37°C in a 5% CO_2 incubator. MSCs in passage 3 were used throughout the experiments.

The cell line of murine lung carcinoma (Lewis lung cancer 1, LLC1) (3LL, H2b), derived from the lungs of C57BL mice implanted with Lew (Lewis) lung cancer, was purchased from the American Type Culture Collection (ATCC) (Catalog number CRL-1642™). Cells were routinely grown in suspension in complete DMEM medium, at 37°C in a 5% CO_2 incubator. LLC1 cells in passage 3 were used throughout the experiments.

2.2. Generation of MSC-Conditioned Medium (MSC-CM). MSCs were seeded at a density of 10,000 cells/cm^2. In order to collect the MSC-CM, MSCs were first cultured in serum-containing complete medium and incubated at 37°C in a humid atmosphere with 5% CO^2. At 80% confluence, the cells were washed twice with 1X phosphate-buffered saline (PBS, Invitrogen), and the medium was then changed to serum-free medium. After 48 h, the medium was collected, centrifuged at 13000 $\times g$ at 4°C for 10 min, and stored at −80°C until used [7].

2.3. Pharmacological Inhibition of Indoleamine 2,3-Dioxygenase (IDO) and Inducible Nitric Oxide Synthase (iNOS). MSCs were cultured for 48 h in culture medium containing 1 mM 1-methyltryptophan, (1-MT, Sigma-Aldrich, St. Louis, MO), an inhibitor of IDO enzymatic activity [8].

To block iNOS activity, MSCs were cultured for 48 h in the presence of 1 mM of an iNOS inhibitor, L-N^G-monomethyl arginine citrate (L-NMMA, Sigma-Aldrich, St. Louis, MO) [9].

2.4. Animals. 6–8-week-old C57Bl/6 male mice were used. All animals received human care, and all experiments were approved by and conducted in accordance with the Guidelines of the Animal Ethics Committee of the Faculty of Medical Sciences of the University of Kragujevac, Serbia. Mice were housed in a temperature-controlled environment with a 12-hour light-dark cycle and were administered with standard laboratory chow and water ad libitum.

2.5. Induction of Experimental Metastasis and Systemic Application of MSCs. Experimental metastases were induced by intravenous injection of 5×10^4 LLC1 cells [10]. Mice intravenously received either 5×10^5 MSCs or saline one week after injection of LLC1 cells. Mice were sacrificed on the 28th day of the experiment, as previously described [5].

2.6. Histopathological Analysis. All mice were sacrificed in an atmosphere saturated with diethyl ether (BETA HEM, Belgrade), and the lungs were isolated for histopathological analysis of metastatic colonies 28 days after tumor induction.

The isolated lungs were fixed in 10% formalin and embedded in paraffin, and consecutive 4 μm tissue sections mounted on slides. Sections were stained with hematoxylin and eosin (H&E) and examined under low-power (100x) light microscopy-equipped digital camera (Zeiss Axioskop 40, Jena, Germany). Metastases were verified by light microscopy (magnification 10x and 40x) as characteristic brown-black pigmented "hot spots" with giant multinucleated cells clearly limited by the surrounding lung tissue.

2.7. Immunohistochemistry. For immunohistochemical staining, paraffin-embedded sections (4 μm) of mouse lung tissue were used. Heat-mediated antigen retrieval in citrate buffer (pH = 6.0) was performed. Deparaffinized tissue-sections were incubated with primary mouse anti-CD3 (sc-20047,

Santa Cruz Biotechnology), anti-CD4 (ab183685, Abcam), anti-CD68 (ab49777, Abcam), anti-TNF-α antibody (ab6671, Abcam), and anti-IL-17 (ab79056, Abcam). Staining was visualized by using Mouse Specific HRP/DAB Detection IHC Kit (ab64259, Abcam) for CD3 and CD68, and rabbit specific HRP/AEC detection IHC Kit (ab94361, Abcam) for CD4, TNF-α, and IL-17. Sections were counterstained with Mayer's hematoxylin. Sections were photomicrographed with a digital camera mounted on light microscope (Olympus BX51, Japan), digitized, and analyzed.

2.8. Isolation of Lung-Infiltrated Immune Cells. The lungs, obtained from control, LLC1 and LLC1 + MSC-treated mice at the 28th day of the experiment, were washed with sterile phosphate-buffered saline (PBS) and placed in Petri dishes with DMEM supplemented with 10% FBS. The dissected lung tissue was incubated in medium that contained Collagenase Type IV (0.5 mg/mL) and type IV bovine pancreatic DNAse (Roche Diagnostic; 1 mg/mL) at 37°C for 45 min. The cells were filtered through a 100 μm nylon cell strainer into a clean 50 mL conical tube. Then, cells were pelleted by centrifuging 10 min at 300 $\times g$, at 10°C. Red blood cells were depleted with a lysis buffer (0.144 M NH4Cl, 0.0169 M TRIS base, pH 7.4) at 37°C in a 5% CO_2 atmosphere for 5 min [11].

2.9. Flow Cytometry Analysis and Intracellular Staining of Lung-Infiltrated Immune Cells. Lung-infiltrated immune cells were screened for various cell surface and intracellular markers with flow cytometry. Briefly, 1×10^6 cells were incubated with anti-mouse CD45, F4/80, CD4, CD8, CD11c, CD11b, CD49b, FasL, CD107, perforin, NKG2D monoclonal antibodies conjugated with fluorescein isothiocyanate (FITC), phycoerythrin (PE), peridinin chlorophyll protein (PerCP), or allophycocyanin (APC) (all from BD Biosciences, San Jose, CA, USA) following the manufacturer's instructions. Immune cells derived from the lungs were concomitantly stained for the intracellular content of TNF-α, IL-10, and IL-17 by using the fixation/permeabilization kit and anti-mouse monoclonal antibodies conjugated with fluorescein isothiocyanate (FITC), phycoerythrin (PE), peridinin chlorophyll protein (PerCP), and allophycocyanin (APC) (BD Biosciences). For intracellular cytokine staining, cells were stimulated with 50 ng/mL PMA and 500 ng/mL ionomycin for 5 h, and GolgiStop (BD Biosciences) was added. Cells were fixed in Cytofix/Cytoperm, permeated with 0.1% saponin, and stained with fluorescent Abs. Flow cytometric analysis was conducted on a BD Biosciences' FACSCalibur and analyzed by using the flowing software analysis program.

2.10. Measurement of Cytokines and Growth Factors in Sera of Tumor-Bearing Mice. Levels of TNF-α, IL-17, IL-10, and HGF in the mouse serum at the 14th, 21st, and 28th days of the experiment were measured using ELISA kits specific for the mouse cytokines (R&D Systems, Minneapolis, MN, USA) according to the manufacturer's instructions.

Serum concentrations of nitric oxide (NO) were measured by Griess reagent while IDO activity was determined by spectrophotometric measuring of kynurenine since IDO catalyzes the metabolism of tryptophan in the kynurenine [12]. Concentrations of NO and kynurenine were determined in mouse sera at the 14th, 21st, and 28th days of the experiment.

2.11. Isolation of NK Cells by Magnetic Cell Sorting. At the 28th day of the experiment, NK cells were isolated from the spleens of LLC1 and LLC1 + MSC-treated mice by magnetic cell sorting according to the manufacturer's instructions. Single-cell suspensions of mononuclear cells derived from the spleens were labeled with monoclonal anti-mouse antibodies against CD49b, and microbeads conjugated to monoclonal anti-biotin antibody (Miltenyi Biotec). The labeled cells were subsequently depleted by separation over a MACS Column (Miltenyi Biotec), which was placed in the magnetic field of a MACS Separator (Miltenyi Biotec). Isolated NK cells were then used in the coculture experiments and cytotoxicity assay as purified NK cells.

2.12. Cytotoxicity Assay. The DP version of the xCELLigence system (Roche) was used in this study for the determination of NK cell cytotoxicity. The DP version comprises a measurement unit housed within a standard tissue culture incubator with 3 stations that each takes E16 plates (each E16 plate has 16 wells). 100 μL of complete medium was added to each well, and background impedance on the plates was measured on the xCELLigence RTCA DP instrument at 37°C and 5% CO_2. LLC1 cells were used as targets for NK cells. Seeding density of 4×10^4 LLC1 cells/well was considered optimal and used for all assays. Effector to target ratio (E : T ratio) 10 : 1 was used [13]. LLC1 cells were resuspended in DMEM with 10% FCS at 4×10^5 cells per milliliter. A total of 100 μL tumor cells were added to each well of the E16 plate, which was then placed in the xCELLigence RTCA DP. NK cells, isolated from LLC1 and LLC1 + MSC-treated mice at the 28th day of the experiment, were counted and resuspended at a concentration of 4×10^6 cells per milliliter in DMEM + 10% FCS media. Then, 100 μL NK cells or media alone were added to the respective wells. The E-plate 16 was placed in the xCELLigence RTCA DP, and impedance measurements were recorded every 15 min for 24 hours at 37°C and 5% CO_2. NK cell-mediated death of tumor cells was monitored in real time and was indicated by a decrease in cell index. Data were analyzed with RTCA Software 1.2 (ACEA Biosciences).

2.13. Statistical Analysis. The results were analyzed using the Student t-test. All data in this study were expressed as the mean ± standard error of the mean (SEM). Values of $p < 0.05$ were considered as statistically significant.

3. Results

3.1. Intravenous Injection of MSCs Significantly Augmented Lung Cancer Metastasis. First, we investigated whether systemic application of MSCs could modulate spontaneous LLC1 tumor cell metastasis to the lungs. We observed that LLC1 + MSC-treated tumor-bearing mice exhibited increased numbers of lung metastasis (Figure 1(a)) compared to animals that received only LLC1 cells. Significantly higher number of tumor cells with pleomorphic nuclei, arranged in aggregated forms, was noticed in

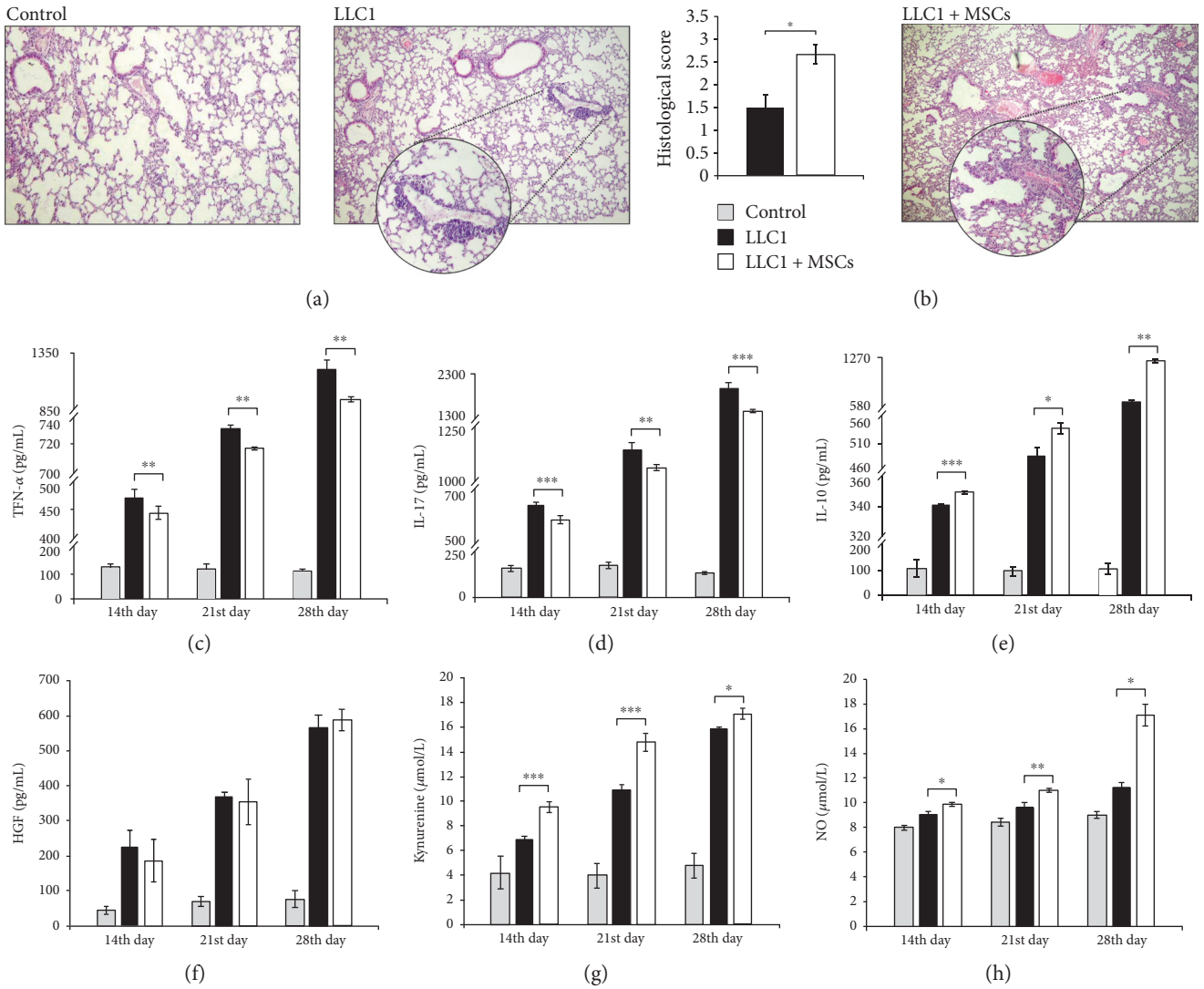

Figure 1: MSCs promote lung cancer metastasis. (a) Representative H&E stained mouse lungs obtained at the 28th day of the experiment. H&E staining images of liver tissue samples are shown at the same magnifications (×100). (b) Histological score of lung tissue determined at the 28th day of the experiment. (c) Serum concentrations of TNF-α, (d) IL-17, (e) IL-10, and (f) HGF measured at the 14th, 21st, and 28th days of the experiment. (g) The level of kynurenine and (h) NO in mouse sera at the 14th, 21st, and 28th days of the experiment. Data presented as mean ± SEM; $n = 10$ mice per experimental groups. $^{*}p < 0.05$, $^{**}p < 0.01$, and $^{***}p < 0.001$.

the lungs of MSC-treated tumor-bearing animals at the 28th day of the experiment. Although perivascular infiltration of tumor cells was also noticed in the lungs isolated from LLC1-treated mice, expansion of malignant tissue in these mice was notably lower in comparison to LLC1 + MSCs-treated animals in which lung tissues were almost completely displaced with tumor cells (Figure 1(a)). Histological score of lung tissue confirmed extensive malignancy in LLC1-treated mice that intravenously received MSCs (Figure 1(b)).

3.2. MSCs Altered Serum Levels of Cytokine and Growth Factors That Played Important Role in Antitumor Immune Response. In order to explore whether MSC-dependent expansion of metastatic lesions in the lungs is a consequence of their effects on systemic immune response, cytokine concentration was determined in sera of tumor-bearing animals at the 14th, 21st, and 28th days of the experiment. In accordance with the histological analysis, MSCs significantly alter serum levels of cytokines and growth factors that play important role in antitumor immune response at all measured time points. The concentrations of antitumor cytokines TNF-α (Figure 1(c)) and IL-17 (Figure 1(d)) were significantly lower while the concentrations of immunosuppressive IL-10 (Figure 1(e)), kynurenine (Figure 1(g)), and NO (Figure 1(h)) were significantly higher in sera of LLC1-treated mice that received MSCs. There was not any significant difference in serum levels of immunomodulatory HGF between experimental groups (Figure 1(f)).

3.3. MSCs Significantly Reduced Total Number of DCs, Macrophages, and CD4+ Helper T Cells in the Lungs of LLC1-Treated Mice and Altered Their Cytokine Profile. Next, we analyzed cellular make-up of the lungs 28 days after tumor injection in order to determine cellular targets

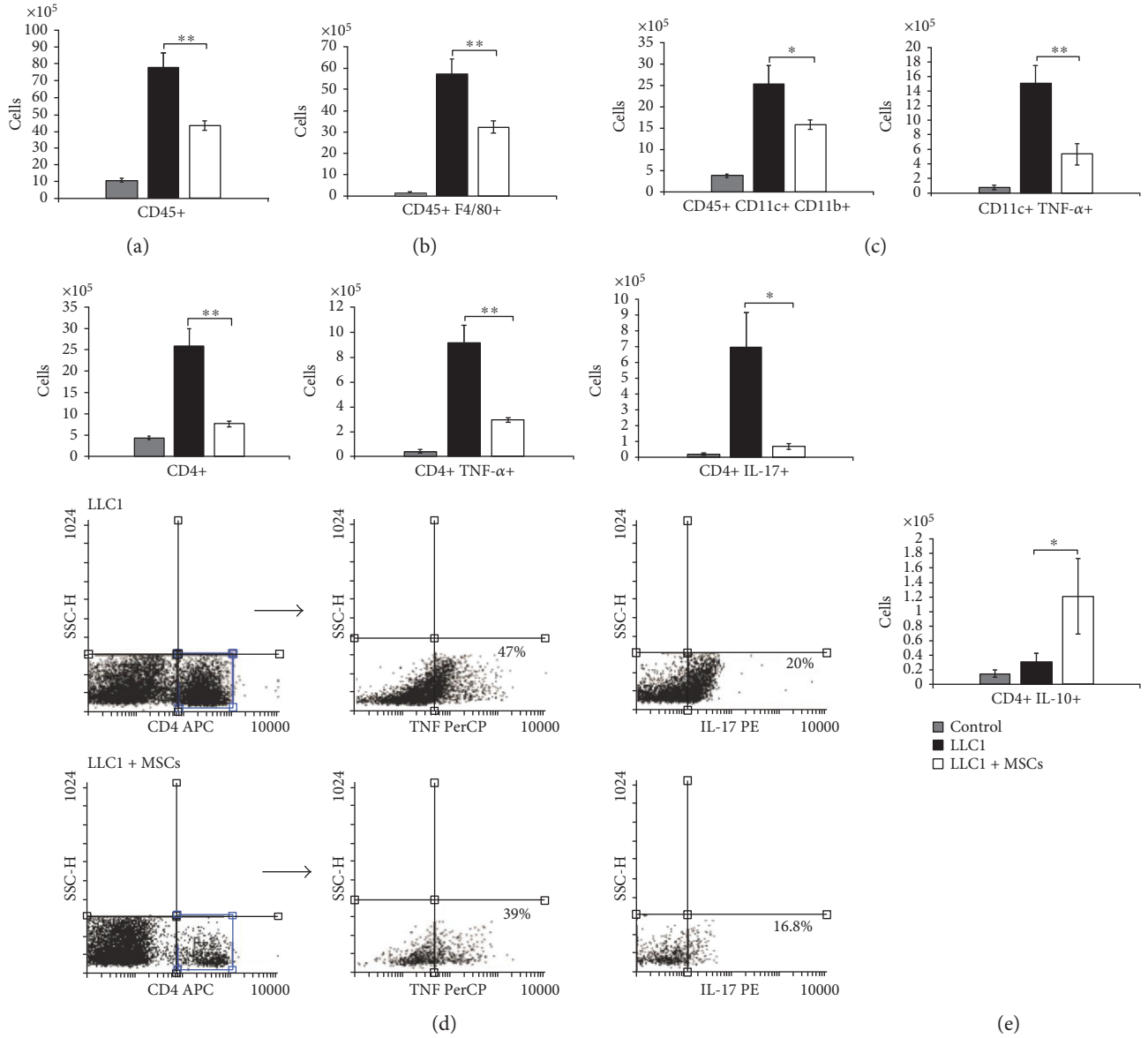

Figure 2: MSC treatment reduces influx of DCs, macrophages, and CD4+ T cells, in the metastatic model of lung cancer, and altered their cytokine profile. Total numbers of (a) CD45+, (b) CD45+ F4/80+, (c) CD45+ CD11c+ CD11b+, and CD11c+ TNF-α+ cells in the lungs of control, LLC1, and LLC1 + MSC-treated mice at the 28th day of the experiment. (d) Total number and representative flow cytometry dot plots of CD4+, TNF-α-, and IL-17-producing CD4+ cells at the 28th day of the experiment. (e) Total numbers of lung-infiltrating CD4+ IL-10+ cells at the 28th day of the experiment. Values are mean ± SEM ($n = 10$ per group). $^*p < 0.05$, $^{**}p < 0.01$.

of MSC-mediated suppression of antitumor immune response in LLC1-treated animals. MSCs profoundly reduced infiltration of CD45+ leukocytes into the lung parenchyma ($p < 0.01$; Figure 2(a)). Flow cytometry analysis showed that a total number of CD45+ F4/80+ macrophages (Figure 2(b), $p < 0.01$), CD45+ CD11c+ CD11b+ inflammatory DCs (Figure 2(c), left panel, $p < 0.05$), and CD4+ helper T cells (Figure 2(d), $p < 0.01$) were significantly lower in the lungs of tumor-bearing mice that received MSCs.

Intracellular staining revealed that systemic application of MSCs reduces infiltration of TNF-α-producing DCs (Figure 2(c), right panel, $p < 0.05$), TNF-α-producing (Figure 2(d), middle panel, $p < 0.01$), and IL-17-producing CD4+ helper T cells (Figure 2(d), right panel, $p < 0.05$) and increases the presence of CD4+ T cells that produce immunosuppressive IL-10 (Figure 2(e), $p < 0.05$).

Immunohistochemical analysis confirmed these findings. Intravenous injection of MSCs reduced the presence of CD3+ T lymphocytes (Figure 3(a)), CD4+ T helper cells (Figure 3(b)), CD68+ macrophages (Figure 3(c)), TNF-α-producing (Figure 3(d)), and IL-17-producing cells (Figure 3(e)) in the lungs of LLC1-treated mice 28 days after tumor induction.

3.4. MSCs Reduced Infiltration of CTLs in the Lungs of LLC1-Treated Mice and Attenuated Expression of FasL, Perforin, and CD107 on Their Surface. Intravenous injection of MSCs significantly reduce total number of cytotoxic CD8+ CTLs

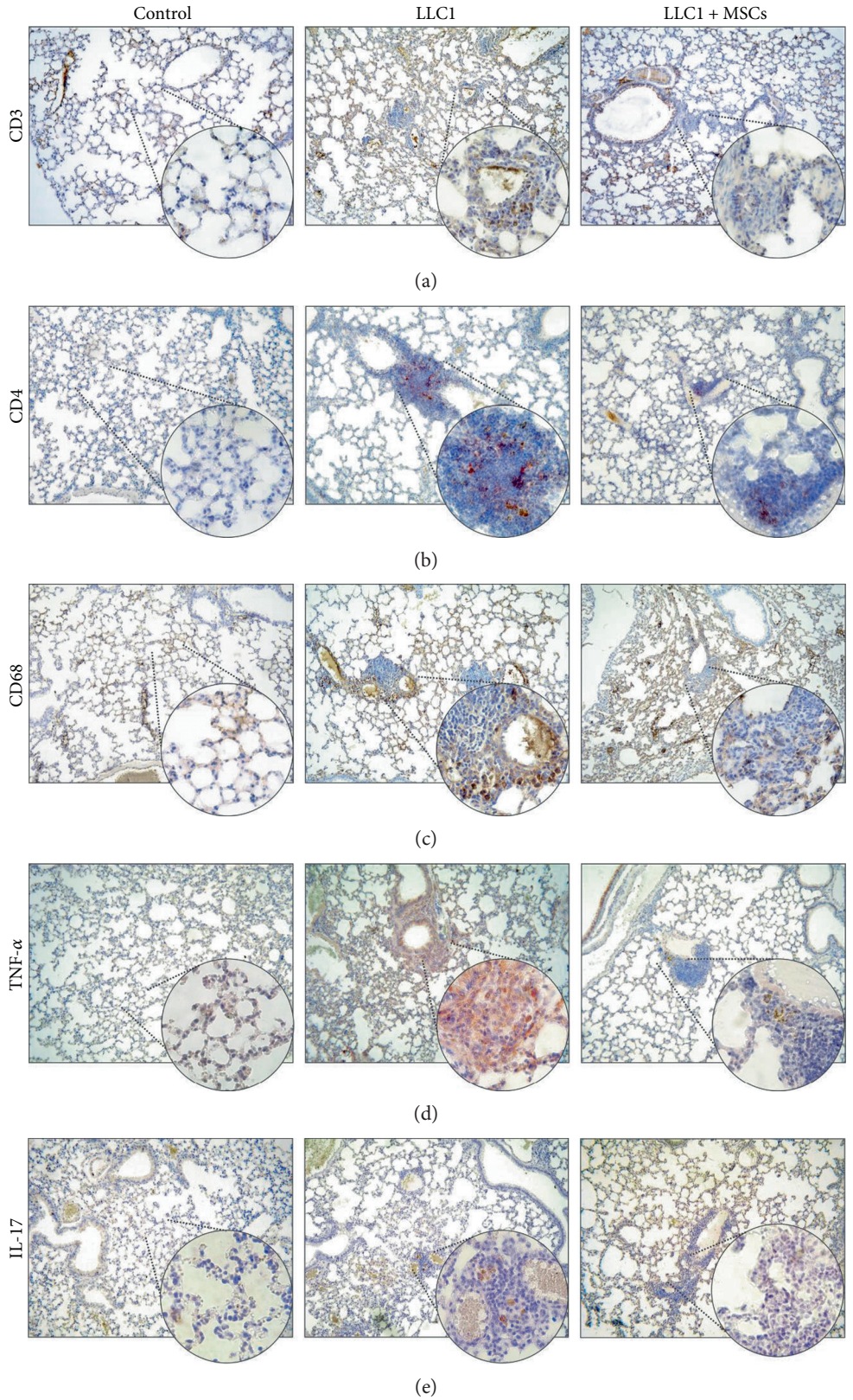

Figure 3: Systemic injection of MSCs reduces the presence of immune cells and inflammatory cytokines in the lungs of LLC1-treated mice. Representative images of CD3, CD4, CD68, TNF-α, and IL-17 immunohistochemical staining on paraffin-embedded lung tissue sections obtained at the 28th day of the experiment (×20, ×40). (a) CD3+ cells, (b) CD4+ cells, and (c) CD68+ macrophages were present in higher numbers in lungs of LLC1-treated mice compared to LLC1 + MSCs and control groups. Expression of (d) TNF-α and (e) IL-17 in lung tissue was higher in lungs of LLC1-treated mice compared to LLC1 + MSC and control groups.

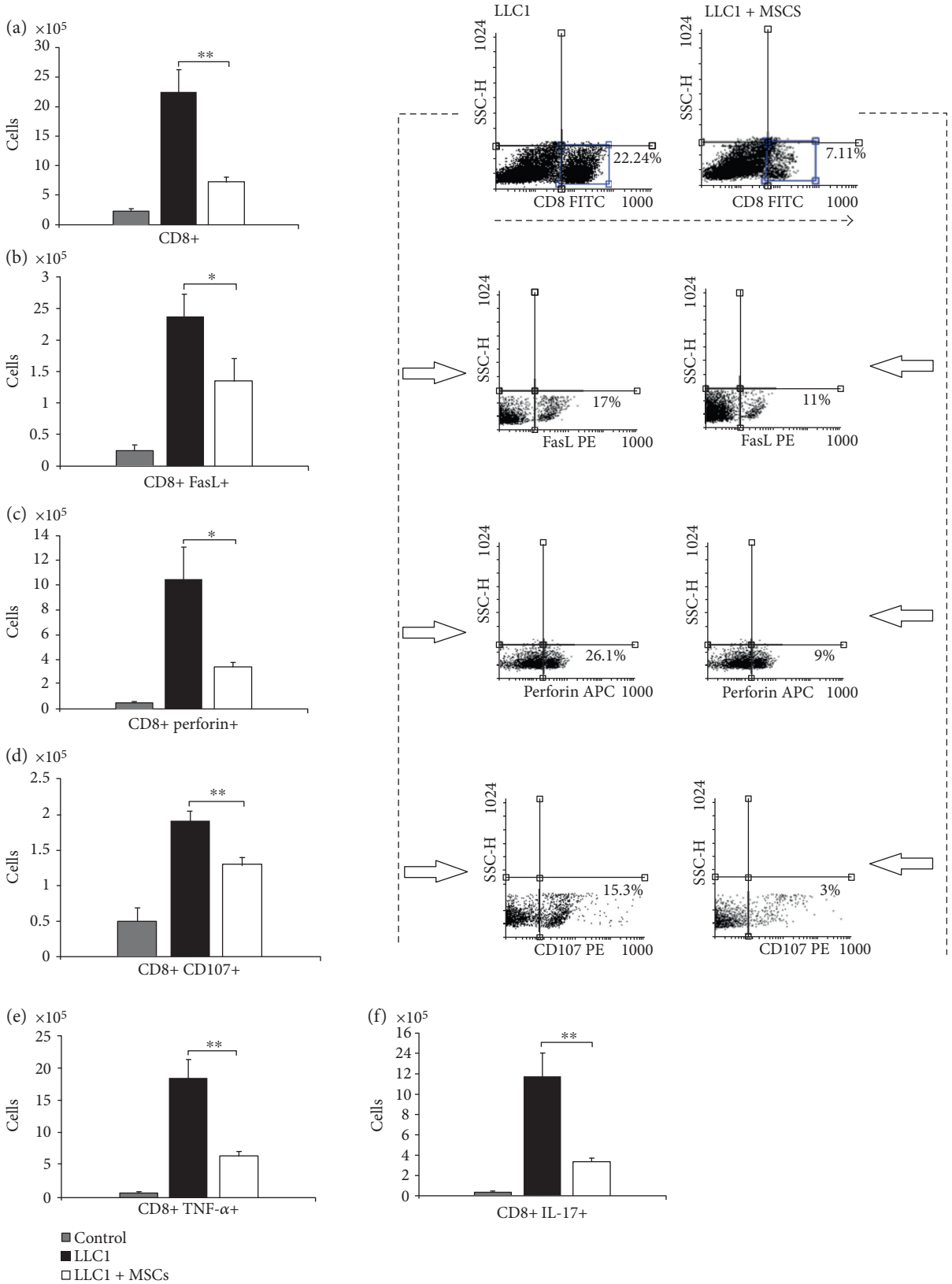

Figure 4: MSCs reduce infiltration of CTLs in the lungs of LLC1-treated mice and attenuate expression of FasL, perforin, and CD107 on their surface. Total number of (a) CD8+, (b) CD8+ FasL+, (c) CD8+ perforin+, (d) CD8+ CD107+, (e) CD8+ TNF-α+, and (f) CD8+ IL-17+ cells in the lungs of control, LLC1, and LLC1 + MSC-treated mice at the 28th day of the experiment, accompanied with representative dot plots. Data presented as mean ± SEM; $n = 10$ mice per experimental groups. $^{*}p < 0.05$, $^{**}p < 0.01$.

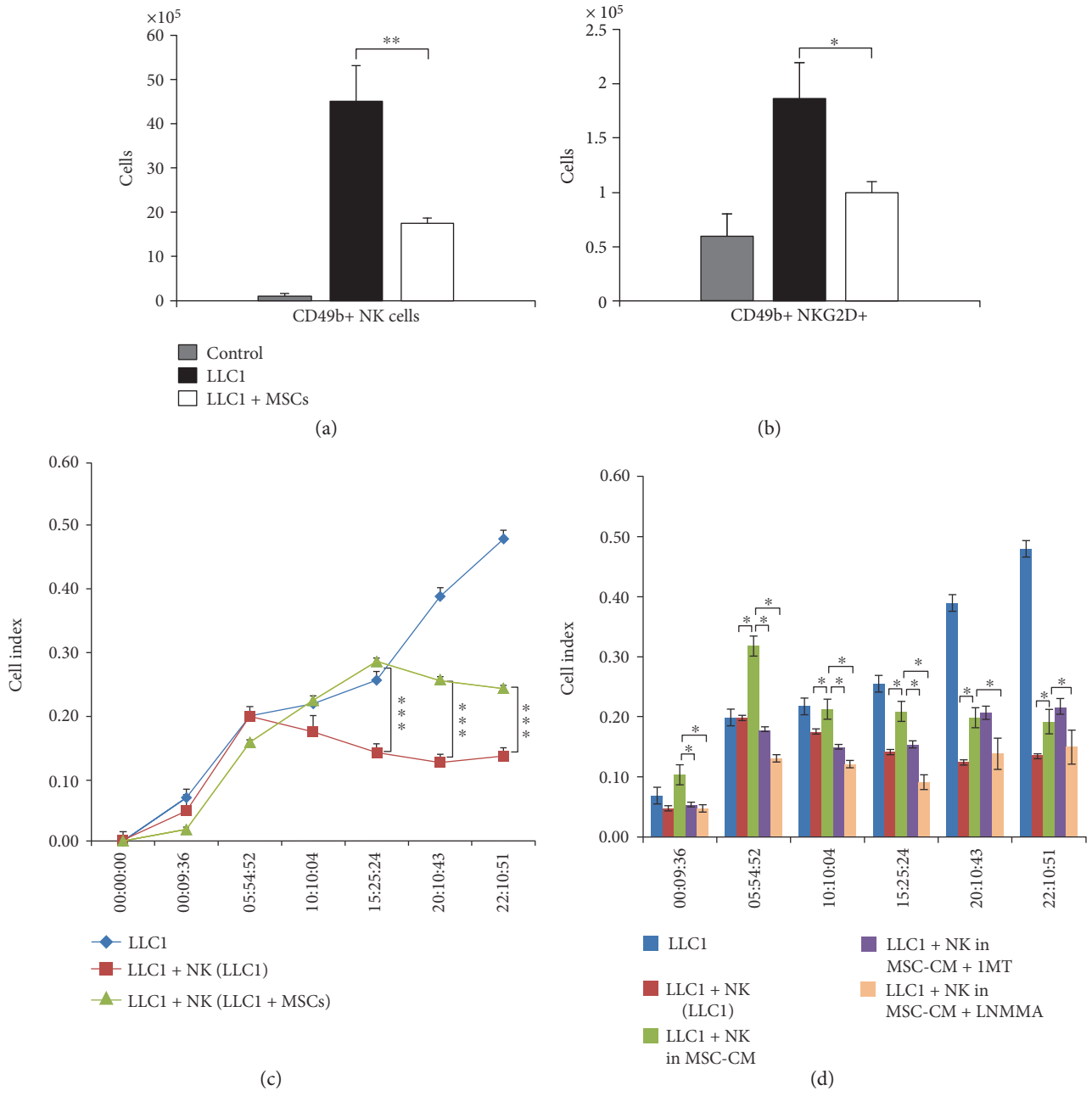

Figure 5: MSCs attenuate antitumor cytotoxicity of NK cells in iNOS and IDO-dependent manner. The total number of (a) CD49b+ and (b) CD49b+ NKG2D+ cells in the lungs of control, LLC1, and LLC1 + MSC-treated mice at the 28th day of the experiment. (c-d). The results obtained by xCELLigence system showed cytotoxic activity of NK cells against LLC1 target cells. Data presented as mean ± SEM; $n = 10$ mice per experimental groups. $^{*}p < 0.05$, $^{**}p < 0.01$, and $^{***}p < 0.001$.

(Figure 4(a), $p < 0.01$) in the lungs of LLC1-treated mice at the 28th day of the experiment. Moreover, analysis of cytotoxic molecules involved in CTL-mediated antitumor immune response (FasL, perforin, and CD107) showed that MSCs managed to attenuate influx of FasL+ CTLs (Figure 4(b), $p < 0.05$), perforin + CTLs (Figure 4(c), $p < 0.05$), and CD107+ CTLs (Figure 4(d), $p < 0.01$) in the lungs of tumor-bearing animals.

Intracellular staining revealed that systemic application of MSCs attenuate the capacity of CTLs to produce antitumor cytokines (Figures 4(e)-4(f)). There were significantly lower number of TNF-α-producing (Figure 4(e), $p < 0.01$) and IL-17-producing CTLs (Figure 4(f), $p < 0.01$) in MSC + LLC1-treated mice when compared to LLC1-only treated animals.

3.5. Antitumor Cytotoxicity of NK Cells Was Significantly Attenuated in MSC + LLC1-Treated Mice in Paracrine, NO, and IDO-Dependent Manner. As determined by flow cytometry, 28 days after tumor induction, the presence of CD49b + NK cells was significantly reduced in LLC1 + MSC-treated

mice when compared to the LLC1-only treated animals (Figure 5(a), $p < 0.01$).

Moreover, the total number of NK cells that express activation receptor NKG2D, involved in antitumor immune response, was notably lower in the lungs of tumor-bearing mice that received MSCs (Figure 5(b), $p < 0.05$). Accordingly, the results obtained by xCELLigence system for monitoring real-time cytotoxicity showed that NK cells isolated from LLC1 + MSC-treated mice were significantly less cytotoxic against LLC1 cells then NK cells isolated from animals that received only LLC1 cells (Figure 5(c)), indicating that intravenous injection of MSCs significantly reduced antitumor cytotoxicity of NK cells.

To directly demonstrate that soluble factors and not cell to cell contact were responsible for the MSC-mediated inhibition of NK cell cytotoxicity against LLC1 cells, effects of MSC-CM were evaluated. As it is shown in Figure 5(d), MSC-CM significantly suppressed cytotoxicity of NK cells against LLC1 cells. This phenomenon was completely abrogated in the presence of iNOS inhibitor (L-NMMA) or IDO inhibitor (1-MT), suggesting iNOS and IDO as important factors for MSC-mediated suppression of antitumor cytotoxicity of NK cells (Figure 5(d)).

4. Discussion

It is well known that MSCs are inherently tumor-homing cells that, few hours after systemic injection, migrate in the lungs [14, 15]. Many receptors, extracellular matrix proteins, and soluble tumor-derived factors have been reported to effect tumor tropism of intravenously injected MSCs [15, 16]. Most recently, it was shown that macrophage migration inhibitory factor (MIF)/CXCR4 and monocyte chemoattractant protein-1 (MCP-1)/CCR2 pathways are responsible for migration of MSCs in the tumor microenvironment of the lungs [15, 16]. MIF secreted from tumor cells attracts MSCs to the lungs in CXCR4-dependent manner. Knockdown of either CXCR4 or MIF abrogates MSC homing to tumors in an in vivo pulmonary metastasis model [15]. Similarly, homing ability of MSCs was suppressed after either knocking down the expression of MCP-1 in lung cancer cells or blocking CCR2 expressed on the surface of MSCs, indicating the important role of MCP-1/CCR2 axis in the tropism of MSCs to lung tumors [16]. Immediately after their engraftment, MSCs interact with tumor-infiltrated immune cells, affecting antitumor immune response [17]. Accordingly, findings related to the MSC-based modulation of antitumor immunity could have important implications for clinical applications of MSCs.

Here, we provide the evidence that systemic application of MSCs in tumorbearing animals promotes expansion of lung metastasis by suppressing antitumor immune response through the inhibition of innate (DCs, NK cells) and adaptive (CD4+ T helper, CD8 + CTLs) immunity.

Significantly lower number of macrophages (Figures 2(b) and 3(c)), DCs (Figure 2(c)), effector CD4+ helper T cells (Figures 2(d) and 3(b)), and CD8+ CTLs (Figures 4(a), 4(b), 4(c), 4(d), 4(e), and 4(f)) as well as reduced number and cytotoxicity of NK cells (Figure 5) indicates that systemic application of MSCs affected both inductive and effector phase of antitumor immune response.

Intravenous injection of MSCs suppresses, almost instantaneously, the migration of DCs to the draining lymph nodes significantly affecting the ability of DCs for antigen presentation to CD4+ T cells and cross-presentation to CD8+ T cells [18, 19]. Accordingly, significantly reduced number of CD11c+ CD11b+ DCs (Figure 2(c)) was accompanied with reduced number of CD4+ (Figures 2(d) and 3(b)) and CD8+ T cells (Figure 3(a)) in the lungs of LLC1-treated mice that received MSCs.

Maturation of DC is also impaired by MSCs [20, 21]. DC exposed to TNF-alpha and MSCs failed to upregulate maturation markers [19]. On turn, immature DCs are strongly hampered in their ability to produce TNF-α and other proinflammatory cytokines that inhibit tumor growth and metastasis [22]. In line with these observations, downregulated serum levels of TNF-α (Figure 1(c)) were accompanied with lower number of TNF-α-producing DCs in the lungs of LLC1 + MSCs-treated mice when compared to LLC1-only treated animals (Figure 2(c)).

In addition to suppression of naïve T cell activation, MSCs are able to induce suppression of effector CD4+ T helper cells that is mainly mediated through the production of soluble factors including IDO, NO, IL-10, prostaglandin E2 (PGE2), HGF, and TGF-β [23]. Accordingly, intravenous injection of MSCs resulted with higher serum levels of IL-10 (Figure 1(e)), kynurenine (Figure 1(g)), and NO (Figure 1(h)) that was followed by reduce number of lung-infiltrated effector CD4+ T cells (Figures 2(d) and 3(b)) that produce antitumor cytokines TNF-α and IL-17 (Figure 2(d)).

Progressive inflammatory diseases, including tumors, are associated with the loss of IL-17-producing CD4+ Th17 cells and a reciprocal increase in the fraction of the immunosuppressive IL-10-producing CD4+ T lymphocytes both in peripheral blood and in inflamed tissues [24]. MSC-derived IDO is an enzyme that has powerful immunomodulatory effects, resulting from its enzymatic activity, which leads to catabolism of the essential aminoacid L-tryptophan to L-kynurenine [25]. Metabolites of the L-kynurenine pathway have been shown to act as critical molecular switch that stimulates immunosuppressive properties of IL-10producing T cells and simultaneously blocks their reprogramming into IL-17-producing effector T cells [26]. Accordingly, herewith, we showed that injection of MSCs increased serum levels of kynurenine in LLC1-treated mice (Figure 1(g)), accompanied with increased number of IL-10-producing CD4+ T lymphocytes and decreased number of IL-17-producing Th17 cells (Figure 2(d)).

As described above, MSCs attenuate the capacity of DC for cross-presentation and activation of CD8+ T cells [18]. Additionally, MSCs suppress the proliferation of CTLs and inhibit surface expression of molecules which are involved in CTL-mediated cytotoxicity against tumor cells [27]. In line with these findings, significantly lower number of lung-infiltrated CD8 + CTLs expressing FasL (Figure 4(b)) and perforin (Figure 4(c)) was noticed in MSC + LLC1-treated mice when compared to LLC1-only treated animals indicating that systemic administration of MSCs suppressed

both perforin- and FasL-mediated mechanisms of antitumor cytotoxicity of CTLs.

MSCs suppress proliferation and cytotoxicity of NK cells, as well [28–30]. This inhibitory effect of MSCs is associated with the downregulated expression of the activating NK cell receptors, such as NKG2D, and is primarily mediated by IDO, PGE2, and TGF-β1 [29, 30]. Herewith, we showed that MSCs reduce total number of lung-infiltrated NKG2D-expressing NK cells in LLC1-treated mice (Figure 5(b)) and significantly attenuate their cytotoxicity against lung cancer cells in vitro (Figure 5(c)). Both iNOS and IDO inhibitors managed to almost completely restore cytotoxic activity of NK cells against LLC1 cells in vitro (Figure 5(d)), suggesting the importance of both iNOS and IDO signaling for MSC-mediated inhibition of NK cell antitumor toxicity. It is well known that inflammatory cytokines, such as TNF-α, provoke MSCs to use iNOS-dependent mechanism for NO production [9, 31]. MSC-derived NO can directly suppress proliferation of lymphocytes or may increase IDO activity which could result with the attenuation of NK cell cytotoxicity [9, 31].

5. Conclusions

Our study provides the evidence that systemic application of MSCs may promote metastasis of lung cancer cells by suppressing antitumor immune response. These findings raised serious concerns regarding the safety of intravenous application of MSCs in patients who have genetic susceptibility for malignant diseases.

Conflicts of Interest

The authors declare that there is no conflict of interests regarding the publication of this paper.

Acknowledgments

This study was supported by the "Start Up for Science" grant funded by Phillip Morris and Center for Leadership Development, Swiss National Science Foundation Project (SCOPES IZ73Z0_152454/1), the Serbian Ministry of Science (ON175069 and ON175103), and the Faculty of Medical Sciences, University of Kragujevac (MP01/14 and MP01/12).

References

[1] M. Gazdic, V. Volarevic, N. Arsenijevic, and M. Stojkovic, "Mesenchymal stem cells: a friend or foe in immune-mediated diseases," *Stem Cell Reviews and Reports*, vol. 11, no. 2, pp. 280–287, 2015.

[2] A. Gebler, O. Zabel, and B. Seliger, "The immunomodulatory capacity of mesenchymal stem cells," *Trends in Molecular Medicine*, vol. 18, no. 2, pp. 128–134, 2012.

[3] H. Tao, Z. Han, Z. C. Han, and Z. Li, "Proangiogenic features of mesenchymal stem cells and their therapeutic applications," *Stem Cells International*, vol. 2016, Article ID 1314709, 2016.

[4] M. M. Lalu, L. McIntyre, C. Pugliese et al., "Safety of cell therapy with mesenchymal stromal cells (SafeCell): a systematic review and meta-analysis of clinical trials," *PLoS One*, vol. 7, no. 10, article e47559, 2012.

[5] P. C. Hackler, S. Reuss, R. L. Konger, J. B. Travers, and R. P. Sahu, "Systemic platelet-activating factor receptor activation augments experimental lung tumor growth and metastasis," *Cancer Growth Metastasis*, vol. 7, pp. 27–32, 2014.

[6] Y. Mao, D. Yang, J. He, and M. J. Krasna, "Epidemiology of lung cancer," *Surgical Oncology Clinics of North America*, vol. 25, no. 3, pp. 439–445, 2016.

[7] I. Linero and O. Chaparro, "Paracrine effect of mesenchymal stem cells derived from human adipose tissue in bone regeneration," *PLoS One*, vol. 9, no. 9, article e107001, 2014.

[8] S. H. Yang, M. J. Park, I. H. Yoon et al., "Soluble mediators from mesenchymal stem cells suppress T cell proliferation by inducing IL-10," *Experimental & Molecular Medicine*, vol. 41, no. 5, pp. 315–324, 2009.

[9] G. Ren, L. Zhang, X. Zhao et al., "Mesenchymal stem cell-mediated immunosuppression occurs via concerted action of chemokines and nitric oxide," *Cell Stem Cell*, vol. 2, no. 2, pp. 141–150, 2008.

[10] M. S. Tsai, C. C. Chang, M. L. Kuo, and Y. T. Wu, "Vascular endothelial growth factor-A and changes in a tumor-bearing mouse model with Lewis lung cancer," *Oncolology Letters*, vol. 2, no. 6, pp. 1143–1147, 2011.

[11] E. P. Amaral, S. C. Ribeiro, V. R. Lanes et al., "Pulmonary infection with hypervirulent mycobacteria reveals a crucial role for the P2X7 receptor in aggressive forms of tuberculosis," *PLoS Pathogens*, vol. 10, no. 7, article e1004188, 2014.

[12] W. Ling, J. Zhang, Z. Yuan et al., "Mesenchymal stem cells use IDO to regulate immunity in tumor microenvironment," *Cancer Research*, vol. 74, no. 5, pp. 1576–1587, 2014.

[13] S. Wang, X. Zhang, Y. Ju et al., "MicroRNA-146a feedback suppresses T cell immune function by targeting Stat1 in patients with chronic hepatitis B," *The Journal of Immunology*, vol. 191, no. 1, pp. 293–301, 2013.

[14] B. Rüster, S. Göttig, R. Ludwig et al., "Mesenchymal stem cells display coordinated rolling and adhesion behavior on endothelial cells," *Blood*, vol. 108, no. 12, pp. 3938–3944, 2006.

[15] S. Lourenco, V. Teixeira, T. Kalber, R. J. Jose, R. A. Floto, and S. M. Janes, "Macrophage migration inhibitory factor-CXCR4 is the dominant chemotactic axis in human mesenchymal stem cell recruitment to tumors," *The Journal of Immunology*, vol. 194, no. 7, pp. 3463–3474, 2015.

[16] C. Yan, X. Song, W. Yu et al., "Human umbilical cord mesenchymal stem cells delivering sTRAIL home to lung cancer mediated by MCP-1/CCR2 axis and exhibit antitumor effects," *Tumour Biology*, vol. 37, no. 6, pp. 8425–8435, 2016.

[17] A. Poggi, A. Musso, I. Dapino, and M. Zocchi, "Mechanisms of tumor escape from immune system: role of mesenchymal stromal cells," *Immunology Letters*, vol. 159, no. 1–2, pp. 55–72, 2014.

[18] S. Chiesa, S. Morbelli, S. Morando et al., "Mesenchymal stem cells impair in vivo T-cell priming by dendritic cells," *Proceedings of the National Academy of Sciences of the United States of America*, vol. 108, no. 42, pp. 17384–17389, 2011.

[19] K. English, F. P. Barry, and B. P. Mahon, "Murine mesenchymal stem cells suppress dendritic cell migration, maturation and antigen presentation," *Immunology Letters*, vol. 115, no. 1, pp. 50–58, 2008.

[20] X. X. Jiang, Y. Zhang, B. Liu et al., "Human mesenchymal stem cells inhibit differentiation and function of

monocyte-derived dendritic cells," *Blood*, vol. 105, no. 10, pp. 4120–4126, 2005.

[21] W. Zhang, W. Ge, C. Li et al., "Effects of mesenchymal stem cells on differentiation, maturation, and function of human monocyte-derived dendritic cells," *Stem Cells and Development*, vol. 13, no. 3, pp. 263–271, 2004.

[22] A. J. Nauta, A. B. Kruisselbrink, E. Lurvink, R. Willemze, and W. E. Fibbe, "Mesenchymal stem cells inhibit generation and function of both CD34+-derived and monocyte-derived dendritic cells," *The Journal of Immunology*, vol. 177, no. 4, pp. 2080–2087, 2006.

[23] V. Volarevic, N. Arsenijevic, M. L. Lukic, and M. Stojkovic, "Concise review: mesenchymal stem cell treatment of the complications of diabetes mellitus," *Stem Cells*, vol. 29, no. 1, pp. 5–10, 2011.

[24] D. Favre, J. Mold, P. W. Hunt et al., "Tryptophan catabolism by indoleamine 2,3-dioxygenase 1 alters the balance of TH17 to regulatory T cells in HIV disease," *Science Translational Medicine*, vol. 2, no. 32, article 32ra36, 2010.

[25] H. Ito, M. Hoshi, H. Ohtaki et al., "Ability of IDO to attenuate liver injury in alpha-galactosylceramide-induced hepatitis model," *Journal of Immunology*, vol. 185, no. 8, pp. 4554–4560, 2010.

[26] G. Matteoli, E. Mazzini, I. D. Iliev et al., "Gut CD103+ dendritic cells express indoleamine 2,3-dioxygenase which influences T regulatory/T effector cell balance and oral tolerance induction," *Gut*, vol. 59, no. 5, pp. 595–604, 2010.

[27] I. Rasmusson, M. Uhlin, K. Le Blanc, and V. Levitsky, "Mesenchymal stem cells fail to trigger effector functions of cytotoxic T lymphocytes," *Journal of Leukocyte Biology*, vol. 82, no. 4, pp. 887–893.

[28] I. Prigione, F. Benvenuto, P. Bocca, L. Battistini, A. Uccelli, and V. Pistoia, "Reciprocal interactions between human mesenchymal stem cells and gammadelta T cells or invariant natural killer T cells," *Stem Cells*, vol. 27, no. 3, pp. 693–702, 2009.

[29] G. M. Spaggiari, A. Capobianco, H. Abdelrazik, F. Becchetti, M. C. Mingari, and L. Moretta, "Mesenchymal stem cells inhibit natural killer-cell proliferation, cytotoxicity, and cytokine production: role of indoleamine 2,3-dioxygenase and prostaglandin E2," *Blood*, vol. 111, no. 3, pp. 1327–1333, 2008.

[30] P. A. Sotiropoulou, S. A. Perez, A. D. Gritzapis, C. N. Baxevanis, and M. Papamichail, "Interactions between human mesenchymal stem cells and natural killer cells," *Stem Cells*, vol. 24, no. 1, pp. 74–85, 2006.

[31] W. Li, G. Ren, Y. Huang et al., "Mesenchymal stem cells: a double-edged sword in regulating immune responses," *Cell Death & Differentiation*, vol. 19, no. 9, pp. 1505–1513, 2012.

Hindawi
Stem Cells International
Volume 2017, Article ID 2353240, 16 pages
https://doi.org/10.1155/2017/2353240

Research Article

Crosstalk with Inflammatory Macrophages Shapes the Regulatory Properties of Multipotent Adult Progenitor Cells

Stylianos Ravanidis,[1] Jeroen F. J. Bogie,[1] Raf Donders,[1] Robert Deans,[2] Jerome J. A. Hendriks,[1] Piet Stinissen,[1] Jef Pinxteren,[3] Robert W. Mays,[2] and Niels Hellings[1]

[1]*Biomedical Research Institute/Transnational University Limburg, School of Life Sciences, Hasselt University, 3590 Diepenbeek, Belgium*
[2]*Department of Regenerative Medicine, Athersys Inc., Cleveland, OH, USA*
[3]*ReGenesys BVBA, Leuven, Belgium*

Correspondence should be addressed to Niels Hellings; niels.hellings@uhasselt.be

Received 9 March 2017; Revised 27 May 2017; Accepted 12 June 2017; Published 12 July 2017

Academic Editor: Vladislav Volarevic

Macrophages and microglia are key effector cells in immune-mediated neuroinflammatory disorders. Driving myeloid cells towards an anti-inflammatory, tissue repair-promoting phenotype is considered a promising strategy to halt neuroinflammation and promote central nervous system (CNS) repair. In this study, we defined the impact of multipotent adult progenitor cells (MAPC), a stem cell population sharing common mesodermal origin with mesenchymal stem cells (MSCs), on the phenotype of macrophages and the reciprocal interactions between these two cell types. We show that MAPC suppress the secretion of tumor necrosis factor alpha (TNF-α) by inflammatory macrophages partially through a cyclooxygenase 2- (COX-2-) dependent mechanism. In turn, we demonstrate that inflammatory macrophages trigger the immunomodulatory properties of MAPC, including an increased expression of immunomodulatory mediators (e.g., inducible nitric oxide synthase (iNOS) and COX-2), chemokines, and chemokine receptors. Macrophage-primed MAPC secrete soluble factors that suppress TNF-α release by macrophages. Moreover, the MAPC secretome suppresses the antigen-specific proliferation of autoreactive T cells and the T cell stimulatory capacity of macrophages. Finally, MAPC increase their motility towards secreted factors of activated macrophages. Collectively, these in vitro findings reveal intimate reciprocal interactions between MAPC and inflammatory macrophages, which are of importance in the design of MAPC-based therapeutic strategies for neuroinflammatory disorders in which myeloid cells play a crucial role.

1. Introduction

Increasing evidence indicates that stem cell transplantation harbors potential to treat neuroinflammatory disorders [1]. For instance, neural precursor cells (NPCs) and mesenchymal stem cells (MSCs) possess functional immunomodulatory and neuroprotective properties as demonstrated by attenuation of disease severity after transplantation in experimental models of central nervous system- (CNS-) associated diseases, namely, multiple sclerosis (MS) and traumatic brain injury (TBI) among others [2–5].

Macrophages and microglia are key effector cells in the pathogenesis of neuroinflammatory disorders [6, 7]. Myeloid cells are regarded to be mainly detrimental in autoimmune diseases of the CNS as they promote neuroinflammation, demyelination, and neurodegeneration [8]. Inflammatory and toxic secretions, such as tumor necrosis factor alpha (TNF-α), interleukin 6 (IL-6), interleukin 1 beta (IL-1β), and nitric oxide (NO), partially underlie the disease-promoting impact of myeloid cells in MS [8, 9]. Furthermore, myeloid cells can promote neuroinflammation through the activation of encephalitogenic T cells and by promoting their recruitment to the CNS [9, 10]. Therefore, driving myeloid cells towards an anti-inflammatory and regenerative phenotype is considered a promising strategy to halt disease progression in neuroinflammatory disorders.

Several types of adult stem cells have been shown to skew myeloid cells towards a neuroprotective phenotype. For instance, MSCs can suppress the release of inflammatory mediators such as TNF-α and IL-6 by macrophages, while simultaneously inducing an "M2-like" anti-inflammatory and reparative phenotype in vitro and in vivo [11–14]. Moreover, macrophages seem to shape MSCs enhancing their immunomodulatory functions and altering their migratory properties [15, 16]. These studies point towards intimate reciprocal interactions between stem cells and macrophages.

Multipotent adult progenitor cells (MAPC) are bone marrow-derived stem cells that share a common mesodermal origin with MSCs. However, compared to MSCs, MAPC show a faster expansion rate and long-term population doublings of MAPC occur without signs of replicative senescence providing sufficient quantities for future therapeutic use [17, 18]. Moreover, MAPC show superior in vitro and in vivo immune suppressive features compared to MSCs [19, 20]. Particularly, using a xenogeneic transplantation approach, human MAPC (hMAPC) induced an "M2-like" polarization of microglia and macrophages in experimental models of TBI and spinal cord injury (SCI) [21–23]. In another study, rat MAPC (rMAPC) reduced the expression of metalloproteinase 9 (MMP-9) in macrophages, thereby preventing the macrophage-mediated induction of axonal dieback in SCI [24]. Moreover, it seems that the plasticity of rMAPC is shaped when they encounter an inflammatory environment [25]. These features make MAPC an attractive alternative for stem cell transplantation in CNS disorders [21–24, 26]. However, to date, the reciprocal interactions between MAPC and myeloid cells remain to be fully characterized.

In this study, we sought to determine the in vitro reciprocal interactions between macrophages and MAPC. We show that MAPC suppress the inflammatory phenotype that macrophages acquire following lipopolysaccharide (LPS) stimulation. In parallel, macrophage-exposed MAPC acquire an enhanced T cell modulatory phenotype. Moreover, MAPC increase their motility towards the inflammatory environment of classically activated macrophages. Collectively, these in vitro findings indicate that intimate interactions between MAPC and macrophages occur, resulting in enhanced therapeutic potency of MAPC. This study warrants in vivo validation and can, in the long run, assist in appropriate tissue targeting in preclinical autologous experimental studies.

2. Materials and Methods

2.1. rMAPC Culture and Chemicals. Lewis rat-derived MAPC (rMAPC) were provided by ReGenesys BVBA (Leuven, Belgium) and maintained according to the standard protocols developed by the supplier (37°C/5% CO_2/5% O_2). Cells were isolated and expanded as described previously [25, 27]. rMAPC medium consisted of 60% Dulbecco's Modified Eagle medium (DMEM; Gibco, Life Technologies Europe B.V., Gent, Belgium) low glucose (1 g/L), 40% MCDB-201 medium (pH 7.2), 1X linoleic acid-bovine serum albumin, 10^{-4} M l-ascorbic acid, 0.05 μM dexamethasone, 55 μM 2-mercapto-ethanol (all from Sigma-Aldrich, Diegem, Belgium), 100 IU/mL penicillin and 100 μg/mL streptomycin (Invitrogen, Life Technologies Europe B.V.), 1X insulin-transferrin-selenium (Lonza, Verviers, Belgium), 10 ng/mL mouse epidermal growth factor, 10 ng/mL recombinant human platelet-derived growth factor (R&D Systems, Abingdon, United Kingdom), and 10^3 units/mL mouse leukemia inhibitory factor (Millipore, Billerica, MA, USA). Finally, medium was supplemented with 2% fetal bovine serum (FBS; Hyclone, EU approved, Cat CH30160.03). Cells were cultured in human-derived fibronectin (10 ng/mL; Sigma-Aldrich) T175 flasks (Cellstar, Greiner Bio-One, Vilvoorde, Belgium) or Petri dishes (Nunc, VWR, Leuven, Belgium) according to the purposes needed.

Prostaglandin E2 (PGE2¸ Enzo Life Sciences, Farmingdale, NY, USA) was added on macrophages in specific experiments. PGE2 was diluted in dimethyl sulfoxide (DMSO; Sigma-Aldrich) which was used also as negative control.

2.2. Peritoneal Macrophages, NR8383 Cells, and Generation of Myelin Basic Protein-Specific T Cells. Macrophages were isolated from the peritoneal cavity of female Lewis rats via peritoneal lavage with 5 mM ethylenediaminetetraacetic acid (EDTA; VWR, Leuven, Belgium) solution in phosphate-buffered saline (PBS) as previously described [28]. Cells were collected and centrifuged at 1400 rpm for 10 minutes. After seeding, cells were allowed to adhere for 3 hours and then were washed twice with Roswell Park Memorial Institute-(RPMI-) 1640 (Invitrogen, Life Technologies Europe B.V.) to remove nonadherent peritoneal exudate cells. Peritoneal macrophages, as well as the alveolar macrophage-like cell line NR8383 [29], were cultured in RPMI-1640 supplemented with 10% fetal calf serum (FCS, Gibco, Life Technologies Europe B.V., Gent, Belgium) and 0.5% penicillin-streptomycin mixture (Gibco).

For the generation of myelin basic protein- (MBP-) specific T cells, the experimental model of MS, experimental autoimmune encephalomyelitis (EAE) [9], was induced in female Lewis rats (Janvier, France). Rats were injected subcutaneously with a 0.1 mL solution of 250 μg/mL guinea pig MBP, 2.5 mg/mL H37RA heat-killed mycobacterium tuberculosis (Difco, Detroit, USA), and 60 μL complete Freund's adjuvant (Sigma-Aldrich) in both hind paws. Ten days post-immunization, rats were sacrificed and popliteal and inguinal lymph nodes were excised. Tissues were grinded through a 70 μm cell strainer to generate a single -cell suspension. MBP-specific T cells were generated as described before [30].

All animal experiments were approved by the Ethical Committee for Animal Experiments of Hasselt University.

2.3. Cocultures. The effect of rMAPC on the phenotype of macrophages was determined in direct and transwell cocultures. Macrophages were seeded in 24-well plates (5×10^5/well), and rMAPC were added in ratios ranging from 1 : 0.5 up to 1 : 4. Cells were allowed for a preconditioning period for 24 hours, and then 100 ng/mL LPS (Sigma-Aldrich) was added for 20 hours. To evaluate the role of cyclooxygenase (COX) in the observed effects,

10 μM indomethacin (Sigma-Aldrich) was added along with LPS stimulation.

2.4. Exposure of rMAPC to Macrophage Supernatant and Generation of Conditioned Media. Macrophages were stimulated with 100 ng/mL LPS for 12 hours, and the supernatant (SN) was collected, filtered through a 0.45 μm filter, and applied to rMAPC for 12 hours. Supernatant of untreated macrophages was used as a control. To define differences in messenger ribonucleic acid (mRNA) expression, rMAPC were incubated with SN of ±LPS-activated macrophages or LPS (7.5×10^5 cells/well). Exposure to the SN of LPS-activated macrophages was prolonged to 18 hours for measuring NO using the Griess reagent assay (Promega, Leuven, Belgium).

To prepare double-conditioned media (DCM), rMAPC (5×10^4 cells/well), previously exposed to the SN of LPS-activated macrophages for 12 hours, were allowed to secrete soluble factors for 24 hours in 50 μL macrophage medium (96-well plate). In specific experiments, rMAPC were stimulated with a mixture of recombinant rat TNF-α, IL-1β, and IL-6 (100 ng/mL each; all from Peprotech, London, UK) to partially mimic the SN of LPS-activated macrophages. This conditioned medium is designated as "licensed-" conditioned medium (LCM). Nonstimulated rMAPC provided the single-conditioned media (CM). The representation of the generation of conditioned media from rMAPC is illustrated in Supplemental Figure 1 available online at https://doi.org/10.1155/2017/2353240. All the conditioned media were collected and filtered through a 0.45 μm filter.

2.5. Application of Soluble Factors Derived by rMAPC to Macrophages and T Cells. Macrophages (1.5×10^5/well/96-well plate) were exposed to LPS (100 ng/mL) and conditioned media from rMAPC for 24 hours. After this period, soluble mediators were measured in the supernatant. In parallel, to determine mRNA expression of M1 and M2 markers, NR8383 cells (7.5×10^5 cells/well/24-well plate) were seeded in the conditioned media with or without polarization stimuli. Control conditions included cells in fresh medium with M1 stimuli (100 ng/mL LPS), M2 stimuli {100 ng/mL interleukin 4 (IL-4), 150 ng/mL interleukin 13 (IL-13), and 250 ng/mL interleukin 10 (IL-10)}, or without any stimuli (M0).

To define the effect of rMAPC-derived conditioned media on antigen-specific T cells, MBP-reactive T cells (2.5×10^5) and irradiated thymocytes (2.5×10^5 cells/well, 3000 rad) were seeded in 96-well U-plates in CM, DCM, or LCM and were exposed to 10 μg/mL MBP. Conditioned media were diluted 1 : 1 with fresh T cell medium. The consistency of T cell medium was as previously described [25]. Control conditions included T cells and thymocytes seeded in a 1 : 1 mixture of nonconditioned and T cell medium with or without MBP. After 48 hours, 1 μCi ^{3}H thymidine (PerkinElmer, Waltham, MA, USA) per well was added for 18 hours. Following this period, cells were harvested (automatic cell harvester) and thymidine incorporation was measured in a β-plate liquid scintillation counter (PerkinElmer). Stimulation index of proliferated cells was calculated based on the individual conditions where no exogenous stimulus (MBP) was added.

2.6. Migration Assay. Migration of rMAPC towards the soluble factors secreted by LPS-activated macrophages was assessed using an 8 μM diameter pore transwell assay. To avoid false positive migration towards increased serum concentrations [31], macrophages were seeded in macrophage medium containing 1% FCS, instead of 10%, and were stimulated with LPS for 24 hours. The conditioned medium from macrophages was seeded in the lower part of the 24-well inserts. rMAPC (3×10^4 cells/well) were suspended in DMEM low glucose 1 g/L (Gibco) containing 1% FCS in the upper chamber. Nonconditioned macrophage medium supplemented with 1% FCS served as negative while rMAPC medium served as positive control [25]. Cells were allowed to migrate for 14 hours at 37°C. Then, the media in the lower chamber were removed and inserts were fixed with 4% solution of paraformaldehyde (PFA) for 20 minutes and then they were washed with PBS (Lonza) twice. Subsequently, cells were stained with 0.1% Crystal Violet (Sigma-Aldrich) solution in ethanol for 10 minutes. Cells on the top side of the insert were removed using a cotton swab. Then, inserts were washed with PBS, allowed to air dry and three pictures per well were taken. Using ImageJ software, pictures were transformed to 8-bit images and the migrated fraction is expressed as percentage of the total covered area of the well [32].

2.7. Antigen Recall Assay. To define the impact of conditioned media from rMAPC on the capacity of macrophages to present antigens, macrophages (5×10^4/well/96-well plate) were pulsed with 25 μg/mL MBP in the presence of conditioned media from rMAPC. Following 18 hours, the conditioned media were removed and 1.5×10^5 carboxyfluorescein diacetate succinimidyl ester- (CFSE-; Invitrogen) labeled MBP-specific T cells (2 μM) were added (T cells/macrophage ratio 3 : 1). After 4 days, T cells were collected and processed for flow cytometry. T cells were stained with rat anti-CD3 (eBioscience, Vienna, Austria) and 7 aminoactinomycin D (7AAD; R&D Systems, Abingdon, UK) to assess cell death.

2.8. Flow Cytometry. The effect of conditioned media from rMAPC on endocytic properties of macrophages was assessed using fluorescein isothiocyanate- (FITC-) labeled dextran beads (Sigma-Aldrich). For this purpose, following an overnight incubation with conditioned media from rMAPC, macrophages were exposed to 100 μg/mL FITC-labeled dextran beads for 2 hours. Macrophages exposed to beads on ice were taken along to correct for background levels generated by spontaneous sticking of the beads to cell membranes. In separate experiments, cells were stained with anti-rat CD86 (eBioscience) and the mean FL2 signal within the CD86 gate was used to evaluate the CD86 expression. In coculture experiments, cells were stained with anti-CD11 b/c (BioLegend, San Diego, CA, USA) along with anti-CD86, and the mean expression of FL2 channel was used to measure CD86 expression.

2.9. Analysis of Gene Expression. RNA was isolated with RNeasy mini kit (Qiagen, Venlo, The Netherlands) and was

transcribed to complementary deoxyribonucleic acid (cDNA) using the Quanta kit (VWR, Leuven, Belgium) following the manufacturer's instructions. Semiquantitative real-time polymerase chain reaction (qPCR) was performed to detect changes in gene expression. Reactions were performed in a StepOnePlus™ Real-Time PCR System (Applied Biosystems) in micro AMP Fast Optical 96-well reaction plates in a total volume of 10 μL per reaction. Master mix consisted of 1x Fast SYBR green master mix (Applied Biosystems), 10 mM of each primer (designed with Primer 3 [33]; Eurogentec, Liege, Belgium), nuclease-free water, and 12.5 ng of cDNA template. Following the amplification, melting curve analysis was performed to test the specificity of the qPCR products. The primer sequences used are listed in Supplemental Table 1. The $2^{-\Delta\Delta Ct}$ method was used to relatively quantify the expression of each gene [34] while data were normalized to the most stable reference genes for each experiment following geNorm analysis [35].

2.10. Measurement of Soluble Mediators and Nitrite Formation. Cytokines were measured with sandwich enzyme-linked immunosorbent assay (ELISA). TNF-α (eBioscience) and IL-6 (R&D Systems, Minneapolis, MN, USA) ELISA were used following the manufacturer's instructions, and absorbance was measured at 450 nm using a spectrophotometer (Bio-Rad Benchmark, Bio-Rad Laboratories, Hercules, CA, USA). The presence of nitrite was measured using Griess reagent system (Promega, Leuven, Belgium) following the manufacturer's instructions, and absorbance was measured at 540 nm.

2.11. Statistical Analysis. Data were analyzed with the GraphPad Prism version 5.00 for Windows (GraphPad Software, San Diego, California, USA, www.graphpad.com) and are presented as mean ± SEM. D'Agostino and Pearson omnibus normality test was used to evaluate whether the data are following normal distribution. For comparisons between two groups, unpaired Student's *t*-test or Mann–Whitney *U* test was used. One-way analysis of variance (ANOVA) followed by Dunnett's multiple comparison test or Kruskal-Wallis followed by Dunn's multiple comparison test was used, depending on whether the data were parametric or nonparametric, for comparisons between multiple groups. Differences with p value ≤ 0.05 were considered significant.

3. Results

3.1. rMAPC Release NO When Cocultured with Inflammatory Macrophages. NO has multimodal functions in neuroinflammatory disorders. While high levels of NO can be detrimental for oligodendrocytes and neurons [36], NO can also inhibit the proliferation of autoreactive T cells [30]. In this part of the study, we sought to determine NO release in cocultures with rMAPC and macrophages. Our data show that NO levels were increased in both direct and transwell cocultures of inflammatory macrophages and rMAPC (Figures 1(a) and 1(b)). Nonstimulated macrophages did not release detectable levels of NO (data not shown). To determine the cellular source of NO in cocultures, rMAPC were incubated with SN of LPS-activated macrophages (Figure 1(c)). We observed that rMAPC released NO above the levels already present in the supernatant due to LPS stimulation of macrophages (Figure 1(d)). In line with this finding, rMAPC showed increased mRNA expression of iNOS upon exposure to SN of LPS-activated macrophages compared to rMAPC stimulated with SN of nonstimulated macrophages or LPS alone (Figure 1(e)).

3.2. rMAPC Suppress the Release of TNF-α by Macrophages Partially through a COX-2-Dependent Mechanism. Adult stem cells hold potential in suppressing the inflammatory properties of classically activated macrophages or even direct them towards an "M2-like" phenotype [12, 14, 37]. Direct and transwell cocultures of rMAPC and LPS-stimulated macrophages were established to determine the effect of rMAPC on the release of inflammatory mediators by macrophages. rMAPC suppressed the release of TNF-α by activated macrophages in a dose-dependent manner (Figure 2(a)). Nonstimulated macrophages did not produce detectable levels of TNF-α (data not shown). A similar inhibition of TNF-α release was observed when cell contact between rMAPC and macrophages was blocked by using transwell inserts (Figure 2(b)). rMAPC did not produce detectable levels of TNF-α following treatment with SN of ±LPS-activated macrophages (data not shown).

Prostaglandin E2 (PGE2) is well known to modulate the phenotype of macrophages. Interestingly, the expression of its rate-limiting enzyme involved in the generation of PGE2, cyclooxygenase 2 (COX-2), is induced in MSCs and MAPC under inflammatory conditions [12, 14, 25]. By using an inhibitor of COX-2, we show that the reduction of TNF-α release by macrophages in direct contact cocultures with rMAPC is partially abrogated (Figure 2(c)). In contrast, inhibition of COX-2 did not significantly counteract the reduced levels of TNF-α in transwell cocultures (Figure 2(d)). To confirm the capacity of PGE2 to reduce TNF-α release, macrophages were exposed to PGE2 along with LPS stimulation. We demonstrate that PGE2 suppressed the release of TNF-α by LPS-stimulated macrophages in a dose-dependent manner (Figure 2(e)). Finally, we found that rMAPC have an increased mRNA expression of COX-2, but not COX-1, when exposed to the SN of LPS-activated macrophages compared to rMAPC treated with SN from naïve macrophages or LPS alone (Figure 2(f) and data not shown). The latter finding strongly suggests that macrophage-driven expression of COX-2 by rMAPC is involved in the regulation of the macrophage phenotype.

3.3. rMAPC Increase IL-6 Secretion in Response to Activated Macrophages. In contrast to TNF-α and similar to NO, levels of IL-6 were increased in both direct and transwell cocultures of macrophages and rMAPC (Figures 3(a) and 3(b)). Application of COX-2 inhibitor did not have any impact on IL-6 secretion (data not shown). In line with this finding, PGE2 did not affect the release of IL-6 by macrophages as seen with TNF-α (Figure 3(c)). To define the cellular source of IL-6 in cocultures, rMAPC were incubated with SN of LPS-activated macrophages for a short period. Then, new

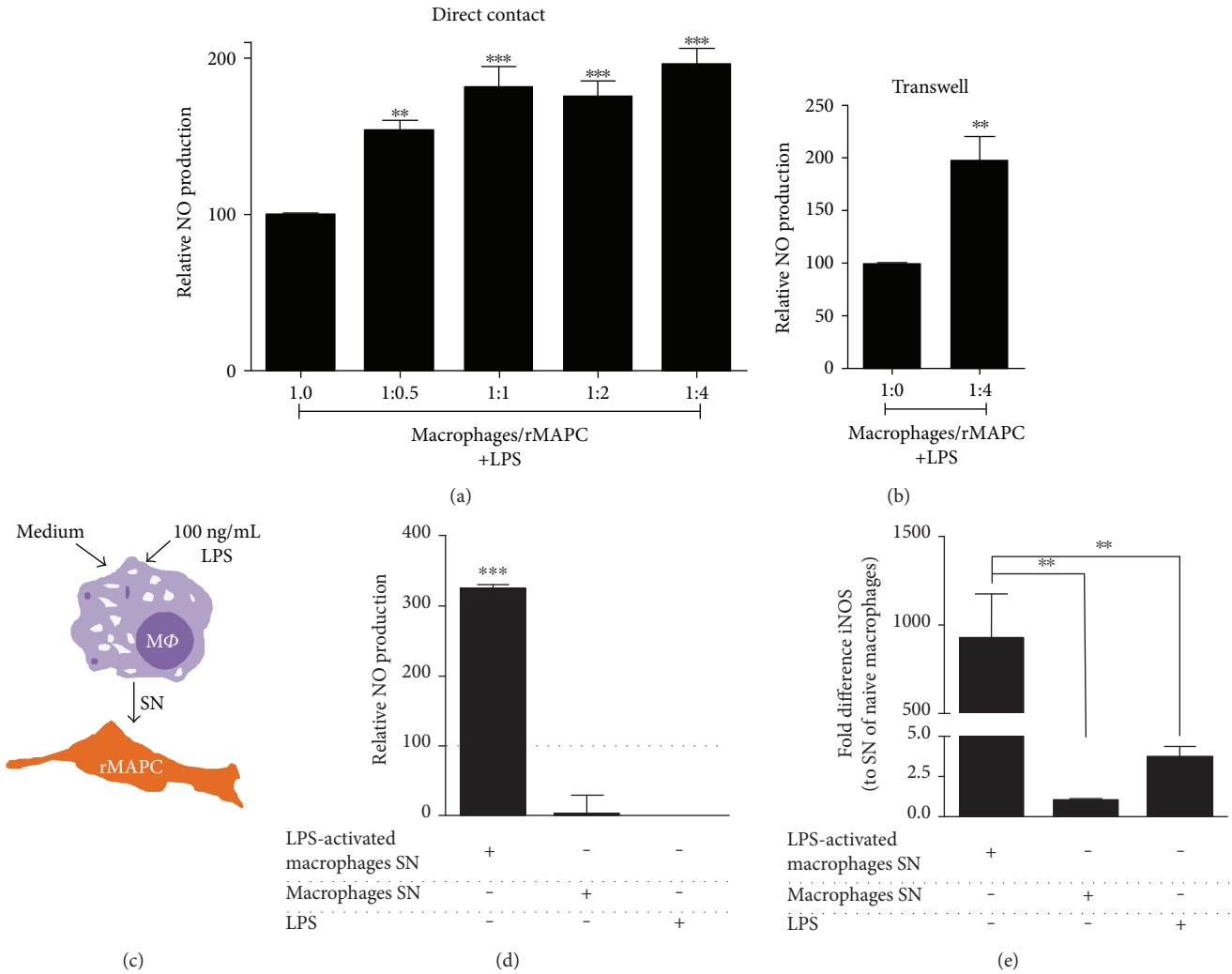

Figure 1: rMAPC increase NO production in the presence of inflammatory macrophages. (a) Direct contact cocultures ($N = 7$ experiments) of macrophages with rMAPC in increasing ratios (1 : 0 to 1 : 4) and (b) transwell cocultures of macrophages with rMAPC (1 : 4, $N = 6$ experiments), supplemented with LPS. The results are shown as percentage of nitrite levels normalized to the positive control (1 : 0 +LPS) with duplicates per experiment. Asterisks (*) indicate statistical significant difference with positive control (1 : 0 +LPS). (c) Schematic illustration of generation of LPS-activated SN (MΦ; macrophages). (d) rMAPC treated with SN of LPS-activated macrophages, SN of naïve macrophages or LPS alone ($N = 4$ experiments). The results are shown as percentage of nitrite levels normalized to the positive control (pure s/n from activated macrophages, dotted line). Asterisks (*) indicate statistical significant difference with positive control. (e) iNOS mRNA expression of rMAPC treated with SN of LPS-activated macrophages, SN of naïve macrophages or LPS ($N = 5$ experiments). The results are shown as fold differences in comparison to SN of naïve macrophages. Asterisks (*) indicate statistical significant differences. Mean values ± SEM. Data were analyzed with one-way ANOVA followed by Dunnett's multiple comparison test or with Kruskal-Wallis test followed by Dunn's multiple comparison test for nonparametric dat ($^{**}p \leq 0.01$ and $^{***}p \leq 0.001$).

medium was applied for 24 hours and this was used for measuring IL-6 levels (Figure 3(d)). Macrophage-primed rMAPC increased their IL-6 secretion (DCM), while naïve or cytokine-primed rMAPC did not produce detectable levels of IL-6 (Figure 3(e)). Also, the mRNA expression of IL-6 in rMAPC was increased compared to rMAPC treated with SN of macrophages or LPS alone (Figure 3(f)). These findings point towards rMAPC as the cellular source of the additional IL-6 release in LPS-stimulated cocultures. Of interest, no IL-6 production was observed in nonstimulated cocultures, indicating that LPS stimulation is necessary for macrophages to induce IL-6 release by rMAPC.

3.4. Macrophage-Primed rMAPC Secrete Factors That Modulate the Macrophage Phenotype. Increasing evidence indicates that inflammatory conditions promote the immunomodulatory features of stem cells [38]. To explore whether rMAPC primed by inflammatory macrophages reciprocally impact macrophage physiology, double-conditioned medium was generated. For this purpose, rMAPC were initially triggered with SN of LPS-activated macrophages, simulating the inflammatory mediators released by "M1-like" macrophages in immune-mediated diseases, and then allowed to secrete factors in their supernatant (Supplemental Figure 1). Macrophages exposed to the double-conditioned

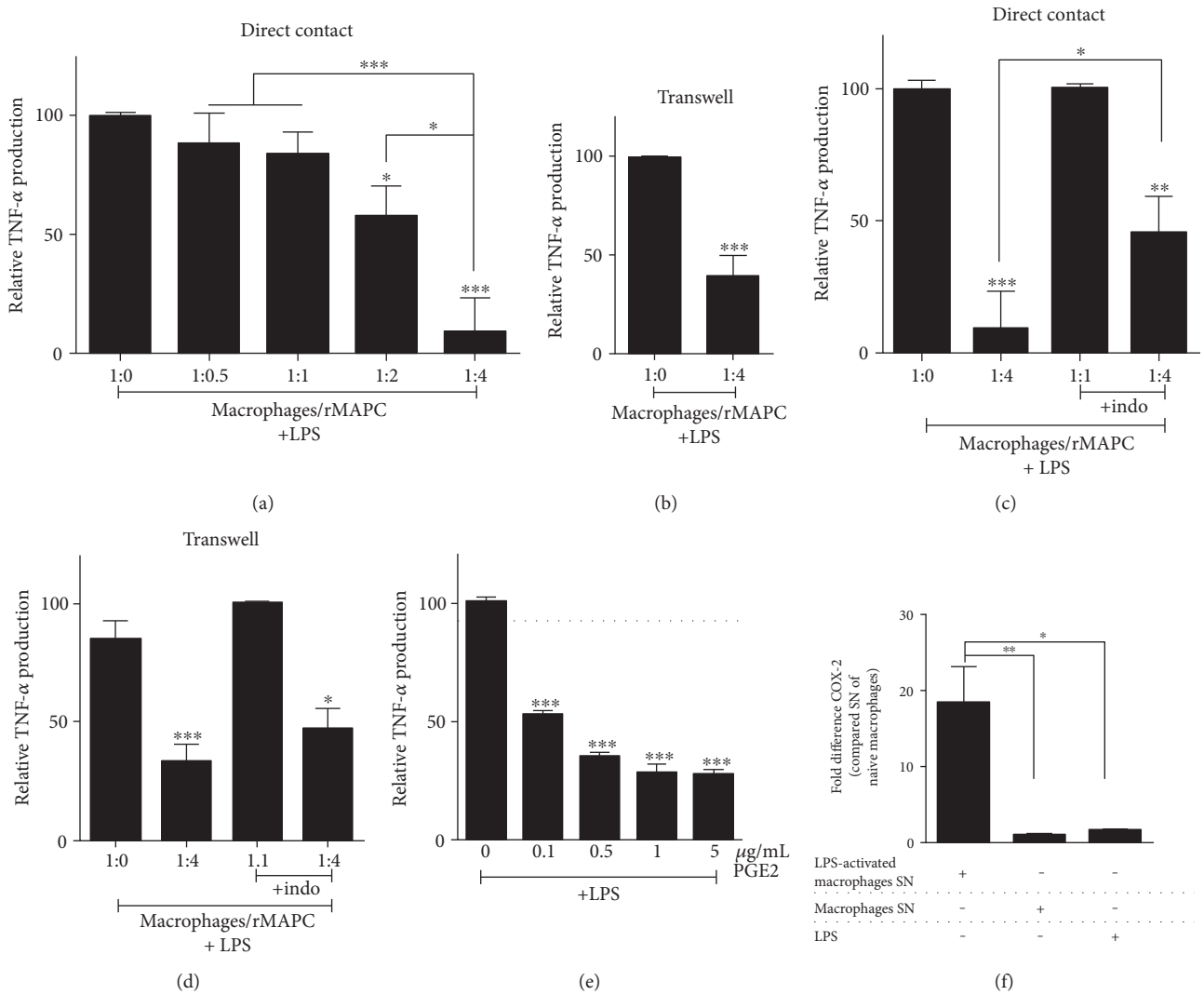

Figure 2: rMAPC suppress TNF-α release by macrophages in a COX-2-dependent mechanism. (a) Direct contact cocultures ($N = 9$ experiments) of macrophages with rMAPC in increasing ratios (1 : 0 to 1 : 4) and (b) transwell cocultures of macrophages with rMAPC (1 : 4, $N = 4$ experiments), supplemented with LPS. The results are shown as percentage of TNF-α levels normalized to the positive control (1 : 0 +LPS) with duplicates per experiment. Asterisks (*) indicate statistical significant difference with positive control. (c) Direct contact ($N = 7$ experiments) and (d) transwell coculture ($N = 4$ experiments) of macrophages with rMAPC supplemented with LPS (1 : 4) and indomethacin. The results are shown as percentage of TNF-α levels normalized to the positive control (1 : 0 +LPS + indo) with duplicates per experiment. Asterisks (*) indicate statistical significant difference with positive control. (e) Effect of PGE2 (0 to 5 μg/mL) on TNF-α release by macrophages after LPS stimulation ($N = 4$ experiments with triplicates per experiment). The results are shown as percentage of TNF-α levels normalized to the positive control (0 μg/mL +LPS). Asterisks (*) indicate statistical significant difference with positive control. Mean values of dimethyl sulfoxide are shown as solvent of PGE2 (dotted line). (f) Cyclooxygenase-2 (COX-2) mRNA expression in rMAPC treated with SN of LPS-activated macrophages, SN of naïve macrophages or LPS ($N = 5$ experiments). The results are shown as fold differences in comparison to SN of naïve macrophages. Asterisks (*) indicate statistical significant differences. Mean values ± SEM. Data were analyzed with one-way ANOVA followed by Dunnett's multiple comparison test. $^{*}p \leq 0.05$, $^{**}p \leq 0.01$, and $^{***}p \leq 0.001$.

media from rMAPC (DCM) (Figure 4(a)) secreted less TNF-α following LPS stimulation (Figure 4(b)). This effect was not due to increased cell death of macrophages (not shown). Single-conditioned media (CM) showed no effect, indicating the necessity of priming of rMAPC to regulate the TNF-α secretion levels by macrophages. IL-6 levels were not affected in any condition (Figure 4(c)). To detect the effects of rMAPC-derived conditioned media on mRNA expression of polarization markers, we used a macrophage-like cell line, NR8383. DCM did not induce spontaneous expression of M1 (iNOS, CD86, and TNF-α; Figures 4(d), 4(e), and 4(f)) or M2 markers {arginase 1 (Arg1) and C-C motif ligand 18 (CCL18); Figures 4(g) and 4(h)} in NR8383 cells. However, when NR8383 cells were simultaneously incubated in DCM and were stimulated with either LPS or M2-inducing cytokines (IL-4/IL-10/IL-13), we observed an increased mRNA expression of Arg1, the prototypical marker for M2 macrophages (Figures 4(i) and 4(j)).

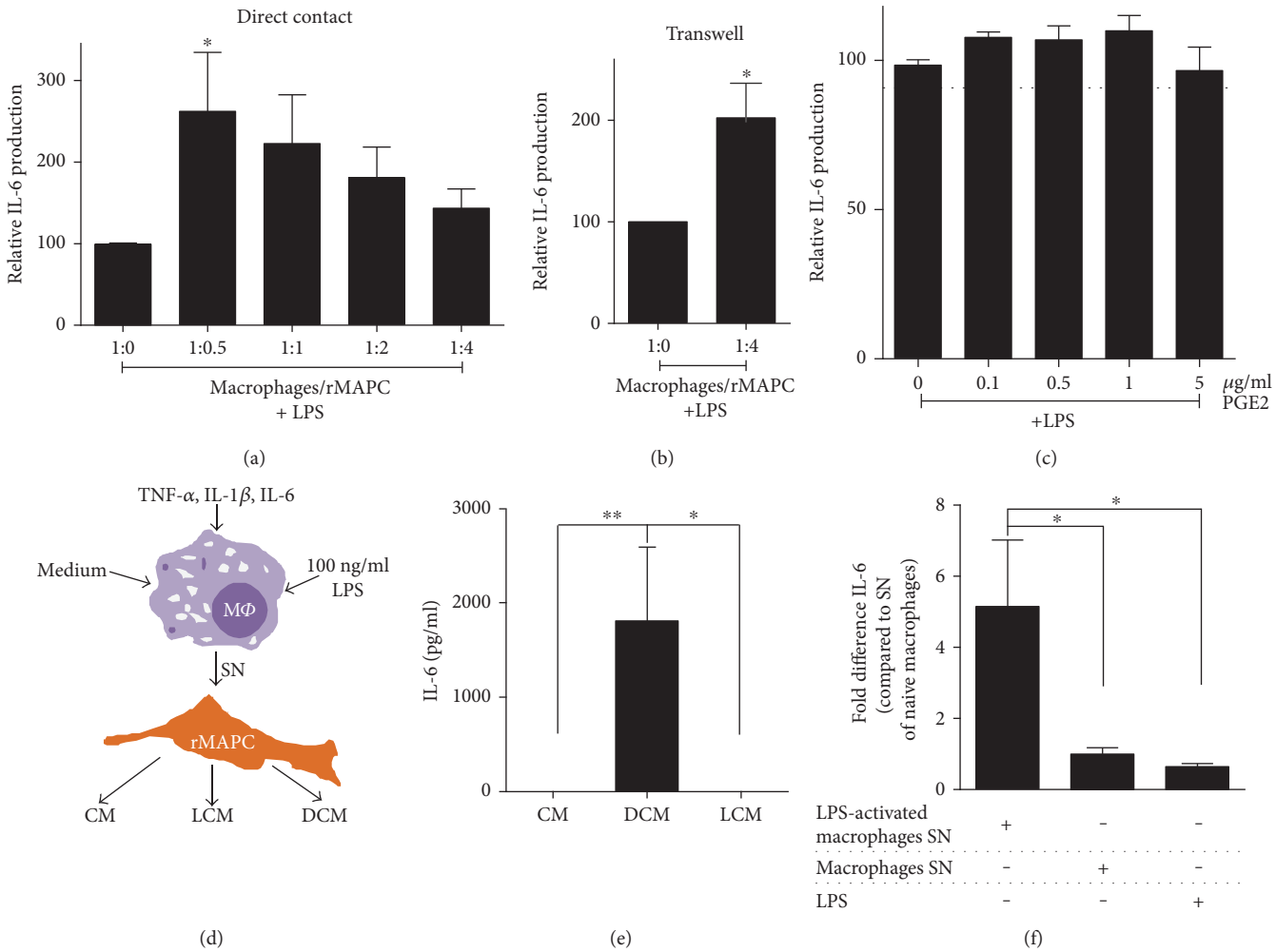

FIGURE 3: Macrophage-primed rMAPC increase their IL-6 expression. (a) Direct contact cocultures ($N = 6$ experiments) of macrophages with rMAPC in increasing ratios (1 : 0.5 to 1 : 4) and (b) transwell cocultures of macrophages with rMAPC (1 : 4, $N = 4$ experiments), supplemented with LPS. The results are shown as percentage of IL-6 levels normalized to the positive control (1 : 0 +LPS) with duplicates per experiment. Asterisks (*) indicate statistical significant difference with positive control. (c) Effect of PGE2 (0 to 5 μg/mL) on TNF-α release by macrophages after LPS stimulation ($N = 4$ experiments with triplicates per experiment). The results are shown as percentage of IL-6 levels normalized to the positive control (0 μg/mL +LPS). Asterisks (*) indicate statistical significant difference with positive control. Mean values of dimethyl sulfoxide are shown as solvent of PGE2 (dotted line). (d) Schematic illustration of generation of rMAPC-conditioned media (SN; supernatant, MΦ; macrophages). (e) IL-6 measurement in rMAPC-derived conditioned media ($N = 6$ experiments) following different stimuli. IL-6 levels are shown as pg/mL. Asterisks (*) indicate statistical significant difference between the different conditioned media. (f) IL-6 mRNA expression in rMAPC treated with SN of LPS-activated macrophages, SN of naïve macrophages or LPS ($N = 5$ experiments). The results are shown as fold differences in comparison to SN of naïve macrophages. Asterisks (*) indicate statistical significant differences. Mean values ± SEM. Data were analyzed with one-way ANOVA followed by Dunnett's multiple comparison test ($^*p \leq 0.05$, $^{**}p \leq 0.01$).

An increased mRNA expression of CCL18 by NR8383 cells incubated in DCM was observed only following LPS stimulation (data not shown).

Collectively, these results indicate that the regulatory activities of rMAPC towards macrophages are shaped by the factors released by macrophages.

3.5. Macrophage-Primed rMAPC Suppress Autoreactive T Cell Proliferation. The proliferation of autoreactive T cells is closely associated with disease severity in neuroinflammatory conditions [39, 40]. As proinflammatory priming is reported to enhance the capacity of MSCs to suppress T cell proliferation [25, 38], we assessed whether macrophage-mediated priming of rMAPC also enhances their capacity to suppress myelin-reactive T cells. For this purpose, MBP-reactive T cells were exposed to cognate antigen and double-conditioned media of rMAPC. Additionally, MBP-reactive T cells were exposed to conditioned medium of rMAPC that were primed with TNF-α, IL-1β, and IL-6, cytokines that are typically secreted by inflammatory macrophages [41]. Our data indicate that cytokine- (LCM) and macrophage- (DCM) primed rMAPC suppress the proliferation of MBP-reactive T cells to a similar extent (Figure 5).

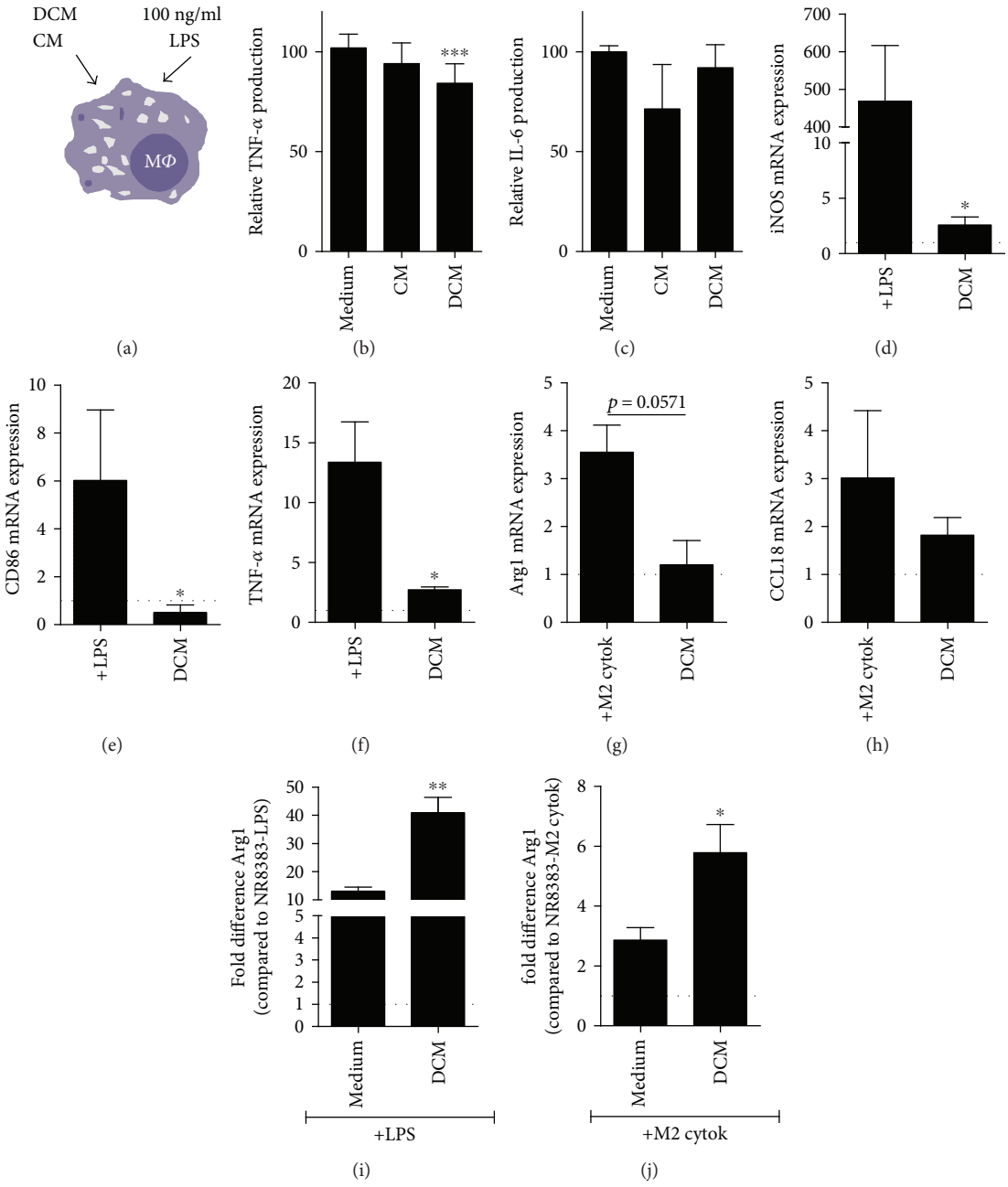

Figure 4: Soluble factors derived by macrophages-primed rMAPC modulate macrophages phenotype. (a) Schematic illustration of application of rMAPC-derived conditioned media to macrophages (MΦ). (b) TNF-α ($N = 6$ independent experiments with triplicates per experiment) and (c) IL-6 ($N = 3$ experiments with triplicates per experiment) secretion levels of macrophages treated with LPS in the presence of rMAPC-derived conditioned media. The results are presented as percentage of to the positive control (medium +LPS). Asterisks (*) indicate statistical significant difference with positive control. (d–h) NR8383 mRNA expression of M1 and M2 polarization markers seeded in DCM ($N = 5$ experiments). iNOS (d), CD86 (e), and TNF-α (f) are compared to their respective positive control (NR8383 +LPS) while Arg1 (g) and CCL18 (h) to NR8383 +M2 cytokines (IL-4/IL-10/IL-13). The results are presented as fold differences to nonstimulated NR8383 cells (dotted line). (i-j) NR8383 mRNA expression of Arg1 seeded in DCM supplemented with polarization stimulus, +LPS (i) and +M2 cytokines (j). The results are presented as fold differences to nonstimulated NR8383 cells (dotted line). Asterisks (*) indicate statistical significant difference with positive control in each case (NR8383 +LPS or NR8383 +M2 cytokines). Relative expressions were normalized against the expression of hydroxymethylbilane synthase (HMBS) and b-actin. Mean values ± SEM. Data were analyzed with one-way ANOVA followed by Dunnett's multiple comparison test or with Kruskal-Wallis test followed by Dunn's multiple comparison test for nonparametric data. Two group comparisons were made with unpaired Student's t-test ($^{*}p \leq 0.05$, $^{**}p \leq 0.01$, and $^{***}p \leq 0.001$).

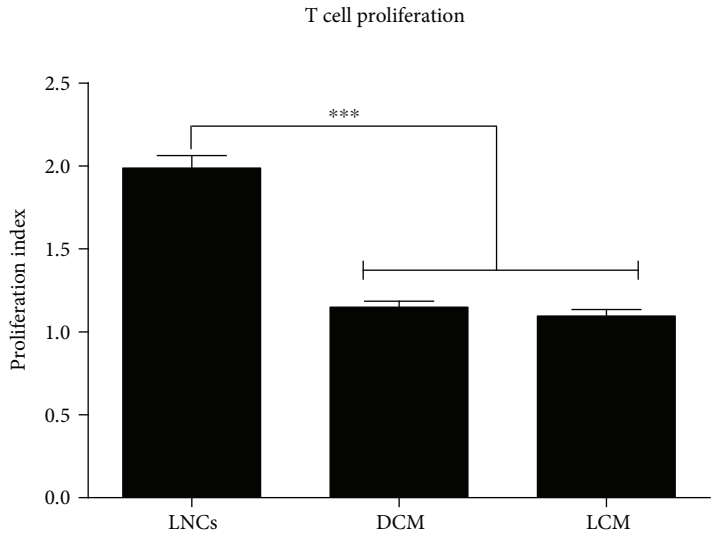

Figure 5: rMAPC suppress antigen-specific T cell proliferation. Myelin basic protein-(MBP-) specific T cells were seeded in rMAPC-derived conditioned media and were stimulated with MBP. Proliferation index was calculated based to conditions without MBP (not shown). Mean values ± SEM are from 3 independent experiments, with triplicates per experiment. Data were analyzed with one-way ANOVA followed by Dunnett's multiple comparison test $^{***}p \leq 0.001$.

3.6. rMAPC-Derived Soluble Factors Interfere with the Antigen Presentation Capacity of Macrophages. Macrophages are specialized antigen-presenting cells. The processing and the subsequent presentation of myelin antigens by macrophages promote neuroinflammation and disease progression [42]. To define whether soluble factors derived from primed rMAPC affect T cell stimulatory capacity of macrophages, macrophages were pulsed with MBP in the presence of conditioned media prior to coculture with MBP-reactive T cells. Macrophages that were exposed to double-conditioned media (DCM) and licensed-conditioned medium (LCM) showed a reduced capacity to stimulate T cells compared to macrophages exposed to control condition (Figure 6(a)). Double- or licensed-conditioned media did not affect the endocytic ability of macrophages (Figure 6(b)). This finding suggests that a reduced uptake of MBP does not underlie the impaired capacity of macrophages to stimulate T cells. Interestingly, macrophages cultured in DCM and LCM showed a reduced surface expression of CD86 (Figure 6(c)). Similarly, macrophages showed a decreased surface expression of CD86 in direct contact coculture with rMAPC following LPS stimulation (Figure 6(d)). These findings suggest that rMAPC affect the T cell stimulatory capacity of macrophages by reducing the expression of costimulatory molecules [6, 7].

3.7. rMAPC Motility Is Increased towards Inflammatory Mediators Secreted from Macrophages. Migration towards inflammatory gradients released by the cells present at the site of tissue injury is an important feature of adult stem cells in the context of neuroinflammation [15, 25]. We observed an enhanced migration of rMAPC towards inflammatory macrophage-conditioned medium as compared to conditioned medium derived by nonstimulated macrophages (Figure 7(a)). An enhanced expression of C-C motif chemokine receptors, CCR1 and CCR3, on rMAPC may account for the observed increase in migration of rMAPC (Figures 7(b) and 7(c)). CCR1 and CCR3 are the receptors of CCL5, which is a chemokine that is typically secreted by classically activated macrophages [10]. These observations suggest that rMAPC increase their motility towards inflammatory gradients generated by activated macrophages. Moreover, rMAPC demonstrated increased mRNA expression of CCL2, CCL5, and CXCL10, after exposure to SN of LPS-activated macrophages (Supplemental Figure 2). Overall, these results indicate that rMAPC's exposure to secretome of classically activated macrophages may assist the establishment of interactions with the immune cells in vivo by altering their migratory and chemoattractive phenotype.

4. Discussion

Stem cell transplantation represents a promising therapeutic approach to treat neuroinflammatory and neurodegenerative disorders. Upon transplantation in inflammatory CNS disorders such as MS, TBI, SCI, and stroke, stem cells are likely to encounter myeloid cells in both the CNS and periphery. Myeloid cells are key effector cells in these disorders [6, 9, 43, 44]. Skewing myeloid cells towards a less inflammatory phenotype is considered to be a promising therapeutic strategy. In this study, we show that macrophages and rMAPC, a similar but functionally different adherent stem cell population than MSCs with superior features, closely interact thereby affecting each other's inflammatory and migratory phenotype. In particular, we found that rMAPC dampen the inflammatory features of classically activated macrophages. Vice versa, rMAPC acquired an immunomodulatory and migratory phenotype when exposed to soluble factors released by inflammatory macrophages. These syngeneic reciprocal interactions between rMAPC and macrophages may suppress features

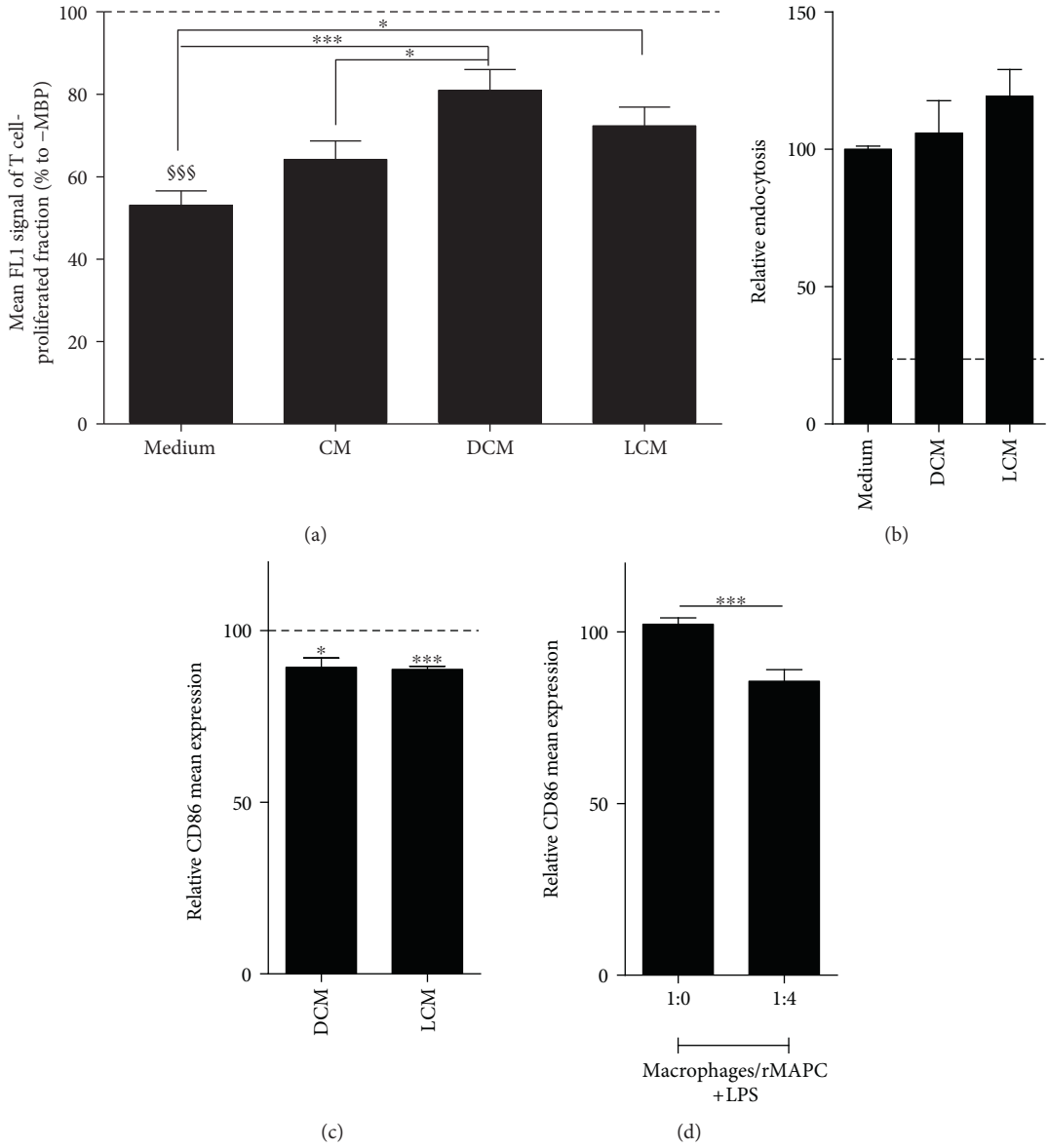

Figure 6: rMAPC suppress antigen presenting features of macrophages. (a) Coculture of macrophages and T cells following macrophages' pulsing with MBP in specified conditioned media from rMAPC or in their own medium ($N = 3$ experiments with quadruplicates per experiment). T cell proliferation was estimated based to the mean FL1 signal of the proliferated fraction of carboxyfluorescein diacetate succinimidyl ester (CFSE) labeling. The results are shown as percentages of negative control (macrophages cocultured with T cells without prior pulsing of MBP, dotted line). Paragraph signs (§) indicate statistical significant difference between positive control (pulsed macrophages with MBP in fresh medium cocultured with T cells) and negative control. Asterisks (*) indicate statistical significant difference with positive control. (b) Endocytosis of FITC-labelled beads of macrophages when incubated with designated media. The results are shown as percentages of positive control (endocytosis in fresh medium). Background levels of endocytosis are shown in *dotted line*. (c) Mean of CD86 expression of macrophages incubated with designated media ($N = 4$ experiments with duplicates per experiment). The results are presented as percentages of positive control (macrophages in fresh medium) (dotted line). Asterisks (*) indicate statistical significant differences with positive control. (d) Mean of CD86 expression of CD11b/c/CD86 fraction of coculture of macrophages and rMAPC (1 : 4) treated with LPS ($N = 4$ experiments with quadruplicates per experiment). The results are presented as percentages of positive control (1 : 0 +LPS). Asterisks (*) indicate statistical significant difference with positive control. Mean values ± SEM. Data were analyzed with one-way ANOVA followed by Dunnett's multiple comparison test or with Kruskal-Wallis test followed by Dunn's multiple comparison test for nonparametric data. $^{§§§}p \leq 0.001$, $^{*}p \leq 0.05$, and $^{***}p \leq 0.001$.

of neuroinflammation and therefore provide further incentive to use rMAPC to treat neuroinflammatory disorders.

Macrophages secrete a plethora of inflammatory mediators that promote neuroinflammation and neurodegeneration. TNF-α is highly expressed by both parenchymal and circulating myeloid cells in neuroinflammation [6] and is well known to promote neurodegeneration [45]. In line with previous studies using MSCs, our data indicate that rMAPC

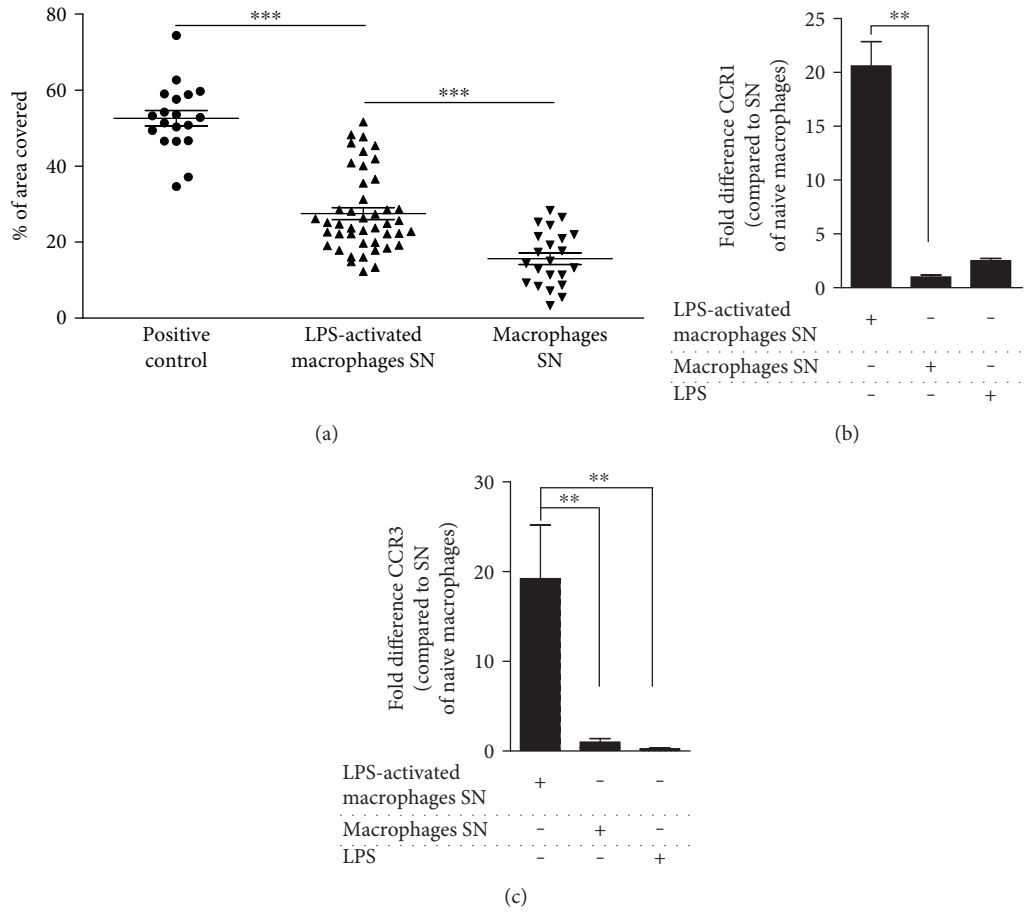

Figure 7: rMAPC acquire a migratory phenotype in response to SN of LPS-activated macrophages. (a) rMAPC migration towards SN of ±LPS-activated macrophages. The results are presented as percentage of area covered from the migrated fraction. A positive control rMAPC medium was used. Asterisks (*) indicate statistical significant differences. (positive control versus SN of naïve macrophages; $p < 0.001$). Mean values ± SEM are from 7 independent experiments, with duplicates per experiment. (b) CCR1 and (c) CCR3 mRNA expression in rMAPC treated with SN of LPS-activated macrophages, SN of naïve macrophages, or LPS ($N = 5$ experiments). The results are shown as fold differences in comparison to the SN of naïve macrophages. Mean values ± SEM. Asterisks (*) indicate statistical significant differences. Data were analyzed with one-way ANOVA followed by Dunnett's multiple comparison test. $^{**}p \leq 0.01$ and $^{***}p \leq 0.001$.

suppress the secretion of TNF-α by LPS-stimulated macrophages [11, 12]. Separation of rMAPC and macrophages did not abrogate the suppression of TNF-α secretion, indicating that soluble factors produced by rMAPC decrease the release of TNF-α by macrophages. Upon transplantation of rMAPC, this reduced expression of TNF-α may decrease oligodendrocytes damage within CNS and thus reduce disease progression [45, 46].

By using an inhibitor for COX-2, the rate-limiting enzyme in the formation of PGE2, we further provide evidence that rMAPC partially modulate TNF-α secretion by macrophages in a COX-2-dependent manner. In line with this finding, activated macrophage-conditioned medium markedly increased the mRNA levels of COX-2 in rMAPC and PGE2 administration decreased the release of TNF-α by macrophages. Previous studies indicate that PGE2 is crucial in mediating the immunosuppressive features of MSCs and MAPC [12, 25, 47, 48]. However, in our experiments, the levels of TNF-α were not completely restored following inhibition of COX-2, indicating that other mechanisms may play a synergistic role in the observed effect. These mechanisms could include IL-6, IL-10, and granulocyte macrophage colony-stimulating factor (GM-CSF) [49, 50]. Moreover, the levels of TNF-α were not restored when COX-2 was inhibited in transwell assays. This suggests that other synergistic mechanisms assist in the suppression of macrophage inflammatory phenotype, such as the binding of integrins to their corresponding receptors on the surface of macrophages [51]. In addition, the immunosuppressive action of PGE2 seems to be enhanced when rMAPC and macrophages are in close proximity [52]. Albeit other studies showed that PGE2 also suppresses IL-6 production by mouse peritoneal macrophages [12], PGE2 did not affect the secretion of IL-6 by macrophages in our experiments. This could be due to the increased IL-6 levels from rMAPC in our cocultures, which disguises the suppression

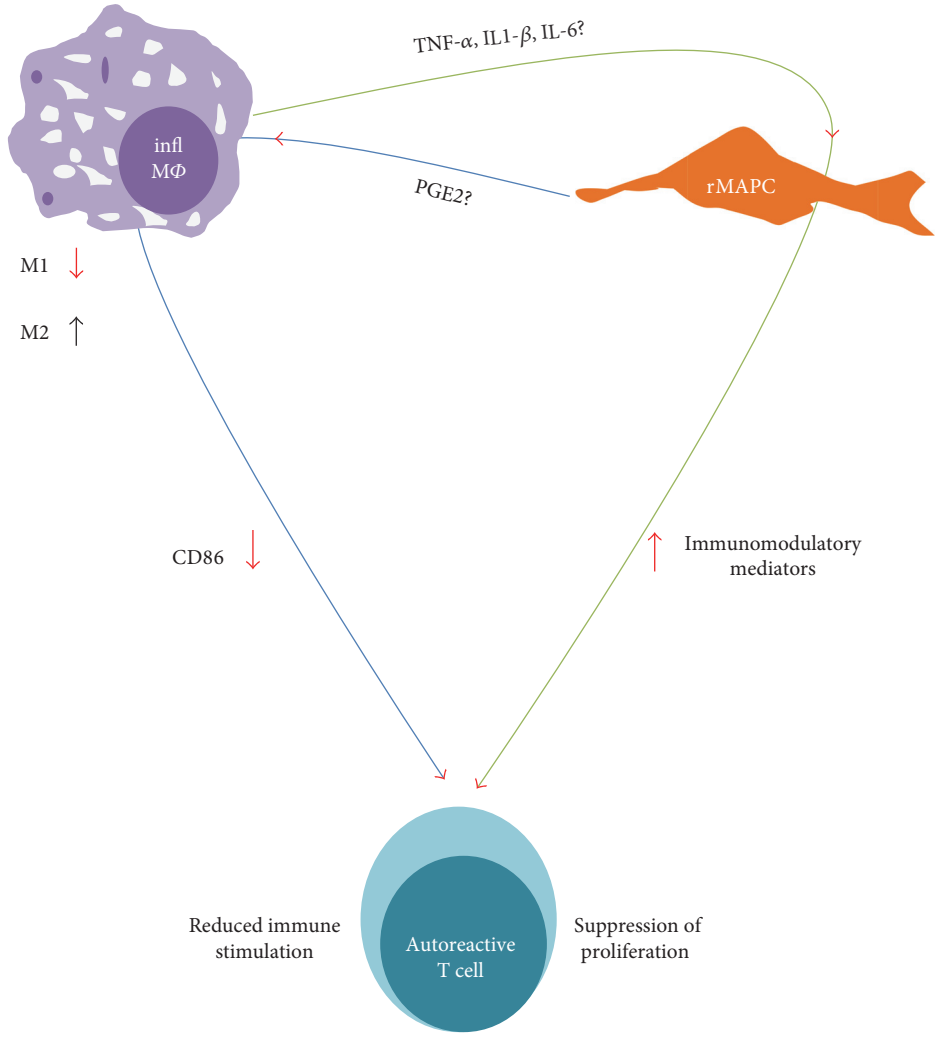

Figure 8: Schematic representation of reciprocal effects between rMAPC and macrophages. Inflammatory macrophages (infl MΦ) secrete vast amounts of proinflammatory cytokines (e.g., TNF-α, IL-1β, and IL-6) that prime rMAPC. rMAPC acquire enhanced immunoregulatory properties secreting immunomodulatory mediators that suppress autoreactive T cell proliferation (green trajectory). Moreover, immunoregulatory properties of rMAPC may suppress the M1 phenotype of MΦ or even induce a shift towards an M2 phenotype via the upregulation of PGE2 for instance. Effects of rMAPC secretome may lead to impaired stimulatory capacity of MΦ towards T cells via the downregulation of expression of surface molecules (e.g., CD86) resulting in suppressed autoreactive T cell proliferation (blue trajectory).

of the IL-6 by macrophages. The impact of rMAPC on IL-6 secretion by macrophages should be further investigated. Eventually, complete abrogation of COX-2 mRNA expression, for example, with the use of siRNA, could provide a better understanding on the role of PGE2 in the MAPC-mediated immunosuppression.

Our data further indicate that soluble factors released by inflammatory macrophages promote IL-6 secretion by rMAPC in cocultures. It has been reported that macrophage-associated MSCs increase their IL-6 secretion [15]. However, while MSCs increase IL-6 secretion by macrophages [11, 50], rMAPC did not impact IL-6 production by LPS-stimulated macrophages in our experiments. IL-6 has a bimodal role as it can have both a pro- and anti-inflammatory effect. IL-6 controls the cascade of proinflammatory responses while it is also necessary for wound-healing processes in immunosuppressed mice based on its ability to induce "M2-" polarized macrophages [53–55]. Since IL-6 has been proposed as key molecule for MSCs to promote the polarization of macrophages towards an "M2" phenotype and PGE2 upregulation in MSCs is IL-6 dependent, its role has to be further explored [50, 56]. Overall, IL-6 secretion by rMAPC in inflammatory environment signifies their wide arsenal of immunomodulatory mechanisms that is triggered in events associated with immune activation.

In inflammatory disorders, macrophages and microglia secrete proinflammatory cytokines that can potentially enhance the secretion of immunomodulatory molecules by adult stem cell types [16, 56]. We found an increased secretion of NO by rMAPC, as well as elevated mRNA abundance of iNOS in rMAPC upon treatment with medium derived from inflammatory macrophages. We have previously demonstrated that rMAPC increase their immunomodulatory and neuroprotective properties when they encounter a

neuroinflammatory environment [25]. Notably, apart from being immunomodulatory [25, 30, 38], NO can induce neuronal and oligodendrocyte damage [57]. Although rMAPC did not increase their expression of other proinflammatory cytokines, such as TNF-α, and did not skew macrophages towards an inflammatory phenotype, we cannot rule out the induction of a proinflammatory "MSC1-like" phenotype in rMAPC [58].

Aside from suppressing the inflammatory phenotype of macrophages, factors secreted by macrophage-primed and cytokines-primed rMAPC also intervened with the T cell stimulatory capacity of macrophages potentially by suppressing the expression of the costimulatory molecule CD86. Of note, cytokine-primed rMAPC-conditioned medium did not impact the T cell stimulatory capacity of macrophages to the same extent as macrophage-primed conditioned medium, while it induced greater suppression of CD86 surface expression. This indicates that other mediators than those used in recombinant form (TNF-α, IL-1β, and IL-6) contribute to the observed effects. Moreover, it suggests that additional mechanisms may mediate the effect of rMAPC on macrophage-associated T cell stimulatory activity beyond suppression of costimulatory molecules. Suppression of scavenger receptors, such as CD36 and CD14, that are involved in the recognition of antigens may be one additional mechanism and deserves further investigation as it has already been demonstrated for MSCs [59].

Furthermore, we observed that soluble factors released by macrophage-primed rMAPC directly suppressed antigen-specific T cell proliferation to the same extent as cytokine-primed rMAPC. Previous findings demonstrated the need for MAPC to interact with monocytes in order to suppress homeostatic proliferation of T cells [60]. This effect was attributed to IL-1β-dependent secretion of PGE2 by hMAPC. In line with this finding, we have previously found that IL-1β increases COX-2 mRNA in rMAPC [25]. Overall, we conclude that these immunoregulatory mechanisms can be triggered by activated macrophages while collectively these observations confirm the notion that "licensing" of MAPC enhances their paracrine effects [25, 58, 61] and renders them as an ideal cell type for transplantation in neuroinflammatory conditions.

Migratory and chemoattractive properties of transplanted cells towards myeloid cells are of paramount importance for them to mediate their immunomodulatory properties [62]. We observed that macrophages release soluble molecules that attract rMAPC and increase the expression of chemokines and chemokine receptors in rMAPC. The increase of CCR1 and CCR3 agrees with the observation that their expression is induced by TNF-α and IL-1β on rMAPC [25]. This result is useful for the direct contact interactions or the effectiveness of paracrine mechanisms [63].

5. Conclusions

Macrophages have a bimodal action in autoimmune-mediated CNS diseases; while demyelinating incidents of the CNS drive macrophages and microglia activation thus contributing to the disease pathogenesis [6, 64, 65], macrophage clearance of myelin debris facilitates remyelination and reshapes their morphology towards acquisition of an anti-inflammatory and neuroprotective phenotype [30, 66–68]. Therefore, it is of high importance to elucidate how MAPC modulate the features of myeloid cell types since intravenously transplanted cells are likely to be localized in close proximity with myeloid cells in the CNS and periphery [37, 61, 69]. Overall, we showed that inflammatory macrophages are able to regulate the immunomodulatory properties of rMAPC in vitro, thereby warranting confirmatory in vivo studies. A hypothetical triangle in which inflammatory macrophages and MAPC exert reciprocal effects, leading to decreased T cell proliferation either due to paracrine effects of MAPC or due to the macrophages' reduced ability to contribute to the continuation of immunopathogenesis, should be considered in the design of experimental cell therapy schemes and is the novelty of this study (Figure 8). The efficient adaptation of MAPC in this microenvironment would favor their use in targeting myeloid cell-mediated neuroinflammation which is considered an important step on ongoing MAPC-based clinical trials [70].

Disclosure

Parts of this study have been presented at international conferences and have been published as journal supplements. The two abstracts have been included as supplements, and the data of the publications are the following: *Regen Med* 2013; 8 (6s):S81-S81 and *Neuroimmunomodulation* 2014; 21 (Suppl 1): S7-S7. The listed abstracts are not included in the References list.

Conflicts of Interest

Jef Pinxteren was an employee of ReGenesys BVBA, the European subsidiary of Athersys Inc. while he is currently affiliated with Promethera Biosciences. Robert W. Mays is an employee of Athersys Inc. Robert Deans was previously an employee of Athersys Inc. while he is currently affiliated with Blue Rock Therapeutics. The rest of the authors declare that they have no conflicts of interest.

Authors' Contributions

Stylianos Ravanidis performed the experiments and wrote the manuscript. Stylianos Ravanidis, Jeroen F. J. Bogie, and Niels Hellings designed the experiments of the current study. Jeroen F. J. Bogie, Raf Donders, Robert Deans, Jef Pinxteren, and Robert W. Mays provided the study material and assisted the interpretation of the results. Jerome J. A. Hendriks and Robert W. Mays participated in the conception and design of the study. Piet Stinissen, Jerome J. A. Hendriks, and Robert W. Mays reviewed thoroughly the manuscript. Niels Hellings supervised the study and gave the final approval for the manuscript.

Acknowledgments

The authors would like to further thank Ms. Katrien Wauterickx and Ms. Christel Bocken (Biomedical Research Institute, Hasselt University) for the technical assistance. Moreover, the authors would like to thank Erwin Leysen (UHasselt) for contributing to real-time PCR experiments. Finally, the authors gratefully thank David Craeye and Kristel Gijbels (employees of ReGenesys BVBA) for the technical and scientific input concerning the culture and properties of rMAPC. The current study was financially supported by the Belgian Charcot Foundation.

References

[1] G. Martino, R. J. Franklin, A. Baron Van Evercooren, D. A. Kerr, and Stem Cells in Multiple Sclerosis (STEMS) Consensus Group, "Stem cell transplantation in multiple sclerosis: current status and future prospects," *Nature Reviews Neurology*, vol. 6, no. 5, pp. 247–255, 2010.

[2] J. Zhang, Y. Li, J. Chen et al., "Human bone marrow stromal cell treatment improves neurological functional recovery in EAE mice," *Experimental Neurology*, vol. 195, no. 1, pp. 16–26, 2005.

[3] S. Ravanidis, K. N. Poulatsidou, R. Lagoudaki et al., "Subcutaneous transplantation of neural precursor cells in experimental autoimmune encephalomyelitis reduces chemotactic signals in the central nervous system," *Stem Cells Translational Medicine*, vol. 4, no. 12, pp. 1450–1462, 2015.

[4] S. Pluchino and G. Martino, "The therapeutic plasticity of neural stem/precursor cells in multiple sclerosis," *Journal of the Neurological Sciences*, vol. 265, no. 1-2, pp. 105–110, 2008.

[5] A. Laroni, G. Novi, N. Kerlero de Rosbo, and A. Uccelli, "Towards clinical application of mesenchymal stem cells for treatment of neurological diseases of the central nervous system," *Journal of Neuroimmune Pharmacology*, vol. 8, no. 5, pp. 1062–1076, 2013.

[6] J. F. Bogie, P. Stinissen, and J. J. Hendriks, "Macrophage subsets and microglia in multiple sclerosis," *Acta Neuropathologica*, vol. 128, no. 2, pp. 191–213, 2014.

[7] M. Kouwenhoven, N. Teleshova, V. Ozenci, R. Press, and H. Link, "Monocytes in multiple sclerosis: phenotype and cytokine profile," *Journal of Neuroimmunology*, vol. 112, no. 1-2, pp. 197–205, 2001.

[8] J. J. Hendriks, C. E. Teunissen, H. E. de Vries, and C. D. Dijkstra, "Macrophages and neurodegeneration," *Brain Research. Brain Research Reviews*, vol. 48, no. 2, pp. 185–195, 2005.

[9] Z. Jiang, J. X. Jiang, and G. X. Zhang, "Macrophages: a double-edged sword in experimental autoimmune encephalomyelitis," *Immunology Letters*, vol. 160, no. 1, pp. 17–22, 2014.

[10] A. Mantovani, A. Sica, S. Sozzani, P. Allavena, A. Vecchi, and M. Locati, "The chemokine system in diverse forms of macrophage activation and polarization," *Trends in Immunology*, vol. 25, no. 12, pp. 677–686, 2004.

[11] J. Kim and P. Hematti, "Mesenchymal stem cell-educated macrophages: a novel type of alternatively activated macrophages," *Experimental Hematology*, vol. 37, no. 12, pp. 1445–1453, 2009.

[12] J. Maggini, G. Mirkin, I. Bognanni et al., "Mouse bone marrow-derived mesenchymal stromal cells turn activated macrophages into a regulatory-like profile," *PLoS One*, vol. 5, no. 2, article e9252, 2010.

[13] H. Nakajima, K. Uchida, A. R. Guerrero et al., "Transplantation of mesenchymal stem cells promotes an alternative pathway of macrophage activation and functional recovery after spinal cord injury," *Journal of Neurotrauma*, vol. 29, no. 8, pp. 1614–1625, 2012.

[14] J. H. Ylostalo, T. J. Bartosh, K. Coble, and D. J. Prockop, "Human mesenchymal stem/stromal cells cultured as spheroids are self-activated to produce prostaglandin E2 that directs stimulated macrophages into an anti-inflammatory phenotype," *Stem Cells*, vol. 30, no. 10, pp. 2283–2296, 2012.

[15] K. Anton, D. Banerjee, and J. Glod, "Macrophage-associated mesenchymal stem cells assume an activated, migratory, pro-inflammatory phenotype with increased IL-6 and CXCL10 secretion," *PLoS One*, vol. 7, no. 4, article e35036, 2012.

[16] Z. Rahmat, S. Jose, R. Ramasamy, and S. Vidyadaran, "Reciprocal interactions of mouse bone marrow-derived mesenchymal stem cells and BV2 microglia after lipopolysaccharide stimulation," *Stem Cell Research & Therapy*, vol. 4, no. 1, p. 12, 2013.

[17] S. A. Jacobs, V. D. Roobrouck, C. M. Verfaillie, and S. W. Van Gool, "Immunological characteristics of human mesenchymal stem cells and multipotent adult progenitor cells," *Immunology and Cell Biology*, vol. 91, no. 1, pp. 32–39, 2013.

[18] Y. Jiang, B. N. Jahagirdar, R. L. Reinhardt et al., "Pluripotency of mesenchymal stem cells derived from adult marrow," *Nature*, vol. 418, no. 6893, pp. 41–49, 2002.

[19] S. Mora-Lee, M. S. Sirerol-Piquer, M. Gutierrez-Perez et al., "Therapeutic effects of hMAPC and hMSC transplantation after stroke in mice," *PLoS One*, vol. 7, no. 8, article e43683, 2012.

[20] G. M. Sindberg, B. A. Lindborg, Q. Wang et al., "Comparisons of phenotype and immunomodulatory capacity among rhesus bone-marrow-derived mesenchymal stem/stromal cells, multipotent adult progenitor cells, and dermal fibroblasts," *Journal of Medical Primatology*, vol. 43, no. 4, pp. 231–241, 2014.

[21] S. S. Bedi, R. Hetz, C. Thomas et al., "Intravenous multipotent adult progenitor cell therapy attenuates activated microglial/macrophage response and improves spatial learning after traumatic brain injury," *Stem Cells Translational Medicine*, vol. 2, no. 12, pp. 953–960, 2013.

[22] M. A. DePaul, M. Palmer, B. T. Lang et al., "Intravenous multipotent adult progenitor cell treatment decreases inflammation leading to functional recovery following spinal cord injury," *Scientific Reports*, vol. 5, article 16795, 2015.

[23] P. A. Walker, S. S. Bedi, S. K. Shah et al., "Intravenous multipotent adult progenitor cell therapy after traumatic brain injury: modulation of the resident microglia population," *Journal of Neuroinflammation*, vol. 9, p. 228, 2012.

[24] S. A. Busch, J. A. Hamilton, K. P. Horn et al., "Multipotent adult progenitor cells prevent macrophage-mediated axonal dieback and promote regrowth after spinal cord injury," *The Journal of Neuroscience*, vol. 31, no. 3, pp. 944–953, 2011.

[25] S. Ravanidis, J. F. Bogie, R. Donders et al., "Neuroinflammatory signals enhance the immunomodulatory and neuroprotective properties of multipotent adult progenitor cells," *Stem Cell Research & Therapy*, vol. 6, no. 1, p. 176, 2015.

[26] R. K. Jellema, D. R. Ophelders, A. Zwanenburg et al., "Multipotent adult progenitor cells for hypoxic-ischemic injury in

the preterm brain," *Journal of Neuroinflammation*, vol. 12, no. 1, p. 241, 2015.

[27] K. Subramanian, M. Geraerts, K. A. Pauwelyn et al., "Isolation procedure and characterization of multipotent adult progenitor cells from rat bone marrow," *Methods in Molecular Biology*, vol. 636, pp. 55–78, 2010.

[28] J. J. Hendriks, H. Slaets, S. Carmans et al., "Leukemia inhibitory factor modulates production of inflammatory mediators and myelin phagocytosis by macrophages," *Journal of Neuroimmunology*, vol. 204, no. 1-2, pp. 52–57, 2008.

[29] K. B. Lane, B. Egan, S. Vick, R. Abdolrasulnia, and V. L. Shepherd, "Characterization of a rat alveolar macrophage cell line that expresses a functional mannose receptor," *Journal of Leukocyte Biology*, vol. 64, no. 3, pp. 345–350, 1998.

[30] J. F. Bogie, P. Stinissen, N. Hellings, and J. J. Hendriks, "Myelin-phagocytosing macrophages modulate autoreactive T cell proliferation," *Journal of Neuroinflammation*, vol. 8, p. 85, 2011.

[31] J. Croitoru-Lamoury, F. M. Lamoury, J. J. Zaunders, L. A. Veas, and B. J. Brew, "Human mesenchymal stem cells constitutively express chemokines and chemokine receptors that can be upregulated by cytokines, IFN-beta, and Copaxone," *Journal of Interferon & Cytokine Research*, vol. 27, no. 1, pp. 53–64, 2007.

[32] C. A. Schneider, W. S. Rasband, and K. W. Eliceiri, "NIH image to ImageJ: 25 years of image analysis," *Nature Methods*, vol. 9, no. 7, pp. 671–675, 2012.

[33] A. Untergasser, I. Cutcutache, T. Koressaar et al., "Primer3—new capabilities and interfaces," *Nucleic Acids Research*, vol. 40, no. 15, article e115, 2012.

[34] K. J. Livak and T. D. Schmittgen, "Analysis of relative gene expression data using real-time quantitative PCR and the 2(−delta delta C(T)) method," *Methods*, vol. 25, no. 4, pp. 402–408, 2001.

[35] J. Vandesompele, K. De Preter, F. Pattyn et al., "Accurate normalization of real-time quantitative RT-PCR data by geometric averaging of multiple internal control genes," *Genome Biology*, vol. 3, no. 7, article RESEARCH0034, 2002.

[36] D. Linares, M. Taconis, P. Mana et al., "Neuronal nitric oxide synthase plays a key role in CNS demyelination," *The Journal of Neuroscience*, vol. 26, no. 49, pp. 12672–12681, 2006.

[37] K. Nemeth, A. Leelahavanichkul, P. S. Yuen et al., "Bone marrow stromal cells attenuate sepsis via prostaglandin E(2)-dependent reprogramming of host macrophages to increase their interleukin-10 production," *Nature Medicine*, vol. 15, no. 1, pp. 42–49, 2009.

[38] G. W. Ren, L. Y. Zhang, X. Zhao et al., "Mesenchymal stem cell-mediated immunosuppression occurs via concerted action of chemokines and nitric oxide," *Cell Stem Cell*, vol. 2, no. 2, pp. 141–150, 2008.

[39] T. B. Jones, D. M. Basso, A. Sodhi et al., "Pathological CNS autoimmune disease triggered by traumatic spinal cord injury: implications for autoimmune vaccine therapy," *The Journal of Neuroscience*, vol. 22, no. 7, pp. 2690–2700, 2002.

[40] K. Kil, Y. C. Zang, D. Yang et al., "T cell responses to myelin basic protein in patients with spinal cord injury and multiple sclerosis," *Journal of Neuroimmunology*, vol. 98, no. 2, pp. 201–207, 1999.

[41] D. Tugal, X. Liao, and M. K. Jain, "Transcriptional control of macrophage polarization," *Arteriosclerosis, Thrombosis, and Vascular Biology*, vol. 33, no. 6, pp. 1135–1144, 2013.

[42] B. Becher, I. Bechmann, and M. Greter, "Antigen presentation in autoimmunity and CNS inflammation: how T lymphocytes recognize the brain," *Journal of Molecular Medicine (Berlin)*, vol. 84, no. 7, pp. 532–543, 2006.

[43] R. Jin, G. Yang, and G. Li, "Inflammatory mechanisms in ischemic stroke: role of inflammatory cells," *Journal of Leukocyte Biology*, vol. 87, no. 5, pp. 779–789, 2010.

[44] A. Katsumoto, H. Lu, A. S. Miranda, and R. M. Ransohoff, "Ontogeny and functions of central nervous system macrophages," *Journal of Immunology*, vol. 193, no. 6, pp. 2615–2621, 2014.

[45] K. W. Selmaj and C. S. Raine, "Tumor necrosis factor mediates myelin and oligodendrocyte damage in vitro," *Annals of Neurology*, vol. 23, no. 4, pp. 339–346, 1988.

[46] J. Beck, P. Rondot, L. Catinot, E. Falcoff, H. Kirchner, and J. Wietzerbin, "Increased production of interferon gamma and tumor necrosis factor precedes clinical manifestation in multiple sclerosis: do cytokines trigger off exacerbations?" *Acta Neurologica Scandinavica*, vol. 78, no. 4, pp. 318–323, 1988.

[47] Q. Li, W. Sun, X. Wang, K. Zhang, W. Xi, and P. Gao, "Skin-derived mesenchymal stem cells alleviate atherosclerosis via modulating macrophage function," *Stem Cells Translational Medicine*, vol. 4, no. 11, pp. 1294–1301, 2015.

[48] G. M. Spaggiari, H. Abdelrazik, F. Becchetti, and L. Moretta, "MSCs inhibit monocyte-derived DC maturation and function by selectively interfering with the generation of immature DCs: central role of MSC-derived prostaglandin E2," *Blood*, vol. 113, no. 26, pp. 6576–6583, 2009.

[49] V. Dayan, G. Yannarelli, F. Billia et al., "Mesenchymal stromal cells mediate a switch to alternatively activated monocytes/macrophages after acute myocardial infarction," *Basic Research in Cardiology*, vol. 106, no. 6, pp. 1299–1310, 2011.

[50] Q. Z. Zhang, W. R. Su, S. H. Shi et al., "Human gingiva-derived mesenchymal stem cells elicit polarization of m2 macrophages and enhance cutaneous wound healing," *Stem Cells*, vol. 28, no. 10, pp. 1856–1868, 2010.

[51] G. Ren, X. Zhao, L. Zhang et al., "Inflammatory cytokine-induced intercellular adhesion molecule-1 and vascular cell adhesion molecule-1 in mesenchymal stem cells are critical for immunosuppression," *Journal of Immunology*, vol. 184, no. 5, pp. 2321–2328, 2010.

[52] M. M. Duffy, J. Pindjakova, S. A. Hanley et al., "Mesenchymal stem cell inhibition of T-helper 17 cell-differentiation is triggered by cell-cell contact and mediated by prostaglandin E2 via the EP4 receptor," *European Journal of Immunology*, vol. 41, no. 10, pp. 2840–2851, 2011.

[53] Z. Xing, J. Gauldie, G. Cox et al., "IL-6 is an antiinflammatory cytokine required for controlling local or systemic acute inflammatory responses," *The Journal of Clinical Investigation*, vol. 101, no. 2, pp. 311–320, 1998.

[54] R. M. Gallucci, P. P. Simeonova, J. M. Matheson et al., "Impaired cutaneous wound healing in interleukin-6-deficient and immunosuppressed mice," *The FASEB Journal*, vol. 14, no. 15, pp. 2525–2531, 2000.

[55] H. Roca, Z. S. Varsos, S. Sud, M. J. Craig, C. Ying, and K. J. Pienta, "CCL2 and interleukin-6 promote survival of human CD11b+ peripheral blood mononuclear cells and induce M2-type macrophage polarization," *The Journal of Biological Chemistry*, vol. 284, no. 49, pp. 34342–34354, 2009.

[56] C. Bouffi, C. Bony, G. Courties, C. Jorgensen, and D. Noël, "IL-6-dependent PGE2 secretion by mesenchymal stem cells inhibits local inflammation in experimental arthritis," *PLoS One*, vol. 5, no. 12, article e14247, 2010.

[57] A. di Penta, B. Moreno, S. Reix et al., "Oxidative stress and proinflammatory cytokines contribute to demyelination and axonal damage in a cerebellar culture model of neuroinflammation," *PLoS One*, vol. 8, no. 2, article e54722, 2013.

[58] M. Krampera, "Mesenchymal stromal cell 'licensing': a multistep process," *Leukemia*, vol. 25, no. 9, pp. 1408–1414, 2011.

[59] L. P. Erwig and P. M. Henson, "Clearance of apoptotic cells by phagocytes," *Cell Death and Differentiation*, vol. 15, no. 2, pp. 243–250, 2008.

[60] J. L. Reading, B. Vaes, C. Hull et al., "Suppression of IL-7-dependent effector T-cell expansion by multipotent adult progenitor cells and PGE2," *Molecular Therapy*, vol. 23, no. 11, pp. 1783–1793, 2015.

[61] R. Donders, M. Vanheusden, J. F. Bogie et al., "Human Wharton's jelly-derived stem cells display immunomodulatory properties and transiently improve rat experimental autoimmune encephalomyelitis," *Cell Transplantation*, vol. 24, no. 10, pp. 2077–2098, 2014.

[62] V. Neirinckx, G. Agirman, C. Coste et al., "Adult bone marrow mesenchymal and neural crest stem cells are chemoattractive and accelerate motor recovery in a mouse model of spinal cord injury," *Stem Cell Research & Therapy*, vol. 6, p. 211, 2015.

[63] E. Eggenhofer, F. Luk, M. H. Dahlke, and M. J. Hoogduijn, "The life and fate of mesenchymal stem cells," *Frontiers in Immunology*, vol. 5, p. 148, 2014.

[64] S. David, A. D. Greenhalgh, and A. Kroner, "Macrophage and microglial plasticity in the injured spinal cord," *Neuroscience*, vol. 307, pp. 311–318, 2015.

[65] C. L. Hsieh, C. C. Kim, B. E. Ryba et al., "Traumatic brain injury induces macrophage subsets in the brain," *European Journal of Immunology*, vol. 43, no. 8, pp. 2010–2022, 2013.

[66] J. F. Bogie, W. Jorissen, J. Mailleux et al., "Myelin alters the inflammatory phenotype of macrophages by activating PPARs," *Acta Neuropathologica Communications*, vol. 1, no. 1, p. 43, 2013.

[67] V. E. Miron, A. Boyd, J. W. Zhao et al., "M2 microglia and macrophages drive oligodendrocyte differentiation during CNS remyelination," *Nature Neuroscience*, vol. 16, no. 9, pp. 1211–1218, 2013.

[68] M. van Zwam, J. N. Samsom, E. E. Nieuwenhuis et al., "Myelin ingestion alters macrophage antigen-presenting function in vitro and in vivo," *Journal of Leukocyte Biology*, vol. 90, no. 1, pp. 123–132, 2011.

[69] B. Wagner and R. Henschler, "Fate of intravenously injected mesenchymal stem cells and significance for clinical application," *Advances in Biochemical Engineering/Biotechnology*, vol. 130, pp. 19–37, 2013.

[70] D. C. Hess, C. A. Sila, A. J. Furlan, L. R. Wechsler, J. A. Switzer, and R. W. Mays, "A double-blind placebo-controlled clinical evaluation of MultiStem for the treatment of ischemic stroke," *International Journal of Stroke*, vol. 9, no. 3, pp. 381–386, 2014.

Hindawi
Stem Cells International
Volume 2017, Article ID 4758930, 12 pages
https://doi.org/10.1155/2017/4758930

Research Article

Human Suprapatellar Fat Pad-Derived Mesenchymal Stem Cells Induce Chondrogenesis and Cartilage Repair in a Model of Severe Osteoarthritis

Ignacio Muñoz-Criado,[1] Jose Meseguer-Ripolles,[2] Maravillas Mellado-López,[2] Ana Alastrue-Agudo,[2] Richard J Griffeth,[2] Jerónimo Forteza-Vila,[3] Ramón Cugat,[4,5] Montserrat García,[4,5] and Victoria Moreno-Manzano[2,6,7]

[1]*Unidad de Traumatología, Hospital Casa de la Salud, Valencia, Spain*
[2]*Neuronal and Tissue Regeneration Lab, Centro de Investigación Príncipe Felipe, Valencia, Spain*
[3]*Molecular Pathology and Translational Research in Oncology, Unidad Mixta Universidad Católica de Valencia y Centro de Investigación Príncipe Felipe, Valencia, Spain*
[4]*Unidad de Artroscopia y Unidad de Traumatología del Hospital Quiron, Barcelona, Spain*
[5]*Fundación García Cugat, Barcelona, Spain*
[6]*Universidad Católica de Valencia, Valencia, Spain*
[7]*FactorStem Ltd., Valencia, Spain*

Correspondence should be addressed to Victoria Moreno-Manzano; vmorenom@cipf.es

Received 5 December 2016; Accepted 23 April 2017; Published 9 July 2017

Academic Editor: Gerald A. Colvin

Cartilage degeneration is associated with degenerative bone and joint processes in severe osteoarthritis (OA). Spontaneous cartilage regeneration is extremely limited. Often the treatment consists of a partial or complete joint implant. Adipose-derived stem cell (ASC) transplantation has been shown to restore degenerated cartilage; however, regenerative differences of ASC would depend on the source of adipose tissue. The infra- and suprapatellar fat pads surrounding the knee offer a potential autologous source of ASC for patients after complete joint substitution. When infrapatellar- and suprapatellar-derived stromal vascular fractions (SVF) were compared, a significantly higher CD105 (+) population was found in the suprapatellar fat. In addition, the suprapatellar SVF exhibited increased numbers of colony formation units and a higher population doubling in culture compared to the infrapatellar fraction. Both the suprapatellar- and infrapatellar-derived ASC were differentiated in vitro into mature adipocytes, osteocytes, and chondrocytes. However, the suprapatellar-derived ASC showed higher osteogenic and chondrogenic efficiency. Suprapatellar-derived ASC transplantation in a severe OA mouse model significantly diminished the OA-associated knee inflammation and cartilage degenerative grade, significantly increasing the production of glycosaminoglycan and inducing endogenous chondrogenesis in comparison with the control group. Overall, suprapatellar-derived ASC offer a potential autologous regenerative treatment for patients with multiple degenerative OA.

1. Introduction

Osteoarthritis (OA) is a degenerative joint disease with no efficient treatment due to limited endogenous regenerative capacity. It affects the knees of nearly a quarter of the population aged 60 and older [1, 2]. Currently, patients with severe OA are inexorably relegated to prosthetic joint substitution. OA is a disorder involving movable joints characterized by cell stress and extracellular matrix degradation initiated by micro- and macroinjury that activates maladaptive repair responses including proinflammatory pathways of innate immunity. The disease is first manifested as a molecular

derangement (abnormal joint tissue metabolism) followed by anatomic and/or physiologic derangements (characterized by cartilage degradation, bone remodelling, osteophyte formation, joint inflammation, and loss of normal joint function) culminating in disease [3, 4].

Since the OA pathological processes are well described involving among others, the loss of functional chondrocytes, several cell-based therapeutic approaches have already been successfully developed including bone-marrow stimulation [5], implantation of osteochondral autograft [6] or allografts (ACI) [7], and transplantation of expanded autologous chondrocytes [8], or amplified mesenchymal stem cells (MSCs) [9], which help to restore articular cartilage. The intra-articular administration of MSC directly in the synovial fluid has been the predominant cell-based approach, with already demonstrated clinical effectiveness, with probed regenerative and immunosuppressant activities [9, 10]. To date, it continues to be an important avenue of research and clinical development due to its extraordinary therapeutic aptitude. However, the direct differentiation of multipotent MSC into cells of the chondrogenic lineage has led to a variety of experimental strategies to investigate whether tissue-specific MSCs are preferential for the regeneration and maintenance of articular cartilage [9]. Additional efforts on engineered cartilage implants are also done by using MSC synergistically activated with biomolecules to potentially improve chondral and osteochondral lesion repair, converting those in specialized trophic producers to initiate endogenous regenerative activities in the OA joint [11–13]. The long-term durability, increased tissue integration, and specific activity depend first on better transplantation survival rates and better adaptation to the hostile environment which still comprises a challenge. To date, there is not a precise description of which donor sample would be more efficient in the generation of MSC for the treatment and repair of joints in a degenerative process. Subcutaneous fat tissue is the most accessible source; however, after prosthetic implementation for joint substitution, the supra- and infrapatellar fat pads are commonly resected, constituting a suitable autologous adipose-derived MSC source (ASC). The infrapatellar or Hoffa's fat pad is an intracapsular but extrasynovial structure, situated in the knee under the patella, between the patellar tendon, femoral condyle, and tibia plateau [14]. The suprapatellar or quadricep fat pad is externally interposed between the joint capsule and the synovium, lined to the joint cavity showing a triangular shape and extended through the patellar base [15]. Previous studies have already described the potential regenerative capability of ASC derived from the infrapatellar pad in a model of OA [16, 17], showing in fact a higher percentage of immunophenotypical positive stromal cells in comparison with those obtained from subcutaneous fat [18]. However, no previous data has been reported regarding the suprapatellar tissue regenerative capacity. In addition, recent reports also focus on the role of the Hoffa's-derived cells, such as inflammatory cells releasing or inducing the release of inflammatory mediators such as IL-6, IL-8, TNFα, and PGE2 when derived from OA patients, suggesting that the infrapatellar fat pad is an active joint tissue in the initiation and progression of knee OA [19–22].

There are stem cell niches with no spontaneous capacity to mobilize to the injury to repair the severe OA defects. The amplification of these cells from these specialized sources could render an optimal source of autologous or even allogenic applications to promote cartilage regeneration. Indeed, the patellar fat pad-derived ASC would offer a potential autologous regenerative treatment for patients with multiple degenerative OA.

2. Material and Methods

2.1. Adipose Tissue Processing, SVF Isolation, and ASC Culture. Twenty-four patients between 50 and 80 years old indicated for complete joint substitution were included in the study. All patients were asked to sign an informed consent for the use of surplus fat tissue in the prosthesis surgery as well as a donation of peripheral blood (~20 ml) for autologous serum isolation. The samples, adipose tissue from supra- or infrapatellar areas, were anonymized and individually housed and collected inside the surgery room in sterile containers with sterile saline. This experimental procedure has been evaluated and accepted by the Regional Ethics Committee for Clinical Research with Medicines and Health Products following the Code of Practice 2014/01. As exclusion criteria, no samples were collected from patients with a history of cancer and infectious diseases active at the time of the surgery (viral or bacterial).

The adipose tissue, from supra- or infrapatellar areas, was transferred from the surgery room to the laboratory in a hermetic container at 4°C in sterile solution. The samples were washed multiple times in PBS plus antibiotics to clean the tissue and remove residual blood. The samples were distributed within 10 g of adipose tissue per 100 mm petri dish, with a solution containing PBS, 100 units/ml penicillin and 100 μg/ml streptomycin (Gibco 15,140), collagenase type IA (0.07%, Sigma C9891 CA, USA), and dispase I (0.2 mM Sigma). The tissue was cut into small pieces using sterile surgical scissors in a laminar flow hood and digested in a closed cell flask overnight in a shaker at 37°C, 20% O_2, 5% CO_2. The following day, the digested adipose tissue was collected and washed multiple times with PBS plus antibiotic by serial centrifugation. The cell pellet constitutes the stromal vascular fraction (SVF) and was suspended in 1 ml of PBS for cell counting via a Neubauer® chamber. For FACS analysis, 10^5 cells were utilized for each pair of antibodies. The remaining cells were employed for cell amplification and posterior analysis, distributed in two groups, growth in 10% human serum containing medium or 10% fetal bovine serum (in DMEM medium containing 2 mM L-glutamine, 30% L-glucose, 100 units/ml penicillin, and 100 μg/ml streptomycin), plated in petri dishes, and incubated overnight. The following day, the medium was removed and replaced with fresh medium and attached cells were allowed to grow until nearly confluent and then subjected to cell proliferative analysis, clonicity assay, morphological assessments, and FACS analysis and cell differentiation assays.

2.2. FACS Analysis. The SVF was assayed for cell surface protein expression by flow cytometry (FC500, Beckman Cultek, USA). 10^5 cells, diluted into 100 μl of PBS were incubated with 1 : 50 dilution for every pair of antibodies: CD90-PE and CD29-APC, CD44-PE-Cy, CD117-APC, CD105-PE, CD45-FITC, and CD34-PE (BD Pharmigen, USA). As a negative control, cell suspension without antibody was employed following the same procedure. Cells were incubated in the dark for 45 min at room temperature and then washed three times with PBS and suspended in 0.3 ml of cold PBS for FACS analysis. The mean ± SD of every identified population (in percentage) of all tested samples was determined.

2.3. Colony Formation Assay. The amplification and expansion of the ASC population from the SVF involves first the colony forming units after attachment onto a substrate and then a subsequent amplification in the presence of appropriate growth factors [23]. Fifty cells at passage three of every sample, supra- and infrapatellar, of four different patients were seeded in 6-well plates in the presence of 10% human serum or 10% fetal bovine serum containing medium for 10 days. The medium was replaced every third day. Subsequently, the cells were fixed with cold methanol for 5 minutes and washed with PBS before incubating in Giemsa solution (Sigma, USA) for 30 minutes. The excess stain was removed by subsequent washes with tap water. The cells were allowed to air dry and then visualized under the microscope. The mean ± SD of the total number of colonies at each condition of all tested samples was determined.

2.4. ASC Proliferative Analysis. At passage three of every sample, supra- and infrapatellar, 10^4 cells were seeded in 24-well plates in the presence of 10% human serum or 10% fetal bovine serum containing medium. Cells were seeded for up to ten days of analysis, by quantifying the number of cells in a Neubauer chamber every day in every well. The mean ± SD at every time point (every consecutive day) was represented.

2.5. Transmission Electron Microscopy. Cells were seeded at 2000 cells/cm^2 in Lab-Tek chamber slides of 2 wells (Nalge Nunc International, Naperville, IL) and were fixed in 3% glutaraldehyde for 1 hour at 37°C. Cells were postfixed in 2% OsO4 for 1 hour at room temperature and stained in 1% uranyl acetate in the dark for 2 h at 4°C. Finally, cells were rinsed in distilled water, dehydrated in ethanol, and infiltrated overnight in Durcupan resin (Fluka, Sigma-Aldrich, St. Louis, USA). Following polymerization, embedded cultures were detached from the chamber slide and glued to araldite blocks. Serial semithin sections (1.5 μm) were cut with an Ultracut UC-6 (Leica, Heidelberg, Germany) and mounted onto slides and stained with 1% toluidine blue. Selected semithin sections were glued with Super Glue-3, Loctite (Henkel, Düsseldorf, Germany), to araldite blocks and detached from the glass slide by repeated freezing (in liquid nitrogen) and thawing. Ultrathin sections (0.06–0.08 μm) were prepared with the Ultracut and stained with lead citrate. Finally, photomicrographs were obtained under a transmission electron microscope FEI Tecnai G2 Spirit (FEI Europe, Eindhoven, Netherlands) using a digital camera Morada (Olympus Soft Image Solutions GmbH, Münster, Germany).

2.6. ASC Directed-Differentiation. ASC at or after passage 4 were subjected to directed differentiation [24], to induce adipogenesis, osteogenesis, and chondrogenesis, for each sample, supra- and infrapatellar from three different patients. All directed-differentiation media were obtained from Lonza (Lonza Co., Basel, Switzerland). *Adipogenesis*: ASC were seeded at a cell density of 10,000 cells/cm^2 and when ASC were >90% confluent, the growth medium was substituted for differentiation medium containing insulin, dexamethasone, IBMX (3-isobutyl-methyl-xantine), and indomethacin (adipose-derived stem cell basal medium; Lonza Co.). The cells were then incubated in standard cell culture conditions for 12 days. The adipogenic differentiation was evaluated by Oil Red staining of the lipid vacuoles in formalin-fixed cultures; Oil Red O stock solution (5 g/l of isopropanol) was diluted 6/10 in water and incubated for 1 hour at RT. Serial washes with water to remove the excess staining were applied. After bright-field picture acquisition, total Oil Red O stain was extracted with 100% isopropanol for 5 min with gentle rocking and the absorbance at 492 nm was quantified. The mean ± SD of the absolute numbers at each condition of all tested samples was determined. *Osteogenesis*: ASC were seeded at a cell density of 10,000 cells/cm^2 in collagen I (Sigma; 10 mM) coated plates in medium containing 0.1 μM dexamethasone, 50 μM Asc2P, and 10 mM μ-glycerophosphate (osteogenic basal medium; Lonza Co.) with 10% human serum. ASC cultures were maintained in this medium for 4 weeks (with medium changes every 3 days). For detection of extracellular calcium deposits, Alizarin red staining was used in formalin-fixed cultures; Alizarin red solution (0.2 g/l water) was incubated for 2-3 minutes, until the reaction was observed microscopically. Excess dye was removed by several washing steps using water. The orange-red calcium precipitates were quantified from at least four different pictures of each sample by using ImageJ software. *Chondrogenesis*: The ASC culture was performed from cell "Micromass" starting with a high concentration of cells in a minimal volume (1×10^5 cells/100 μl) in the presence of TGF-β 1 and 3 (10 ng/ml), Asc 2P (50 μM), and insulin (6.25 μg/ml) (Chondro BulletKit; Lonza Co.) for four weeks with medium changes every 3 days. Alcian blue (0.1 g/l in water, pH 1.0) was used to detect the presence of enrichment of sulphated proteoglycans in the extracellular matrix. Before staining, the micromass cultures were fixed in formalin, embedded in paraffin, and sectioned into 10 μm. Blue staining was quantified from 4 different pictures of each sample with ImageJ software.

2.7. OA Mouse Model and Cell Transplantation. Twelve-week old adult male C57BL6 mice were experimentally induced to have severe OA in both knees by a single injection of 13 U collagenase II in 6 μl of 5 mM $CaCl_2$ [25]. Five days later, when the OA by severe cartilage damage was induced, all animals were distributed into 4 groups ($n = 6$ per group). The *control* group was injected with 6 μl of growth cell culture medium; 10^5 cells in 6 μl of SVF or hASC (from suprapatellar

fat pad) were injected in the SVF or hASC groups, respectively. Six μl of thawed pooled human platelet rich plasma (PRP) was injected in the PRP group. All intra-articular injections were performed by using a 30G Hamilton syringe connected to a Remote Infuse/withdraw pump 11 elite nanomite programmable syringe pump (Harvard Apparatus) at a 2 μl/min infusion rate. The PRP was isolated from blood collected from all patients in citrate tubes and was prepared following the standardized method described in Anitua et al. [26] and pooled to minimize individual modifications. All animals were sacrificed one month after OA induction, and knee joints were collected. The experimental protocol was approved by the Animal Care Committee of the Centro de Investigación Principe Felipe (Valencia, Spain) in accordance with the National Guide to the Care and Use of Experimental Animals (Real Decreto 53/2013). The leg was isolated and osteomized in the middle of the femoral shaft and in the middle of the tibia and fibula to get the whole joint. Most of the adherent connective tissue, including muscle, ligaments, and tendons, surrounding the knee were removed preventing any damage to the cartilage. One knee was used for histological analysis and the other knee for the quantification of glycosaminoglycans (GAGs).

2.8. GAG Analysis. Immediately after tissue dissections, GAGs were individually quantified for tibia and femur portions from one treated knee of all animals in all groups. Weighted samples were digested in 2.5% papain solution by overnight incubation at 65°C. The supernatant was incubated with 10% Alcian blue working solution containing 0.25% of Triton X-100 in 18 mM H_2SO_4 and then incubated with dissociation solution (4 M guanidine HCl, 0.375 Triton X-100 in 0.027 M H_2SO_4) for 30 min. The precipitated GAGs were suspended in 8 M guanidine HCl and quantified at 570 nm. A chondroitin sulfate standard curve was prepared in parallel.

2.9. Safranin-O Staining and Histological OA Scoring. Bones fixed in 4% PFA were incubated for 7 days in 0.1 M ethylene diamine tetra-acetic acid (EDTA) for decalcification before paraffin embedding and frontally sectioning the entire knee into 5 μm sections. Deparaffinized and hydrated slices were first stained for 5 min with hematoxylin (Sigma) and, after several washes, quickly destained in acid EtOH, stained with fast green (0.001%) solution for 5 minutes, quickly rinsed with 1% acetic acid solution, and then stained with 0.1% safranin-O solution for 5 minutes. Dehydrated samples were mounted in Eukit. Bright-field pictures of all series (every 4th section) were acquired for OA score quantification following the recommendations established by Glasson et al. [27]. The entire joint was analysed at all four quadrants and through multiple step sections through the joint following the 0–6 subjective scoring system, where 0 is normal; 0.5 means loss of safranin-O without structural changes; 1, small fibrillations without loss of cartilage; 2, vertical clefts down to the layer immediately below the superficial layer and some loss of surface lamina; 3, vertical clefts/erosion to the calcified cartilage extending to <25% of the articular surface; 4, vertical clefts/erosion to the calcified cartilage extending to 25–50% of the articular surface; 5, vertical clefts/erosion to the calcified cartilage extending to 50–75% of the articular surface; and 6, vertical clefts/erosion to the calcified cartilage extending to >75% of the articular surface.

2.10. Immunoassay. Both fixed cells on a cover slip from osteogenic-directed differentiation or the chondrogenic-directed differentiated as well as fixed bone (after demineralization by EDTA immersion) paraffin-embedding sections were subjected to protein expression analysis by specific immunostaining. The paraffin-embedded sections were first deparaffinized. Both were fixed with 4% paraformaldehyde at room temperature for 10 min and washed with PBS, permeabilized with a PBS solution containing 0.1% Triton X-100, and blocked with 5% goat serum in PBS for 1 h. The following primary antibodies were diluted in blocking solution and incubated overnight at 4°C. Polyclonal rabbit α-Sox9 (Millipore (1 : 200) or monoclonal mouse α-Connexin 43 (Invitrogen; (1 : 200). After being rinsed three times with PBS, the cells were incubated with Alexa647 dye conjugated goat anti-mouse IgG (1 : 400; Invitrogen, CA, USA) secondary antibody and Phalloidin-Alexa 488 (Invitrogen, CA, USA) for 1 h at room temperature. Tissues were incubated with Oregon Green-488 dye conjugated goat anti-rabbit IgG (1 : 400; Invitrogen, CA, USA) secondary antibody. All samples were counterstained by incubation with 4,6-diamidino-2-phenylindole hydrochloride (DAPI) from Molecular Probes (Invitrogen, USA) for 3 min at room temperature followed by washing steps. Samples were mounted using Fluor Save Reagent (Calbiochem, USA). Signals were visualized by confocal microscopy (Leica, Germany); at least 6 different fields per condition and assay were analysed.

2.11. PET Analysis. For PET image acquisition (Albira Si PET subsystem; Oncovision, Spain), an additional group of animals was included. After OA induction, the right knee was injected with medium (control) and the left knee was injected with 10^5 hASC in 6 μl each, in order to minimize individual differences of the NaF-18 probe signal distribution and acquisition. The probe was i.v. injected though the tail with a range of activities between 177 and 199 uCi with uptake times that varied between 83 and 110 min. In all cases, the whole body PET scan time was 10 minutes. The images were analysed by using Amide® software. The mean ± SD of the ROIs at each condition of all animals was determined.

2.12. Statistical Analysis. Statistical comparisons were assessed by Student's *t*-test. All *P* values were derived from a two-tailed statistical test using the SPSS 11.5 software. A *P* value <0.05 was considered statistically significant.

3. Results

3.1. Suprapatellar Fat Pad SVF Is Enriched in CD105 Positive Cells. The supra- and infrapatellar fat pads of twenty-four patients with severe OA were resected during the surgical intervention for prosthetic implantation. After tissue processing, total cell counting rendered no significant differences in the amount of nucleated cells between the supra- or infrapatellar samples ($7.8 \times 10^5 \pm 2.8 \times 10^5$ infrapatellar cells versus $8.8 \times 10^5 \pm 4.4 \times 10^5$ suprapatellar cells/g of

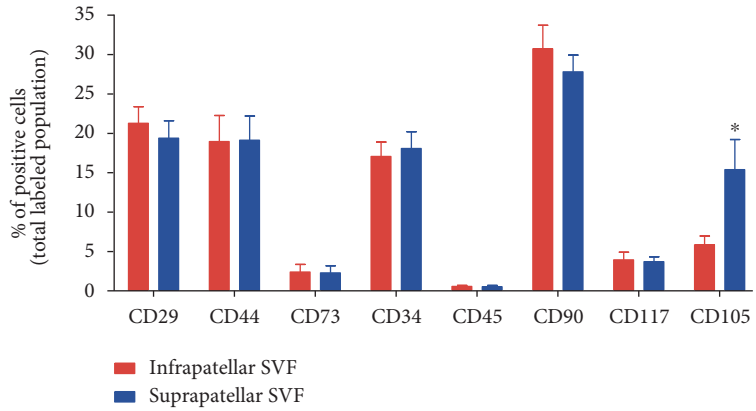

Figure 1: Supra- and infrapatellar fat pad cell populations in the SVF. The SVF derived from the mechanical and enzymatic homogenization of each fat pad of the knee were subjected to FACS analysis for immunodetection of mesenchymal superficial cell markers CD29, CD90, CD44, CD117, and CD105 as well as the hematopoietic cell marker CD34 and the mature leukocyte marker CD45. The positive cell populations were expressed as a percentage of the total analysed cell population. The mean ± SD of the identified population (in percentage) of twenty-four different samples was shown. $^*P < 0.05$ in comparison with infrapatellar group.

adipose tissue; Supplementary Figure available online at https://doi.org/10.1155/2017/4758930). The immunophenotypic analysis of the SVF showed in both cases a positive population for a panel of typical human mesenchymal cell markers including CD90, CD29, CD44, CD117, and CD105 (Figure 1) [28]. Interestingly, the suprapatellar-derived SVF contained a significant enrichment of CD105(+) cells in comparison with the infrapatellar-derived cell suspension (Figure 1). No significant differences were detected in any other assayed marker, including the hematopoietic precursor cell marker CD34 or the mature leucocyte cell marker CD45.

3.2. The Suprapatellar ASC Show a Faster Proliferative Profile. ASC cultures derived from both supra- and infrapatellar tissues were allowed to reach cell confluency and were kept for three passages before cell proliferative analysis in the presence of human serum (HS) or fetal bovine serum (FBS). For colony-forming unit (CFU) quantification, a clonogenic assay was performed (Figure 2(a)). When ASC were grown in the presence of FBS, no differences were found. However, when ASC were grown in the presence of HS, there was a significant increase in the number of CFU and indeed the suprapatellar-derived ASC showed a higher CFU in comparison with the infrapatellar fraction (Figure 2(a)). The colonies formed from the suprapatellar SVF were not only more abundant, but they were always bigger (Figure 2(a), right panel) and exhibited a faster proliferative profile. In fact, when the ASC were cultured with either FBS or HS, the proliferative rates, in terms of the number of cells per growth area, within a cell growth curve daily analysis, were significantly higher from those cells amplified from the suprapatellar fat tissue compared with infrapatellar. The differential growth rate was significantly different eight days after culture in the presence of HS and ten days after culture in FBS (Figure 2(b)). The ultrastructural analysis of the suprapatellar cell cultures grown in FBS or HS showed higher inclusion body accumulation (indicated by white arrows) and higher distribution of intermediate filaments (indicated by black arrows) in the presence of HS-containing medium (Figure 2(c)).

3.3. In Vitro Osteogenesis and Chondrogenesis Are Favored in Suprapatellar ASC. To further assess the stem cell characteristics from both adipose tissue sources, the supra- and infrapatellar fat pads, we compared the differentiation multipotency between both samples (Figure 3). Both underwent induced differentiation into the adipogenic, osteogenic, and chondrogenic lineages (Figure 3). However, the extent of differentiation was not identical. Suprapatellar-derived ASC showed higher osteogenic and chondrogenic potential in comparison with the infrapatellar-derived and infrapatellar-differentiated cells as indicated by quantification of Alizarin red and Alcian blue staining, respectively (Figure 3, right panels). The higher chondrogenic potential of the suprapatellar-derived cells was also supported by the increased expression of Sox9 (green), a chondrocyte precursor marker [29]. This differential multipotency yields the suprapatellar fat pad a promising cell source for cartilage tissue repair.

3.4. Suprapatellar-Derived ASC Significantly Improves Cartilage Regeneration in a Mouse Model of Severe OA. To assess whether the increased cell proliferative and cell differentiation properties shown in vitro of the suprapatellar-derived MSCs would be functionally efficient in cartilage regeneration, in vivo cell transplantation assay in a severe OA mouse model was performed.

For the therapeutic efficacy testing of the suprapatellar-derived human ASC (hASC), severe OA was induced by single intra-articular injection of collagenase II (13 U) in both knees of 12-week old adult male C57BL6 mice. Five days after injection, when total cartilage destruction occurs (previously evaluated by histological analysis; data not shown), 10^5 hASC or the SVF or growth medium (control) was injected into the intra-articular space. It has been shown that PRP infiltration, increasingly implemented in regular clinical

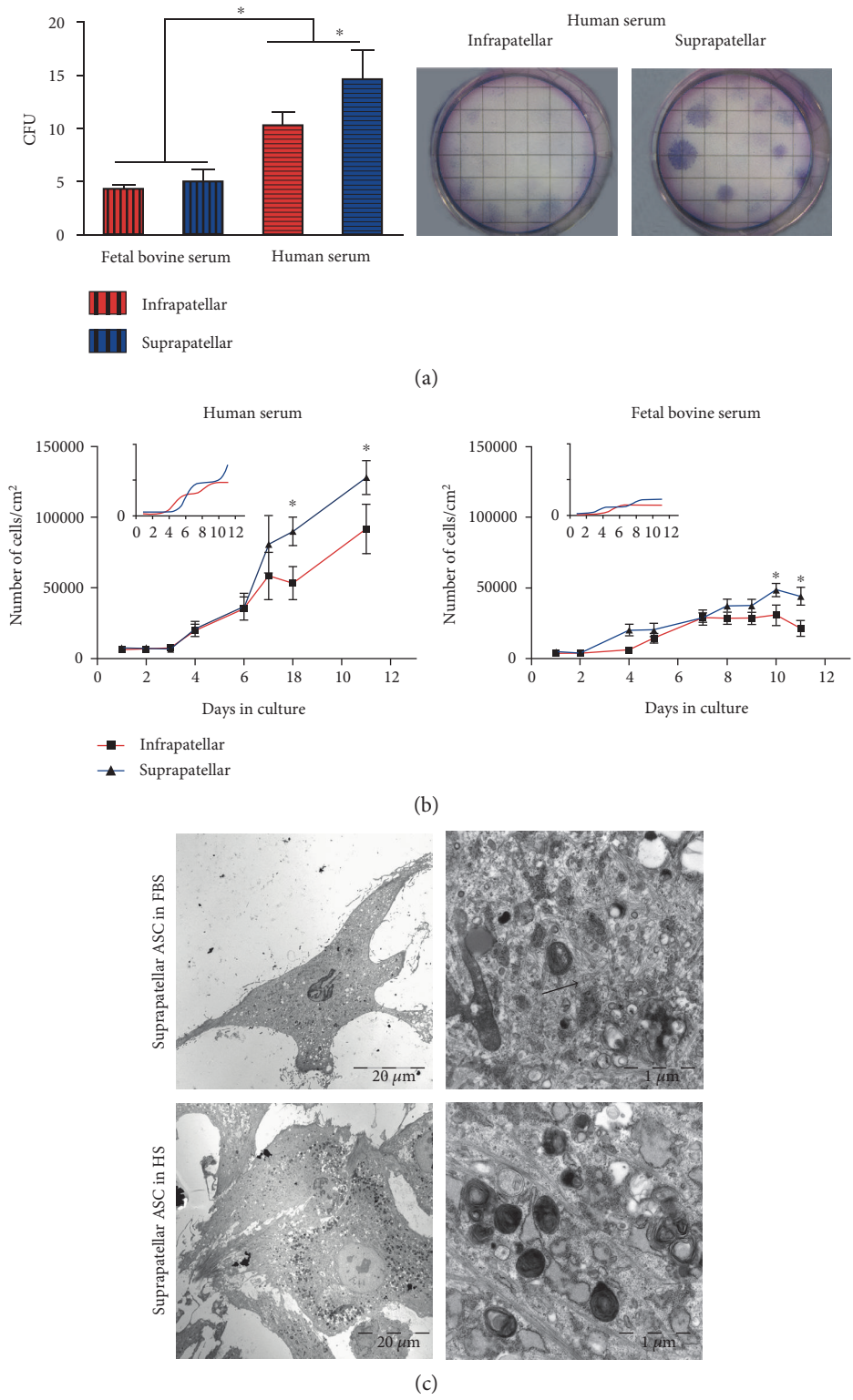

Figure 2: Supra- and infrapatellar ASC proliferative activity. (a) Colony-forming unit (CFU) assay was performed from infra and suprapatellar SVF from four different patients in the presence of 10% human serum (HS) or 10% fetal bovine serum- (FBS-) containing medium for 10 days. The generated colonies were counted after Giemsa staining (right panel). The mean ± SD of the total number of colonies at each condition of all tested samples was shown. $^*P < 0.05$ at the indicated comparisons. (b) 10^4 cells at passage three of every sample, suprapatellar (blue line)- and infrapatellar (red line)-derived ASC were allowed to grow in multiple wells in the presence of 10% HS or 10% FBS and quantified every day up to 10 days. The mean ± SD of the total number of cells at every time point was represented. $^*P < 0.05$ versus infrapatellar. (c) Representative images after TEM acquisition of suprapatellar ASC growth in HS (left panels) or FBS (right panels) are shown. White arrows: inclusion bodies; black arrows: intermediate filaments.

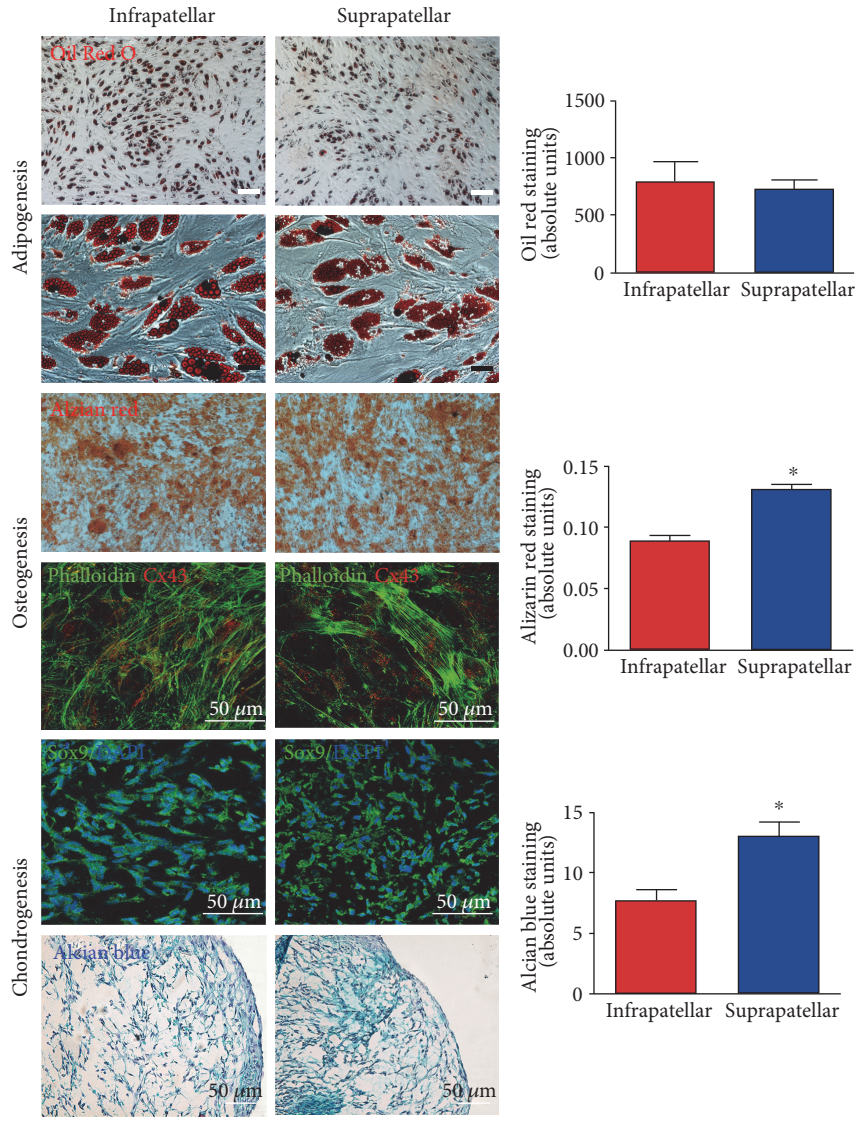

Figure 3: Multilineage potential of suprapatellar- and infrapatellar-derived ASC. All directed differentiation processes were induced from both samples, suprapatellar- and infrapatellar-derived ASC at passages after 4. To quantify the efficiency of cell differentiation, specific staining was employed for each process: Oil Red O staining for adipogenesis, Alizarin red for osteogenesis and Alcian blue for chondrogenesis, $^{*}P < 0.05$ versus infrapatellar. In addition, immunodetection of Connexin 43 (red; osteocyte marker) and phalloidin (green; cytoskeletal marker) was performed to evaluate osteocyte maturation. Sox9 (green) counterstained with DAPI (blue, nucleus) stained newly generated chondrocytes.

practice, can reduce pain and improve joint function with a notable improvement on the quality of life of patients [30, 31]. Therefore, PRP was also injected in an additional group of animals (PRP) in order to compare the regenerative effectiveness on cell transplantation in comparison with growth factor infiltration (Figure 4).

Once a week after treatments, the volume of the knees was measured using an automatic caliper. As shown in Figure 4(a), a significant increase in knee size occurs in all three groups after OA induction during the whole experiment. However, all treated groups, hASC, SVF, and PRP, showed a significant reduction of this increased volume one month after OA induction compared to the control group (Figure 4(a)). This result indicates a significant anti-inflammatory effect of the treatments. However, when we examined the structural regenerative effect by quantifying GAG (Figure 4(b)) and the OA damage score (Figure 4(c)), we observed a unique consistent structural regeneration of the loss of cartilage when the animals were treated with hASC in comparison with the control group (Figures 4(b) and 4(c)). Thus, PRP or SVF acts as an effective anti-inflammatory agent, but the regenerative effects of the stem cells do not seem to be bolstered by PRP or SVF. A representative safranin-O staining image for each treated group showed a complete absence of articular cartilage in the control animal and safranin-O-positive areas compatible with regenerating cartilage more prominent in the hASC-treated animal (Figure 4(d)).

To explore the contribution of the ectopic ASC to the regeneration of the articular cartilage, we evaluated the

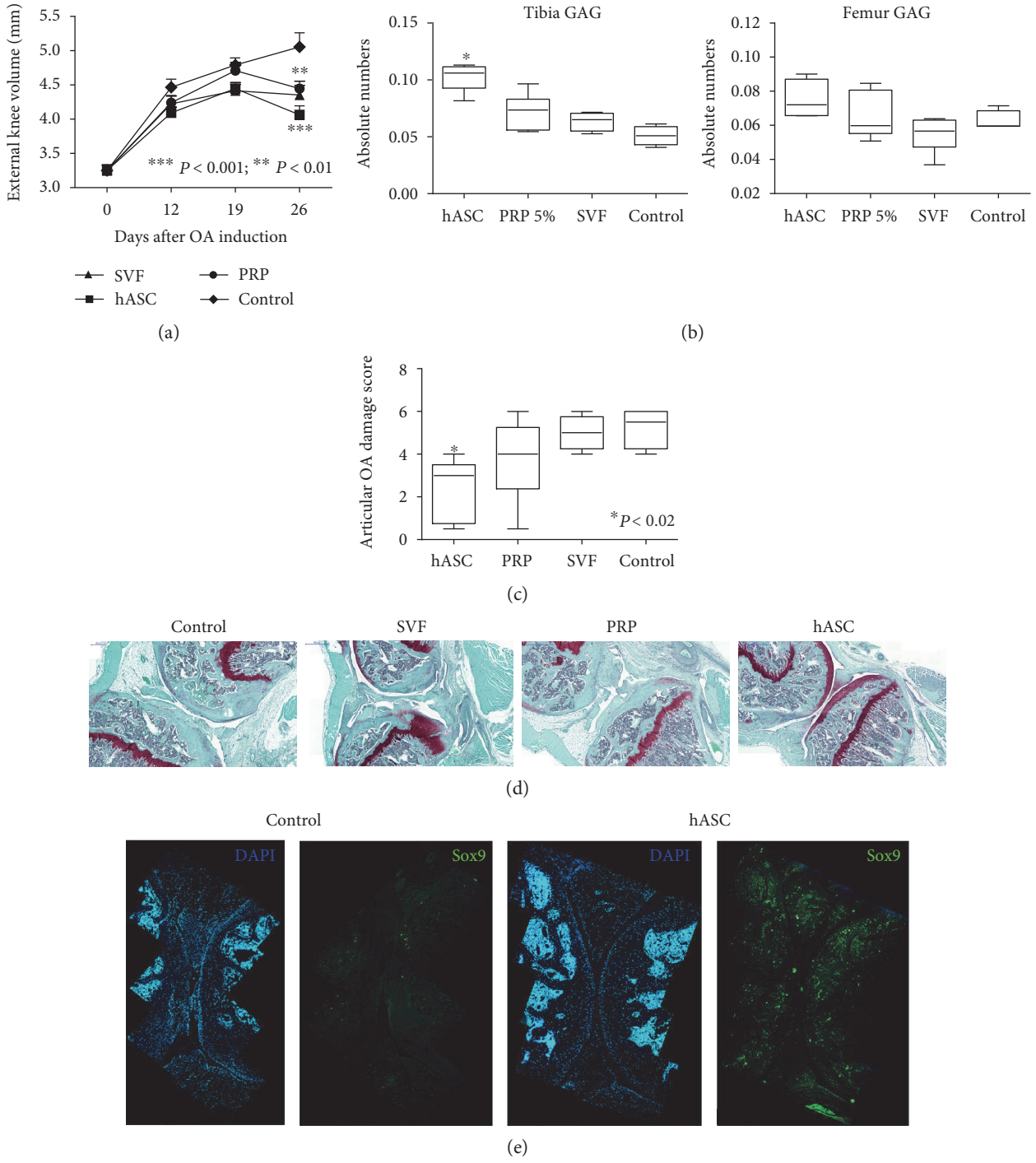

FIGURE 4: Functional and structural cartilage regeneration. The therapeutic activity of suprapatellar-derived ASC (supra-hASC) in comparison with control-, SVF-, and PRP- treated groups was studied in a mouse model of severe OA. (a) Swelling-related inflammation was measured by quantifying once a week the external volume of the knees, $^{**}P < 0.01$ $^{***}P < 0.001$ versus control. (b) Glycosaminoglycan (GAG) quantification at both, tibia and femur, $^{*}P < 0.05$ versus control. (c) Articular OA damage score was performed from 5 μm frontally sectioned knees stained with safranin-O and following the recommendations established by Glasson et al. [27]. $^{*}P < 0.05$ versus control. Representative images of a frontal section stained with safranin-O are shown for each group. (d) Immunostaining of Sox9 (green) to evaluate the endogenous chondrogenic activity. All cell nuclei were detected with DAPI staining (blue).

induced chondrogenic activity by the detection of Sox9 (a chondrocyte progenitor marker) positive cells in the control and supra-hASC-treated joints (Figure 4(e)). As shown in the representative images, an increase in Sox9 positive cells was detected in the hASC group (Figure 4(e)). However, few of the Sox9 positive cells costained with the specific

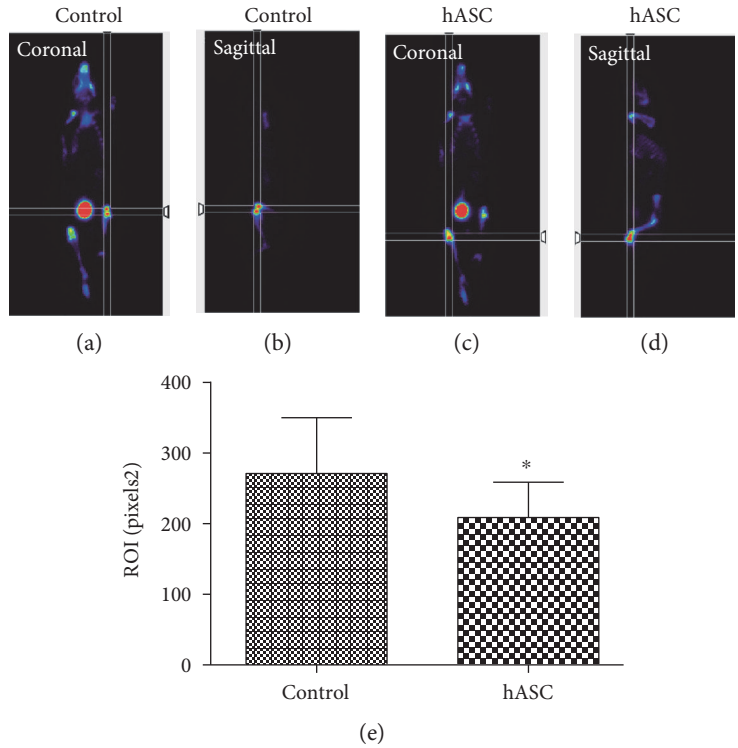

Figure 5: Translational PET image analysis after hASC transplantation in the OA mouse model. PET acquisition (a, c) and quantification (e) of NaF-18 detection of the control knee (a, b) and hASC transplanted knee (c, d). The images were analysed by using Amide software. The mean ± SD of the region of interest at each condition of all animals was determined. $^{*}P < 0.05$ versus control.

immunodetection for human cells (antinuclei; data not shown) indicating an endogenous induction of the cartilage repair by the hASC transplantation.

3.5. Positron Emission Tomography (PET) Analysis Shows In Vivo Cartilage Regeneration Process after ASC Trasplantation. 18F-NaF PET/CT is a high-performance diagnostic tool utilized by clinical practitioners and produces high-quality images within a shorter period from injection time in bone and joint disorders including osteoarthritis [32, 33]. PET analysis was employed to evaluate cartilage regeneration in vivo in a group of animals with induced OA in both knees. In order to minimize the individual differences of the NaF-18 probe signal distribution and acquisition (injected one month after OA induction), both conditions were included in the same animal; the left knee was transplanted with hASC and the right knee served as a control (Figure 5). After quantification of the ROIs from the acquired images at equivalent coronal and sagittal planes, a significantly lower detection of NaF-18 on the joints transplanted with hASC (Figure 5, right graph) compared to the control joints was observed. The bone at the hASC transplanted joints was less exposed, and the signal was masked by the regenerated cartilage.

4. Discussion

ASC-based therapies have already been tested in clinical trials, at the safety and efficacy phases, with remarkable restorative activity in the treatment of OA from subcutaneous abdominal fat [34, 35]. However, tissue-specific-derived stem cells would guarantee the improvement of ASC repair capabilities for instance, in terms of improved chondrogenic efficiency for cartilage repair [9]. In the knee, there are two major sources of ASC, the supra- and infrapatellar fat pads [14, 15]. Both fat pads are commonly resected during knee joint arthroplasty in patients with acute OA and are a suitable source of ASC for the autologous treatment of additional affected joints. Previous studies have already described the potential regenerative capability of ASC derived from the infrapatellar pad, recently shown to have demonstrated increased chondrogenic potential compared with those from subcutaneous fat in vitro [36] and in vivo in a model of OA [16, 17, 37]. However, no data have been reported yet with the suprapatellar-derived cells. Here, we show for the first time the regenerative capacity of the suprapatellar-derived ASC population in a severe OA mice model. The infrapatellar pad-derived cells have been considered an active joint tissue in the initiation and progression of knee OA, activating the inflammatory cells by producing inflammatory mediators influencing the cartilage and synovium metabolism [38]. When we compare in vitro the proliferative and differentiated properties among both derived ASCs, we demonstrate improved proliferative, chondrogenic, and osteogenic rates from the suprapatellar-derived ASC, showing a promising and improved source for efficient cell therapeutic resolution of joint degeneration [33].

The CD105 or endoglin receptor has been related to the more proliferative, migrating, and invading MSC size populations in the injury area during endogenous regeneration

[39]. Moreover, transplantation of a CD105-negative stem cell population showed significant chondroid degeneration features compared to the CD105-positive transplanted group [40], showing an influence on chondrogenic cell fate induction. In fact, when we compare the directed chondrogenic capability between the two samples, we found a better yield from the suprapatellar-derived ASC that shows an enrichment of CD105-positive population versus those from the infrapatellar fat.

The ASC amplification in vitro with human serum was always better than with fetal bovine serum. Previous reports from subcutaneous adipose tissue have already shown detrimental proliferative activity of ASC in the presence of FBS [41]. Differential gene expression analysis of ASC cultured with HS or FBS showed a significant overexpression of a number of genes related with regulatory roles in cell cycle progression [42].

For translational and functional proof of concept, an in vivo model of severe OA [25] for intra-articular administration of the hASC was explored comparing the efficiency of cartilage regeneration in the SVF- and PRP-treated animals. Interestingly, all treated groups showed significantly reduced knee joint diameter (swelling).

PRP contains a multitude of growth factors including TGF-β, PDGF, IGF, bFGF, VEGF, and EGF [43] with anabolic chondral-promoting and chondral-protective properties [44, 45]. Abundant preclinical and clinical findings support that PRP is a promising coadjutant treatment for cartilage repair and relieving symptoms based on its anabolic effect on the resident cells and due to its potential to inhibit inflammation and alleviate OA symptoms with a clinically acceptable safety profile [46]. PRP treatment has shown additional benefits in the regeneration of other related tissues such as bone defects, indicating PRP plays a crucial role by influencing the local tissue microenvironment and thereby enhancing progenitor cell recruitment and proper matrix deposition [47]. Although only the ASC transplantation showed significant tissue regeneration, the PRP combination could create a synergistic effect by bridging and interfacing between the MSCs and the endogenous tissue, an effect not produced by an individual treatment alone. Chemically induced OA in the mice led to aggressive joint degeneration; however, even in such a severe condition, ASC transplantation reduced and rescued functional anatomy in the intra-articular space, reducing the OA damage scores and increasing the cartilage-like tissue. Continued expression of Sox9 is required to maintain hyaline-like cartilage, avoiding chondrocyte hypertrophy for efficient regeneration [29]. Only the amplified hASC were able to induce efficient regeneration one month after treatment showing a significant increase in SOX9 expression in the growing cartilage. One month after cell transplantation, very few human cells were found in the transplanted joints (data not shown), which is in accordance with previous reports [48, 49]. Rather than assuming cell replacement by ASC transplantation, the most contemporary hypothesis is that their actions are mostly associated with paracrine activity by secreting modulating factors. Accordingly, ASC secrete PGE2 which induces dendritic cells to upregulate the anti-inflammatory cytokine IL10 while reducing the proinflammatory TNFα and IL12 contributing to its known immune-modulatory effect and related promotion of tissue repair [50, 51]. However, this hypothesis needs to be addressed with further research to demonstrate its relevance for the treatment of OA.

5. Conclusion

Our results show that the human suprapatellar fat pad offers a proper ASC source for cartilage regeneration by promoting efficient endogenous chondrogenesis in a mouse model of severe OA.

Conflicts of Interest

The authors declare that they have no conflicts of interest.

Authors' Contributions

Ignacio Muñoz-Criado, Victoria Moreno-Manzano, Ramón Cugat, and Montserrat García contributed to the conception, design, collection, and/or assembly of data, data analysis and interpretation, manuscript writing, and final approval of manuscript. Victoria Moreno-Manzano, Ramón Cugat, and Montserrat García provided financial support and approved the final manuscript. Jose Meseguer-Ripolles, Ana Alastrue-Agudo, Jerónimo Forteza-Vila, Richard J Griffeth, and Maravillas Mellado-López contributed to the collection and/or assembly of data and data analysis and interpretation. Ignacio Muñoz-Criado and Jose Meseguer-Ripolles equally contributed to this work.

Acknowledgments

The authors specifically acknowledge the Fundación García Cugat for its valuable financial and intellectual support. This work was also supported by Ministerio de Economía y Competitividad (grants CONSOLIDER-INGENIO 2010 CSD2008-00005 and MAT2015-66666-C3-2-R, MINECO/FEDER, UE) and the Instituto de Salud Carlos III (PI13/00319). The authors also thank Oncovision for performing the PET analysis and for directly contributing to acquisition and analysis.

References

[1] J. W. Bijlsma, F. Berenbaum, and F. P. Lafeber, "Osteoarthritis: an update with relevance for clinical practice," *Lancet*, vol. 377, no. 9783, pp. 2115–2126, 2011.

[2] M. Hiligsmann and J. Y. Reginster, Eds., *The Economic Weight of Osteoarthritis in Europe*, 2013, http://www.medicographia.com/2013/10/the-economic-weight-of-osteoarthritis-in-europe/.

[3] M. B. Goldring and S. R. Goldring, "Articular cartilage and subchondral bone in the pathogenesis of osteoarthritis," *Skeletal Biology and Medicine*, vol. 1192, pp. 230–237, 2010.

[4] http://oarsi.org/research/standardization-osteoarthritis-definitions.

[5] T. Minas and S. Nehrer, "Current concepts in the treatment of articular cartilage defects," *Orthopedics*, vol. 20, no. 6, pp. 525–538, 1997.

[6] L. Peterson, "Articular cartilage injuries treated with autologous chondrocyte transplantation in the human knee," *Acta Orthopaedica Belgica*, vol. 62, Supplement 1, pp. 196–200, 1996.

[7] M. Brittberg, A. Lindahl, A. Nilsson, C. Ohlsson, O. Isaksson, and L. Peterson, "Treatment of deep cartilage defects in the knee with autologous chondrocyte transplantation," *New England Journal of Medicine*, vol. 331, no. 14, pp. 889–895, 1994.

[8] A. Panagopoulos, L. van Niekerk, and I. Triantafillopoulos, "Autologous chondrocyte implantation for knee cartilage injuries: moderate functional outcome and performance in patients with high-impact activities," *Orthopedics*, vol. 35, no. 1, pp. E6–E14, 2012.

[9] A. Vega, M. A. Martín-Ferrero, F. Del Canto et al., "Treatment of knee osteoarthritis with allogeneic bone marrow mesenchymal stem cells: a randomized controlled trial," *Transplantation*, vol. 99, no. 8, pp. 1681–1690, 2015.

[10] H. Orbay, M. Tobita, and H. Mizuno, "Mesenchymal stem cells isolated from adipose and other tissues: basic biological properties and clinical applications," *Stem Cells International*, vol. 2012, Article ID 461718, 9 pages, 2012.

[11] Y. Gong, H. Ma, and J. Liu, "Controlled WISP-1 shRNA delivery using thermosensitive biodegradable hydrogel in the treatment of osteoarthritis," *Journal of Bionic Engineering*, vol. 12, no. 2, pp. 285–293, 2015.

[12] Z. P. Chen, W. Liu, D. Liu et al., "Development of brucine-loaded microsphere/thermally responsive hydrogel combination system for intra-articular administration," *Journal of Controlled Release*, vol. 162, no. 3, pp. 628–635, 2012.

[13] U. Noth, A. F. Steinert, and R. S. Tuan, "Technology insight: adult mesenchymal stem cells for osteoarthritis therapy," *Nature Clinical Practice. Rheumatology*, vol. 4, no. 7, pp. 371–380, 2008.

[14] D. Saddik, E. G. McNally, and M. Richardson, "MRI of Hoffa's fat pad," *Skeletal Radiology*, vol. 33, no. 8, pp. 433–444, 2004.

[15] H. U. Staeubli, C. Bollmann, R. Kreutz, W. Becker, and W. Rauschning, "Quantification of intact quadriceps tendon, quadriceps tendon insertion, and suprapatellar fat pad: MR arthrography, anatomy, and cryosections in the sagittal plane," *AJR. American Journal of Roentgenology*, vol. 173, no. 3, pp. 691–698, 1999.

[16] W. J. Jurgens, A. van Dijk, B. Z. Doulabi et al., "Freshly isolated stromal cells from the infrapatellar fat pad are suitable for a one-step surgical procedure to regenerate cartilage tissue," *Cytotherapy*, vol. 11, no. 8, pp. 1052–1064, 2009.

[17] Y. G. Koh and Y. J. Choi, "Infrapatellar fat pad-derived mesenchymal stem cell therapy for knee osteoarthritis," *The Knee*, vol. 19, no. 6, pp. 902–907, 2012.

[18] P. Pires de Carvalho, K. M. Hamel, R. Duarte et al., "Comparison of infrapatellar and subcutaneous adipose tissue stromal vascular fraction and stromal/stem cells in osteoarthritic subjects," *Journal of Tissue Engineering and Regenerative Medicine*, vol. 8, no. 10, pp. 757–762, 2014.

[19] C. Ballegaard, R. G. Riis, H. Bliddal et al., "Knee pain and inflammation in the infrapatellar fat pad estimated by conventional and dynamic contrast-enhanced magnetic resonance imaging in obese patients with osteoarthritis: a cross-sectional study," *Osteoarthritis and Cartilage*, vol. 22, no. 7, pp. 933–940, 2014.

[20] F. Eymard, A. Pigenet, D. Citadelle et al., "Induction of an inflammatory and prodegradative phenotype in autologous fibroblast-like synoviocytes by the infrapatellar fat pad from patients with knee osteoarthritis," *Arthritis & Rhematology*, vol. 66, no. 8, pp. 2165–2174, 2014.

[21] W. Han, S. Cai, Z. Liu et al., "Infrapatellar fat pad in the knee: is local fat good or bad for knee osteoarthritis?" *Arthritis Research & Therapy*, vol. 16, no. 4, p. R145, 2014.

[22] F. Pan, W. Han, X. Wang et al., "A longitudinal study of the association between infrapatellar fat pad maximal area and changes in knee symptoms and structure in older adults," *Annals of the Rheumatic Diseases*, vol. 74, no. 10, pp. 1818–1824, 2014.

[23] M. L. Dominici, K. Le Blanc, I. Mueller et al., "Minimal criteria for defining multipotent mesenchymal stromal cells. The International Society for Cellular Therapy position statement," *Cytotherapy*, vol. 8, no. 4, pp. 315–317, 2006.

[24] S. P. Johnson, J. M. Catania, R. J. Harman, and E. D. Jensen, "Adipose-derived stem cell collection and characterization in bottlenose dolphins (*Tursiops truncatus*)," *Stem Cells and Development*, vol. 21, no. 16, pp. 2949–2957, 2012.

[25] E. L. Kuyinu, G. Narayanan, L. S. Nair, and C. T. Laurencin, "Animal models of osteoarthritis: classification, update, and measurement of outcomes," *Journal of Orthopaedic Surgery and Research*, vol. 11, p. 19, 2016.

[26] E. Anitua, C. Carda, and I. Andia, "A novel drilling procedure and subsequent bone autograft preparation: a technical note," *The International Journal of Oral & Maxillofacial Implants*, vol. 22, no. 1, pp. 138–145, 2007.

[27] S. S. Glasson, M. G. Chambers, W. B. Van Den Berg, and C. B. Little, "The OARSI histopathology initiative - recommendations for histological assessments of osteoarthritis in the mouse," *Osteoarthritis and Cartilage*, vol. 18, Supplement 3, pp. S17–S23, 2010.

[28] L. Zimmerlin, V. S. Donnenberg, J. P. Rubin, and A. D. Donnenberg, "Mesenchymal markers on human adipose stem/progenitor cells," *Cytometry. Part a*, vol. 83, no. 1, pp. 134–140, 2013.

[29] K. Hiramatsu, S. Sasagawa, H. Outani, K. Nakagawa, H. Yoshikawa, and N. Tsumaki, "Generation of hyaline cartilaginous tissue from mouse adult dermal fibroblast culture by defined factors," *The Journal of Clinical Investigation*, vol. 121, no. 2, pp. 640–657, 2011.

[30] M. Napolitano, S. Matera, M. Bossio et al., "Autologous platelet gel for tissue regeneration in degenerative disorders of the knee," *Blood Transfusion*, vol. 10, no. 1, pp. 72–77, 2012.

[31] C. J. Meheux, M. C. PC, D. M. Lintner, K. E. Varner, and J. D. Harris, "Efficacy of intra-articular platelet-rich plasma injections in knee osteoarthritis: a systematic review," *Arthroscopy*, vol. 32, no. 3, pp. 495–505, 2016.

[32] J. W. Lee, S. M. Lee, S. Kim, J. W. Choi, and K. W. Baek, "Clinical utility of fluoride-18 positron emission tomography/CT in temporomandibular disorder with osteoarthritis: comparisons with 99mTc-MDP bone scan," *Dento Maxillo Facial Radiology*, vol. 42, no. 2, p. 29292350, 2013.

[33] H. Jadvar, B. Desai, and P. S. Conti, "Sodium 18F-fluoride PET/CT of bone, joint, and other disorders," *Seminars in Nuclear Medicine*, vol. 45, no. 1, pp. 58–65, 2015.

[34] Y. M. Pers, L. Rackwitz, R. Ferreira et al., "Adipose mesenchymal stromal cell-based therapy for severe osteoarthritis of the

knee: a phase I dose-escalation trial," *Stem Cells Translational Medicine*, vol. 5, no. 7, pp. 847–856, 2016.

[35] J. Burke, M. Hunter, R. Kolhe, C. Isales, M. Hamrick, and S. Fulzele, "Therapeutic potential of mesenchymal stem cell based therapy for osteoarthritis," *Clinical and Translational Medicine*, vol. 5, no. 1, p. 27, 2016.

[36] P. Hindle, N. Khan, L. Biant, and B. Péault, "The infrapatellar fat pad as a source of perivascular stem cells with increased chondrogenic potential for regenerative medicine," *Stem Cells Translational Medicine*, vol. 6, no. 1, pp. 77–87, 2017.

[37] P. Tangchitphisut, N. Srikaew, S. Numhom et al., "Infrapatellar fat pad: an alternative source of adipose-derived mesenchymal stem cells," *Arthritis*, vol. 2016, Article ID 4019873, 10 pages, 2016.

[38] S. Clockaerts, Y. M. Bastiaansen-Jenniskens, J. Runhaar et al., "The infrapatellar fat pad should be considered as an active osteoarthritic joint tissue: a narrative review," *Osteoarthritis and Cartilage*, vol. 18, no. 7, pp. 876–882, 2010.

[39] L. L. Zhou, H. W. Liu, X. X. Wen, and H. Xie, "Involvement of bone marrow stem cells in periodontal wound healing," *The Chinese Journal of Dental Research*, vol. 17, no. 2, pp. 105–110, 2014.

[40] S. Asai, S. Otsuru, M. E. Candela et al., "Tendon progenitor cells in injured tendons have strong chondrogenic potential: the CD105-negative subpopulation induces chondrogenic degeneration," *Stem Cells*, vol. 32, no. 12, pp. 3266–3277, 2014.

[41] C. Escobedo-Lucea, C. Bellver, C. Gandia et al., "A xenogeneic-free protocol for isolation and expansion of human adipose stem cells for clinical uses," *PloS One*, vol. 8, no. 7, article e67870, 2013.

[42] B. Lindroos, K. L. Aho, H. Kuokkanen et al., "Differential gene expression in adipose stem cells cultured in allogeneic human serum versus fetal bovine serum," *Tissue Engineering. Part a*, vol. 16, no. 7, pp. 2281–2294, 2010.

[43] A. T. Nurden, P. Nurden, M. Sanchez, I. Andia, and E. Anitua, "Platelets and wound healing," *Frontiers in Bioscience*, vol. 13, pp. 3532–3548, 2008.

[44] A. Brandl, P. Angele, C. Roll, L. Prantl, R. Kujat, and B. Kinner, "Influence of the growth factors PDGF-BB, TGF-beta1 and bFGF on the replicative aging of human articular chondrocytes during in vitro expansion," *Journal of Orthopaedic Research*, vol. 28, no. 3, pp. 354–360, 2010.

[45] L. A. Fortier, H. O. Mohammed, G. Lust, and A. J. Nixon, "Insulin-like growth factor-I enhances cell-based repair of articular cartilage," *Journal of Bone and Joint Surgery. British Volume (London)*, vol. 84, no. 2, pp. 276–288, 2002.

[46] X. Xie, C. Zhang, and R. S. Tuan, "Biology of platelet-rich plasma and its clinical application in cartilage repair," *Arthritis Research & Therapy*, vol. 16, no. 1, p. 204, 2014.

[47] R. M. El Backly, S. H. Zaky, B Canciani et al., "Platelet rich plasma enhances osteoconductive properties of a hydroxyapatite-beta-tricalcium phosphate scaffold (Skelite) for late healing of critical size rabbit calvarial defects," *Journal of Cranio-Maxillo-Facial Surgery*, vol. 42, no. 5, pp. e70–e79, 2014.

[48] P. Bianco, X. Cao, P. S. Frenette et al., "The meaning, the sense and the significance: translating the science of mesenchymal stem cells into medicine," *Nature Medicine*, vol. 19, no. 1, pp. 35–42, 2013.

[49] D. J. Prockop, "Repair of tissues by adult stem/progenitor cells (MSCs): controversies, myths, and changing paradigms," *Molecular Therapy*, vol. 17, no. 6, pp. 939–946, 2009.

[50] J. L. Spees, R. H. Lee, and C. A. Gregory, "Mechanisms of mesenchymal stem/stromal cell function," *Stem Cell Research & Therapy*, vol. 7, no. 1, p. 125, 2016.

[51] S. Aggarwal and M. F. Pittenger, "Human mesenchymal stem cells modulate allogeneic immune cell responses," *Blood*, vol. 105, no. 4, pp. 1815–1822, 2005.

Hindawi
Stem Cells International
Volume 2017, Article ID 9198328, 12 pages
https://doi.org/10.1155/2017/9198328

Research Article

Intra-Articular Injection of Human Synovial Membrane-Derived Mesenchymal Stem Cells in Murine Collagen-Induced Arthritis: Assessment of Immunomodulatory Capacity In Vivo

Minglu Yan, Xin Liu, Qiujie Dang, He Huang, Fan Yang, and Yang Li

Department of Rheumatology and Immunology, The Second Affiliated Hospital of Harbin Medical University, Harbin 150000, China

Correspondence should be addressed to Yang Li; liyang@hrbmu.edu.cn

Received 2 March 2017; Accepted 26 April 2017; Published 21 June 2017

Academic Editor: Vladislav Volarevic

The aim of this study was to evaluate the efficacy of human synovial membrane-derived MSCs (SM-MSCs) in murine collagen-induced arthritis (CIA). Male mice (age 7–9 weeks) were injected intra-articularly with SM-MSCs obtained from patients with osteoarthritis, on days 28, 32, and 38 after bovine type II collagen immunization. The efficacy of SM-MSCs in CIA was evaluated clinically and histologically. Cytokine profile analyses were performed by real-time polymerase chain reaction and multiplex analyses. Splenic helper T (Th) cell and regulatory B cell subsets were analyzed by flow cytometry. Intra-articular SM-MSC injection ameliorated the clinical and histological severity of arthritis. Decrease in tumor necrosis factor-α, interferon-γ, and interleukin- (IL-) 17A and increase in IL-10 production were observed after SM-MSC treatment. Flow cytometry showed that Th1 and Th17 cells decreased, whereas Th2, regulatory T (Treg), and PD-1^{+}CXCR5^{+}FoxP3^{+} follicular Treg cells increased in the spleens of SM-MSC-treated mice. Regulatory B cell analysis showed that CD21^{hi}CD23^{hi} transitional 2 cells, CD23^{low}CD21^{hi} marginal zone cells, and CD19^{+}CD5^{+}CD$1d^{+}$IL-10^{+} regulatory B cells increased following SM-MSC treatment. Our results demonstrated that SM-MSCs injected in inflamed joints in CIA had a therapeutic effect and could prevent arthritis development and suppress immune responses via immunoregulatory cell expansion.

1. Introduction

Rheumatoid arthritis (RA) is a systemic autoimmune disorder characterized by persistent inflammation, extensive synovial hyperplasia, and, ultimately, cartilage and bone destruction [1]. Loss of self-tolerance leads to imbalance of effector and regulatory cells, which plays a crucial role in the onset and pathogenesis of RA [2, 3]. In particular, interferon- (IFN-) γ-helper T (Th) 1 and interleukin- (IL-) 17-Th17 cells are thought to be the etiologic populations, whereas regulatory T (Treg) cells and B cells, with an IL-10-secreting profile, are capable of recovering self-tolerance and preventing autoimmune diseases [4–6]. Hence, the recovery of immune tolerance by expansion of regulatory cells may be a rational approach for RA treatment.

MSCs are adult multipotent cells that are present in the bone marrow (BM), adipose tissue, synovial membrane, synovial fluid, and perinatal tissues. These cells have been characterized with respect to colony-forming unit fibroblast (CFU-F), surface marker expression, and in vitro multidifferentiation potential, according to the International Society for Cellular Therapy (ISCT) criteria [7]. During the last several decades, MSCs have been largely investigated for their potent immunomodulatory and anti-inflammatory capacities, emerging as a promising therapy for autoimmune diseases such as RA [8–10].

Although an accumulating body of work clearly demonstrates that MSCs harvested from BM and placental cultures possess potent immunomodulatory effects in vitro and in vivo [11–13], relative little is known about the role of synovial membrane-derived MSCs (SM-MSCs) in the immune system. SM-MSCs were first identified in 2001; it was reported that the synovial membrane from the knee joints of human donors could give rise to a fibroblast-like cell population possessing great expansion potential, typical antigen expression, and multidifferentiation capability [14].

Recently, several studies demonstrated that SM-MSCs from patients with osteoarthritis (OA) could suppress T cell proliferation and maintain the Treg population in vitro when cocultured with allogeneic lymphocytes [15, 16], suggesting that SM-MSCs can also be employed to develop a distinct immunomodulatory approach. However, the in vivo regulatory role of SM-MSCs in RA is yet unclear.

In this study, we employed a murine collagen-induced arthritis (CIA) model to evaluate the therapeutic effect of SM-MSCs following repeated intra-articular injection. To our knowledge, this study is the first to show that SM-MSCs can exert immunomodulatory effects in CIA via expansion of $FoxP3^+$ Treg cells and $CD21^{hi}CD23^{hi}$ transitional 2 (T2), $CD23^{low}CD21^{hi}$ marginal zone (MZ), and IL-10-competent regulatory B cells. Our data indicate that SM-MSC administration may provide a promising approach for RA treatment.

2. Materials and Methods

2.1. Isolation and Expansion of MSCs from Human Synovial Membranes. MSCs were isolated from human synovial membranes as previously described [17]. Synovial membranes were obtained aseptically from the knee joints of human donors (age 64 ± 8 years, 21 females and 18 males) at the time of surgical knee replacement for degenerative OA at the Second Affiliated Hospital of Harbin Medical University, with the donors' understanding and informed consent. Exclusion criteria for these donors were rheumatic diseases, infections at the time of this study, and a history of malignancy.

Synovial membranes were rinsed twice in Hank's balanced salt solution (HBSS; Hyclone) supplemented with antibiotic-antimycotic solution (100 U/mL penicillin, 100 μg/mL streptomycin, and 0.25 μg/mL amphotericin B, Life Technologies), finely minced, and digested with 0.2% type I collagenase (Life Technologies) in Dulbecco's modified Eagle's medium-low glucose (DMEM-LG; Hyclone) containing 10% fetal bovine serum (FBS; Excell Bio) and 1% penicillin/streptomycin (P/S; Invitrogen). Following 8 h incubation at 37°C, undigested tissues were removed using a 70 μm nylon sieve, and cells were collected, washed twice, resuspended in DMEM-LG supplemented with 10% FBS and 1% P/S solution (referred to as growth medium), and plated in a T25 culture flask for expansion at 37°C in a humidified 5% CO_2 atmosphere for 3-4 days. Nonadherent cells were removed, and the growth medium was refreshed every 3 days until confluence was achieved. The MSC monolayer was detached using trypsin-ethylenediaminetetraacetic acid (EDTA) (0.25% trypsin, 0.53 mM EDTA; Invitrogen) and subsequently passaged twice before use.

For the CFU-F assay, cells were seeded at a density of 10^4 cells/well in 6-well plates and cultured in growth medium for 10 days. The cells were subsequently fixed and stained with 0.5% crystal violet in 4% paraformaldehyde for 5 min. All visible colonies were counted.

2.2. Identification of SM-MSCs. The immunophenotype of SM-MSCs was identified by flow cytometry analysis (FACS Canto II, BD Biosciences) by using the following fluorescent antibodies: phycoerythrin- (PE-) conjugated mouse antihuman CD34, CD45, and CD90 antibodies; fluorescein isothiocyanate- (FITC-) conjugated CD73 antibodies; and allophycocyanin- (APC-) conjugated CD105 antibodies. As an isotype control, the appropriate mouse immunoglobulin (Ig) G_1 was substituted for the primary antibody. All the antibodies were purchased from BD Pharmingen (San Diego, CA, USA).

SM-MSCs were next tested for their capacity to differentiate toward the adipogenic and osteogenic lineages. For adipogenic induction, 2.5×10^5 MSCs were plated in a 6-well plate and treated with hMSC Adipogenic Differentiation BulletKit™ Medium (Lonza) and maintained for 14 days before being subjected to Oil Red O staining (Sigma-Aldrich). For osteogenic induction, MSCs were digested and seeded in a 6-well plate at a density of 10^5 cells/well and then maintained in hMSC Osteogenic Differentiation BulletKit Medium (Lonza) for 21 days before being subjected to Alizarin Red S staining (Sigma-Aldrich).

2.3. Induction of CIA and SM-MSC Treatment. CIA was induced in male DBA/1J mice (age 7–9 weeks) purchased from Shanghai Laboratory Animal Center (SLAC, Shanghai, China). The mice ($n = 20$) were maintained under standard conditions in our university's central animal laboratory and randomly placed in cages. Bovine type II collagen (CII; Chondrex) was dissolved in 50 mM acetic acid and emulsified with an equal volume of Freund's complete adjuvant (Sigma-Aldrich). The mice were immunized at the base of the tail with 100 μL emulsion containing 200 μg CII. After 21 days, the mice were administered a booster dose of 100 μg CII (2 mg/mL) emulsified with Freund's incomplete adjuvant (Chondrex) via intradermal injection into the tail. On days 28, 32, and 38 after the first immunization, the mice were anesthetized and 10^6 MSCs in 7 μL PBS were injected intra-articularly into the right knee for the SM-MSC treatment group ($n = 8$); the control mice received 7 μL PBS intra-articularly ($n = 8$).

2.4. Clinical and Histological Assessment of Arthritis. Clinical arthritis and severity scores of each individual mouse ($n = 8$ per group) were evaluated every 2 days by using the mean arthritis severity index, with scores on a scale of 0–4, as previously reported [18]. The mean thickness of the hind paw was measured with vernier calipers. The mice were anesthetized and euthanized on day 70 after CII immunization, and the ankle joints (right) were harvested for histological assessment. The joints were fixed in 4% paraformaldehyde, decalcified in 10% EDTA for 48 h, and embedded in paraffin. Tissues were sectioned at 7 μm thickness and stained with hematoxylin and eosin (H&E). All stained joint sections were observed in a blinded manner with light microscopy.

2.5. Quantitative Polymerase Chain Reaction (PCR). The synovia from the right knee joints of the mice was harvested at the end of the experiment. Total RNA was extracted using TRIzol reagent (Invitrogen) and reverse transcribed to cDNA with a Primescript RT Kit (Takara) according to the manufacturer's instructions. SYBR Green-based real-time PCR

Table 1: Sequences for primers.

Target genes	Sequences (5′ to 3′)	
	Forward	Reverse
TNF-α	CAGGCGGTGCCTATGTCTC	CGATCACCCCGAAGTTCAGTAG
IFN-γ	TGAAAGACAATCAGGCCATC	TTGCTGTTGCTGAAGAAGGT
IL-17A	ATCCACCTCACACGAGGCACA	AGATGAAGCTCTCCCTGGACTC
IL-10	CCAGGGAGATCCTTTGATGA	CATTCCCAGAGG AATTGCAT
IL-4	GGTCTCAACCCCCAGCTAGT	GCCGATGATCTCTCTCAAGTGA
TGF-β	CTCCCGTGGCTTCTAGTGC	GCCTTAGTTTGGACAGGATCTG
β-actin	GGCTGTATTCCCCTCCATCG	CCAGTTGGTAACAATGCCATGT

was performed using the 7500 Fast Real-Time PCR System (Applied Biosystems, USA) to quantify the mRNA levels of TNF-α, IFN-γ, IL-17A, IL-10, IL-4, and transforming growth factor- (TGF-) β. Relative changes in gene expression were calculated using the comparative C_T method. The mRNA levels of the target genes were normalized to those of the β-actin gene. Sequences of primers used in this study were obtained from primer bank of Harvard University and were listed in Table 1.

2.6. Multiplex Analysis. Peripheral blood samples were collected from the angular vein of mice on day 70 after etherization, and serum was obtained following a standard protocol. The cytokine (TNF-α, IFN-γ, IL-17A, IL-10, and IL-4) concentrations in serum were determined with the Multiplex Cytokine Bead Array System (Merck, Germany) according to the manufacturer's instructions.

2.7. Flow Cytometry. Splenocytes were freshly prepared on day 70, and single-cell suspensions were stained with the following antibodies for cell surface analysis: anti-CD4-FITC, anti-PD-1-peridinin chlorophyll (PerCP), anti-CXCR5-APC, anti-B220-APC, anti-CD21-FITC, anti-CD23-PE, anti-CD19-PerCP, anti-CD5-FITC, and anti-CD1d-APC antibodies. For transcription factor staining, the cells were fixed and permeabilized using a commercial FoxP3 staining kit (eBioscience, USA) according to the manufacturer's protocols. For intracellular cytokine staining, isolated splenocytes were stimulated with phorbol myristic acetate (PMA; 50 ng/mL)/ionomycin (1 μg/mL) for 4 h in the presence of brefeldin (3 μg/mL) and monomycin (1.4 μg/mL). The following antibodies were used: anti-IFN-γ-PE, anti-IL-4-PE, anti-IL-17-PE, and anti-IL-10-PE antibodies. Appropriate isotype-matched control antibodies were used to determine nonspecific staining. All the antibodies were bought from BD Biosciences. Data were acquired with a FACS Canto II flow cytometer (BD Biosciences, USA) and analyzed using the FlowJo software.

2.8. Statistical Analysis. Data were presented as mean ± standard deviation (SD). Comparisons of parametric data between the two groups were analyzed with Student's *t*-test. Statistical analysis was performed with GraphPad Prism (version 6 for Mac; GraphPad Software). p values less than 0.05 were considered significant.

2.9. Ethics Statement. The use of human materials in this study was approved by the Medical Ethical Committee of Harbin Medical University. All mouse experiments were conducted with the permission of the local ethics committee on animal research and were in compliance with the national guidelines for laboratory animal use.

3. Results

3.1. Characterization of Human SM-MSCs. The SM-MSCs displayed a spindle-like, fibroblast morphology (Figure 1(a)), which is a typical characteristic of MSCs. Since the CFU-F assay is considered to provide the closest estimate of MSC levels [19], we evaluated the colony-forming efficacy of cells isolated from the human synovial membranes. The cells developed large colonies as the culture continued for 10 days (Figure 1(b)), suggesting the high yield and expansion potential of the isolated MSCs. Flow cytometry analysis revealed that SM-MSCs were negative for the hematopoietic lineage markers CD34 and CD45, whereas they were positive for CD73, CD90, and CD105 (Figure 1(c)). SM-MSCs were able to differentiate toward mature adipocytes and osteocytes revealed by Oil Red O staining and Alizarin Red S staining (Figure 1(d)).

3.2. Administration of SM-MSC Ameliorated Collagen-Induced Arthritis. We injected the prepared cells intra-articularly into the right knees of the mice on days 28, 32, and 38 after the first immunization (Figure 2(a)). Repeated intra-articular injection of 10^6 SM-MSCs in the right knee efficiently attenuated the arthritis symptoms (Figure 2(b)) and decreased the mean arthritis scores ($p < 0.05$) (Figure 2(c)). The hind paw thicknesses of SM-MSC-injected mice were significantly lower than those of control mice ($p < 0.05$) (Figure 2(d)). Histologically CIA treated with PBS was characterized by the accumulation of inflammatory infiltrates in the synovial tissue, synovial hyperplasia of the synovial lining layer, followed by the formation of pannus and joint damage. Histological analysis of the ankle joints in SM-MSC-treated mice revealed a rather normal joint architecture, exhibiting markedly decreased cellular infiltration, without or limited synovitis and pannus formation (Figure 2(e)). Thus, repeated intra-articular injection of SM-MSCs exerted a profound therapeutic effect in CIA.

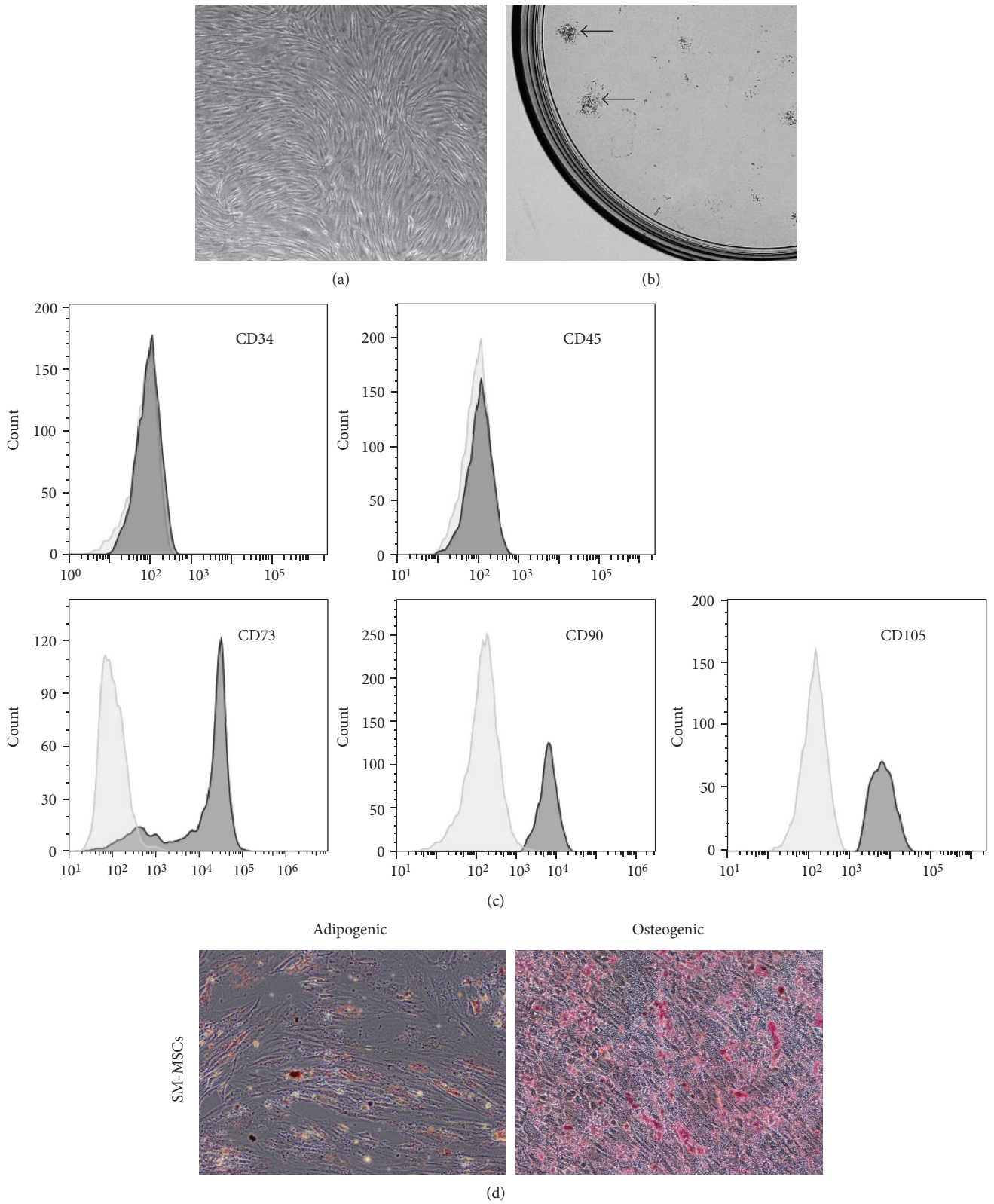

Figure 1: Characterization of MSCs isolated from human synovial membranes. (a) SM-MSCs from passage 3 exhibited a typical spindle-shaped morphology under an inverted microscope. (b) Representative colony-forming unit analysis. (c) Phenotypic analysis of SM-MSCs by flow cytometry. Histograms showed levels of surface antigen expression and their corresponding isotype control. (d) Multilineage differentiation potential of SM-MSCs. Samples were stained with Oil Red O, indicating differentiated adipocytes, and with Alizarin Red S staining, indicating mature osteoblasts. Original magnification, ×100. SM-MSCs, synovial membrane-derived MSCs.

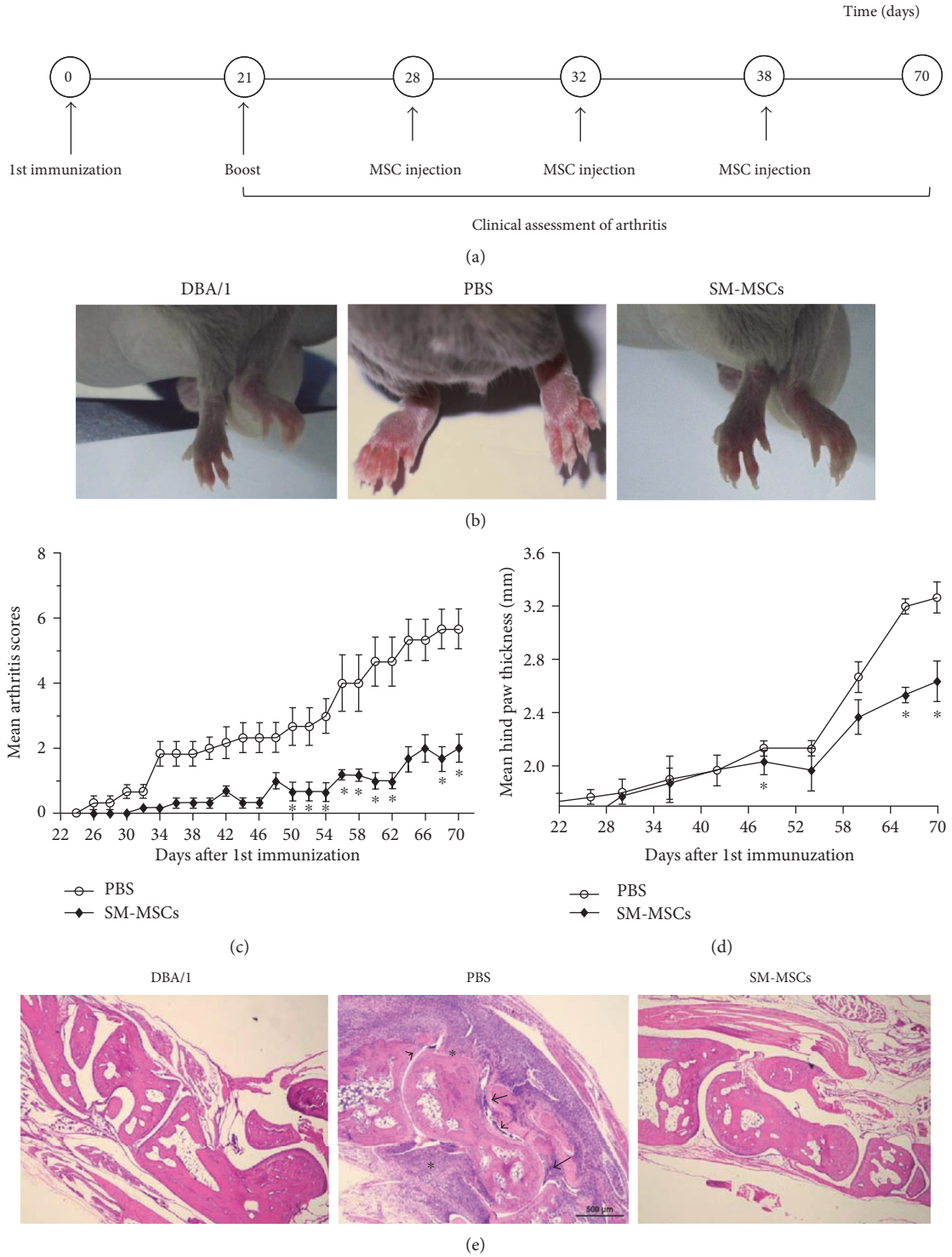

Figure 2: Decrease in severity of CIA following SM-MSC treatment. (a) Experimental design. DBA/1 mice were subcutaneously immunized with 200 μg CII in Freund's complete adjuvant on day 0 and administered a booster dose via intradermal injection of 100 μg CII into the tail on day 21. The CII-immunized mice were treated three times with SM-MSCs (10^6) in 7 μL PBS or PBS alone intra-articularly when arthritis had been established ($n = 8$ per group). The arthritis index score and hind paw thickness of mice in each group were recorded following booster immunization. (b) Representative photos of the paws in normal mice, PBS-treated mice, and SM-MSC-treated mice. (c) Arthritis severity was scored every 2 days, and (d) hind paw thickness was measured every 6 days. (e) Histological sections of the ankle joints (right) were stained with H&E (magnification, ×40). The asterisks denote the presence of inflammatory infiltrates, the arrows indicate synovial hyperplasia, and the arrowheads show the formation of pannus layer. Data have been presented as mean±SD values. $^*p < 0.05$, compared with corresponding time point.

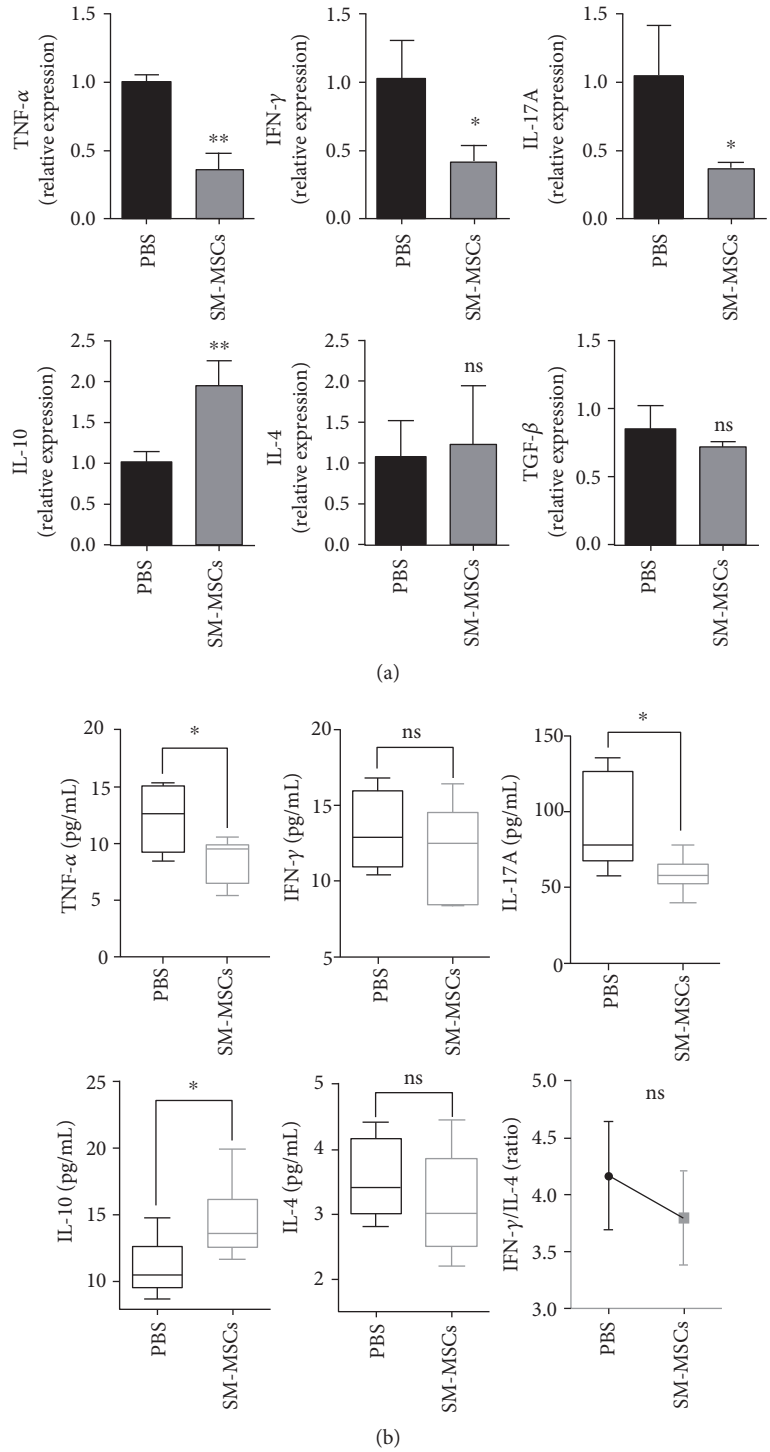

Figure 3: Effect of local SM-MSC administration on cytokine profiles in CIA mice. (a) Synovia of the right knee joints was harvested from five mice of each group at the end of the experiment, and quantitative PCR was performed to measure mRNA levels of several cytokines in resident synoviocytes. The mRNA levels of the target genes were normalized to those of the β-actin gene. (b) Peripheral blood from SM-MSC-treated mice and PBS-treated mice was obtained on day 70, and serum samples were tested for TNF-α, IFN-γ, IL-17A, IL-10, and IL-4 concentrations by using Milliplex analysis. The IFN-γ/IL-4 ratio was calculated. Data have been shown as mean±SD values. $^{*}p < 0.05$, $^{**}p < 0.01$; ns, no significance.

3.3. Reprogramming Cytokine Profiles following SM-MSC Treatment. We analyzed the cytokine gene expression of resident synoviocytes in the absence or presence of allogeneic SM-MSCs. The synovial tissues (right knee joints) were harvested from the mice on day 70, and mRNA levels of TNF-α, IFN-γ, IL-17A, IL-10, IL-4, and TGF-β were quantified. Compared with the findings for PBS-treated controls, the synoviocytes in the presence of SM-MSCs showed

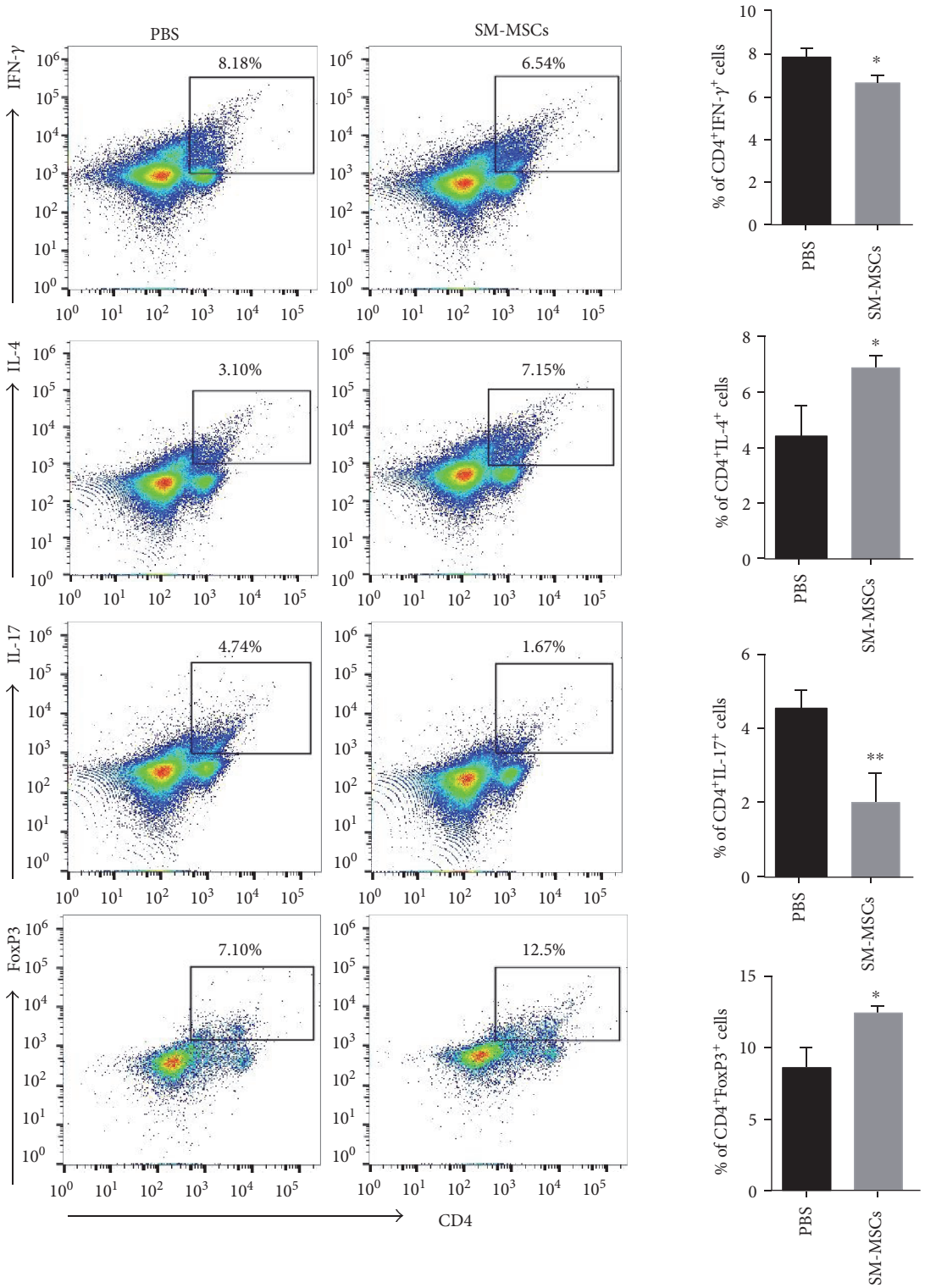

(a)

Figure 4: Continued.

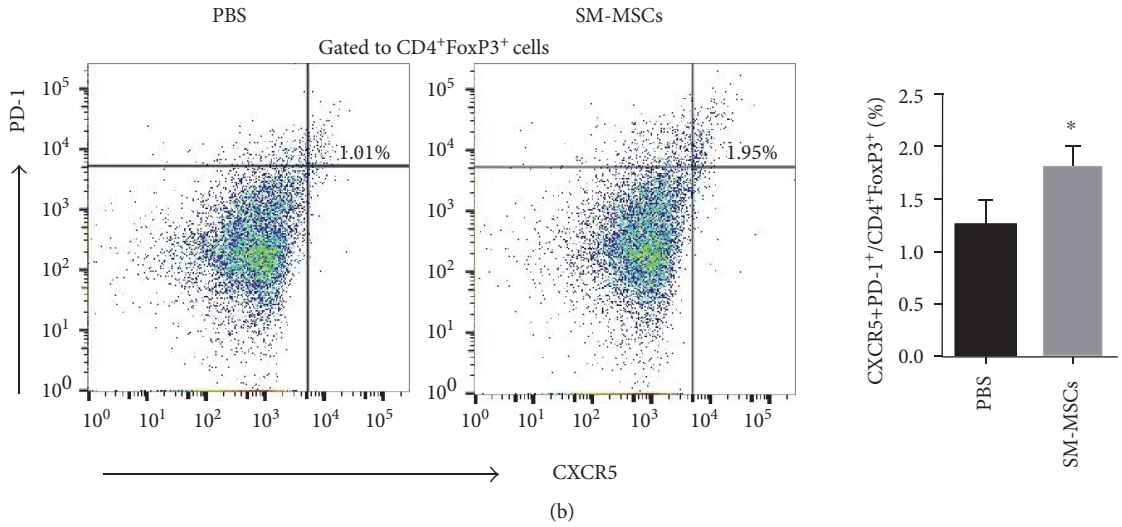

Figure 4: Effect of SM-MSC treatment on the frequency of Th cell subsets in mice with CIA. Splenocytes from the mice in each group ($n = 5$ per group) were prepared and stimulated with PMA/ionomycin for 4 h, following which they were analyzed by flow cytometry. (a) Left, frequencies of Th1 ($CD4^+IFN\text{-}\gamma^+$), Th2 ($CD4^+IL\text{-}4^+$), Th17 ($CD4^+IL\text{-}17^+$), and Treg ($CD4^+FoxP3^+$) cells in the spleens of mice treated or not treated with SM-MSCs. Right, corresponding bar graphs show quantification of cell percentages. (b) Left, Tfr cells were assessed for the expression of $PD\text{-}1^+CXCR5^+$ cells gated from $CD4^+FoxP3^+$ cells by flow cytometry. Right, quantification of the percentage of $CD4^+CXCR5^+PD\text{-}1^+FoxP3^+$ cells. Data have been presented as mean±SD values. $^*p < 0.05$, $^{**}p < 0.01$.

decreased TNF-α, IFN-γ, and IL-17A expression (TNF-α: $p = 0.0013$, IFN-γ: $p = 0.0268$, and IL-17A: $p = 0.0323$), accompanied with an important increase in IL-10 transcripts ($p = 0.0067$). IL-4 and TGF-β expression did not significantly differ between the SM-MSC-treated and PBS-treated groups (IL-4: $p = 0.7568$, TGF-β: $p = 0.3141$) (Figure 3(a)).

Next, we analyzed the cytokine concentrations in serum. Multiplex analysis revealed that TNF-α and IL-17A concentrations in serum significantly decreased in SM-MSC-treated mice, whereas the titers of the anti-inflammatory mediator IL-10 significantly increased (TNF-α: $p = 0.0264$, IL-17A: $p = 0.0424$, and IL-10: $p = 0.0438$). No significant difference was observed in IFN-γ and IL-4 levels after SM-MSC treatment in CIA mice (IFN-γ: $p = 0.4603$, IL-4: $p = 0.3976$). However, the IFN-γ/IL-4 ratio was much lower in mice treated with SM-MSCs than in PBS controls ($p = 0.1845$) (Figure 3(b)). Collectively, these data demonstrated that local administration of SM-MSCs resulted in a systemic regulatory effect on cytokine profiles in CIA mice.

3.4. SM-MSC Treatment Corrected the Balance between Th1/Th17 and FoxP3-Expressing Treg Cells in the Spleen. Dysregulated Th cell subsets have been proved to be major players in triggering the cytokine cascade responsible for tissue injury [20]. Hence, we next addressed whether repeated SM-MSC treatment for mice with CIA could correct the balance of Th cell subsets in the spleen. Splenocytes were isolated and stimulated with PMA/ionomycin before flow cytometry analysis. The frequency of Th1 cells, defined as IFN-γ-expressing $CD4^+$ T cells, was significantly lower in SM-MSC-treated mice than in PBS-treated mice, whereas Th2 cells, defined as IL-4-expressing $CD4^+$ T cells notably increased (Th1: $p = 0.0190$, Th2: $p = 0.0247$). Moreover, there were fewer IL-17-expressing $CD4^+$ T cells and much more $FoxP3^+CD4^+$ Treg cells in SM-MSC-treated mice (Th17: $p = 0.0087$, Treg: $p = 0.0121$) (Figure 4(a)). Thus, SM-MSCs could help recover the Th1/Th2 and Th17/Treg cell balance in CIA.

The critical enhancement of $FoxP3^+$ T cells by SM-MSCs prompted further analysis of the subpopulation of Treg cells. Follicular Treg (Tfr) cells, originating from natural Treg precursors, have been documented to have a suppressive effect upon T cell proliferation in vitro and germinal center (GC) B cell responses in vivo [21, 22]. In our study, a significant increase in $CD4^+CXCR5^+PD\text{-}1^+FoxP3^+$ Tfr cells was observed in SM-MSC-treated mice as compared to PBS controls ($p = 0.0368$) (Figure 4(b)). Together, these data indicated that increase in FoxP3-expressing Treg cells, accompanied by decrease in Th1 and Th17 responses, was involved in the mechanisms underlying arthritis remission under SM-MSC treatment.

3.5. SM-MSCs Favored the Development of Regulatory B Cells in the Spleen. Previous research showed that regulatory B cells play a key role in the maintenance of peripheral tolerance via Th1 and Th17 response inhibition and $FoxP3^+$ Treg cell pool induction [23]. Furthermore, Tfr cells in the spleen require regulatory B cells for optimal expansion and differentiation [24]. To determine whether increase in Treg cells in SM-MSCs-treated mice was accompanied by increase in regulatory B cells, we analyzed the proportion of several B cell subsets that have previously been characterized in the case of mechanisms underlying immune tolerance [25]. $B220^+$ cells were phenotypically analyzed for CD21 and CD23 expression. SM-MSC-treated mice had a considerably higher frequency of $CD21^{hi}CD23^{hi}$ T2 cells and $CD23^{low}CD21^{hi}$ MZ

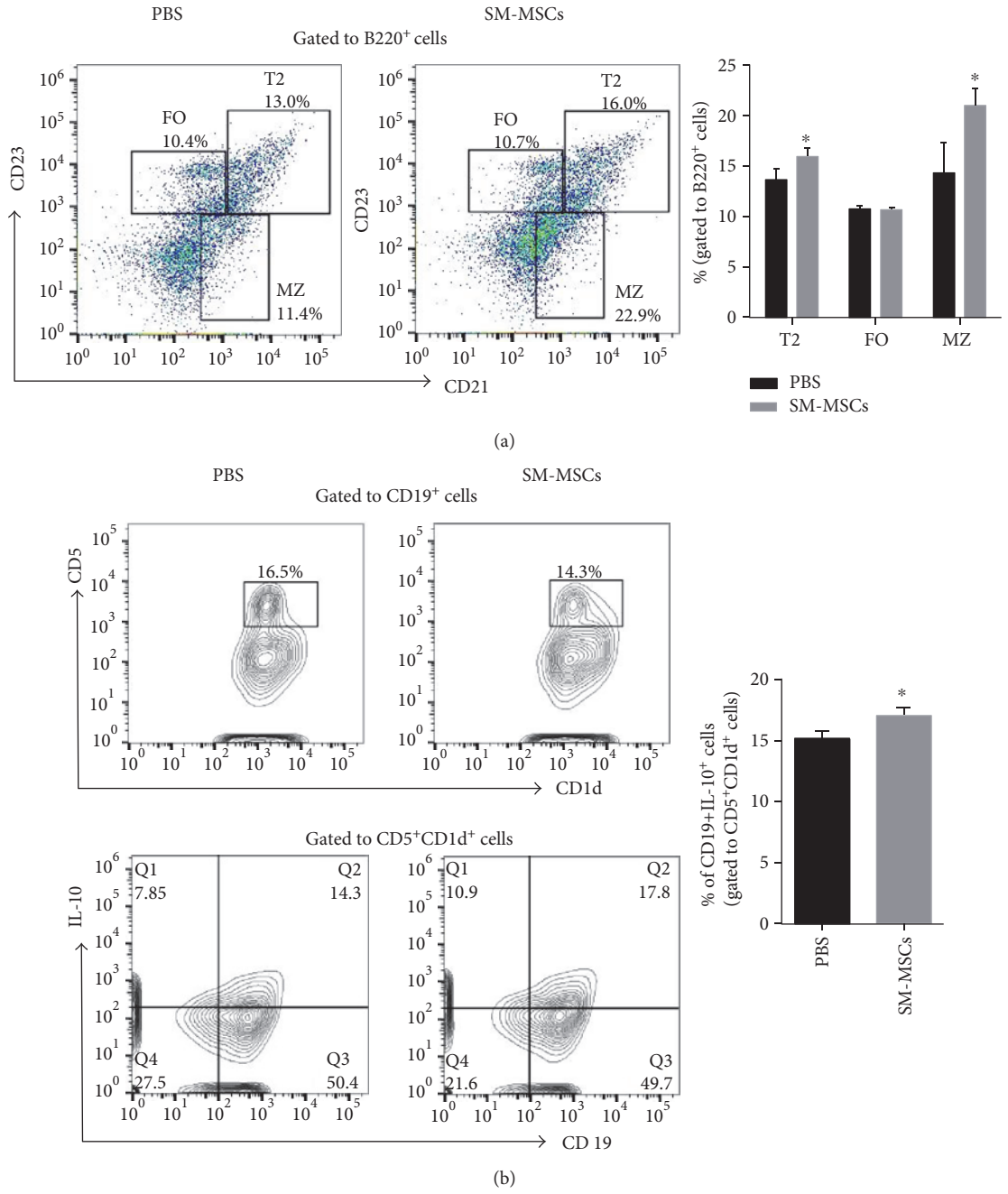

Figure 5: SM-MSCs favored the development of regulatory B cells in the spleen. (a) Surface expression of CD21 and CD23 on $B220^+$ gated B cells derived from mice treated or not treated with SM-MSCs ($n = 5$ per group). The proportions of T2 ($CD21^{hi}CD23^{hi}$), FO ($CD21^{int}CD23^{int}$), and MZ ($CD23^{low}CD21^{hi}$) cells were analyzed by flow cytometry. (b) Splenocytes were stimulated with PMA/ionomycin for 4 h and analyzed for the frequency of B10 ($CD19^+CD5^+CD1d^+IL\text{-}10^+$) cells in mice. Data have been presented as mean±SD values. $^*p < 0.05$.

cells than PBS controls, while the proportion of $CD21^{int}CD23^{int}$ follicular (FO) B cells was similar between the two groups (T2: $p = 0.03963$, FO: $p = 0.88202$, and MZ: $p = 0.03065$) (Figure 5(a)). The cells with a $CD19^+CD5^+CD1d^+IL\text{-}10^+$ phenotype, that is, B10 cells, increased in SM-MSC-treated mice ($p = 0.0277$) (Figure 5(b)). Collectively, our results demonstrated that SM-MSCs induced increase in regulatory B subsets, comprising T2, MZ, and B10 cells, in the spleen of CIA mice.

4. Discussion

RA is a typically chronic and progressive autoimmune disease, which is associated with the breakdown of immune tolerance and with aberrant inflammatory responses. Although new therapeutic agents such as biologicals are now available, a considerable proportion of patients are still resistant to these therapies. MSC-based cell therapy is a promising option for patients with RA because of the anti-

inflammatory, immunomodulatory, and regenerative properties of these cells. Appropriate sources of MSCs, ideal administration route, and optimal disease timing/stage are essential factors for achieving valid therapeutic effects.

In this study, human SM-MSCs were selected from among numerous cell sources because of their strong immunomodulatory properties during coculture with T lymphocytes in vitro and high proliferation capability with limited senescence [14]. Furthermore, the "off-the-shelf" property of MSCs makes the allogeneic human-derived MSCs available for murine CIA [26]. MSCs from the synovial membranes of osteoarthritic joints were found to be capable of suppressing $CD4^+$ T cell proliferation upon CD3/CD28 stimulation, whereas BM-MSCs from the same patient could not [16]. In addition, human synovial membranes are an accessible source of MSCs. They are routinely removed in patients with OA, during arthroscopy and knee replacement surgery, which offers the advantage of excellent supply for future clinical applications. Moreover, previous research on SM-MSCs highlighted the important properties of these cells in tissue repair; these data suggest that SM-MSCs would be a promising option for the treatment of destructive diseases of the bone and cartilage [27].

To our knowledge, our study is the first to show the therapeutic effect of SM-MSCs in CIA. CIA is the most commonly studied murine model of RA and generally thought to be dependent on collagen-specific $CD4^+$ T cells during the initial phase of autoimmune responses in the joints [28]. Repeated administration of SM-MSCs into inflamed joints could attenuate arthritis severity with reduction in inflammatory cytokines and increase in IL-10 production in serum, suggesting that local MSC treatment could exert a systemic therapeutic effect in mice. Recent studies reported that repeated intra-articular administration of allogeneic MSCs could be a safe strategy, leading to enhanced MSC availability [29]. Similarly, a study using proteoglycan-induced arthritis (PGIA), a well-studied inflammatory arthritis model, showed that intra-articular administration of BM-MSCs effectively reduced cumulative arthritis scores and PG-specific IgG2a antibody levels in the serum [30]. Another study using murine antigen-induced arthritis also addressed the systemic anti-inflammatory effect of MSCs, reflected in reduced TNF-α concentrations in serum following injection of BM-MSCs into the knee joints [31]. It has been well documented that MSCs exert immunoregulatory effects via locally cell-cell contact or secretion of soluble modulatory mediators, where in particular MSC-derived indoleamine 2,3-dioxygenase (IDO) in human and inducible nitric oxide synthase (iNOS) in mouse [32]. Besides, the modulatory effects of MSCs on immune responses, especially by means of secreting soluble factors, are critically linked to the "license" by inflammatory signals occurred in which MSCs are applied to [33]. We assumed that the interplay between exogenous MSCs and resident synoviocytes may trigger a series of biological processes participating in the paracrine actions in MSCs, which is most likely responsible for the therapeutic effect of MSCs in CIA.

Although our results are promising, a limitation of the current study is that we did not track the distribution of the injected SM-MSCs in vivo. Previous studies have shown that MSCs injected intra-articularly are retained at the injection site for 1–4 weeks, without migration to distant organs such as the lungs, spleen, and liver [30, 31].

Our data presented here suggest that the therapeutic effect of SM-MSCs in CIA mice was paralleled by increase in regulatory $FoxP3^+$ T cells (Treg and Tfr) and induction of regulatory B cells (T2, MZ, and B10), both of which are essential for inhibiting dysregulated immune responses to self-antigens and are involved in self-tolerance mechanisms. Previous research documented that infusion of human gingiva-derived MSCs significantly ameliorated CIA via suppression of Th1 and Th17 responses and increase in FoxP3-expressing $CD4^+$ T cells in the spleen [34], which is in agreement with our findings. In addition, SM-MSCs appeared to hamper the maturation and differentiation of B cells and induce the IL-10-competent regulatory B cells in our study. This was supported by the increase in immature-transitional stage B cells such as $CD21^{hi}CD23^{hi}$ transitional 2 (T2) cells and $CD23^{low}CD21^{hi}$ MZ cells, as well as $CD5^+CD1d^+IL\text{-}10^+$ cells, in the spleens of SM-MSC-treated mice. Transfer of immature T2 cells from mice with arthritis at the remission stage could help recover the balance between Treg and Th1/Th17 responses in $IL\text{-}10^{-/-}$ hosts [35, 36]. Similarly, adoptive transfer of $CD5^+CD1d^+IL\text{-}10^+$ regulatory B cells prevented CIA development in mice with suppression of Th17 cells in the spleen and draining lymph nodes [25]. Clinical data also revealed that patients with new-onset RA had lesser IL-10-competent B cells, comprising $CD19^+CD5^+CD1d^+$ cells and $CD19^+$ $TIM1^+$ cells, than healthy controls and that this decrease was positively correlated with the number of $CD4^+CD25^+FoxP3^+$ Treg cells in peripheral blood [37]. Given the above and previous data, we hypothesize that, not only $FoxP3^-$ Treg cells but also T2-, MZ-, and IL-10-expressing regulatory B cells were responsible for the suppression of inflammatory responses in mice with CIA, suggesting that the cellular interactions between regulatory B cells and Treg cells were pivotal in determining the beneficial outcome of SM-MSCs in CIA. A functional feed-forward loop between immunoregulatory T cells and B cells during SM-MSC treatment is of great interest and requires further study.

5. Conclusions

To our knowledge, the current study is the first to show that intra-articular injection of SM-MSCs could prevent arthritis development and suppress immune responses via expansion of $FoxP3^+$ Treg cells and T2, MZ, and IL-10-competent regulatory B cells, thus recovering peripheral tolerance in mice with CIA. Our findings established the in vivo effect of SM-MSCs in CIA mice, indicating that intra-articular administration of SM-MSCs may constitute a potential approach for RA cell therapy.

Conflicts of Interest

The authors declare that there is no conflict of interest regarding the publication of this paper.

Acknowledgments

This study was supported by the National Natural Science Foundation of China (81373202) and National High Technology Research and Development Program of China (2015AA042401). The authors would like to thank Editage (www.editage.com) for the English language editing.

References

[1] G. S. Firestein, "Evolving concepts of rheumatoid arthritis," *Nature*, vol. 423, no. 6937, pp. 356–361, 2003.

[2] F. A. Cooles, J. D. Isaacs, and A. E. Anderson, "Treg cells in rheumatoid arthritis: an update," *Current Rheumatology Reports*, vol. 15, no. 9, p. 352, 2013.

[3] A. Alunno, E. Bartoloni, G. Nocentini et al., "Role of regulatory T cells in rheumatoid arthritis: facts and hypothesis," *Autoimmunity Highlights*, vol. 1, no. 1, pp. 45–51, 2010.

[4] M. Haque, K. Fino, F. Lei, X. Xiong, and J. Song, "Utilizing regulatory T cells against rheumatoid arthritis," *Frontiers in Oncology*, vol. 4, p. 209, 2014.

[5] X. Niu, S. Deng, S. Li et al., "Therapeutic effect of ergotope peptides on CIA by down-regulation of inflammatory and Th1/Th17 responses and induction of regulatory T cells," *Molecular Medicine*, vol. 22, pp. 608–620, 2016.

[6] A. M. Gizinski and D. A. Fox, "T cell subsets and their role in the pathogenesis of rheumatic disease," *Current Opinion in Rheumatology*, vol. 26, no. 2, pp. 204–210, 2014.

[7] M. Dominici, K. Le Blanc, I. Mueller et al., "Minimal criteria for defining multipotent mesenchymal stromal cells. The International Society for Cellular Therapy position statement," *Cytotherapy*, vol. 8, no. 4, pp. 315–317, 2006.

[8] Y. Liu, R. Mu, S. Wang et al., "Therapeutic potential of human umbilical cord mesenchymal stem cells in the treatment of rheumatoid arthritis," *Arthritis Research & Therapy*, vol. 12, no. 6, p. R210, 2010.

[9] E. I.-J. JJ, E. I.-S. YM, E. A. Jones, and D. McGonagle, "Mesenchymal stem cells, autoimmunity and rheumatoid arthritis," *QJM*, vol. 107, no. 7, pp. 505–514, 2014.

[10] A. Papadopoulou, M. Yiangou, E. Athanasiou et al., "Mesenchymal stem cells are conditionally therapeutic in preclinical models of rheumatoid arthritis," *Annals of the Rheumatic Diseases*, vol. 71, no. 10, pp. 1733–1740, 2012.

[11] J. Xie, D. Xiao, Y. Xu et al., "Up-regulation of immunomodulatory effects of mouse bone-marrow derived mesenchymal stem cells by tetrahydrocannabinol pre-treatment involving cannabinoid receptor CB2," *Oncotarget*, vol. 7, no. 6, pp. 6436–6447, 2016.

[12] T. H. Shin, H. S. Kim, T. W. Kang et al., "Human umbilical cord blood-stem cells direct macrophage polarization and block inflammasome activation to alleviate rheumatoid arthritis," *Cell Death & Disease*, vol. 7, no. 12, p. e2524, 2016.

[13] M. Ayatollahi, T. Talaei-Khozani, and M. Razmkhah, "Growth suppression effect of human mesenchymal stem cells from bone marrow, adipose tissue, and Wharton's jelly of umbilical cord on PBMCs," *Iranian Journal of Basic Medical Sciences*, vol. 19, no. 2, pp. 145–153, 2016.

[14] C. De Bari, F. Dell'Accio, P. Tylzanowski, and F. P. Luyten, "Multipotent mesenchymal stem cells from adult human synovial membrane," *Arthritis and Rheumatism*, vol. 44, no. 8, pp. 1928–1942, 2001.

[15] S. Hagmann, T. Gotterbarm, T. Müller et al., "The influence of bone marrow- and synovium-derived mesenchymal stromal cells from osteoarthritis patients on regulatory T cells in co-culture," *Clinical and Experimental Immunology*, vol. 173, no. 3, pp. 454–462, 2013.

[16] S. Hagmann, C. Rimmele, F. Bucur et al., "Mesenchymal stromal cells from osteoarthritic synovium are a distinct population compared to their bone-marrow counterparts regarding surface marker distribution and immunomodulation of allogeneic CD4+ T-cell cultures," *Stem Cells International*, vol. 2016, Article ID 6579463, 17 pages, 2016.

[17] C. H. Jo, H. J. Ahn, H. J. Kim, S. C. Seong, and M. C. Lee, "Surface characterization and chondrogenic differentiation of mesenchymal stromal cells derived from synovium," *Cytotherapy*, vol. 9, no. 4, pp. 316–327, 2007.

[18] K. Toupet, M. Maumus, P. Luz-Crawford et al., "Survival and biodistribution of xenogenic adipose mesenchymal stem cells is not affected by the degree of inflammation in arthritis," *PloS One*, vol. 10, no. 1, article e0114962, 2015.

[19] P. Bianco, S. A. Kuznetsov, M. Riminucci, and P. Gehron Robey, "Postnatal skeletal stem cells," *Methods in Enzymology*, vol. 419, pp. 117–148, 2006.

[20] L. T. Osnes, B. Nakken, E. Bodolay, and P. Szodoray, "Assessment of intracellular cytokines and regulatory cells in patients with autoimmune diseases and primary immunodeficiencies-novel tool for diagnostics and patient follow-up," *Autoimmunity Reviews*, vol. 12, no. 10, pp. 967–971, 2013.

[21] M. A. Linterman, W. Pierson, S. K. Lee et al., "Foxp3+ follicular regulatory T cells control the germinal center response," *Nature Medicine*, vol. 17, no. 8, pp. 975–982, 2011.

[22] P. T. Sage and A. H. Sharpe, "T follicular regulatory cells," *Immunological Reviews*, vol. 271, no. 1, pp. 246–259, 2016.

[23] R. X. Wang, C. R. Yu, I. M. Dambuza et al., "Interleukin-35 induces regulatory B cells that suppress autoimmune disease," *Nature Medicine*, vol. 20, no. 6, pp. 633–641, 2014.

[24] S. M. Kerfoot, G. Yaari, J. R. Patel et al., "Germinal center B cell and T follicular helper cell development initiates in the interfollicular zone," *Immunity*, vol. 34, no. 6, pp. 947–960, 2011.

[25] M. Yang, J. Deng, Y. Liu et al., "IL-10-producing regulatory B10 cells ameliorate collagen-induced arthritis via suppressing Th17 cell generation," *Immunity*, vol. 180, no. 6, pp. 2375–2385, 2012.

[26] O. W. Gramlich, A. J. Burand, A. J. Brown, R. J. Deutsch, M. H. Kuehn, and J. A. Ankrum, "Cryopreserved mesenchymal stromal cells maintain potency in a retinal ischemia/reperfusion injury model: toward an off-the-shelf therapy," *Scientific Reports*, vol. 23, no. 6, p. 26463, 2016.

[27] X. Song, Y. Xie, Y. Liu, M. Shao, and W. Wang, "Beneficial effects of coculturing synovial derived mesenchymal stem cells with meniscus fibrochondrocytes are mediated by fibroblast growth factor 1: increased proliferation and collagen synthesis," *Stem Cells International*, vol. 2015, Article ID 926325, 11 pages, 2015.

[28] N. Komatsu and H. Takayanagi, "Inflammation and bone destruction in arthritis: synergistic activity of immune and mesenchymal cells in joints," *Frontiers in Immunology*, vol. 3, p. 77, 2012.

[29] N. Ardanaz, F. J. Vazquez, A. Romero et al., "Inflammatory response to the administration of mesenchymal stem cells in an equine experimental model: effect of autologous, and single

and repeat doses of pooled allogeneic cells in healthy joints," *BMC Veterinary Research*, vol. 12, p. 65, 2016.

[30] J. F. Swart, S. de Roock, F. M. Hofhuis et al., "Mesenchymal stem cell therapy in proteoglycan induced arthritis," *Annals of the Rheumatic Diseases*, vol. 74, no. 4, pp. 760–777, 2015.

[31] O. Kehoe, A. Cartwright, A. Askari, A. J. El Haj, and J. Middleton, "Intra-articular injection of mesenchymal stem cells leads to reduced inflammation and cartilage damage in murine antigen-induced arthritis," *Journal of Translational Medicine*, vol. 12, no. 157, 2014.

[32] G. Ren, J. Su, L. Zhang et al., "Species variation in the mechanisms of mesenchymal stem cell-mediated immunosuppression," *Stem Cells*, vol. 27, no. 8, pp. 1954–1962, 2009.

[33] M. Krampera, J. Galipeau, Y. Shi, K. Tarte, L. Sensebe, and MSC Committee of the International Society for Cellular Therapy (ISCT), "Immunological characterization of multipotent mesenchymal stromal cells—the International Society for Cellular Therapy (ISCT) working proposal," *Cytotherapy*, vol. 15, no. 9, pp. 1054–1061, 2013.

[34] M. Chen, W. Su, X. Lin et al., "Adoptive transfer of human gingiva-derived mesenchymal stem cells ameliorates collagen-induced arthritis via suppression of Th1 and Th17 cells and enhancement of regulatory T cell differentiation," *Arthritis and Rheumatism*, vol. 65, no. 5, pp. 1181–1193, 2013.

[35] N. A. Carter, R. Vasconcellos, E. C. Rosser et al., "Mice lacking endogenous IL-10-producing regulatory B cells develop exacerbated disease and present with an increased frequency of Th1/Th17 but a decrease in regulatory T cells," *Journal of Immunology*, vol. 186, no. 10, pp. 5569–5579, 2011.

[36] J. G. Evans, K. A. Chavez-Rueda, A. Eddaoudi et al., "Novel suppressive function of transitional 2 B cells in experimental arthritis," *Journal of Immunology*, vol. 178, no. 12, pp. 7868–7878, 2007.

[37] L. Ma, B. Liu, Z. Jiang, and Y. Jiang, "Reduced numbers of regulatory B cells are negatively correlated with disease activity in patients with new-onset rheumatoid arthritis," *Clinical Rheumatology*, vol. 33, no. 2, pp. 187–195, 2014.

Hindawi
Stem Cells International
Volume 2017, Article ID 4960831, 7 pages
https://doi.org/10.1155/2017/4960831

Research Article

Adipose Tissue-Derived Mesenchymal Stem Cells Have a Heterogenic Cytokine Secretion Profile

Yongkang Wu,[1,2] Martin J. Hoogduijn,[1] Carla C. Baan,[1] Sander S. Korevaar,[1] Ronella de Kuiper,[1] Lin Yan,[1,2] Lanlan Wang,[2] and Nicole M. van Besouw[1]

[1]*Nephrology & Transplantation, Department of Internal Medicine, Erasmus MC, University Medical Center Rotterdam, Rotterdam, Netherlands*
[2]*West China Hospital, Department of Laboratory Medicine, Sichuan University, Chengdu, China*

Correspondence should be addressed to Nicole M. van Besouw; n.vanbesouw@erasmusmc.nl

Received 7 March 2017; Revised 9 May 2017; Accepted 16 May 2017; Published 31 May 2017

Academic Editor: Vladislav Volarevic

Mesenchymal stem cells derived from adipose tissue (ASC) have immune regulatory function, which makes them interesting candidates for cellular therapy. ASC cultures are however heterogeneous in phenotype. It is unclear whether all ASC contribute equally to immunomodulatory processes. ASC are also responsive to cytokine stimulation, which may affect the ratio between more and less potent ASC populations. In the present study, we determined IL-6 receptor (CD126 and CD130 subunits) and IFN-γ receptor (CD119) expression on ASC by flow cytometry. The production of IL-6 and IFN-γ was measured by ELISA and the frequency of IL-6 and IFN-γ secreting cells by ELISPOT. The results showed that ASC did not express CD126, and only 10–20% of ASC expressed CD130 on their surface, whereas 18–31% of ASC expressed CD119. ASC produced high levels of IL-6 and 100% of ASC were capable of secreting IL-6. Stimulation by IFN-γ or TGF-β had no effect on IL-6 secretion by ASC. IFN-γ was produced by only 1.4% of ASC, and TGF-β significantly increased the frequency to 2.7%. These results demonstrate that ASC cultures are heterogeneous in their cytokine secretion and receptor expression profiles. This knowledge can be employed for selection of potent, cytokine-producing, or responsive ASC subsets for cellular immunotherapy.

1. Introduction

Mesenchymal stem cells (MSC) are adult stem cells with the ability to differentiate into several lineages, such as osteoblasts, chondrocytes, myocytes, and adipocytes [1]. Initial studies focused on MSC derived from the bone marrow but subsequently the presence of MSC in, amongst others, adipose tissue was demonstrated [2], so-called adipose tissue-derived mesenchymal stem cells (ASC). Adipose tissue has some advantages above the bone marrow as a source of MSC as it is relatively easy to access, it is abundant, and the procedure for isolating ASC is easy [3]. It is well known that ASC have a broad immune regulatory function [4, 5], which makes them suitable for cellular therapy.

ASC suppress the proliferation and inflammatory cytokine production of activated immune cells and induce the formation of immunoregulatory cell types, such as regulatory T cells and alternatively activated macrophages [6, 7]. Bone marrow and adipose tissue-derived MSC employ similar mechanisms for immunomodulation [8]. These include targeting immune cells via both cell contact-dependent and cell contact-soluble interactions, such as via the inhibitory costimulatory programmed death ligand 1 (PD-L1) pathway [9] and via the secretion of soluble factors [10]. A multitude of factors have been proposed to play a role in the immunomodulatory effect of MSC, including hepatocyte growth factor (HGF) [11], HLA-G [10], and IL-6 [12]. Although generally seen as a proinflammatory cytokine, IL-6 has a clear dual function and can enforce as well as suppress immune responses, depending on the conditions [13]. Furthermore, the tryptophan-depleting enzyme indoleamine 2,3-dioxygenase (IDO) plays a major contribution to the antiproliferative effect of MSC [14]. MSC in their turn

respond to inflammatory cytokines, in particular IFN-γ, but also TNF-α and IL-17, by dramatically increasing IDO and PD-L1 expression thereby strongly enhancing their immunosuppressive properties [15–17]. MSC are potent secretors of anti-inflammatory TGF-β which contributes to their immune regulatory effects [18], and in addition, TGF-β affects the immune regulatory function of MSC themselves too [19].

Although MSC are clearly involved in cross talk with immune cells, not all MSC may do this in the same way as there is considerable heterogeneity within MSC populations. There is heterogeneity in the differentiation potential of MSC [20, 21], and there is heterogeneity in the expression of cell surface markers such as STRO-1 and CD271, and STRO-1 and CD271 expressing MSC have been demonstrated to possess enhanced immunomodulatory capacity [22, 23]. The heterogeneity of MSC may impair their therapeutic efficacy and introduce variations between studies [24]. One the other hand, it offers opportunities to isolate super-potent MSC from heterogenic populations.

ELISPOT assays are widely used for nonadherent lymphocytes and is more sensitive than ELISA. The ELISPOT assay had not been described for adherent ASC. The advantage of ELISPOT is the sensitive technique for detecting a cytokine at single cell level and allowing frequency analysis [25–27].

We questioned whether ASC populations are heterogenic in their cytokine secretion and cytokine receptor expression profile. Furthermore, we examined whether potential heterogeneity was affected by cytokine stimulation of ASC. In the present study, we enumerate IL-6 and IFN-γ in single-secreting ASC by ELISPOT assay. Furthermore, we studied the frequency of IL-6 and IFN-γ receptor expressing ASC and examined the effect of IFN-γ and TGF-β stimulation on ASC cytokine production.

2. Materials and Methods

2.1. Isolation and Culture of ASC. ASC were isolated from human subcutaneous adipose tissue that became available upon donation of living kidney donors after written informed consent (protocol number MEC-2006-190 approved by the Medical Ethics Committee of the Erasmus MC, Rotterdam) as previously described [28]. In brief, after mechanical disruption and enzymatic digestion of the adipose tissue, the cells were collected in minimum essential medium-α (MEM-α) (Sigma-Aldrich, St. Louis, MO); supplemented with 1% penicillin/streptomycin solution (P/S; 100 IU/mL penicillin, 100 IU/mL streptomycin; Lonza, Verviers, Belgium), 2 mM L-glutamine (Lonza), and 15% fetal bovine serum (FBS; Lonza) (MSC medium); and seeded in T175 culture flasks (Greiner Bio-One, Kremsmunster, Germany) at 37°C, 5% CO_2, and 95% humidity. Cultures were refreshed twice weekly. When the cultures reached 90% confluence, ASC were removed from the culture flasks using 0.05% trypsin-EDTA (Life Technologies, Bleiswijk, Netherlands). ASC were used for experiments between passages 1 and 5.

2.2. Flow Cytometric Analysis. ASC were immunophenotypically characterized by staining for CD45-FITC, CD31-FITC, CD13-PECy7, CD73-PE, and CD90-APC (all BD Biosciences, San Jose, CA). For detection of IL-6 and IFN-γ receptors, 400,000 ASC ($n = 3$) were stained for two IL-6 receptor subunits (CD126 and CD130) and IFN-γ receptor (CD119). The cells were incubated with anti-CD126-PECy7 (BioLegend, San Diego, CA), anti-CD130-BV421 (BD Biosciences, San Jose, CA), anti-CD119-APC (SB Sino Biological Inc., Beijing, China), or isotype-matched control antibodies (eBioscience, San Diego, CA) in the dark for 30 min at room temperature. Thereafter, the cells were washed twice with FACSFlow (BD Biosciences) and measured on a FACS Canto II flow cytometer (BD Biosciences) and analyzed with Kaluza Analysis 1.3 software (Beckman-Coulter, Brea, CA).

2.3. Stimulation of ASC. ASC were stimulated for 72 hours with 50 ng/mL IFN-γ (Life Technologies, USA) or 10 ng/mL TGF-β (Peprotech, USA) prior to experiments in MEM-α with P/S, 2 mM L-glutamine, and 15% FBS. Unstimulated control cells were cultured in parallel.

2.4. IL-6 and IFN-γ ELISPOT Assay. PVDF membrane-bottomed 96-wells plates (multiscreen, Millipore Ireland) were incubated with 70% ethanol for 1 minute at room temperature. After washing the wells with PBS, the wells were precoated with anti-IL-6 mAb or anti-IFN-γ mAb (U-CyTech Biosciences, Utrecht, Netherlands) and blocked with PBS containing 1% BSA according to the manufacturer's protocol. In brief, ASC ($n = 4$: unstimulated, IFN-γ stimulated, and TGF-β stimulated) were seeded in triplicate at a concentration of 4000, 2000, 1000, 500, 250, 125, 62.5, and 31.25 ASC per well. Cells were incubated for 24 hours at the coated ELISPOT plate at 37°C, 5% CO_2, and 95% humidity to allow spot formation to occur. After incubation, the cells were lysed with ice-cold milli-Q water and the plates washed extensively. Subsequently, the wells were incubated with a biotinylated goat antihuman IL-6 or antihuman IFN-γ polyclonal Ab (U-CyTech Biosciences) for 1 hour at 37°C. After washing the wells, IL-6 spots were detected by streptavidin-HRP conjugate and an AEC substrate for IL-6 (U-Cytech Biosciences). IFN-γ spots were detected with phi-labeled goat antibiotin Ab (U-Cytech Biosciences) and a reagent that activates phi (reagent I + II, U-Cytech Biosciences). The reactions were stopped when spots were visualized by adding milli-Q water to the wells. The spots were counted by Bioreader 6000 Elispot-reader (BioSys GmbH, Karben, Germany).

2.5. ELISA. After pretreating ASC ($n = 5$) with IFN-γ or TGF-β for 72 hours, the cells were trypsinised and seeded at 50 (IL-6 ELISA) and 4000 (IFN-γ ELISA) cells per well in 96-well plates (Greiner Bio-One, Kremsmünster, Austria). After 24 hours, conditioned medium was collected. The production of IL-6 and IFN-γ was determined using ELISA kits (U-CyTech Biosciences, Utrecht, Netherlands) according to the manufacturer's instructions.

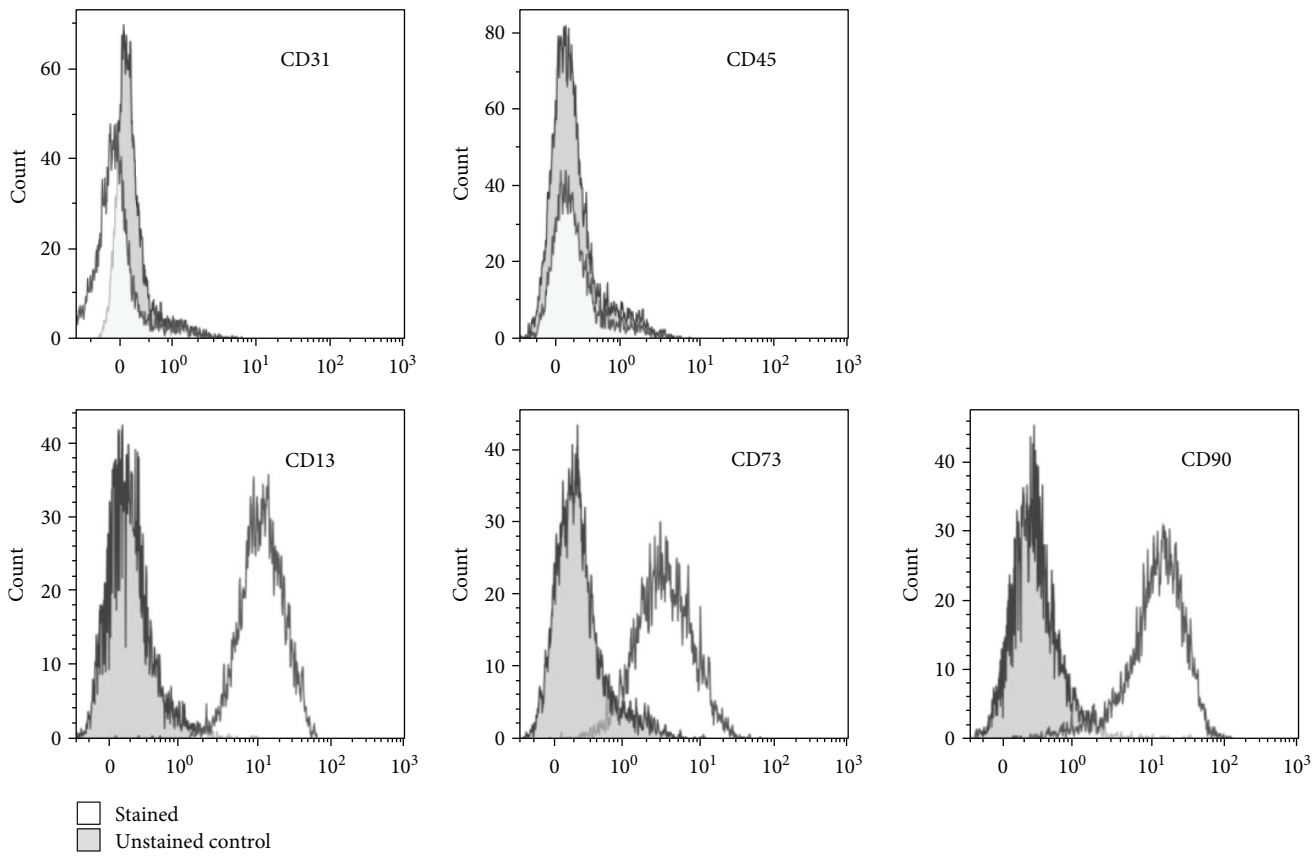

Figure 1: Immunophenotype of ASC. Flow cytometric analysis of the immunophenotype of ASC, demonstrating a lack of CD31 and CD45 expression and positive expression of CD13, CD73, and CD90.

2.6. Statistical Analysis. The effect of ASC pretreated with IFN-γ or TGF-β were analyzed by one-way ANOVA to compare differences in number of cytokine producing IFN-γ and IL-6 producing ASC and by two-tailed paired t-test to compare differences in IFN-γ and IL-6 ELISA. p values < 0.05 were considered significant.

3. Results

3.1. Immunophenotype of ASC. ASC showed a typical spindle-shaped morphology (data not shown) and lacked expression of the hematopoietic cell marker CD45 and of the endothelial cell marker CD31 (Figure 1). Nearly all cells expressed the markers CD13, CD73, and CD90, confirming the ASC phenotype of the cells.

3.2. Heterogeneity in ASC Cytokine Secretion Profiles. To determine whether control ASC and ASC pretreated with IFN-γ or TGF-β were capable of secreting IL-6 and IFN-γ, ELISA were performed on conditioned medium samples. IL-6 was detectable in a conditioned medium from 96-well plates containing as few as 50 ASC per well, demonstrating that IL-6 was abundantly secreted by ASC. There was no difference between control ASC and IFN-γ- or TGF-β-pretreated cultures in the level of IL-6 secretion (Figure 2). IFN-γ secretion by 4000 ASC was hardly detectable. TGF-β treatment of MSC significantly increased IFN-γ secretion (mean $\pm$ SD, OD 0.0248 ± 0.0102 versus 0.1035 ± 0.0268; $p = 0.02$: Figure 2).

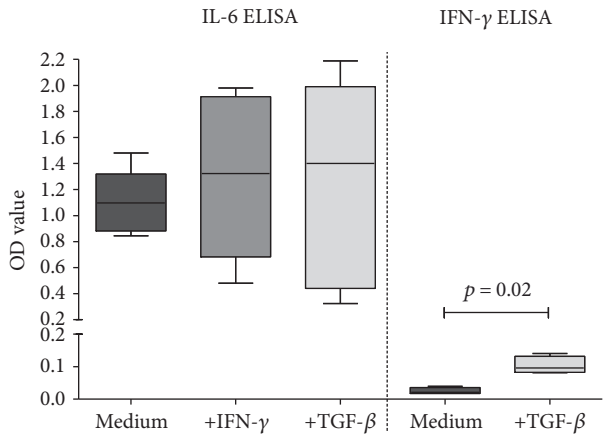

Figure 2: Secretion of IL-6 and IFN-γ by ASC. ASC ($n = 5$) (50 ASC for IL-6, 4000 ASC for IFN-γ) were cultured without or in the presence of IFN-γ or TGF-β for 72 h and washed and reseeded. IL-6 and IFN-γ ELISA were performed in 20 h conditioned medium. Data is presented as box and whisker plot (median and range). More IFN-γ was produced after pretreatment with TGF-β ($p = 0.02$, two-tailed paired t-test).

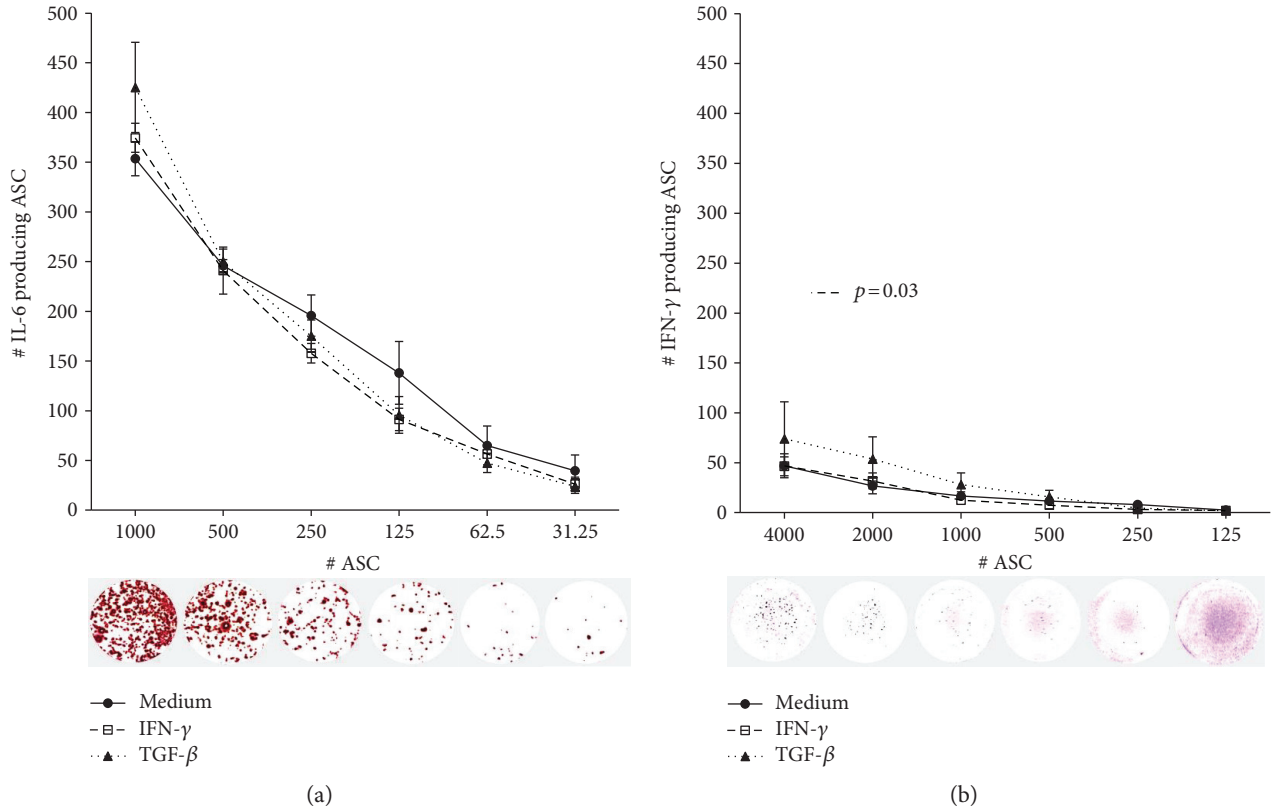

Figure 3: Frequency of IL-6 and IFN-γ secreting ASC. ASC ($n = 4$) were cultured without or in the presence of IFN-γ or TGF-β for 72 h and washed and reseeded at different cell densities. Frequencies of IL-6 (a) and IFN-γ (b) secreting ASC were determined by ELISPOT assay. Representative examples of the ELISPOT assay are shown. After TGF-β treatment, a higher frequency of IFN-γ producing ASC was found ($p = 0.03$, one-way ANOVA).

To examine whether IL-6 is secreted by all ASC, or whether a subpopulation of the cells is responsible for the IL-6 levels found, ELISPOT assay was performed. ASC were seeded in 96-well plates at different densities, ranging from 31 to 1000 cells per well to determine the frequency of IL-6 producing cells. At the lower ranges (31–125 ASC), we found approximately one IL-6 spot per ASC seeded (Figure 3(a)). At higher ASC ranges, the relative number of spots declined to less than 400 spots per 1000 ASC seeded. This is probably due to the crowding of spots at higher ASC numbers, which will start to overlap and subsequently be read as a single spot [29]. Pretreatment of ASC with IFN-γ or TGF-β had no effect on the frequency of IL-6 producing ASC. Although IFN-γ secretion by ASC was hardly detectable by ELISA, we detected a frequency of 1.2%, 1.4%, and 1.7% of IFN-γ secreting ASC, detectable for the 4000, 2000, and 1000 seeded ASC, respectively (Figure 3(b)). After TGF-β treatment, a significantly higher frequency of IFN-γ producing ASC were found; 1.9%, 2.7%, and 2.8%, respectively ($p = 0.03$). These results demonstrate that whereas all ASC secrete IL-6, a small subpopulation secretes IFN-γ, thereby demonstrating heterogeneity in ASC cultures concerning cytokine secretion.

3.3. Heterogeneity in ASC Cytokine Receptor Expression. IL-6 secreted by ASC may have a paracrine and/or an autocrine function. To examine whether ASC-secreted IL-6 has an autocrine function, we measured the expression of the IL-6 receptor α-chain (CD126) and the IL-6 receptor β-chain (CD130) by flow cytometry (Figure 4). CD126 was not detected on the surface of ASC. A subpopulation (10%) of

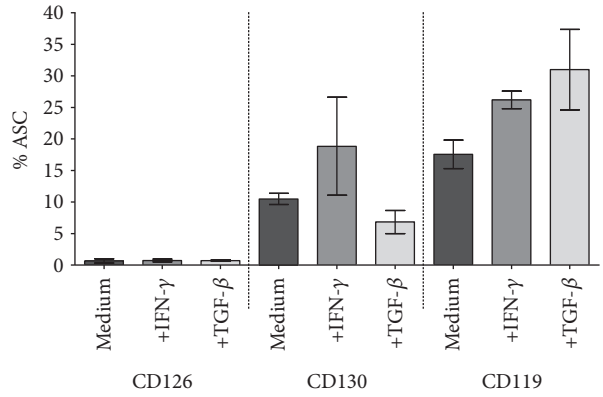

Figure 4: Expression of IL-6 receptor and IFN-γ receptor on ASC. ASC ($n = 3$) were cultured without or in the presence of IFN-γ or TGF-β for 72 h and trypsinised and analyzed by flow cytometry. The IL-6 receptor subunit CD126 was not detected, and CD130 was detected in a small percentage of the ASC. The IFN-γ receptor (CD119) was detected on a subpopulation of ASC. Presented as mean and SEM.

ASC expressed CD130, and pretreatment with IFN-γ resulted in an increased expression of CD130 to 18% of ASC (Figure 4). However, the absence of CD126 indicates that no functional IL-6 receptors are present on ASC. We also measured the expression of the IFN-γ receptor 1 (CD119). CD119 was expressed on a subpopulation of 18% of ASC. Pretreatment with IFN-γ or TGF-β resulted in a higher percentage of CD119 positive ASC, 26% and 31%, respectively (Figure 4).

4. Discussion

MSC are found in all tissues [30] and in the search of finding the most assessable, best expandable, and most effective MSC type for therapy, remarkable similarities concerning surface antigen expression, immunosuppressive activity, and differentiation ability between MSC of different tissue sources have been observed [3, 31]. There are, however, subtle differences between MSC of different sources, such as in levels of chemokine receptor expression and paracrine factor production, and in the resistance to apoptosis, which may reflect different therapeutic efficacy [32–34].

Even within populations of MSC from one tissue source subpopulations of MSC can be identified. For instance, LNGFR^{+}THY-1^{+}VCAM-1^{hi+} MSC have been identified as a population of MSC with enhanced clonogenic properties [35]. James et al. have demonstrated that bone marrow MSC contain distinct immunomodulatory and differentiation-competent subtypes [36] and, for example, STRO-1-enriched MSC display a more suppressive effect on lymphocyte proliferation than MSC [22]. Data from the present study suggests that within populations of ASC there is variation in the immunoregulatory function of ASC. A small fraction of ASC produced IFN-γ, and a subpopulation of ASC expressed the IFN-γ receptor, which distinguishes these cells from other ASC with respect to their response to inflammatory conditions where IFN-γ is around. It is very likely that similar selective expression patterns are found for other receptors and soluble factors. We found no selective secretion of IL-6. All ASC secreted IL-6 at single cell level whereas no expression of the IL-6 receptor α-chain was found on ASC and only 10% expressed the IL-6 receptor β-chain. This demonstrates that IL-6 secreted by ASC has a paracrine signaling role. This has been demonstrated in studies showing that IL-6 secreted by MSC plays a role in the regulation of monocytes [37] and dendritic cells [38].

It is well established that ASC change their immunomodulatory function after exposure to cytokines. It is therefore surprising that the secretion of IFN-γ and expression of IFN-γ receptor or IL-6 receptor was only slightly affected by pretreatment of the ASC with IFN-γ or TGF-β. We furthermore found no changes in the level of IL-6 secretion, while significantly more IFN-γ was produced after pretreatment with TGF-β. This effect of TGF-β was also found in the IFN-γ ELISPOT. It is possible that pretreatment with IFN-γ or TGF-β affects the secretion by ASC of other cytokines that were not examined in the present study or that pretreatment with other cytokines has a more profound effect on ASC. Ageing of ASC in culture may be another factor influencing the function of ASC. We recently demonstrated that the MSC phenotype remains stable until passage 12 and that the immunosuppressive capacity of MSC was reduced from passage 8 onwards [39]. In the present study, ASC between passages 1–5 were used. At these passages, there is no evidence of effects on the phenotype and function of MSC.

This preliminary study demonstrates to our knowledge for the first time that the ELISPOT assay can be used to determine the heterogeneity of MSC with respect to their cytokine secretion. Although MSC are adherent cells and thus physically block patches of the ELISPOT plates, the cytokines secreted by MSC do form spots that are detectable after lysis of the MSC. At high-seeding densities, it was observed that the frequency of IL-6 secreting ASC was decreased. This could have a biological origin stemming from an inhibitory effect of MSC on their neighbors' cytokine secretion. Alternatively, the reason for this observation may be that spots start to overlap at high cell densities leading to an underestimation of spots. It is therefore important to take different seeding densities of MSC in consideration.

5. Conclusions

The ASC population is heterogenic in their cytokine secretion and cytokine receptor expression profile. Determining the frequency of cytokine or growth factor producing ASC by ELISPOT assay is a useful novel tool in the characterization of (clinical) ASC batches that can be used as a potency assay.

Conflicts of Interest

The authors declare that the research was conducted in the absence of any commercial or financial relationships that could be construed as a potential conflict of interest.

Acknowledgments

This work was supported by a fund from the Science and Technology Department of Sichuan Province, China, Grant no. 2016JY0035.

References

[1] M. F. Pittenger, A. M. Mackay, S. C. Beck et al., "Multilineage potential of adult human mesenchymal stem cells," *Science*, vol. 284, no. 5411, pp. 143–147, 1999.

[2] P. A. Zuk, M. Zhu, H. Mizuno et al., "Multilineage cells from human adipose tissue: implications for cell-based therapies," *Tissue Engineering*, vol. 7, no. 2, pp. 211–228, 2001.

[3] S. Kern, H. Eichler, J. Stoeve, H. Kluter, and K. Bieback, "Comparative analysis of mesenchymal stem cells from bone marrow, umbilical cord blood, or adipose tissue," *Stem Cells*, vol. 24, no. 5, pp. 1294–1301, 2006.

[4] E. Gonzalez-Rey, P. Anderson, M. A. Gonzalez, L. Rico, D. Buscher, and M. Delgado, "Human adult stem cells derived from adipose tissue protect against experimental colitis and sepsis," *Gut*, vol. 58, no. 7, pp. 929–939, 2009.

[5] M. A. Gonzalez, E. Gonzalez-Rey, L. Rico, D. Buscher, and M. Delgado, "Treatment of experimental arthritis by inducing immune tolerance with human adipose-derived mesenchymal stem cells," *Arthritis and Rheumatism*, vol. 60, no. 4, pp. 1006–1019, 2009.

[6] A. U. Engela, M. J. Hoogduijn, K. Boer et al., "Human adipose-tissue derived mesenchymal stem cells induce functional de-novo regulatory T cells with methylated FOXP3 gene DNA," *Clinical and Experimental Immunology*, vol. 173, no. 2, pp. 343–354, 2013.

[7] P. Anderson, L. Souza-Moreira, M. Morell et al., "Adipose-derived mesenchymal stromal cells induce immunomodulatory macrophages which protect from experimental colitis and sepsis," *Gut*, vol. 62, no. 8, pp. 1131–1141, 2013.

[8] B. Puissant, C. Barreau, P. Bourin et al., "Immunomodulatory effect of human adipose tissue-derived adult stem cells: comparison with bone marrow mesenchymal stem cells," *British Journal of Haematology*, vol. 129, no. 1, pp. 118–129, 2005.

[9] A. Augello, R. Tasso, S. M. Negrini et al., "Bone marrow mesenchymal progenitor cells inhibit lymphocyte proliferation by activation of the programmed death 1 pathway," *European Journal of Immunology*, vol. 35, no. 5, pp. 1482–1490, 2005.

[10] A. Nasef, N. Mathieu, A. Chapel et al., "Immunosuppressive effects of mesenchymal stem cells: involvement of HLA-G," *Transplantation*, vol. 84, no. 2, pp. 231–237, 2007.

[11] M. Di Nicola, C. Carlo-Stella, M. Magni et al., "Human bone marrow stromal cells suppress T-lymphocyte proliferation induced by cellular or nonspecific mitogenic stimuli," *Blood*, vol. 99, no. 10, pp. 3838–3843, 2002.

[12] M. J. Crop, C. C. Baan, S. S. Korevaar, J. N. Ijzermans, W. Weimar, and M. J. Hoogduijn, "Human adipose tissue-derived mesenchymal stem cells induce explosive T-cell proliferation," *Stem Cells and Development*, vol. 19, no. 12, pp. 1843–1853, 2010.

[13] C. A. Hunter and S. A. Jones, "IL-6 as a keystone cytokine in health and disease," *Nature Immunology*, vol. 16, no. 5, pp. 448–457, 2015.

[14] R. Meisel, A. Zibert, M. Laryea, U. Gobel, W. Daubener, and D. Dilloo, "Human bone marrow stromal cells inhibit allogeneic T-cell responses by indoleamine 2,3-dioxygenase-mediated tryptophan degradation," *Blood*, vol. 103, no. 12, pp. 4619–4621, 2004.

[15] M. J. Crop, C. C. Baan, S. S. Korevaar et al., "Inflammatory conditions affect gene expression and function of human adipose tissue-derived mesenchymal stem cells," *Clinical and Experimental Immunology*, vol. 162, no. 3, pp. 474–486, 2010.

[16] M. Krampera, L. Cosmi, R. Angeli et al., "Role for interferon-gamma in the immunomodulatory activity of human bone marrow mesenchymal stem cells," *Stem Cells*, vol. 24, no. 2, pp. 386–398, 2006.

[17] K. N. Sivanathan, D. M. Rojas-Canales, C. M. Hope et al., "Interleukin-17A-induced human mesenchymal stem cells are superior modulators of immunological function," *Stem Cells*, vol. 2, 2015.

[18] H. S. Kim, J. W. Yun, T. H. Shin et al., "Human umbilical cord blood mesenchymal stem cell-derived PGE2 and TGF-beta1 alleviate atopic dermatitis by reducing mast cell degranulation," *Stem Cells*, vol. 33, no. 4, pp. 1254–1266, 2015.

[19] P. Gao, Y. Zhou, L. Xian et al., "Functional effects of TGF-beta1 on mesenchymal stem cell mobilization in cockroach allergen-induced asthma," *Journal of Immunology*, vol. 192, no. 10, pp. 4560–4570, 2014.

[20] P. Li, H. Tian, Z. Li et al., "Subpopulations of bone marrow mesenchymal stem cells exhibit differential effects in delaying retinal degeneration," *Current Molecular Medicine*, vol. 16, no. 6, pp. 567–581, 2016.

[21] M. Mo, S. Wang, Y. Zhou, H. Li, and Y. Wu, "Mesenchymal stem cell subpopulations: phenotype, property and therapeutic potential," *Cellular and Molecular Life Sciences*, vol. 73, no. 17, pp. 3311–3321, 2016.

[22] A. Nasef, Y. Z. Zhang, C. Mazurier et al., "Selected Stro-1-enriched bone marrow stromal cells display a major suppressive effect on lymphocyte proliferation," *International Journal of Laboratory Hematology*, vol. 31, no. 1, pp. 9–19, 2009.

[23] Z. Kuci, J. Seiberth, H. Latifi-Pupovci et al., "Clonal analysis of multipotent stromal cells derived from CD271+ bone marrow mononuclear cells: functional heterogeneity and different mechanisms of allosuppression," *Haematologica*, vol. 98, no. 10, pp. 1609–1616, 2013.

[24] D. G. Phinney, "Functional heterogeneity of mesenchymal stem cells: implications for cell therapy," *Journal of Cellular Biochemistry*, vol. 113, no. 9, pp. 2806–2812, 2012.

[25] J. H. Gerrits, J. van de Wetering, W. Weimar, and N. M. van Besouw, "T-cell reactivity during tapering of immunosuppression to low-dose monotherapy prednisolone in HLA-identical living-related renal transplant recipients," *Transplantation*, vol. 87, no. 6, pp. 907–914, 2009.

[26] N. M. van Besouw, K. Caliskan, A. M. Peeters et al., "Interleukin-17-producing CD4(+) cells home to the graft early after human heart transplantation," *The Journal of Heart and Lung Transplantation*, vol. 34, no. 7, pp. 933–940, 2015.

[27] N. M. van Besouw, P. T. van Hal, J. M. Zuijderwijk et al., "Herpes zoster after lung transplantation boosts varicella zoster virus-specific adaptive immune responses," *The Journal of Heart and Lung Transplantation*, vol. 35, no. 12, pp. 1435–1442, 2016.

[28] M. Roemeling-van Rhijn, M. Khairoun, S. S. Korevaar et al., "Human bone marrow- and adipose tissue-derived mesenchymal stromal cells are immunosuppressive in vitro and in a humanized allograft rejection model," *Journal of Stem Cell Research and Therapy*, vol. 25, no. 1, Supplement 6, p. 20780, 2013.

[29] J. H. Cox, G. Ferrari, and S. Janetzki, "Measurement of cytokine release at the single cell level using the ELISPOT assay," *Methods*, vol. 38, no. 4, pp. 274–282, 2006.

[30] M. L. da Silva, P. C. Chagastelles, and N. B. Nardi, "Mesenchymal stem cells reside in virtually all post-natal organs and tissues," *Journal of Cell Science*, vol. 119, Part 11, pp. 2204–2213, 2006.

[31] H. J. Jin, Y. K. Bae, M. Kim et al., "Comparative analysis of human mesenchymal stem cells from bone marrow, adipose tissue, and umbilical cord blood as sources of cell therapy," *International Journal of Molecular Sciences*, vol. 14, no. 9, pp. 17986–18001, 2013.

[32] N. Ahmadian Kia, A. R. Bahrami, M. Ebrahimi et al., "Comparative analysis of chemokine receptor's expression in mesenchymal stem cells derived from human bone marrow and adipose tissue," *Journal of Molecular Neuroscience*, vol. 44, no. 3, pp. 178–185, 2011.

[33] G. Ertas, E. Ural, D. Ural et al., "Comparative analysis of apoptotic resistance of mesenchymal stem cells isolated from

human bone marrow and adipose tissue," *The Scientific World Journal*, vol. 2012, Article ID 105698, 2012.

[34] S. T. Hsiao, A. Asgari, Z. Lokmic et al., "Comparative analysis of paracrine factor expression in human adult mesenchymal stem cells derived from bone marrow, adipose, and dermal tissue," *Stem Cells and Development*, vol. 21, no. 12, pp. 2189–2203, 2012.

[35] Y. Mabuchi, S. Morikawa, S. Harada et al., "LNGFR(+)THY-1(+)VCAM-1(hi+) cells reveal functionally distinct subpopulations in mesenchymal stem cells," *Stem Cell Reports*, vol. 1, no. 2, pp. 152–165, 2013.

[36] S. James, J. Fox, F. Afsari et al., "Multiparameter analysis of human bone marrow stromal cells identifies distinct immunomodulatory and differentiation-competent subtypes," *Stem Cell Reports*, vol. 4, no. 6, pp. 1004–1015, 2015.

[37] Y. Deng, Y. Zhang, L. Ye et al., "Umbilical cord-derived mesenchymal stem cells instruct monocytes towards an IL10-producing phenotype by secreting IL6 and HGF," *Scientific Reports*, vol. 6, p. 37566, 2016.

[38] Y. Deng, S. Yi, G. Wang et al., "Umbilical cord-derived mesenchymal stem cells instruct dendritic cells to acquire tolerogenic phenotypes through the IL-6-mediated upregulation of SOCS1," *Stem Cells and Development*, vol. 23, no. 17, pp. 2080–2092, 2014.

[39] S. F. H. de Witte, E. E. Lambert, A. Merino et al., "Ageing of bone marrow and umbilical cord derived MSC during expansion," *Cytotherapy*, 2017, in press.

Hindawi
Stem Cells International
Volume 2017, Article ID 1798260, 11 pages
https://doi.org/10.1155/2017/1798260

Research Article

Therapeutic Effect and Location of GFP-Labeled Placental Mesenchymal Stem Cells on Hepatic Fibrosis in Rats

Jiong Yu,[1] Guangshu Hao,[2] Dan Wang,[1] Jingqi Liu,[1] Xiaotian Dong,[1] Yanni Sun,[1] Qiaoling Pan,[1] Yang Li,[3] Xiaowei Shi,[4] Lanjuan Li,[1] and Hongcui Cao[1]

[1]*State Key Laboratory for the Diagnosis and Treatment of Infectious Diseases, First Affiliated Hospital, College of Medicine, Zhejiang University and Collaborative Innovation Center for Diagnosis and Treatment of Infectious Diseases, 79 Qingchun Road, Hangzhou 310003, China*
[2]*Gansu Provincial Maternity and Child-Care Hospital, 143 Qilihe North Street, Lanzhou 730050, China*
[3]*Obstetrical Department, First Affiliated Hospital, College of Medicine, Zhejiang University, 79 Qingchun Road, Hangzhou 310003, China*
[4]*Chu Kochen Honors College, Zhejiang University, 866 Yuhangtang Road, Hangzhou 310058, China*

Correspondence should be addressed to Hongcui Cao; hccao@zju.edu.cn

Received 24 January 2017; Accepted 8 March 2017; Published 12 April 2017

Academic Editor: Vladislav Volarevic

Background. Liver fibrosis is a chronic progressive liver disease, but no established effective treatment exists except for liver transplantation. The present study was designed to investigate the effect of human placenta mesenchymal stem cells (hPMSCs) expressing green fluorescent protein (GFP) on carbon tetrachloride- (CCl_4-) induced liver fibrosis in rats. *Methods*. Liver fibrosis was induced by subcutaneous injection with CCl_4; hPMSCs were directly transplanted into rats through the caudal vein. The therapeutic efficacy of hPMSCs on liver fibrosis was measured by liver function tests, liver elastography, histopathology, Masson's trichrome and Sirius red staining, and immunohistochemical studies. The expression levels of fibrotic markers, transforming growth factor β1 (TGF-β1) and α-smooth muscle actin (α-SMA), were assessed using real-time polymerase chain reaction. *Results*. We demonstrated that liver fibrosis was significantly dampened in the hPMSC transplantation group according to the Laennec fibrosis scoring system and histological data. The Sirius red-stained collagen area and the elastography score were significantly reduced in the hPMSC-treated group. Meanwhile, hPMSC administration significantly decreased TGF-β1 and α-SMA expression and enhanced liver functions in CCl_4-induced fibrotic rats. *Conclusion*. This study indicates that transplantation of hPMSCs could repair liver fibrosis induced by CCl_4 in rats, which may serve as a valuable therapeutic approach to treat liver diseases.

1. Introduction

Liver fibrosis is a common chronic progressive liver disease caused by one or more etiologies such as viruses, alcohol, parasites, autoimmune reactions, long-term drug damage, or repeated effects of the formation of diffuse liver damage [1]. At home and abroad, orthotopic liver transplantation is currently recognized as the most effective treatment, but a shortage of donor organs and other issues limit the wide application of the treatment [2, 3]. Therefore, it is extremely important to find other effective methods to treat liver fibrosis.

With the development of cell transplantation in recent years, mesenchymal stem cells (MSCs) have attracted more and more attention in the treatment of liver fibrosis [4, 5]. MSCs are a class of mesoderm-derived adult stem cells with a high self-renewal capacity and multidirectional differentiation potential. In addition, MSCs also have low immunogenicity, immunomodulatory, and anti-inflammatory effects [6, 7].

MSCs are widely found in the bone marrow, adipose tissue, placenta, and cord blood as well as other tissues and organs [8–10]. Among them, bone marrow-derived MSC (BMSC) is currently the most widely studied MSC, but

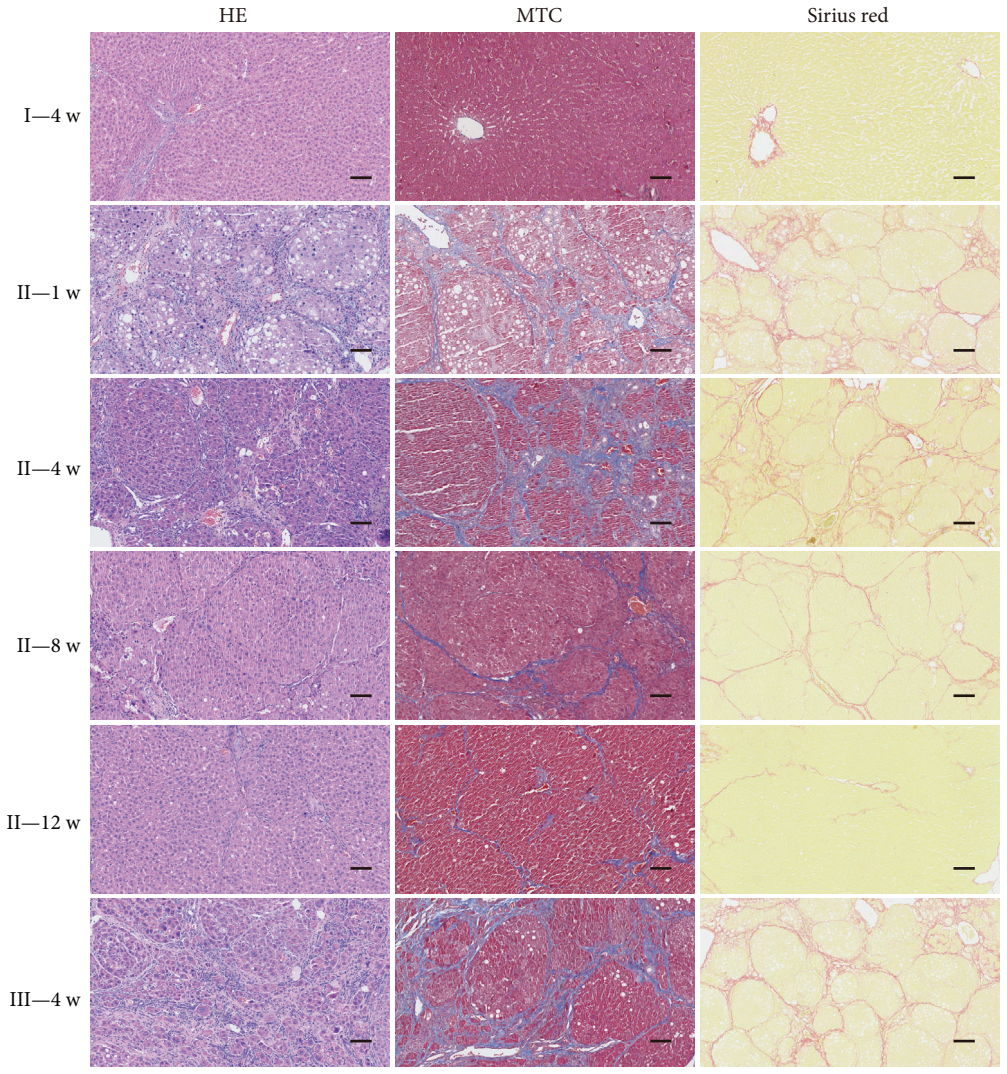

Figure 1: Assessment of liver fibrosis in the different experimental groups by tissue dyes. (a) Histological analysis was evaluated by H&E and MTC staining; (b-c) representative micrograph of hepatic tissue stained with Sirius red (b), and the relative expression of collagen was quantified using ImageJ analysis (c), $n = 6$.

Table 1: Histological stage of hepatic fibrosis.

Group	Stage 0	Stage 1	Stage 2	Stage 3	Stage 4A	Stage 4B	Stage 4C	Average
Score	0	1	2	3	4	5	6	
Group I	24							0
Group II			1	5	8	10		4.125
Group III						9	15	5.625

limited by its potential damages to the donors, its low quantities available, and the existence of ethical problems. Human placenta-derived mesenchymal stem cell (hPMSC), a promising source of MSCs, has biological characteristics similar to those of BMSC and is readily available from a rich source through noninvasive methods, is free of ethical issues, and has a higher differentiation capacity and lower immunogenicity, as well as other advantages [11–14]. All of these advantages indicate the broad potential applications for hPMSCs.

In this study, we used hPMSCs with green fluorescent protein (GFP^+ hPMSCs) and the corresponding imaging modality to provide a novel approach to continuously track and quantify the fate of hPMSCs in vivo, investigated the effect of GFP^+ hPMSCs on hepatic fibrosis in a carbon tetrachloride- (CCl_4-) induced fibrotic rat model [15], and provided an experimental and theoretical basis for the clinical use of hPMSC transplantation for the treatment of liver diseases.

2. Materials and Methods

2.1. Cell Culture and Gene Transduction. hPMSCs were obtained and transduced as previously described [12, 16]. Briefly, hPMSCs were cultured in special medium (Mesen Cult® Human Basal Medium plus MesenCult® Human Supplement, STEMCELL Technologies Inc., Vancouver, Canada) with a standard humidified incubator (HERAcell®150, Thermo Fisher Scientific Inc.) with 5% CO_2 at 37°C. When the hPMSCs were stabilized and reached 50% confluence, the recombinant lentivirus (Gene Pharma, Shanghai, China) was added to the medium to perform the transfection experiment as previously described. Then, the culture medium was replaced with fresh medium mixed with 10 μg puromycin (Sigma-Aldrich Co. LLC, St. Louis, MO, USA); the cells were continuously cultured and trypsinized using 0.25% (*w*/*v*) trypsin/ethylenediaminetetraacetic acid (EDTA, Invitrogen, Carlsbad, CA, USA) and passaged at a 1 : 3 dilution upon reaching 70–80% confluence. Finally, the verification of GFP successful expression was done following the previous experiment. All protocols for human tissue and cell handling were approved by the Research Ethics Committee of First Affiliated Hospital, School of Medicine, Zhejiang University (Reference number 2013-272).

2.2. Liver Fibrosis Animal Model. Six-week-old, specific-pathogen-free, male Sprague Dawley rats weighing 180 g to 200 g were obtained from the Experimental Animal Center of Zhejiang Academy of Medical Sciences and housed in an air-conditioned animal room with 50% humidity and a 12 h daylight/darkness cycle. All rats were treated according to protocols approved by the Research Ethics Committee of the First Affiliated Hospital, School of Medicine, Zhejiang University. To induce liver fibrosis, rats were given a subcutaneous injection of 50% CCl_4 (Wuxi Zhanwang Chemical Co. Ltd., Wuxi, China) mixed with olive oil (Sangon Biotech Co. Ltd., Shanghai, China) at a dose of 0.5 mL per 100 g of body weight twice per week for 8 weeks. After 8 weeks, five model rats were selected randomly to verify liver fibrosis by pathological testing of liver tissue.

2.2.1. Experimental Groups and Cell Transplantation. The animals were randomly divided into three groups as follows: group I (saline control group, $n = 24$), which received saline instead of carbon tetrachloride injection and cell transplantation (passages 3 to 6; 2.0×10^6 hPMSCs in 1 mL saline) by caudal vein injection; group II (hPMSC-treated group, $n = 24$), fibrosis models with hPMSC transplantation via the caudal vein (passages 3 to 6; 2.0×10^6 hPMSCs in 1 mL saline); and group III (untreated fibrosis group, $n = 24$), which received saline by caudal vein injection instead of cell transplantation. Fluorescence imaging and liver shear-wave elastography were performed on the rats, and the rats were then killed at 1 week (1 w), 4 weeks (4 w), 8 weeks (8 w), and 12 weeks (12 w) post transplantation, after which liver tissue and serum were extracted for follow-up analyses.

2.2.2. Biochemical Analysis and Serum Determination. Blood samples were acquired from rats at each time point, placed at room temperature for 30 minutes, and then centrifuged for 15 minutes at 3000 rpm (Sorvall® Biofuge Stratos, Thermo, Germany), and the serum was collected. Then, albumin (ALB), alanine aminotransferase (ALT), aspartate aminotransferase (AST), alkaline phosphatase (ALP), and total bilirubin (TBIL), direct bilirubin (DBIL), gamma-glutamyl transpeptidase (γ-GT) concentrations were assessed using an automated biochemical analyzer (Abbott Aeroset, Abbott Laboratories, Chicago, IL, USA). The levels of hepatic fibrogenesis indicators, such as laminin (LN) and hyaluronan (HA), were measured using commercial enzyme-linked immunosorbent assay (ELISA) kits (R&D Systems Inc., Minneapolis, USA and Abnova Corporation, Taiwan) according to the manufacturer's instructions.

2.2.3. Liver Evaluation with Elastography and Histology. First, we performed liver shear-wave elastography (Siemens AG, Berlin, Germany) to assess the degree of hepatic fibrosis in rats at various time points. In the assessment of chronic liver damage, hepatic elastography is the most reproducible. In the

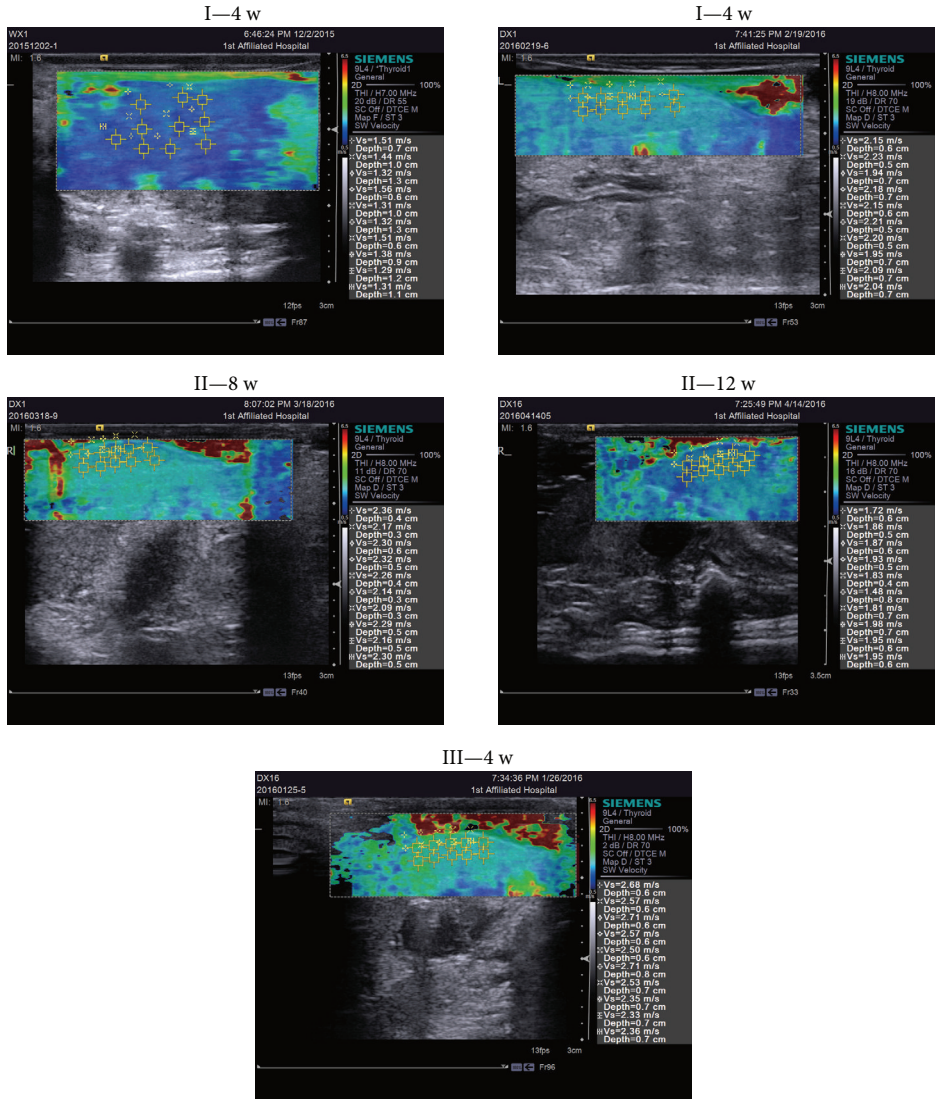

Figure 2: Semiquantitative assessment of liver fibrosis in the different experimental groups by shear-wave elastography. (a) Representative micrograph of liver elastography in the three groups. Saline control group rats (group I), untreated fibrosis animals (group III), fibrotic animals transplanted with hPMSCs (group II) at four weeks, eight weeks, and twelve weeks after transplantation (4 w, 8 w, and 12 w). Images are representative images from $n = 3$ rats at each time point. The data are presented as the mean ± SD (error bars) and were statistically analyzed using one-way ANOVA.$^{***}p < 0.001$.

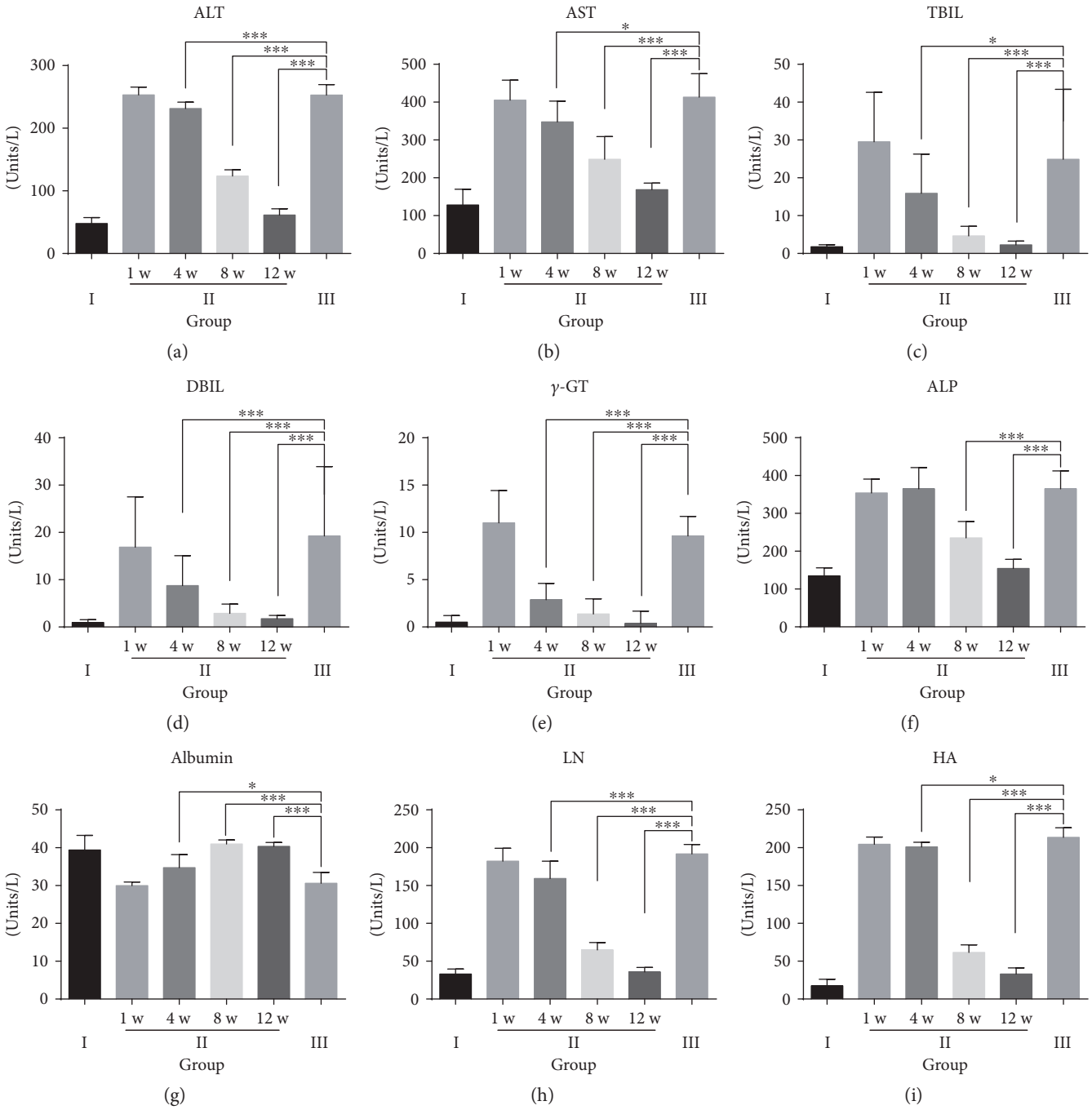

Figure 3: Biochemical analyses. (a) Alanine aminotransferase (ALT); (b) aspartate aminotransferase (AST); (c) total bilirubin (TBIL); (d) direct bilirubin (DBIL); (e) gamma glutamyl transpeptidase (γ-GT); (f) alkaline phosphatase (ALP); (g) albumin (ALB); (h) laminin (LN); (i) hyaluronic acid (HA). Saline control group rats (group I), untreated fibrosis animals (group III), and fibrotic animals transplanted with hPMSCs (group II) and sacrificed one week, four weeks, eight weeks, or twelve weeks after transplantation (1 w, 4 w, 8 w, or 12 w). (a–g) Group I, $n = 20$; group II, $n = 8$; and group III, $n = 8$. (h–i) Group I, $n = 9$; group II, $n = 8$; and group III, $n = 8$. Data represent the means ± SD and were statistically analyzed by one-way ANOVA. $^{*}p < 0.05$, $^{**}p < 0.01$, and $^{***}p < 0.001$.

scoring system, liver fibrosis is evaluated semiquantitatively [17, 18]. As described below, the rats were weighed and anesthetized by subcutaneous injection of chloral hydrate (Sangon Biotech Co. Ltd., Shanghai, China) at a dose of 0.3 mL/100 g, and then the liver shear-wave elastography of rats was examined after rat thoracic hair was removed with a shaver.

To further verify the extent of the rat liver fibrosis, the hepatic specimens were fixed in 4% paraformaldehyde and embedded in paraffin, then deparaffinized and rehydrated with distilled water, and stained with hematoxylin and eosin (H&E), Masson's trichrome (MTC) and Sirius red using a Masson's trichrome staining kit (Sigma-Aldrich Co. LLC, MO, USA) and Sirius red staining kit (Wuhan Goodbio

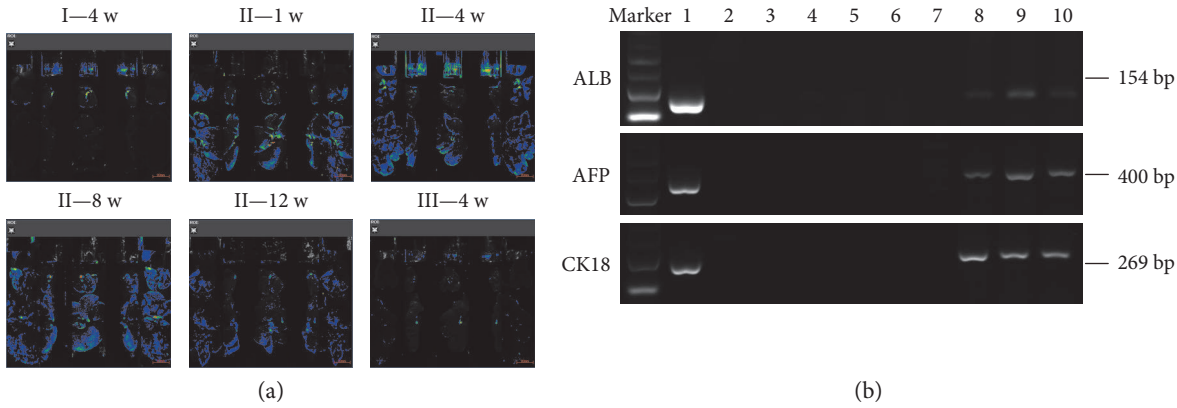

Figure 4: Localization and fate of the transplanted hPMSCs in rat livers of different experimental groups. (a) Representative figures of liver fluorescence are from $n = 6$ rats from each group at each time point; (b) RT-PCR of human-specific markers. Lane 1, positive control (human liver for ALB and CK18, human liver cancer for AFP); lane 2, the liver of group III as a negative control; lane 3 to 6, hPMSC transplantation at 1 w, 4 w, 8 w, and 12 w in group I. Human AFP and CK18 were not detected at the four time points, but ALB was detected in lane 4. Lane 7 to 10, hPMSC transplantation at 1 w, 4 w, 8 w, and 12 w in group II. Human ALB, AFP, and CK18 were all detected at the three later time points but not at 1 w.

Technology Co. Ltd., Wuhan, China) according to the manufacturer's instructions. First, the Laennec fibrosis scoring system was used for quantitative analysis of fibrosis [19]. Additionally, Sirius red staining was performed to estimate the amount of collagen in the liver tissue; the collagen content was quantified as a percentage of the total area positive for Sirius red stain using ImageJ version 1.35s (National Institutes of Health, Bethesda, MD).

2.2.4. Liver Immunohistochemistry. The paraffin sections were deparaffinized and rehydrated. To inactivate the endogenous peroxidase, the sections were incubated in 3% hydrogen peroxide-methanol solution for 10 minutes. Then, antigen retrieval was performed by microwave (Midea Group Co. Ltd., Guangdong, China) treatment in 0.01 M citrate salt buffer (pH 6.0, Wuhan Goodbio Technology Co. Ltd., Wuhan, China) for 15 minutes and blocked in 5% BSA for 45 minutes at room temperature. Sections were incubated overnight at 4°C with the diluted primary antibody against human ALB (1 : 250; Abcam, UK), alpha-fetoprotein (AFP, 1 : 100; Abcam, UK), cytokeratin 18 (CK18, 1 : 100; Abcam, UK) as well as antirat α-smooth muscle actin (α-SMA, 1 : 400; Abcam, UK) and TGF-β1 (1 : 500; Abcam, UK). The next day, the sections were washed 3 times with phosphate-buffered saline (PBS, pH 7.2 ± 0.1, GenomSciences, Hangzhou, China) and then incubated at 37°C in an incubator for 60 minutes with horseradish peroxidase-conjugated secondary antibodies (1 mg/mL, 1 : 1000; Abcam, UK). A brown color was developed with diaminobenzidine tetrahydrochloride solution (DAB kit, Abcam, UK) for 10 min, washed in distilled water 3 times, and counterstained with hematoxylin for 5 minutes at room temperature. Finally, the liver sections were sealed with neutral resin and examined microscopically.

2.2.5. Reverse Transcription-Polymerase Chain Reaction and Quantitative Real-Time Polymerase Chain Reaction. Total RNA from each sample was extracted with the Trizol reagent (Invitrogen, USA). The RNA purity and quantity were measured by determining absorbance at 260 and 280 nm, and 1 μg of RNA was used as the template for cDNA synthesis using the QuantiTect Reverse Transcription Kit (TAKARA Biotechnology (Dalian) Co. Ltd., Dalian, China) according to the manufacturer's instructions. The primers for the target products were designed as shown in Supplementary Table S1 available online at https://doi.org/10.1155/2017/1798260. Polymerase chain reaction (PCR) amplification was subsequently carried out in a PCR thermal cycler (Life Technologies, Carlsbad, California, USA). The PCR products were separated by 1.2% agarose gel electrophoresis containing gelred. Then, the images were acquired using a gel documentation system (Syngene GBox-HR Gel Doc System, UK). The quantitative real-time polymerase chain reaction (qRT-PCR) was performed to measure the mRNA levels of TGF-β1 and α-SMA (QuantiTect SYBR Green RT-PCR kit, TAKARA Biotechnology (Dalian) Co. Ltd.) with a 7500 Real Time System (Life Technologies, Carlsbad, California, USA). All PCR products were normalized to the expression levels of β-actin used as an internal standard.

2.3. Statistical Analysis. Statistical analysis was performed using the SPSS 19.0 software (SPSS Inc., Chicago, IL, USA). All data were presented as the mean ± standard deviation (SD). Statistical comparison among three groups was performed using a one-way ANOVA analysis, and a comparison between the groups was evaluated using Student's t-test. $p < 0.05$ was considered statistically significant.

3. Results

3.1. Construction of hPMSCs Transfected with Green Fluorescent Protein. hPMSCs that were cultured in normal conditions showed a fibroblast-like morphology (see Supplementary Figure S1A). Then, hPMSCs were transduced with a lentiviral vector encoding GFP at a multiplicity of infection (MOI) of 100 : 1. The expression of GFP visualized

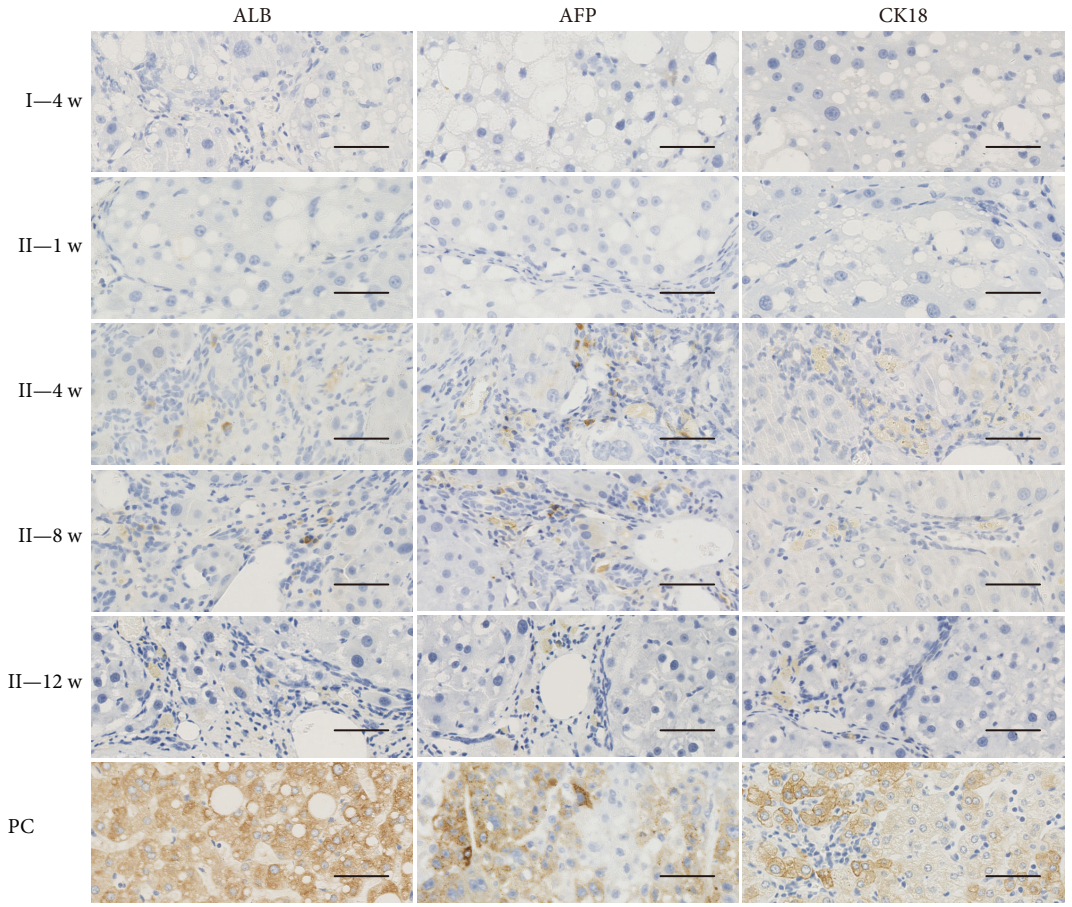

Figure 5: Hepatogenic differentiation of transplanted hPMSCs in rat livers (20x). Immunohistochemistry staining for human hepatic markers ALB, AFP, and CK18, light-brown coloration in cells means the positive staining results. Group III as a negative control; PC: human liver as positive control for ALB and CK18 and human liver cancer as a positive control for AFP; group II: fibrotic animals transplanted with hPMSCs and sacrificed one week, four weeks, eight weeks, or twelve weeks after transplantation (1 w, 4 w, 8 w, or 12 w). Scale bars: 100 μm.

by fluorescence/phase-contrast microscopy was used to evaluate the successful lentiviral transduction in cultured hPMSCs (see Supplementary Figure S1B).

3.2. Enhanced Resolution of Liver Fibrosis by Transplantation of hPMSCs. The results from the histologic liver evaluation showed that transplantation of hPMSCs (group II) had a more beneficial effect on the recovery of liver fibrosis than saline treatment in the untreated fibrosis group (group III), exhibited as strong H&E and MTC staining, showing regenerative nodules and progressive reduction in the amount of collagen occurred in the fibrous septa, especially after the eighth week of transplantation. The degree of fibrosis was significantly improved by hPMSC transplantation. In group II rats on twelve weeks after cell transplantation, the liver was close to the normal structure of the liver, and the architecture of the impaired hepatic lobule returned to normal, as it was no different from the liver structure of rats in the saline control group (group I) (Figure 1(a)). Consistently, the results from the Laennec fibrosis scoring system showed that group II had a relatively lower average score than group III (Table 1). The Sirius red staining results revealed that the collagen-stained area in liver sections was more decreased in the hPMSC-treated group than that in the untreated fibrosis group, and the collagen-stained area decreased with time in the hPMSC-treated group. However, the collagen-stained area maintained a high level in the untreated fibrosis group. Almost no collagen deposition was observed in group I (Figures 1(b) and 1(c)).

The liver elastography showed a similar result. In the untreated fibrosis group, the stiffness score was significantly upregulated, but it was significantly decreased in the hPMSC-treated group (Figure 2). All of these data clearly suggest that hPMSCs were an effective therapeutic method for rat hepatic fibrosis and attenuated the extent of hepatic fibrosis in experimental rats.

3.3. Biochemical Analysis. Biochemical analyses were performed to assess the restoration of the liver functions and hepatic fibrosis. The results showed that ALT, AST, TBIL, DBIL, and γ-GT levels were significantly decreased in the hPMSC-treated group (Figures 3(a)–3(e)) and approached normal levels 12 weeks after cell transplantation. The levels of ALP showed a similar pattern (Figure 3(f)). In addition,

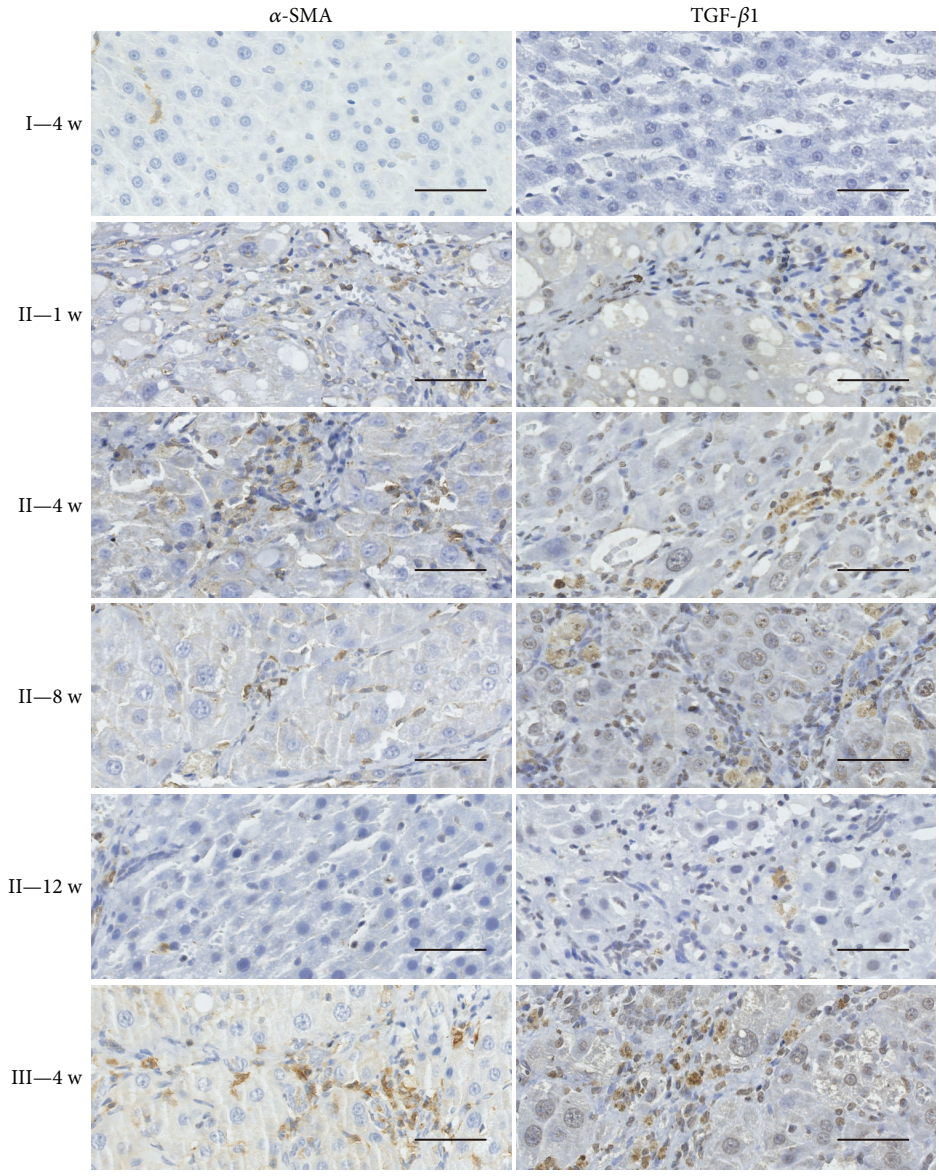

Figure 6: Immunohistochemistry results of α-SMA and TGF-β1 in the different experimental groups. Light-brown coloration in cells means the positive staining results. Immunohistochemical staining for α-SMA and TGF-β1 (20x), with a young rat liver as a negative control (NC), fibrotic animals (group II), fibrotic animals transplanted with hPMSCs (group II) sacrificed at one week, four weeks, eight weeks, or twelve weeks after transplantation (1 w, 4 w, 8 w, or 12 w). Scale bars: 100 μm.

the serum level of albumin in the hPMSC-treated group was higher than that in the untreated fibrosis group and approached the normal level of the saline control group at 12 weeks after transplantation (Figure 3(g)).

The serum levels of LN and HA in the hPMSC-treated group were lower than those in the untreated fibrosis group. The level of LN approached the level in the saline control group at the last time point examined, but the level of HA was still higher than the normal level at that time (Figures 3(h) and 3(i)).

3.4. Localization and Fate of the Transplanted hPMSCs in the Liver. To detect the colonization and differentiation of hPMSCs in the rat after transplantation, we used fluorescence microscopy to image the liver of the rats at the corresponding time points. As shown in Figure 4(a), in group II, fluorescence was detected in the liver tissue at all four time points after hPMSC transplantation, but the fluorescence signal was very weak at 12 weeks. However, in groups I and III, no fluorescence signal was detected in the liver. The liver tissue samples were photographed and fixed paraffin sections, and the expression of liver-specific markers AFP, ALB, and CK18 were detected by immunohistochemistry.

AFP, ALB, and CK18 mRNA were all detected in the liver tissue at 4 weeks, 8 weeks, and 12 weeks after transplantation through RT-PCR analysis using human-specific primers. Human AFP, ALB, and CK18 mRNA were not detected in the livers at 1 week after hPMSC transplantation, which was also confirmed by immunohistochemistry.

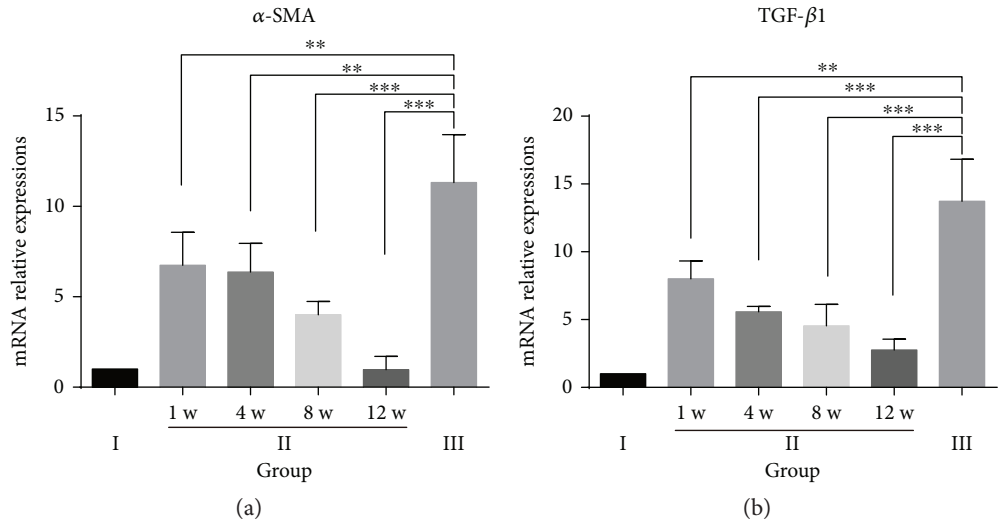

Figure 7: Relative mRNA expression levels of α-SMA and TGF-β1 in the different experimental groups. Quantitative real-time polymerase chain reaction (qRT-PCR) results from $n = 6$ rats from each group at each time point. The tests were performed in triplicate. The data are presented as the mean ± SD (error bars) and were statistically analyzed using Student's t-test. $^{**}p < 0.01$, $^{***}p < 0.001$.

No expression of human AFP, ALB, or CK18 was detected in group I or group III liver samples, except that human ALB mRNA expression was detected in one rat from group I (Figure 4(b)).

We obtained similar results through immunohistochemistry. As shown in Figure 5, in group II, positive staining for AFP, ALB, and CK18 was not observed in any liver specimen at 1 week after hPMSC transplantation. However, the expression of AFP-, ALB-, and CK18-positive cells was detected in all liver tissue of rats at 4 weeks after transplantation, and the positive cells were mainly scattered along the perivascular and the fibrous septa around the portal area. In addition, AFP-, ALB-, and CK18-positive cells were also detected at 8 and 12 weeks after hPMSC transplantation, but the number of positive cells decreased with time. In group III liver samples, no human AFP-, ALB-, or CK18-positive staining was detected (data not shown).

3.5. Inhibition of Hepatic Stellate Cell Activation by hPMSCs. It is well known that activation of hepatic stellate cells (HSCs) is currently recognized as a central event in the development of hepatic fibrosis, in which activated HSCs participate in the formation of hepatic fibrosis through proliferation and secretion of α-SMA protein, which is a marker of activated HSCs and plays a central role in extracellular matrix (ECM) production in response to liver damage. In addition, TGF-β1 is a fibrogenic master cytokine that plays a central role in the progression of ECM degradation. The results through immunohistochemistry (Figure 6) and qRT-PCR (Figure 7) revealed that α-SMA and TGF-β1 levels reached the highest value in the untreated fibrosis group (group III). However, α-SMA and TGF-β1 expression was significantly lower in the hPMSC-treated group (group II) than that in the untreated fibrosis group (group III). In addition, in group II, the levels of α-SMA and TGF-β1 decreased with time and approached normal levels (saline control group) 12 weeks after cell transplantation. These results indicated that hPMSC transplantation may prevent HSC differentiation and inhibit HSC activity.

4. Discussion

Recently, MSCs have been reported to potentially secrete organotrophic factors that protect cells from damage or activate endogenous restorative mechanisms to enhance fibrous matrix degradation and restore the injured liver [20, 21]. In this study, we investigated the therapeutic effect of hPMSCs in a CCl_4-induced rat liver fibrosis model. We found that hPMSC transplantation exhibited an enhanced therapeutic effect compared to that observed without hPMSC transplantation. We performed fluorescence imaging of the rat liver at multiple time points to determine whether GFP-labeled hPMSCs were expressed in the rat liver. As an important means of tracking cells, GFP tagging has a strong advantage. Using fluorescent imaging devices, it was fairly easy to see whether GFP-labeled hPMSCs colonized in the liver as well as analyze the number and distribution of cells in the rat liver. These results, combined with the data from RT-PCR and immunohistochemistry, were much more credible. As the images showed, the expression of the fluorescent signal was detected at all four time points in the hPMSC-treated group (group II), but the signal intensity was weakest at 12 weeks. Nevertheless, our data clearly demonstrated the presence of transplanted hPMSCs in the damaged rat liver.

Cirrhosis and advanced fibrosis are generally considered irreversible conditions and are not diagnosed until the condition has reached an advanced stage [22]. Therefore, early diagnosis of liver fibrosis has become very important. In general, liver fibrosis and its severity are determined through H&E, MTC, and Sirius red and α-SMA staining of histological sections. In addition, we used B-ultrasonography, which has the advantages of less trauma, providing intuitive results and having less of an effect on the experimental animals and biological events that need to be

observed to evaluate liver fibrosis in rats [23, 24]. In this study, shear-wave elastography of the liver was also a supplement to the results of the pathological analysis, making the experimental results more credible. Some studies have used the Metavir scoring system to classify liver fibrosis. However, due to a lack of accurate subclassification of cirrhosis using the Metavir scoring system, liver pathologists will often come to the wrong conclusions when assessing the therapeutic effect. Therefore, further better histological subclassification of cirrhosis is required. In this study, we applied the new Laennec system; these histologic criteria have been better defined to provide a more exact and detailed classification of cirrhotic stage [19, 25].

HSC activation and increased ECM synthesis paired with insufficient degradation play a central role in the change induced by hepatic fibrosis. The expression of α-SMA in the liver is an indicator for the HSC activation, indicating that activated HSCs expressing α-SMA are involved in the development and progression of hepatic fibrosis [26, 27]. In the present study, levels of α-SMA in the rat liver significantly decreased after hPMSC transplantation. This result may explain the reduced fibrogenesis in the hPMSC-transplanted liver.

The balance between ECM deposition and degradation is regulated by a variety of cytokines, the most important of which is TGF-β1 [28, 29]. TGF-β1 can inhibit the proliferation of hepatocytes, induce hepatocyte apoptosis, activate HSCs, promote the production of extracellular matrix, and inhibit the degradation of extracellular matrix. Furthermore, TGF-β1 can inhibit the production of collagenase and protease, promote tissue inhibitors such as tissue inhibitor of metalloproteinase production, and reduce ECM degradation [30, 31]. TGF-β1 can also indirectly affect ECM synthesis by acting on other cytokines [32]. As shown in this study, hPMSC transplantation into the rat liver reduced the level of TGF-β1, resulting in a decrease in the activation of hepatic stellate cells and reduction in hepatic fibrosis.

In conclusion, our study showed that MSCs from the human placenta could effectively cure liver fibrosis, reduce the activation of hepatic stellate cells, and restore liver functions. However, the underlying mechanism remains to be further clarified. Therefore, hPMSC therapy may be a new and effective strategy for the treatment of fibrotic liver disease in the future.

Abbreviations

AFP: Alpha-fetoprotein
ALB: Albumin
ALP: Alkaline phosphatase
ALT: Alanine aminotransferase
AST: Aspartate aminotransferase
CCl_4: Carbon tetrachloride
CK18: Cytokeratin 18
DBIL: Direct bilirubin
ECM: Extracellular matrix
EDTA: Ethylenediaminetetraacetic acid
ELISA: Enzyme-linked immunosorbent assay
GFP: Green fluorescent protein
H&E: Hematoxylin and eosin
HA: Hyaluronan
hPMSCs: Human placental mesenchymal stem cells
HSC: Hepatic stellate cell
LN: Laminin
MOI: Multiplicity of infection
MSCs: Mesenchymal stem cells
MTC: Masson's trichrome
PBS: Phosphate-buffered saline
PCR: Polymerase chain reaction
RT-PCR: Reverse transcription-polymerase chain reaction
TBIL: Total bilirubin
TGF-β1: Transforming growth factor β1
α-SMA: α-Smooth muscle actin
γ-GT: Gamma-glutamyl transpeptidase.

Additional Points

Highlights. The following are the highlights of the paper:

(i) Green fluorescent protein gene-transduced human placenta-derived mesenchymal stem cells (hPMSCs) and the corresponding imaging modality were used to provide a novel approach to continuously track and quantify the fate of hPMSCs in vivo and to investigate the effect of their transplantation on the carbon tetrachloride- (CCl_4-) induced liver fibrosis in rats.

(ii) Biochemical analyses, histology, immunohistochemistry, and liver shear-wave elastography were used to evaluate the improvement on hepatic fibrosis after hPMSC transplantation.

(iii) hPMSCs had an enhanced therapeutic effect for hepatic fibrosis compared to non-hPMSCs possibly via their differentiation and inhibition of hepatic stellate cell activation.

Conflicts of Interest

No competing financial interests exist.

Authors' Contributions

Jiong Yu and Guangshu Hao contributed equally to this work.

Acknowledgments

The authors would like to thank Dr. Tianan Jiang and Dr. Danxia Xu of the Department of Ultrasound and Dr. Ke Sun of the Department of Pathology at First Affiliated Hospital of Zhejiang University for their professional review on the B-ultrasonography and histopathology. This study was supported by the National Natural Science Foundation of China (no. 81471794) and Stem Cell and Translational Research, the National Key Research and Development Program of China (no. 2016YFA0101001).

References

[1] R. Bataller and D. A. Brenner, "Liver fibrosis," *Journal of Clinical Investigation*, vol. 115, no. 2, pp. 209–218, 2005.

[2] R. Pais, A. S. Barritt, Y. Calmus et al., "NAFLD and liver transplantation: current burden and expected challenges," *Journal of Hepatology*, vol. 65, no. 6, pp. 1245–1257, 2016.

[3] G. Addolorato, A. Mirijello, P. Barrio, and A. Gual, "Treatment of alcohol use disorders in patients with alcoholic liver disease," *Journal of Hepatology*, vol. 65, no. 3, pp. 618–630, 2016.

[4] G. Ali, S. Mohsin, M. Khan et al., "Nitric oxide augments mesenchymal stem cell ability to repair liver fibrosis," *Journal of Translational Medicine*, vol. 10, no. 1, p. 75, 2012.

[5] B. M. Stutchfield, S. J. Forbes, and S. J. Wigmore, "Prospects for stem cell transplantation in the treatment of hepatic disease," *Liver Transplantation*, vol. 16, no. 7, pp. 827–836, 2010.

[6] A. R. Zekri, H. Salama, E. Medhat et al., "The impact of repeated autologous infusion of haematopoietic stem cells in patients with liver insufficiency," *Stem Cell Research & Therapy*, vol. 6, no. 1, p. 118, 2015.

[7] Y. O. Jang, M. Y. Kim, M. Y. Cho, S. K. Baik, Y. Z. Cho, and S. O. Kwon, "Effect of bone marrow-derived mesenchymal stem cells on hepatic fibrosis in a thioacetamide-induced cirrhotic rat model," *BMC Gastroenterology*, no. 1, p. 14, 2014198, 2014.

[8] Y. H. Jiang, B. N. Jahagirdar, R. L. Reinhardt et al., "Pluripotency of mesenchymal stem cells derived from adult marrow," *Nature*, vol. 418, pp. 41–49, 2002.

[9] P. S. In 't Anker, S. A. Scherjon, C. Kleijburg-van der Keur et al., "Isolation of mesenchymal stem cells of fetal or maternal origin from human placenta," *Stem Cells*, vol. 22, no. 7, pp. 1338–1345, 2004.

[10] O. K. Lee, T. K. Kuo, W. M. Chen, K. D. Lee, S. L. Hsieh, and T. H. Chen, "Isolation of multipotent mesenchymal stem cells from umbilical cord blood," *Blood*, vol. 103, no. 5, pp. 1669–1675, 2004.

[11] Z. Miao, J. Jin, L. Chen et al., "Isolation of mesenchymal stem cells from human placenta: comparison with human bone marrow mesenchymal stem cells," *Cell Biology International*, vol. 30, no. 9, pp. 681–687, 2006.

[12] H. C. Cao, J. F. Yang, J. Yu et al., "Therapeutic potential of transplanted placental mesenchymal stem cells in treating Chinese miniature pigs with acute liver failure," *BMC Medicine*, no. 1, p. 10, 201256, 2012.

[13] O. Parolini, F. Alviano, G. P. Bagnara et al., "Concise review: isolation and characterization of cells from human term placenta: outcome of the first international workshop on placenta derived stem cells," *Stem Cells*, vol. 26, no. 2, pp. 300–311, 2008.

[14] P. Mattar and K. Bieback, "Comparing the immunomodulatory properties of bone marrow, adipose tissue, and birth-associated tissue mesenchymal stromal cells," *Frontiers in Immunology*, vol. 3, no. 6, p. 560, 2015.

[15] P. Starkel and I. A. Leclercq, "Animal models for the study of hepatic fibrosis," *Best Practice & Research. Clinical Gastroenterology*, vol. 25, no. 2, pp. 319–333, 2011.

[16] J. Yu, X. Su, C. Zhu et al., "GFP labeling and hepatic differentiation potential of human placenta-derived Mesenchymal stem cells," *Cellular Physiology and Biochemistry*, vol. 35, no. 6, pp. 2299–2308, 2015.

[17] W. K. Jeong, H. K. Lim, H. K. Lee, J. M. Jo, and Y. Kim, "Principles and clinical application of ultrasound elastography for diffuse liver disease," *Ultrasonography*, vol. 33, no. 3, pp. 149–160, 2014.

[18] T. Jiang, G. Tian, Q. Zhao et al., "Diagnostic accuracy of 2D-shear wave elastography for liver fibrosis severity: a meta-analysis," *PLoS One*, vol. 11, no. 6, article e0157219, 2016.

[19] M. Y. Kim, M. Y. Cho, S. K. Baik et al., "Histological subclassification of cirrhosis using the Laennec fibrosis scoring system correlates with clinical stage and grade of portal hypertension," *Journal of Hepatology*, vol. 55, no. 5, pp. 1004–1009, 2011.

[20] M. D. Kim, S. S. Kim, H. Y. Cha et al., "Therapeutic effect of hepatocyte growth factor-secreting mesenchymal stem cells in a rat model of liver fibrosis," *Experimental & Molecular Medicine*, vol. 46, no. 8, article e110, 2014.

[21] W. H. Liu, F. Q. Song, L. N. Ren et al., "The multiple functional roles of mesenchymal stem cells in participating in treating liver diseases," *Journal of Cellular and Molecular Medicine*, vol. 19, no. 3, pp. 511–520, 2015.

[22] D. Schuppan and M. Pinzani, "Anti-fibrotic therapy: lost in translation?" *Journal of Hepatology*, vol. 56, Supplement 1, pp. S66–S74, 2012.

[23] B. E. Van Beers, J. L. Daire, and P. Garteiser, "New imaging techniques for liver diseases," *Journal of Hepatology*, vol. 62, no. 3, pp. 690–700, 2015.

[24] K. M. Moon, G. Kim, S. K. Baik et al., "Ultrasonographic scoring system score versus liver stiffness measurement in prediction of cirrhosis," *Clinical and Molecular Hepatology*, vol. 19, no. 4, pp. 389–398, 2013.

[25] P. Bedossa, G. Garcia-Tsao, and D. Jain, "Cirrhosis regression and subclassification," *Surgical Pathology Clinics*, vol. 6, no. 2, pp. 295–309, 2013.

[26] F. J. Eng and S. L. Friedman, "Fibrogenesis I. New insights into hepatic stellate cell activation: the simple becomes complex," *American Journal of Physiology - Gastrointestinal and Liver Physiology*, vol. 279, no. 1, pp. G7–G11, 2000.

[27] S. Lindert, L. Wickert, I. Sawitza et al., "Transdifferentiation-dependent expression of alpha-SMA in hepatic stellate cells does not involve TGF-beta pathways leading to coinduction of collagen type I and thrombospondin-2," *Matrix Biology*, vol. 24, no. 3, pp. 198–207, 2005.

[28] A. Weiss and L. Attisano, "The TGFbeta superfamily signaling pathway," *Wiley Interdisciplinary Reviews: Developmental Biology*, vol. 2, no. 1, pp. 47–63, 2013.

[29] S. Dooley, B. Delvoux, B. Lahme, K. Mangasser-Stephan, and A. M. Gressner, "Modulation of transforming growth factor beta response and signaling during transdifferentiation of rat hepatic stellate cells to myofibroblasts," *Hepatology*, vol. 31, no. 5, pp. 1094–1106, 2000.

[30] G. R. Grotendorst, "Connective tissue growth factor: a mediator of TGF-β action on fibroblasts," *Cytokine & Growth Factor Reviews*, vol. 8, no. 3, pp. 171–179, 1997.

[31] F. Verrecchia and A. Mauviel, "Transforming growth factor-β and fibrosis," *World Journal of Gastroenterology*, vol. 13, no. 22, pp. 3056–3062, 2007.

[32] K. Sakai, S. Jawaid, T. Sasaki, G. Bou-Gharios, and T. Sakai, "Transforming growth factor-beta-independent role of connective tissue growth factor in the development of liver fibrosis," *The American Journal of Pathology*, vol. 184, no. 10, pp. 2611–2617, 2014.